DETECTING PHYTOPLANKTON SIZE CLASS USING SATELLITE EARTH OBSERVATION

R. J. W. BREWIN

Ph.D. 2011

DETECTING PHYTOPLANKTON SIZE CLASS USING SATELLITE EARTH OBSERVATION

ROBERT J W. BREWIN

A thesis submitted to the University of Plymouth
in partial fulfilment for the degree of

DOCTOR OF PHILOSOPHY

School of Marine Science and Engineering
Faculty of Science

In collaboration with
Plymouth Marine Laboratory
UK Met Office

FEBRUARY 2011

Detecting Phytoplankton Size Class using Satellite Earth Observation

Robert J. W. Brewin

A new range of multi-plankton biogeochemical models have recently been developed, designed to advance our understanding of the ocean carbon cycle to improve predictions of its future influence on climate. Synoptic measurements of the different phytoplankton communities are required to validate and ultimately improve such models. Measuring ocean colour from satellite is the only method currently available for synoptically monitoring wide-area properties of ocean ecosystems, such as phytoplankton chlorophyll biomass. Recently, a variety of bio-optical methods have been established that use satellite data to identify and differentiate between either phytoplankton functional types (PFTs) or phytoplankton size classes (PSCs). In this thesis, several of these techniques were evaluated against *in situ* observations (6504 samples) to determine their ability to detect dominant phytoplankton size classes (micro-, nano- and picoplankton). Results show that spectral-response, ecological and abundance-based approaches can all perform with similar accuracy. However, abundance-based approaches provide better spatial retrieval of PSCs.

Based on insights into the abundance-based models, and by utilising a large pigment database, a new three-component model was developed which calculates the fractional contributions of three phytoplankton size classes (micro-, nano- and picoplankton) to the overall chlorophyll-a concentration. Using a globally representative, independent, coupled pigment and satellite dataset the model estimates fractional contributions with a mean accuracy of 9.2% for microplankton, 17.1% for nanoplankton and 16.1% for picoplankton. The effect of optical depth on the model parameters was also investigated and explicitly incorporated into the model.

Using the three-component model, the two-component absorption model of Sathyendranath et al. (2001) and Devred et al. (2006) was extended to three-component populations of phytoplankton, namely, pico-, nano- and microplankton. The new model infers total and size-dependent phytoplankton absorption as a function of the total chlorophyll-a concentration. A main characteristic of the model is that all the parameters that describe it have biological or optical interpretation. The three-component model performs better than the two-component model, at retrieving total phytoplankton absorption. Accounting for the contribution of pico- and nanoplankton, rather than the combination of both used in the two-component model, improved significantly the retrieval of phytoplankton absorption at low chlorophyll-a concentrations.

The three-component model was applied to a decade of ocean colour observations. In the equatorial region of the Pacific and Indian Oceans, phytoplankton size class anomalies (% total chlorophyll-a) were highly correlated with indices of both the El Niño (La Niña) Southern Oscillation and the Indian Ocean Dipole. Furthermore, in these regions, micro- and nanoplankton size class anomalies were negatively correlated with anomalies of the sea surface temperature, sea surface height and stratification. Whereas, the picoplankton size class anomalies were positively correlated with these physical variables. Results from this thesis indicate that phytoplankton size class can be retrieved from Earth Observation with reasonable accuracy. It is recommended that such information can now be assimilated into multi-plankton biogeochemical models, or alternatively, verify them.

Contents

List of Figures

List of Tables

Acronyms

ACE	Accumulated Cyclone Energy
AMO	Atlantic Multidecadal Oscillation
AMSR	Advanced Microwave Scanning Radiometer
AMT	Atlantic Meridional Transect
ANN	Artificial Neural Network
AOP	Apparent Optical Property
AVHRR	Advanced Very High Resolution Radiometer
AVISO	Archive, Validate and Interpret Satellite Ocean Data
BATS	Bermuda Atlantic Time-series Study
BE	BioEnergetic status
BE-BOT	BioEnergetic status and Bio-Optical Trait hypothesis
BODC	British Oceanographic Data Centre
BOT	Bio-Optical Traits
CASIX	Centre for the study of Air-Sea Interactions and FluXes
CDM	Coloured Dissolved and detrital Matter
CDOM	Coloured Dissolved Organic Matter
CPR	Continuous Plankton Recorder survey
CTD	Conductivity Temperature and Depth
CZCS	Coastal Zone Color Scanner
DMI	Indian Ocean Dipole Mode Index
DMS	DiMethyl Sulfide
DNA	DeoxyriboNucleic Acid
DOAS	Differential Optical Absorption Spectroscopy
DPA	Diagnostic Pigment Analysis
EM	ElectroMagnetic spectrum
ENSO	El Niño (La Niña) Southern Oscillation
EO	Earth Observation
ERS-2	European Remote-Sensing Satellite number 2
ESA	European Space Agency
EUC	Eastern Equatorial Undercurrent
GCM	General Circulation Models

GMES	Global Monitoring for Environment and Security programme
GSM	Garver-Siegel-Maritorena IOP algorithm
HOTS	Hawaii Ocean Time-Series
HPLC	High Performance Liquid Chromatography
IOD	Indian Ocean Dipole
IOP	Inherent Optical Property
ITCZ	InterTropical Convergence Zone
JAMSTEC	Japanese Agency for Marine-Earth Science and Technology
LUT	Look-Up Table
MBA	Marine Biological Association
ME	Mean Absolute Error, ME% refers to ME in relative values
MEI	Multivariate ENSO Index
MERIS	Medium Resolution Imaging Spectrometer
MODIS	Moderate Resolution Imaging Spectrometer
MOS	Modular Optical Scanner
NAO	North Atlantic Oscillation
NASA	National Aeronautics and Space Administration U.S.A.
NCEO	National Centre for Earth Observation
NEODAAS	NERC Earth Observation Data Acquisition and Analysis Service
NERC	National Environmental Research Council UK
NOAA	U.S. National Oceanic and Atmospheric Administration
NOMAD	NASA bio-Optical Marine Algorithm Dataset
NPOESS	National Polar-orbiting Operational Environment Satellite System
NPZD	Nutrient Phytoplankton Zooplankton and Detritus model
NSF	U.S. National Science Foundation
OBPG	NASA Ocean Biology Processing Group
OC2	Ocean Chlorophyll version 2 algorithm
OC4	Ocean Chlorophyll version 4 algorithm
OC4-SD	Ocean Chlorophyll version 4 Species Dependent algorithm
OCTS	Ocean Color and Temperature Sensor
PAR	Photosynthetically-Active Radiation
PDO	Pacific Decadal Oscillation
PFT	Phytoplankton Functional Type
PHY	Phytoplankton
PML	Plymouth Marine Laboratory
PSC	Phytoplankton Size Class
PSD	Particle Size Distribution
QAA	Quasi-Analytical Algorithm (Lee et al., 2002)
QS	NASA QuikSCAT sensor

RSPSoc	Remote Sensing and Photogrammetry Society
SeaBASS	SeaWiFS Bio-optical Archive and Storage System
SeaWiFS	Sea-viewing Wide Field-of-view Sensor
SO-CPR	Southern Ocean Continuous Plankton Recorder
SODA	Simple Ocean Data Assimilation
SPM	Suspended Particular Matter
SSH	Sea-Surface Height
SSHA	Sea-Surface Height Anomaly
SST	Sea Surface Temperature
T865	Optical aerosol thickness
VIIRS	Visible Infrared Imaging Spectro-Radiometer Suite

Symbols

a	Absorption coefficient of phytoplankton (m^{-1})
a_{CDOM}	Absorption coefficient of CDOM (m^{-1})
a_m	Absorption coefficient of microplankton (m^{-1})
a_n	Absorption coefficient of nanoplankton (m^{-1})
a_p	Absorption coefficient of picoplankton (m^{-1})
a^s	Absorption coefficient of phytoplankton derived from R_{rs} (m^{-1})
a^s_m	Absorption coefficient of microplankton derived from R_{rs} (m^{-1})
a^s_n	Absorption coefficient of nanoplankton derived from R_{rs} (m^{-1})
a^s_p	Absorption coefficient of picoplankton derived from R_{rs} (m^{-1})
a_{SPM}	Absorption coefficient of SPM (m^{-1})
a_t	Total absorption coefficient (m^{-1})
a_w	Absorption coefficient for water (m^{-1})
a^*	Specific absorption coefficient of phytoplankton (m^2 [mg C]$^{-1}$)
a^*_{CDOM}	Specific absorption coefficient of CDOM ($m^2\,mg^{-1}$)
a^*_m	Specific absorption coefficient of microplankton (m^2 [mg C]$^{-1}$)
a^*_n	Specific absorption coefficient of nanoplankton (m^2 [mg C]$^{-1}$)
a^*_p	Specific absorption coefficient of picoplankton (m^2 [mg C]$^{-1}$)
$a^*_{p,n}$	Specific absorption coefficient of combined pico-nanoplankton (m^2 [mg C]$^{-1}$)
a^*_{sol}	*In vivo* weight-specific absorption coefficient of a particulate pigment ($m^2\,mg^{-1}$)
a^*_{SPM}	Specific absorption coefficient of SPM ($m^2\,mg^{-1}$)
A	Numerical constant for a power-law model (Equation 5.9)
b	Scattering coefficient of phytoplankton (m^{-1})
b_{SPM}	Scattering coefficient of SPM (m^{-1})
b_t	Total scattering coefficient (m^{-1})
b^b_t	Backward scattering coefficient (m^{-1})
b^f_t	Forward scattering coefficient (m^{-1})
b_w	Scattering coefficient for water (m^{-1})
b^*	Specific scattering coefficient for phytoplankton (m^2 [mg C]$^{-1}$)
b^*_{SPM}	Specific scattering coefficient for SPM ($m^2\,mg^{-1}$)

B	Numerical constant for a power-law model (Equation 5.9)
c	Speed of light ($\mathrm{m\,s^{-1}}$)
C	Total chlorophyll-a concentration derived from High Performance Liquid Chromatography ($\mathrm{mg\,m^{-3}}$)
$\mathbf{C}$	Carbon ($\mathrm{mg\,m^{-3}}$)
$CaCO_3$	Calcium carbonate ($\mathrm{mg\,m^{-3}}$)
C_{DIM}	Dimensionless chlorophyll-a concentration for the model of Uitz et al (2006)
C_m	Chlorophyll-a concentration of microplankton ($\mathrm{mg\,m^{-3}}$)
C_{max}	Represents the maximum vertical chlorophyll-a concentration for the vertical dimensionless C profile of Uitz et al (2006)
C_n	Chlorophyll-a concentration of nanoplankton ($\mathrm{mg\,m^{-3}}$)
CO_2	Carbon dioxide
C_p	Chlorophyll-a concentration of picoplankton ($\mathrm{mg\,m^{-3}}$)
$C_{p,n}$	Chlorophyll-a concentration of combined pico-nanoplankton ($\mathrm{mg\,m^{-3}}$)
C_{sur}	Surface chlorophyll-a concentration where $\tau<1$ ($\mathrm{mg\,m^{-3}}$)
C_w	Total chlorophyll-a concentration ($\mathrm{mg\,m^{-3}}$) derived from P and W according to Uitz et al (2006)
$\overline{C_{Zp}}$	The average chlorophyll-a concentration within the euphotic layer ($\mathrm{mg\,m^{-3}}$)
C_ζ	Chlorophyll-a concentration at a particular dimensionless depth ζ ($\mathrm{mg\,m^{-3}}$)
C^m	Maximum chlorophyll-a concentration of a particular size class ($\mathrm{mg\,m^{-3}}$)
$C^m_{p,n}$	Maximum chlorophyll-a concentration of combined pico-nanoplankton ($\mathrm{mg\,m^{-3}}$)
C^m_p	Maximum chlorophyll-a concentration of picoplankton ($\mathrm{mg\,m^{-3}}$)
C^s	Total chlorophyll-a concentration derived from $R_{rs}(\lambda)$ following O'Reilly et al. (1998) ($\mathrm{mg\,m^{-3}}$)
C^s_p	Chlorophyll-a concentration of picoplankton retrieved from satellite ($\mathrm{mg\,m^{-3}}$)
C^s_n	Chlorophyll-a concentration of nanoplankton retrieved from satellite ($\mathrm{mg\,m^{-3}}$)
C^s_m	Chlorophyll-a concentration of microplankton retrieved from satellite ($\mathrm{mg\,m^{-3}}$)
D_b	Surface value for the vertical dimensionless C profile of Uitz et al (2006)
E_d	Downward Irradiance ($\mathrm{W\,m^{-2}\,sr^{-1}}$)
F_m	Microplankton fraction of total chlorophyll-a

F_n	Nanoplankton fraction of total chlorophyll-a
F_p	Picoplankton fraction of total chlorophyll-a
$F_{p,n}$	Combined pico-nanoplankton fraction of total chlorophyll-a
F_p^s	Picoplankton fraction of total chlorophyll-a retrieved from satellite
F_n^s	Nanoplankton fraction of total chlorophyll-a retrieved from satellite
F_m^s	Microplankton fraction of total chlorophyll-a retrieved from satellite
g	Proportionality factor describing the directional effect at the air-surface interface
k	The decrease in the vertical mass flux of carbon with depth
K	Diffuse attenuation coefficient for downwelling irradiance (m^{-1})
L	Radiance ($W\,m^{-2}\,sr^{-1}$)
L_w	Water-leaving radiance ($W\,m^{-2}\,sr^{-1}$)
L_{wn}	Normalised water-leaving radiance ($W\,m^{-2}\,sr^{-1}$)
m	Microplankton
ME%	Relative mean error [%]
ME	Mean absolute error
n	Nanoplankton
N_2	Nitrogen gas fixation
N	Refers to the number of samples
p	Picoplankton
P	Diagnostic Pigments (fucoxanthin; peridinin; 19'-hexanoyloxyfucoxanthin; 19'-butanoyloxyfucoxanthin; alloxanthin; chlorophyll-b and divinyl chlorophyll b; zeaxanthin)
PAR	Photosynthetically-active radiation ($E\,m^{-2}\,d^{-1}$)
pCO_2	Partial pressure of CO_2 in the atmosphere and the ocean
q	Beam attenuation coefficient (m^{-1})
r	Pearson correlation coefficient
R	Size-specific slopes describing the variations in the size-specific $a^*(\lambda)$ of the Uitz et al. (2008) model along the vertical z/Z_p
R_{rs}	Remote sensing reflectance (sr^{-1})
s	Linear decrease in slope for the dimensionless C profile of Uitz et al. (2006)
S	Slope describing the rate of increase in the chlorophyll-a concentration of a particular size class as a function of the total chlorophyll-a concentration
S_{CDM}	The spectral slope of CDM absorption
S_f	Size parameter of phytoplankton which represents the fractional contribution of picoplankton to a according to Ciotti et al. (2002)
Si	Silica

S_p	Slope describing the rate of increase in the chlorophyll-a concentration of picoplankton as a function of the total chlorophyll-a concentration
$S_{p,n}$	Slope describing the rate of increase in the chlorophyll-a concentration of combined pico-nanoplankton as a function of the total chlorophyll-a concentration
SSH	Sea-surface height (cm)
SSHA	Sea-surface height anomaly (cm)
SST	Sea surface temperature (°C)
T865	Optical aerosol thickness (dimensionless)
u	Standard deviation of all samples for a type of phytoplankton
v	Frequency (Hz or s^{-1})
w	Phytoplankton cell count
W	Chlorophyll-a to diagnostic pigment ratios derived by Uitz et al. (2006) (1.41, 1 41, 1.27, 0 35, 0 6, 1 01; 0 86)
x	A concentration
$\overline{x}$	Overall mean of all cell counts for each type of phytoplankton
X	A particular variable
z	Geometric depth (m)
Z	Z-factor
Z_m	Mixed-layer depth (m)
Z_p	Euphotic depth (m)
β_a	Represent the change in $C^m_{p,n}$ with increasing τ
β_b	Represent the change in $S_{p,n}$ with increasing τ
β_c	Represent the change in C^m_p with increasing τ
β_d	Represent the change in S_p with increasing τ
$\Delta\zeta$	Depicts the width of the peak for the dimensionless C profile of Uitz et al (2006)
χ	Volume scattering function (m^{-1})
λ	Wavelength (nm)
τ	Optical depth (m)
ζ	Dimensionless depth (z/Z_p)
ζ_{max}	The depth at which C_{max} occurs for the dimensionless C profile of Uitz et al (2006)

Acknowledgements

This thesis constitutes the apex of three years of work at the University of Plymouth. From a personal and academic perspective, I have been supported and helped by many individuals who have provided invaluable assistance. Firstly, I am hugely indebted to my supervisors Sam Lavender, Nick Hardman-Mountford, Paul Russell and Rosa Barciela. Individually, Sam, I thank you for giving me a chance. There are not many academics that would have considered me for a PhD in marine remote sensing, given my unique background qualifications. Sam, I also thank you for providing me with countless opportunities over the past three years, teaching, travelling and getting involved with external activities, and providing guidance, support and much of your time teaching me to become a scientist.

Nick, like Sam, I cannot thank you enough for providing guidance, support and much of your time to help me get through these three years. I also thank you for motivating me and pushing me, always encouraging investigation into ideas and offering thought-provoking viewpoints. Nick, I thank you for being positive and confident in my abilities which has helped me get through the PhD. I have been enormously fortunate to have both you and Sam as supervisors. Paul, I thank you for stepping in as my director of studies, providing encouragement through the latter stages of the PhD and instilling confidence in me to achieve my goal. Rosa, thank you for your insightful viewpoints during the PhD meetings and for providing your intuition from a modelling perspective.

In addition to my supervisors, I would also like to personally thank five more individuals, Takafumi Hirata, Shubha Sathyendranath, Emmanuel Devred, Dionysios Raitsos and Jim Aiken who, throughout my PhD, provided hours of their invaluable time to collaborate, critique and encourage. I cannot thank these individuals enough! Additionally, I would like to thank Julia Uitz, Annick Bricaud, Aurea Ciotti, Trevor Platt, Tim Smyth and Yaswant Pradhan for providing comments to help refine ideas. I thank Professors Richard Geider and Phil Dyke for a challenging and stimulating *viva voce* examination.

With regard to data used in this thesis, all contributors to the SeaBASS and NOMAD datasets are acknowledged. All present and past staff who are involved with the maintenance, collection, analysis and processing of the BATS and HOTS pigment databases are acknowledged. I also acknowledge the crew of RRS James

Clark Ross and RRS Discovery and all scientists who helped in the acquisition and analyses of AMT data. All present and past staff of SAHFOS who have contributed to the maintenance of the CPR time-series are acknowledged, and I thank the present and past PML staff that have contributed to the maintenance, collection, analysis and processing of the L4 data. I would also like to thank Séverine Alvain for providing the PHYSAT look-up table, Dionysios Raitsos for help running his ANN, and Annick Bricaud, Aurea Ciotti and Bernard Gentili for help running their nonlinear-optimisation code. I would like to acknowledge Declan Schroeder of the Marine Biological Association and Abigail McQuatters-Gollop, based at SAHFOS, for comments on the CPR data, Claire Widdicombe based at PML for help on the L4 data and Peter Miller for cooperation processing satellite data over the L4 site. I acknowledge NASA and the SeaWiFS project at the Goddard Space Flight Centre for AVHRR and SeaWiFS data, AVISO for SSH data and the Department of Atmospheric and Oceanic Science at the University of Maryland for free access to SODA data. I would like to acknowledge the financial support of the National Environmental Research Council, UK, and the Centre for the study of Air-Sea Interactions and FluXes (which recently merged into the National Centre for Earth Observation).

A big "shout out" goes to B528, George, Jon, Kat, Sola, Faye, French Tom, Jaimie and Emlyn. You guys, and all the Plymouth post-docs (e.g. Dan B, Tim S, Ian F, Rob S, Bex and Martin A) and PhDers (e.g. Tim P, Gabi, Rob M, Emma L and Kieran) really made these three years worth living! Also, for the standard Friday night, much needed, beverages (JSV or Nowhere Inn) and associated madness (French Tom particularly!). Also, I would like to thank JB and Kate, who were around for the first two years of the PhD and always keen for some fun (JB particularly for joining me on the hunt for that elusive barrel!). From a personal viewpoint, big thanks to my brother Tom, Sid, Alan, "George Best" (particularly for bringing out Gazza), Mic, Horse, Bob and Joy and all my other friends and family for support or escapism.

I can't thank my immediate family enough (Mum, Dad and Aunty B) for support, encouragement and love. Finally, I could not have achieved anything without the support of *ma femme*. I cannot thank you enough for always being there and tolerating an obsessive man (*à la folie*). Seven years ago I came to Plymouth, young, fit and in search of a barrel. Seven years later I am not so young, not so fit, and still in search of a barrel. I do however, have some letters behind my name and have some very interesting experiences to remember. One thing I have learned during the past three years is summed up nicely by a quote from Edward R. Murrow "The obscure we see eventually. The completely obvious, it seems, takes longer."

Author's declaration

At no time during the registration for the degree of Doctor of Philosophy has the author been registered for any other University award without prior agreement of the Graduate Committee. This study was financed with the aid of a studentship from the Natural Environment Research Council (NERC). It was carried out in collaboration the NERC Centre for the study of Air-Sea Interactions and FluXes (CASIX) that recently merged into the National Centre for Earth Observation (NCEO), Plymouth Marine Laboratory and the UK Met Office.

A programme of advanced study was undertaken which included; two taught modules at the University of Plymouth, Laboratory based teaching methods and practice (ENV 5101) and Marine Applications of Remote Sensing and Geographical Systems (IMS5109); Multi-level modelling with 'R', University of Plymouth, October 2007; Graduate Teaching Associates Course, University of Plymouth, March 2008; Analysis of Multivariate Data from Ecology and Environmental Science using PRIMER v6, Plymouth, February 2008; ESA 2008 4th Earth Observation Summer School, Earth System monitoring and modelling, ESA ESRIN Frascati, Rome, Italy, August 2008; and various courses supplied by the Graduate training school including, introduction to Endnote XI, the transfer process and preparing for the viva.

Relevant scientific seminars and conferences were regularly attended at which work was often presented; external institutions were visited for consultation purposes and several papers were published in peer-reviewed journals. A list of oral presentations, poster presentations, newsletters, conference papers and peer-reviewed scientific articles are outlined below.

Peer-reviewed scientific articles

- Hirata, T., Hardman-Mountford, N.J., Barlow, R., Lamont, T., **Brewin, R.J.W.**, Smyth, T. and Aiken, J. (2009). An inherent optical property approach to the estimation of size-specific photosynthetic rates in eastern boundary upwelling zones from satellite ocean colour: an initial assessment. Progress in Oceanography 83, 393-397, doi:10.1016/j.pocean.2009.07.019.

- **Brewin, R.J.W.**, Lavender, S J , Hardman-Mountford, N J. and Hirata, T. (2010) A spectral response approach for detecting dominant phytoplankton size class from satellite remote sensing Acta Oceanologica Sinica 29 (2), 14-32, doi:10.1007/s13131-010-0018-y

- **Brewin, R.J.W.**, Lavender, S.J and Hardman-Mountford, N. J. (2010) Mapping size-specific phytoplankton primary production on a global scale. Journal of Maps, v2010, 448-462, doi:10.4113/jom 2010 1122

- **Brewin, R.J.W.**, Lavender, S.J. and Hardman-Mountford, N. J. (2010) Published Map In Brewin, R J.W., Lavender, S J and Hardman-Mountford, N J (2010). Mapping size-specific phytoplankton primary production on a global scale Journal of Maps, v2010, 448-462, doi 10 4113/jom 2010 1122

- **Brewin, R.J.W.**, Sathyendranath, S , Hirata, T , Lavender, S.J , Barciela, R and Hardman-Mountford, N.J (2010) A three-component model of phytoplankton size class for the Atlantic Ocean Ecological Modelling 221, 1472-1483, doi 10 1016/j.ecolmodel 2010.02 014

- **Brewin, R.J.W.**, Hardman-Mountford, N J and Hirata, T (2010) Detecting phytoplankton community structure from ocean colour, in J Morales, V Stuart, T Platt and S. Sathyendranath (eds), Handbook of Satellite Remote Sensing Image Interpretation Applications to Marine Living Resources Conservation and Management, EU PRESPO Project, Spain

- Hirata, T , Hardman-Mountford, N J , **Brewin, R.J.W.**, Aiken, J , Barlow, R , Suzuki, K , Isada, T , Howell, E , Hashioka, T , Noguchi-Aita, M. and Yamanaka, Y (2011) Synoptic relationships between surface Chlorophyll-a and diagnostic pigments specific to phytoplankton functional types Biogeosciences 8, 311-327, doi.10 5194/bg-8-311-2011

- **Brewin, R.J.W.**, Hardman-Mountford, N J., Lavender, S J , Raitsos, D E , Hirata, T , Uitz, J , Devred, E , Bricaud, A , Ciotti, A and Gentili, B (2011) An intercomparison of bio-optical techniques for detecting dominant phytoplankton size class from satellite remote sensing Remote Sensing of Environment 115, 325-339, doi·10 1016/j rse 2010 09 004.

- **Brewin, R.J.W.**, Devred, E., Sathyendranath, S., Hardman-Mountford, N J and Lavender, S.J (In revision) A model of phytoplankton absorption based on three size classes Applied Optics

Conference papers

- **Brewin, R.J.W.**, Lavender, S J , Hardman-Mountford, N J , Barciela, R ,

Barker, K., Hirata, T. and Smyth, T. (2008) Examining the influence of phytoplankton functional types in CO_2 flux variability. Stage 1 PFT Intercomparision: Microplankton. Proceedings of the RSPSoc conference 2008, PDF No. 19 (CDROM), University of Exeter, UK, 15-17th September 2008.

- **Brewin, R.J.W.**, Lavender, S.J., Hardman-Mountford, N.J., Hirata, T., Raitsos, D.E. and Barciela, R. (2008). An intercomparison of bio-optical techniques for detecting phytoplankton functional types from space. Ocean Optics XIX, SPIE proceedings, PDF No. oo080577 (CDROM), Castelvecchio Pascoli, Italy, 6-10th October 2008.

- **Brewin, R.J.W.**, Lavender, S.J., Hardman-Mountford, N.J., Barciela, R. and Hirata, T. (2009) A Phytoplankton Size Class Model: Exploring Beyond the View of a Satellite. Proceedings of the RSPSoc conference 2009, PDF No. 212 (CDROM), University of Leicester, UK, 8-11th September 2009.

- Hirata, T., **Brewin, R.J.W.**, Hardman-Mountford, N.J., Smyth, T., Hirawake, T., Saitoh, S., Ishizaka, J., Toratani, M. and Murakami, H. (2010) New Challenges in Satellite Retrievals of Marine Products under Global Climate Observation Mission. Ocean Optics XX, SPIE proceedings, PDF No. 100996 (CDROM), Anchorage, Alaska, 27th September - 1st October 2010.

Newsletter Articles

- Hirata, T., **Brewin, R.J.W.** (2009). Phytoplankton community structure from space. GLOBEC International Newsletter 15 (1), 5-6.

Oral presentations

- **Brewin, R.J.W.**, Lavender, S.J., Hardman-Mountford, N.J., Hirata, T., Raitsos, D.E. and Barciela, R. (2008). An intercomparison of bio-optical techniques for detecting phytoplankton functional types from space. Ocean Optics XIX, Castelvecchio Pascoli, Italy, 6-10th October 2008 (Travel Bursary awarded from the Oceanography Society ($500)).

- **Brewin, R.J.W.**, Lavender, S.J., Hardman-Mountford, N.J., Barciela, R., Raitsos, D.E. and Hirata, T. (2009). Assessing the accuracy of remote sensing of phytoplankton functional types. ALSO Aquatic Sciences Meeting 2009: A cruise through Nice waters, Nice, France, 25-30th January 2009 (Travel Bursary awarded from AGU ($250)).

- **Brewin, R.J.W.**, Lavender, S.J., Hardman-Mountford, N.J., Barciela, R., Hirata, T. and Sathyendranath, S. (2009). A chlorophyll-a based phytoplank-

ton size class mixing model: theory and applications. Plymouth Marine Science Partnership Symposium: Marine Science for a Changing World, University of Plymouth, 7th April 2009.

- **Brewin, R.J.W.**, Lavender, S.J and Hardman-Mountford, N J (2009) Mapping size-specific phytoplankton primary production on a global scale RSPSoc Annual Student Meeting 2009, Glaramara, Lake District, 14-16th April 2009

- **Brewin, R.J.W.**, Lavender, S J , Hardman-Mountford, N J , Barciela, R , Hirata, T and Sathyendranath, S. (2009) Phytoplankton-type algorithm intercomparison and model development NCEO Ocean Carbon Cycle Meeting, Dartington Hall, Totnes, UK, 9-10th June 2009

- **Brewin, R.J.W.**, Lavender, S.J , Hardman-Mountford, N.J , Barciela, R , Hirata, T. and Sathyendranath, S (2009) Including vertical light attenuation in Earth Observation assessments of phytoplankton types NCEO Annual Science Meeting 2009, University of Oxford, UK, 8-11th September 2009

- **Brewin, R.J.W.**, Lavender, S.J., Hardman-Mountford, N.J , Barciela, R , Hirata, T and Sathyendranath, S (2009) Phytoplankton Size Class changes with depth MAREMIP workshop, University of Cambridge, UK, 28-30th October 2009

- **Brewin, R.J.W.**, Hardman-Mountford, N J , Lavender, S J and Barciela, R (2010) Deriving size-specific photosynthetic rates from globally representative *in situ* measurements Application to Earth Observation. 14th Biennial Challenger Conference for Marine Science, NOC, Southampton, UK, 6-9th September 2010

Poster presentations

- **Brewin, R.J.W.**, Lavender, S.J , Hardman-Mountford, N.J and Barciela, R (2007) Investigation of the role of phytoplankton functional types in CO_2 flux variability CASIX Annual Science Meeting, Met Office, Exeter, UK, 17-18th December 2007.

- **Brewin, R.J.W.**, Lavender, S J , Hardman-Mountford, N J and Barciela, R (2008) Investigation of the role of phytoplankton functional types in CO_2 flux variability Illuminating Ocean Ecosystems Developments in bio-optics for observing the ocean carbon cycle, Plymouth, UK, 19th February 2008.

- **Brewin, R.J.W.**, Lavender, S J., Hardman-Mountford, N J. and Barciela, R (2008) Investigation of the role of phytoplankton functional types in CO_2 flux

variability. RSPSoc Annual Student Meeting 2008, Foxlease, New Forest, UK, 10-11th March 2008.

- **Brewin, R.J.W.**, Lavender, S.J., Hardman-Mountford, N.J., Barciela, R., Hirata, T., Barker, K. and Smyth, T. (2008) Investigation of the role of phytoplankton functional types in CO_2 flux variability Stage 1 Intercomparision of PFT techniques: Microplankton. AMEMR conference 2008, University of Plymouth, Plymouth, UK, 23-26th June 2008.

- **Brewin, R.J.W.**, Lavender, S.J., Hardman-Mountford, N.J., Barciela, R., Hirata, T., Barker, K. and Smyth, T. (2008) Investigation of the role of phytoplankton functional types in CO_2 flux variability Stage 1 Intercomparision of PFT techniques: Microplankton. ESA 2008 4th Earth Observation Summer School: Earth System monitoring and modelling, ESA ESRIN Frascati, Rome, Italy, 4-14th August 2008.

- **Brewin, R.J.W.**, Lavender, S.J., Hardman-Mountford, N.J., Barciela, R., Hirata, T., Barker, K. and Smyth, T. (2008) An analysis of bio-optical techniques for detecting phytoplankton functional types from space and their potential influence in our understanding of CO_2 fluxes. 13th Biennial Challenger Conference for Marine Science, University of Bangor, UK, 8-11th September 2008.

- **Brewin, R.J.W.**, Lavender, S.J., Hardman-Mountford, N.J., Barciela, R., Barker, K., Hirata, T. and Smyth, T. (2008) Examining the influence of phytoplankton functional types in CO_2 flux variability. Stage 1 PFT Intercomparision: Microplankton. RSPSoc conference 2008, University of Exeter, UK, 15-17th September 2008.

- **Brewin, R.J.W.**, Lavender, S.J., Hardman-Mountford, N.J., Hirata, T., Raitsos, D.E. and Barciela, R. (2008). An intercomparison of bio-optical techniques for detecting phytoplankton functional types from space. Ocean Optics XIX, Castelvecchio Pascoli, Italy, 6-10th October 2008.

- **Brewin, R.J.W.**, Hardman-Mountford, N.J., Lavender, S.J., Hirata, T., Sathyendranath, S., Aiken, J., Russell, P.E. and Barciela, R. (2010) Decadal scale variability in phytoplankton functional types as seen from satellite remote sensing. AGU Ocean Sciences Meeting 2010, Oregon Convention Center, Portland, Oregon, 22-26th February 2010.

- **Brewin, R.J.W.** (2010) Decadal changes in phytoplankton size class as seen from Earth Observation. RSPSoc Annual Student Meeting 2010, Mount Batten, Plymouth, UK, 15-17th March 2010.

- **Brewin, R.J.W.**, Hardman-Mountford, N J , Lavender, S J., Hirata, T , Sathyendranath, S , Aiken, J , Russell, P.E and Barciela, R (2010) Decadal scale variability in phytoplankton functional types as seen from satellite remote sensing. Ocean 2025 Annual Science Meeting, 11-13th May 2010

Other

- Attended a GEO Workshop "Observing system requirements for managing and mitigating the impacts of human activities and coastal inundation in the Mediterranean region", Biomedical research foundation (IIBEAA), Academy of Athens, Athens, Greece, 9-13th June 2008

- Associate lecturer and associate demonstrator for the School of Earth, Ocean and Environmental Sciences and the School of Marine Science and Engineering, University of Plymouth Taught and demonstrated on Marine Remote Sensing master and undergraduate level modules (IMS5109, EOE3308 and EOE1305), October 2008 to October 2011

- Invited Lecturer in "Ocean colour data overview and examples of use": African Monitoring of Environment for Sustainable Development (AMESD) Regional training course in "Physical oceanography and Ocean Remote Sensing", Meteorological Services Mauritius, Vacoas, Mauritius, 8-20th June 2009

- Student representative for the RSPSoc society (2008-2010) This involved writing frequent articles in the RSPSoc newsletter "*Sensed*", attending RSPSoc council meetings predominately held in the Chadwick Building, University College London, and organising the 2010 RSPSoc Annual Student Meeting (Mount Batten, Plymouth, 15-17th March 2010). This meeting was a three-day event which involved organising advertisement, sponsorship (£2100 raised), conference facilities, accommodation, activities and social events.

- Invited Lecturer in "Remote Sensing of Phytoplankton Functional Types" workshop, Ocean Optics XX conference, Anchorage, Alaska, 26th September 2010 (Travel Bursary awarded from the Challenger Society (£150) and also the RSPSoc Society (£150))

Word count of main body of thesis 57,095

Signed Bob Brewin

Date 21/03/2011

Chapter 1

Introduction

1.1 Thesis introduction and motivation

Global climate change is one of the major concerns facing human society in the 21st Century (Patz et al., 2005). Since the establishment of the industrial revolution at the beginning of the 19th Century there has been a vast increase in anthropogenic emissions of carbon dioxide (CO_2) from the burning of fossil fuels and deforestation (Sabine et al., 2004). CO_2 released into the atmosphere may have three possible fates: it may be absorbed by the terrestrial ecosystem, absorbed by the ocean, or it may continue to reside in the atmosphere (Nair et al., 2008). The process of photosynthesis is partly responsible for the absorption of atmospheric CO_2. It has been estimated that the ocean absorbs approximately 26 % of anthropogenically emitted CO_2 acting as an essential component of the carbon cycle (House et al., 2002; Canadell et al., 2007; Le Quéré et al., 2009).

The majority of oceanic photosynthesisers are microscopic single or multi celled free-floating algae called phytoplankton, from the Greek word *phyton*, meaning plant, and *planktos*, meaning wandering (Jeffrey and Mantoura, 1997). They are globally distributed, consisting of tens of thousands of species, and contribute to over 25 % of the total planetary vegetation (Jeffrey and Hallegraeff, 1990). Phytoplankton use inorganic carbon to photosynthesise organic matter, which in turn is recycled in the water column or exported towards the sediments.

Phytoplankton are responsible for between 40-50 % of the total primary production on Earth (Longhurst et al., 1995; Field et al., 1998; Falkowski et al., 2004) and contribute to modulating the total CO_2 concentration and pH of the ocean, which together with physical processes (e.g. solar energy input, sea-air heat exchanges, upwelling of subsurface waters and mixed layer thickness) dictates air-sea CO_2 gas exchanges (Takahashi et al., 2002). Improving models of the flux of atmospheric carbon dioxide to the oceans depends on the accurate depiction of phytoplankton community abundance, distributions and physiology, which ultimately dictates the drawdown of CO_2. Phytoplankton, therefore, play a major role in the ocean carbon

cycle. In light of rising concern about the accelerating greenhouse effect, there is an increasing urgency to advance our understanding of the ocean carbon cycle to improve predictions of its future influence on climate

Traditionally, simple Nutrient Phytoplankton Zooplankton and Detritus (NPZD) models have been coupled to General Circulation Models (GCM) to study the ocean's carbon cycle (e g Sarmiento et al , 1993, Six and Maier-Reimer, 1996, Oschlies and Garcon, 1998, Palmer and Totterdell, 2001). Such coupled ocean-ecosystem models manifest many essential aspects of the pelagic ecosystem (Anderson, 2006) However, NPZD models categorise phytoplankton under a single group (P) when, in reality, phytoplankton groups can differ greatly in their biogeochemical functions More recently, biogeochemical models have been developed that use different phytoplankton functional types (PFTs) (e.g Taylor et al , 1993, Vanden Berg et al , 1996, Gregg et al , 2003, Blackford et al , 2004, Le Quéré et al., 2005) PFT-based models have been criticized for being both unnecessarily complex (Anderson, 2005) and for not mirroring natural complexity (e.g neglecting trophic functionality, Flynn, 2006) Such models, however, present a major development in ecosystem analysis as they have the potential to improve our understanding of how phytoplankton interact with their environment (Hood et al , 2006; Le Quéré, 2006)

In regard to primary production and the ocean carbon cycle, cell size, hereafter referred to as phytoplankton size class (PSC), has been used to classify the functional groups (Sieburth et al., 1978) The size of the phytoplankton is intimately linked with a variety of processes that influence the ocean carbon cycle (Probyn, 1985, Michaels and Silver, 1988, Chisholm, 1992, Bricaud et al , 1995, Raven, 1998, Boyd and Newton, 1999, Laws et al , 2000, Bouman et al , 2005, Platt et al , 2005, Marañón, 2009). To verify and improve PFT-based (or PSC-based) models, synoptic measurements of the different PFTs (or PSCs) are required This has typically been conducted by use of *in situ* measurements However, sampling limitations of ships and buoys which involve comparing measurements widely separated in space and time, limit their use in validating such models

Earth Observation (EO), defined as the gathering of information about planet Earth's physical, chemical and biological systems (GEO, 2010), can be used to monitor wide areas synoptically which is not possible by conventional *in situ*-based methods This has led to the development of a variety of bio-optical models that are designed for use in remote sensing to map PFTs or PSCs on global and regional scales (e g Sathyendranath et al , 2004, Alvain et al , 2005, 2008, Ciotti and Bricaud, 2006; Devred et al , 2006, Uitz et al , 2006, Raitsos et al , 2008; Hirata et al., 2008a) Platt et al (2006) describe the detection of different phytoplankton communities from satellite as a major challenge in ocean optics, which is further complicated by the sparseness of *in situ* data required to validate these algorithms.

Phytoplankton size class measurements from satellite have been incorporated

into primary production EO models, resulting in a greater understanding of the contribution of different PSCs to global ocean primary production (Claustre et al., 2005; Mouw and Yoder, 2005; Uitz et al., 2008, 2009, 2010; Silió-Calzada et al., 2008; Hirata et al., 2009b). Of particular importance to such models, is the absorption coefficient of phytoplankton which is influenced by pigment composition and size structure (Morel and Bricaud, 1981; Sathyendranath et al., 1987; Lohrenz et al., 2003; Bricaud et al., 2004). There is evidence to suggest that models of phytoplankton size structure may be used to improve the retrieval of the phytoplankton absorption coefficient (Devred et al., 2006).

In order to confidently use satellite models that estimate PSCs, as with any satellite derived geophysical or biogeochemical product, validation exercises need to be conducted to ascertain accuracy and limitations. This is especially important when a field of research, such as the detection of phytoplankton communities from satellite data, is in its early stages of development, known as the research mode (Platt et al., 2008). In such cases, validation exercises may be used to raise questions that can guide future efforts in the field.

EO models that accurately depict phytoplankton communities from satellite have enormous potential in viewing how marine ecology may be adapting in the face of our changing climate. With access to over a decade of ocean colour satellite observations, researchers have begun to investigate interannual and decadal trends in phytoplankton biomass and link such trends with climatic variability (McClain et al., 2004; Gregg et al., 2003, 2005; Antoine et al., 2005; Behrenfeld et al., 2006; Martinez et al., 2009). However, little work has been conducted on interannual trends in phytoplankton size structure and its relationship with physical forcing.

This thesis intends to take the field of detecting PSCs from satellite one step further. By applying these PSC-based satellite models to 10-years of ocean colour data and by comparing the results with *in situ* data, a better understanding of the performance of these algorithms can be gained. The results of this intercomparison could then be used to develop a new modified PSC model, with advantages over its predecessors. Furthermore, equipped with over a decade of satellite ocean colour observations, EO PSC models can be used to assess relationships between interannual climatic variability and phytoplankton size structure. Such information could be hugely beneficial for future carbon cycle studies.

1.2 Thesis aims, research questions and objectives

The primary aim of this thesis is to compare a variety of existing approaches that have been designed to detect phytoplankton size class from EO. As an outcome of this comparison, a new modified approach can be developed and applied to 10-years of satellite ocean colour observations to investigate relationships between phyto-

plankton size structure and physical forcing. Based on the aim of this thesis, the following research questions will be addressed

- How accurately can we detect phytoplankton size class from EO in the global ocean?
- What is the most robust method for detecting phytoplankton size class from EO in the global ocean?
- Can EO estimates of phytoplankton size class be used to improve estimates of phytoplankton light absorption needed for input to satellite-based primary production models?
- How is phytoplankton size structure influenced by climate variability?

In order to answer the above research questions, several objectives have been set:

- Conduct an intercomparison of the current bio-optical techniques for detecting phytoplankton size class from EO through use of a concurrent and co-located *in situ* and satellite database of phytoplankton size measurements
- Based on the results from the intercomparison, and through either merging the output of several techniques or developing a modified version, produce an improved bio-optical technique for detecting phytoplankton size class from EO
- Investigate methods for improving estimates of the phytoplankton absorption coefficient from EO by introducing phytoplankton size structure
- Implement and run the new improved bio-optical technique for detecting phytoplankton size class from EO on 10-years of satellite data to investigate seasonal cycles, interannual variability, and compare the relationship between interannual variability and climatic indices
- Draw conclusions and make suggestions for future work.

1.3 Thesis structure

This thesis adheres to the following structure: A literature review of the current state of knowledge in the context of the aims and objectives of the thesis is provided in Chapter 2 In Chapter 3, an intercomparison of bio-optical techniques for detecting dominant phytoplankton size class from EO is conducted Based on the results from Chapter 3, a new model is developed in Chapter 4, designed to calculate the fractional contributions of three phytoplankton size classes for a continuum of chlorophyll-a concentrations. In Chapter 5, the model developed in Chapter 4

is used to estimate size-fractionated phytoplankton absorption as a function of the total chlorophyll-a concentration, and in Chapter 6, the model developed in Chapter 4 is run on a decade of ocean colour observations to investigate seasonal cycles and the relationship between interannual variability and physical forcing. Chapters 3 to 6 are synthesised with existing research in Chapter 7, in addition to summarising the main findings of the thesis and outlining future work. A flow chart of the thesis methodology is given in Figure 1.1, guiding the reader through Chapters 3 to 6.

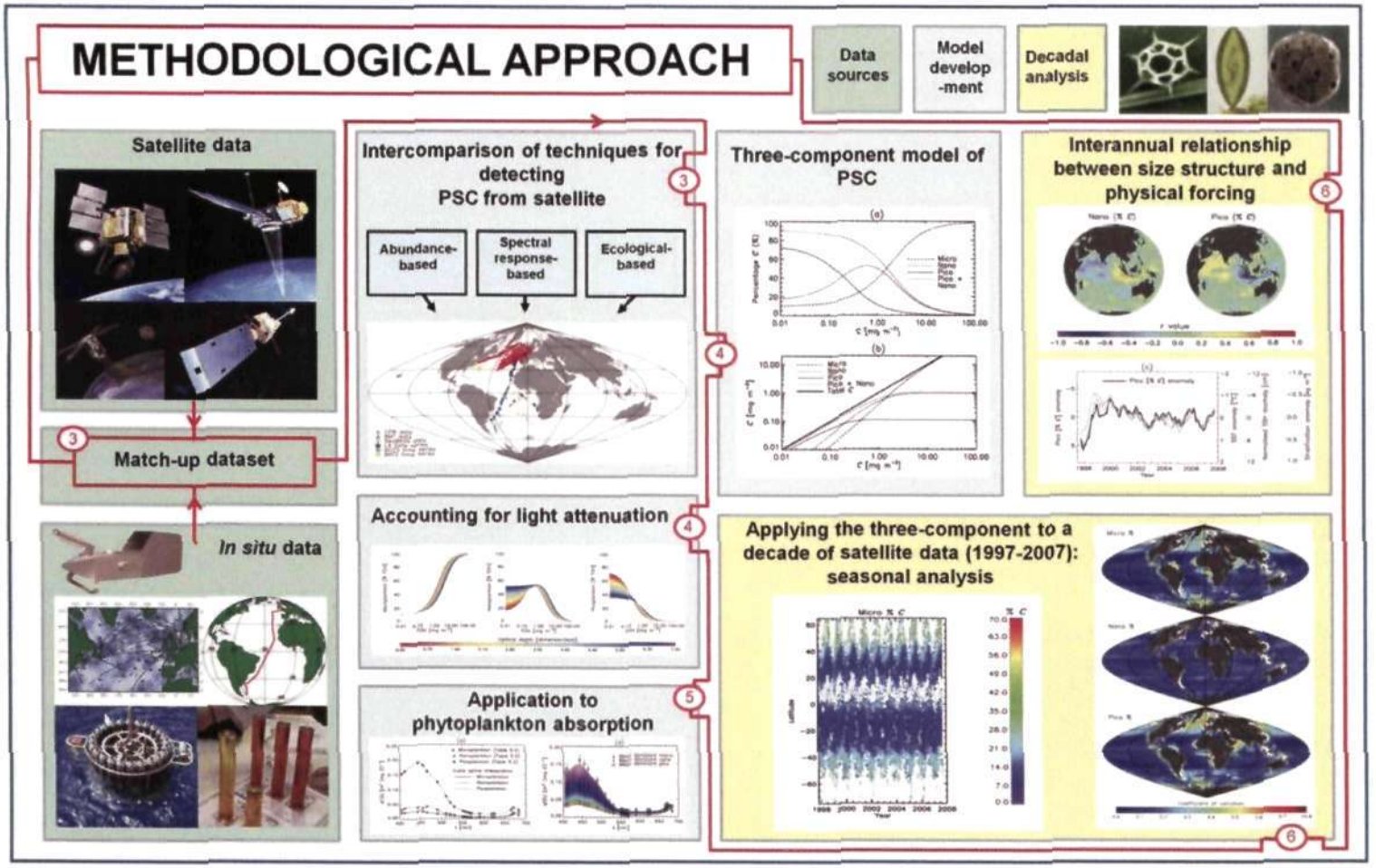

Figure 1.1: A flow chart of the thesis methodology. Chapters are shown in the red circles (3 to 6).

Chapter 2

A Review of the Current State of Knowledge

2.1 Introduction

In this chapter, a comprehensive review of the subject area is undertaken in the context of the aims and objectives of the thesis. The chapter is partitioned into four sections; the first section address the determination of phytoplankton communities *in situ*, including a description of a variety of long-term biological programmes; the second section focuses on the underlying bio-optical knowledge required for detecting phytoplankton communities from EO; the third section introduces methods for detecting phytoplankton communities from EO; and the final section assesses current research into decadal and interannual changes in phytoplankton biomass and community structure.

2.2 Phytoplankton classification

2.2.1 Phytoplankton Functional Types

Phytoplankton functional types (PFTs) refer to phytoplankton that have a specific function with regard to the scientific question being addressed (Le Quéré et al., 2005; Nair et al., 2008). In terms of primary production and the global carbon cycle, cell size, or phytoplankton size class (PSC), has previously been adopted to classify the functional groups (Sieburth et al., 1978). According to the conceptual model of Sieburth et al. (1978), the autotrophic pool is split into picoplankton ($<2\,\mu$m), nanoplankton (2-20 μm) and microplankton ($>20\,\mu$m) contributions.

While from a biogeochemical perspective the cell size functional classification may not be fully satisfactory (see Nair et al., 2008), many ecological and biogeochemical processes are related to cell size. These processes include light absorption, as influenced by the cellular pigment composition and packaging effect (Duysens, 1956;

Kirk, 1975, Morel and Bricaud, 1981, Prieur and Sathyendranath, 1981; Bricaud et al , 1995, 2004), nutrient uptake (Probyn, 1985; Sunda and Huntsman, 1997), sinking rate and export (Michaels and Silver, 1988, Boyd and Newton, 1999, Laws et al , 2000) There is also an established connection between the size and the physiology of phytoplankton (Platt and Denman, 1976, Geider et al , 1986; Chisholm, 1992; Raven, 1998), the marine food web (Parsons and Lalli, 2002), areas of high fish production (Caddy et al., 1995) and various metabolic rates (Platt and Denman, 1977, 1978) Strong links have also been established between size and environmental characteristics (availability of nutrients and light) that regulate photosynthesis, phytoplankton selection and succession (Chisholm, 1992, Bouman et al , 2005, Platt et al , 2005, Aiken et al , 2008) The phytoplankton taxonomic and functional groups are closely related to size class (Table 2 1).

This thesis concentrates on three phytoplankton functional types according to the conceptual model of Sieburth et al. (1978); picoplankton (<2 μm), nanoplankton (2-20 μm) and microplankton (>20 μm) (Note that from this point onward the terms *picoplankton*, *nanoplankton* and *microplankton refer specifically to phytoplankton*)

Table 2 1 Linkages between phytoplankton taxonomy, functional group and size class (adapted from Hirata and Brewin (2009))

Taxonomic group	Major biogeochemical function	Typical Cell Size
Diatoms	C, Si	Micro (> 20 μm)
Dinoflagellates	C, DMS	Micro (>20 μm)
Haptophytes	C, $CaCO_3$, DMS	Nano (2-20 μm)
Cyanobacteria	C, N_2	Pico (<2 μm)

Si = silica, C = carbon, DMS = dimethyl sulfide, $CaCO_3$ = calcium carbonate, N_2 = nitrogen gas fixation

2.2.1.1 Microplankton

Microplankton consist mainly of the diatoms and dinoflagellates and form the largest celled phytoplankton in the ocean Microplankton generally prosper in high-nutrient environments, have high photosynthetic rates, carbon biomass, total chlorophyll-a and export rates, and generally account for most of the phytoplankton biomass in regions where light or nutrients are not limiting (Sze, 1993, Aiken et al., 2009, Marañón, 2009) Diatoms are taxonomically partitioned into the centrics, which are radically symmetric, and the pennates, which are bilaterally symmetric (Miller, 2004) Diatoms are responsible for ~20 % of global carbon fixation (Nelson et al , 1995) and are major contributors to the biogeochemical cycling of silicon (Falciatore et al , 2000) Dinoflagellates can contribute to the production of dimethyl

sulfide (DMS) (Keller, 1988) which can effect cloud and aerosol production in the atmosphere which may alter the Earth's radiation budget (Charlson et al., 1987). Dinoflagellates have also been known to produce toxins, possibly for competition with other algal groups (Sze, 1993) and are responsible for some harmful algal blooms in coastal areas (Millie et al., 1997).

2.2.1.2 Nanoplankton

Nanoplankton are generally abundant in environments with some inorganic nutrients and additional re-cycled nutrients (organic). According to Aiken et al. (2009) and Marañón (2009), they generally have moderate photosynthetic rates, carbon biomass, total chlorophyll-a and export rates. They incorporate the nanoflagellates, which includes Prymnesiophytes, Chrysophytes and Cryptophytes. Nanoplankton include both calcifying phytoplankton such as coccolithophores, and also dimethyl sulfide producers such as *Phaeocystis*. The coccolithophore *Emiliania huxleyii* is generally considered to be abundant in a number of areas of the ocean ranging from high latitude eutrophic waters to oligotrophic areas of the ocean such as the subtropical gyres (Brown and Yoder, 1994).

2.2.1.3 Picoplankton

Picoplankton are generally abundant in low nutrient environments. According to Aiken et al. (2009) and Marañón (2009), they are associated with lower photosynthetic rates, carbon biomass, total chlorophyll-a and export rates, when compared with the larger size classes. In the open ocean, picoplankton consist mainly of the cyanobacteria (*Prochlorococcus* and *Synechococcus*) and picoeukaroytes (Zubkov et al., 2000). *Prochlorococcus* use chlorophyll-a in its di-vinyl form, as opposed to the mono-vinyl form used by all other phytoplankton groups (Partensky et al., 1999). Nitrogen-fixing phytoplankton, such as the cyanobacterium *Trichodesmium*, the dominant nitrogen-fixing organism in the oligotrophic oceans, utilise atmospheric nitrogen as a raw material for growth and thus impact the nitrogen cycle (Nair et al., 2008).

2.2.2 Identification of phytoplankton size class from *in situ* data

Phytoplankton groups can be identified from various types of *in situ* measurements with each method exhibiting limitations and advantages. Common approaches include microscopic analysis, flow cytometry, High Performance Liquid Chromatography (HPLC) analysis of marker pigments, size-fractionation and deoxyribonucleic acid (DNA) sequencing.

2.2.2.1 Microscopic analysis

Traditionally phytoplankton have been identified using a light microscope. Nair et al. (2008) highlight that microscopes (including both light and electron) are unsurpassed in the information they can provide on the type and species of phytoplankton However, the disadvantage with such techniques is that they can be time consuming (unsuitable for analysis of a large number of samples) and often rely on the taxonomic skill of the observer, using morphological characteristics to identify the phytoplankton Picoplankton can be difficult to identify to the species level due to the lack of distinct morphological characteristics (Nair et al , 2008) To overcome this, epifluoroscence microscopes and electron microscopes have been used to differentiate picoplankton from heterotrophs (e g Li et al., 1983) Once the taxonomic groups have been identified using a microscope, the plankton can be partitioned into typical size classes (as in Table 2 1)

2.2.2.2 Flow cytometry

During the 1980's there was a rapid development in the use of flow cytometry to analyse photosynthetic plankton, both in the laboratory and in the field (Chisholm et al., 1986, 1988, Burkill, 1987, Vaulot et al., 1989) Flow cytometry involves partitioning cells in liquid suspension and allowing them to individually pass though a light field. The fluorescence and scattering properties are then recorded, in addition to cell size, and used to differentiate between the different phytoplankton communities. Flow cytometry is particularly useful at identifying different types of picoplankton such as *Prochlorococcus*, *Synechococcus* and picoeukaroytes, due to their unique fluorescence and scattering signatures.

Flow cytometers are capable of making rapid measurements of cells, with typical commercial instruments making measurements at rates of up to 1000 cells per second, while specialised instruments can make measurements at rates in excess of 25,000 cells per second (Davey and Winson, 2003) This is a clear advantage of flow cytometers over microscopes The disadvantage of flow cytometers is that they generally have a limited particle size range (upper limit is typically 15-20 μm) which poses a problem when obtaining information on the larger size classes of phytoplankton. However, recent efforts have been made to enumerate and characterise microplankton and larger filamentous phytoplankton (Sieracki et al., 1998, van Dijk et al , 2010) Autonomous flow cytometers have also been developed (Olson et al , 2003; Olson and Sosik, 2007) allowing long-term flow cytometric measurements

2.2.2.3 High Performance Liquid Chromatography (HPLC) analysis of diagnostic marker pigments

Phytoplankton groups can also be separated on the basis of their marker pigments (Jeffrey and Mantoura, 1997). This is usually conducted by performing chromatographic analysis of pigments using HPLC. The total chlorophyll-a concentration (C) (which includes, chlorophyll-a, di-vinyl chlorophyll-a, chlorophyllide-a, chlorophyll-a allomers and epimers) is a ubiquitous pigment in all phytoplankton. However, other accessory pigments vary depending on the taxonomic group. Automated HPLC allows for the rapid processing of pigments to determine phytoplankton groups from *in situ* data. Various methods have been proposed to determine phytoplankton taxa and size class using HPLC data. Mackey et al. (1996) proposed a method known as CHEMTAX which is a matrix factorization program that derives the taxonomic structure of phytoplankton from pigment ratios. This has been used throughout the world's ocean to determine phytoplankton taxonomic groups (e.g. Wright et al., 1996; Wright and van den Enden, 2000; Landry et al., 2000; Muylaerta et al., 2006). HPLC analysis has the advantage to be comprehensive in terms of phytoplankton size range (Claustre, 1994) and has been used to derive phytoplankton size structure from diagnostic pigments (diagnostic pigments are defined as biomarker-pigments of specific phytoplankton taxa).

Table 2.2: Diagnostic pigments of phytoplankton and their taxonomic and size class association (adapted from Uitz et al. (2010))

Diagnostic Pigment	Taxonomic Association	Typical Cell Size
Fucoxanthin	Diatoms	Micro (>20 μm)
Peridinin	Dinoflagellates	Micro (>20 μm)
19'-Hexfucoxanthin	Prymnesiophytes	Nano (2-20 μm)
19'-Butfucoxanthin	Pelagophytes	Nano (2-20 μm)
Alloxanthin	Cryptophytes	Nano (2-20 μm)
Zeaxanthin	Cyanobacteria, Prochlorophytes	Pico (<2 μm)
Total chlorophyll b*	Chlorophytes, Prochlorophytes	Pico (<2 μm)

* Total chlorophyll b = chlorophyll b + divinyl-chlorophyll b

Vidussi et al. (2001) selected seven diagnostic pigments to obtain the fractions [F] of picoplankton (F_p), nanoplankton (F_n) and microplankton (F_m) from *in situ* HPLC pigment data (see Table 2.2). These diagnostic pigments include fucoxanthin, peridinin, 19'-hexanoyloxyfucoxanthin, 19'-butanoyloxyfucoxanthin, alloxanthin, chlorophyll-b and divinyl chlorophyll-b and zeaxanthin. Uitz et al. (2006) carried out multiple regression analyses of chlorophyll-a and the seven diagnostic pigments, to calculate the chlorophyll-a concentration from the combined sum of the

diagnostic pigments proposed by Vidussi et al. (2001) According to this approach, the chlorophyll-a concentration (C) can be reconstructed from the coefficients [W] and the pigments [P] according to

$$C_w = \sum_{i=1}^{7} W_i P_i, \tag{2.1}$$

where, [W] = {1.41, 1.41; 1.27; 0.35; 0.6, 1.01, 0.86}, [P] = {fucoxanthin; peridinin; 19'-hexanoyloxyfucoxanthin; 19'-butanoyloxyfucoxanthin, alloxanthin, chlorophyll-b and divinyl chlorophyll-b, zeaxanthin} and C_w refers to the reconstructed chlorophyll-a concentration. According to Uitz et al (2006), the fractions [F] of the chlorophyll-a concentration (C) associated with each size class can be inferred as

$$F_m = \frac{\sum_{i=1}^{2} W_i P_i}{C_w}, \tag{2.2}$$

$$F_n = \frac{\sum_{i=3}^{5} W_i P_i}{C_w}, \tag{2.3}$$

$$F_p = \frac{\sum_{i=6}^{7} W_i P_i}{C_w}, \tag{2.4}$$

where, the subscripts p, n and m refer to picoplankton, nanoplankton and microplankton respectively. Furthermore, following Devred et al. (2006), the picoplankton and nanoplankton fractions can be combined into a single class $F_{p,n}$.

$$F_{p,n} = \frac{F_p + F_n}{F_p + F_n + F_m} \tag{2.5}$$

Applying the method of Vidussi et al (2001) as modified by Uitz et al (2006), the fractions of each size class can then be applied to the *in situ* chlorophyll-a concentration (C) to derive the size-specific chlorophyll concentrations

$$C_m = F_m C, \tag{2.6}$$

$$C_{p,n} = F_{p,n} C, \tag{2.7}$$

$$C_n = F_n C, \tag{2.8}$$

$$C_p = F_p C. \tag{2.9}$$

Hirata et al (2008a) developed a slight modification to the method proposed by Vidussi et al (2001) and Uitz et al (2006), extended to account for picoeukaryotes. In the Hirata et al. (2008a) approach, the pigment total chlorophyll-b is included in the discrimination of the nanoplankton size class, as opposed to the picoplankton size class, as higher levels were found in moderate chlorophyll-a waters Furthermore, all samples with chlorophyll-a $<0.25\,\mathrm{mg\,m^{-3}}$ are defined as picoplankton

The HPLC diagnostic pigment analysis (DPA), as highlighted by Vidussi et al. (2001) and Uitz et al. (2006), does not strictly reflect the true size of phytoplankton. Diatoms, for example, have been observed in the nano-size range, whereas, in this procedure, they are only identified as microplankton. Some taxonomic pigments might be shared by various phytoplankton groups, such as fucoxanthin (the main indicator of diatoms) which may also be found in some prymnesiophytes. Despite these disadvantages, in recent years HPLC data has been extensively used as a proxy for size class (e.g. Vidussi et al., 2001; Bricaud et al., 2004, 2007; Claustre et al., 2005; Devred et al., 2006; Uitz et al., 2006, 2008, 2009; Hirata et al., 2008a; Ras et al., 2008; Aiken et al., 2008, 2009).

2.2.2.4 Size-fractionation, determining the particle size distribution and DNA sequencing

A common approach used to determine the chlorophyll-a biomass or the absorption coefficient of different size classes of phytoplankton is through filtration (Glover et al., 1988; Clarke and Leakey, 1996; Ciotti et al., 2002). This involves filtering water (normally under low pressure) though filters of different sizes (e.g. $20\,\mu$m and $2\,\mu$m). The concentration of chlorophyll-a and particulate absorption in each size fraction is then determined. Size-fractionation has advantages in that the sizes of phytoplankton are explicitly partitioned. However, there are also disadvantages. The filtrates often retain a certain portion of particles smaller than the determined pore size, which in turn depends on the filter types and the cohesive properties of the particles (Sheldon, 1972; Logan, 1993; Logan et al., 1994; Chavez et al., 1995; Knefelkamp et al., 2007; Dall'Olmo et al., 2009). The clogging of filters and the inability to accurately define the pore size of filters appears to be the main reason for the mismatch between retained particles and nominal pore sizes (Droppo, 2000).

Other techniques to estimate the size of phytoplankton include determining the particle size distribution (PSD). Common methods include the Coulter counter (Sheldon and Parsons, 1967; Sheldon et al., 1972; Milligan and Kranck, 1991), using a laser scatter particle size instrument to determine the scattering properties of the sample and associate this with a particle size distribution (Agrawal and Pottsmith, 2000; Slade and Boss, 2006; Karp-Boss et al., 2007), video (Eisma and Kalf, 1996; Manning and Dyer, 1999) or holographic imagery (Nimmo Smith, 2008; Graham and Nimmo Smith, 2010) and using acoustics (Thorne et al., 2007).

There are advantages and disadvantages to all these approaches. Coulter counters are sensitive to particle volume (Sheldon and Parsons, 1967; Milligan and Kranck, 1991), furthermore edge and shape effects can cause errors in diameter estimation of up to 14% (Boyd and Johnson, 1995). A laser scatter particle size instrument relies on inversion algorithms between particle size and scattering signatures. These inversions often use Mie theory which assumes particle sphericity

and is sensitive to deviations from sphericity (Karp-Boss et al , 2007) Digital and holographic imagery often involves a large amount of computer processing and the systems tend to be restricted to particles greater than 10 μm in size. Deriving particle size distributions from acoustic backscattering signatures is also limited to particles greater than 10-100 μm in size (Libicki et al , 1989) A further limitation of approaches that determine the particle size distribution, is difficulty differentiating between biogenic and non-biogenic particles, a limitation that is of considerable importance when applying such approaches to determine field estimates of phytoplankton size

Molecular methods use genetic variations in the phytoplankton to distinguish at taxonomic levels These include DNA sequencing and probing techniques (Fuller et al , 2006, Bouman et al , 2006, Zwirglmaier et al , 2007, 2008) Such approaches are not available for all possible phytoplankton taxonomic groups and specificity of probes remains an area of ongoing research (Nair et al , 2008)

There are positives and negatives to using any of the proposed methods for determining phytoplankton size class *in situ* This leads to the conclusion, also noted by Nair et al (2008), that the use of any one of these techniques, in isolation, may not be entirely dependable Therefore, when determining phytoplankton size class *in situ*, it would seem sensible to incorporate different types of *in situ* methods which should lead to a more accurate diagnosis. Nonetheless, HPLC analysis has the advantage to be comprehensive in terms of phytoplankton size range (Claustre, 1994) and, despite having limitations, it is the only method for which a sufficient amount of globally representative data is currently available.

2.2.3 Available *in situ* biological datasets

Long-time-period *in situ* observations are recognised as being extremely important in an era of accelerated global change (Harris, 2010) The true capabilities of EO data can be realised when used in conjunction with *in situ* measurements, for calibration and validation purposes There are a variety of decade-long *in situ* monitoring programmes that have been used for such purposes, and have the potential to be used to validate and improve available methods for detecting phytoplankton size class from EO

2.2.3.1 Continuous Plankton Recorder (CPR) survey

The longest multi-decadal plankton monitoring programme in the world is the Continuous Plankton Recorder (CPR) survey (Richardson et al., 2006) First tested to sample Krill in the Antarctic on the "Discovery" cruises of 1925-27 (Hardy, 1926), then initiated by Alister Hardy in 1931 (Hardy, 1939), the CPR has measured near-surface phyto- and zooplankton for nearly 80 years (207,619 samples were recorded by late 2004 (Richardson et al., 2006)) It is considered to be one of the largest and

most valuable biological databases in the world (Edwards, 2001). Data have been available in paper form since 1931, and from 1946 a computerised database was created. The survey has particular value since 1948, as it has been based on consistent methods of sampling and analysis (Warner and Hayes, 1994). As a result it provides unique information on the spatial and temporal distribution, annual and interannual cycle, and abundance of plankton over a large time scale, and has been used as a baseline to assess impacts of global change on marine ecosystems (Beaugrand et al., 2003, 2002; Edwards and Richardson, 2004; Raitsos et al., 2005).

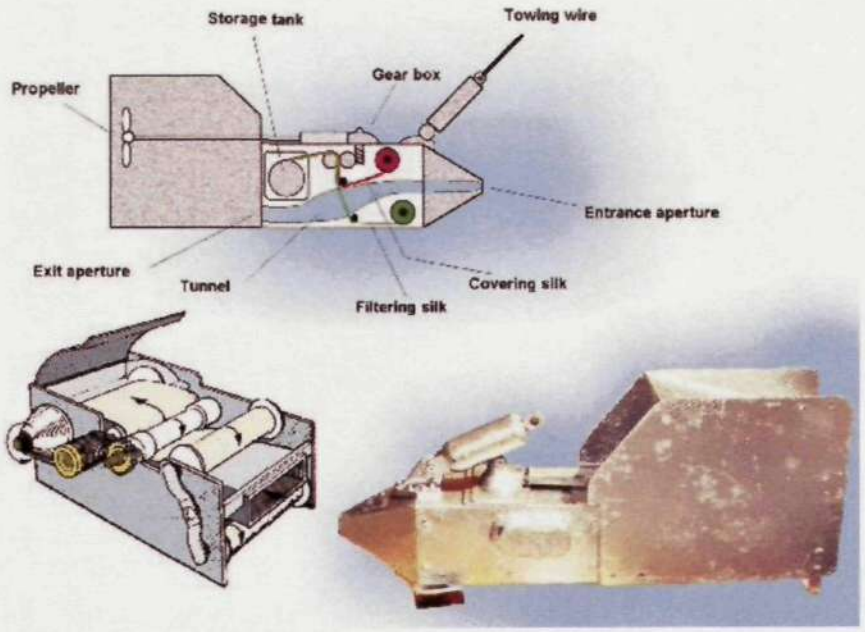

Figure 2.1: A cross-section of the CPR, its internal mechanism and CPR body, taken from Richardson et al. (2006).

Measurements of plankton abundance (cell counts) from the CPR are collected by a high-speed plankton recorder towed behind "ships-of-opportunity" in the surface layer of the ocean ~6-10 m deep. The CPR device filters plankton on a constantly moving band of mesh silk (mesh size 270 μm). As water enters the CPR body, plankton is filtered on a band of filtering silk (see Figure 2.1) and then a second band of silk (the covering silk, see Figure 2.1) sandwiches the first band of silk in order to enclose the plankton. This is then rolled into the storage chamber and the plankton is preserved in a formaldehyde solution (SAHFOS, 2010). Once the tow has finished, the CPR body is taken back to the laboratory and analysed for phytoplankton biomass, phytoplankton taxa, and zooplankton taxa (Warner and Hayes, 1994). The CPR device can operate at speeds of up to 25 knots and it is designed to operate in rough sea states with successful tows taken in wind force 11 (Beaufort scale) conditions (SAHFOS, 2010).

Each measurement represents ~18 km of tow. Post 1997, ships typically moved at 14.8 knots meaning each measurement is representative of ~32 minutes of tow,

and each sample equates to $\sim 3\,m^3$ of filtered seawater (Richardson et al., 2006). The CPR has been used extensively in the Atlantic Ocean and the North Sea since 1946. The sampling routes taken in this area from the period 1946-2005 are shown in Figure 2.2.

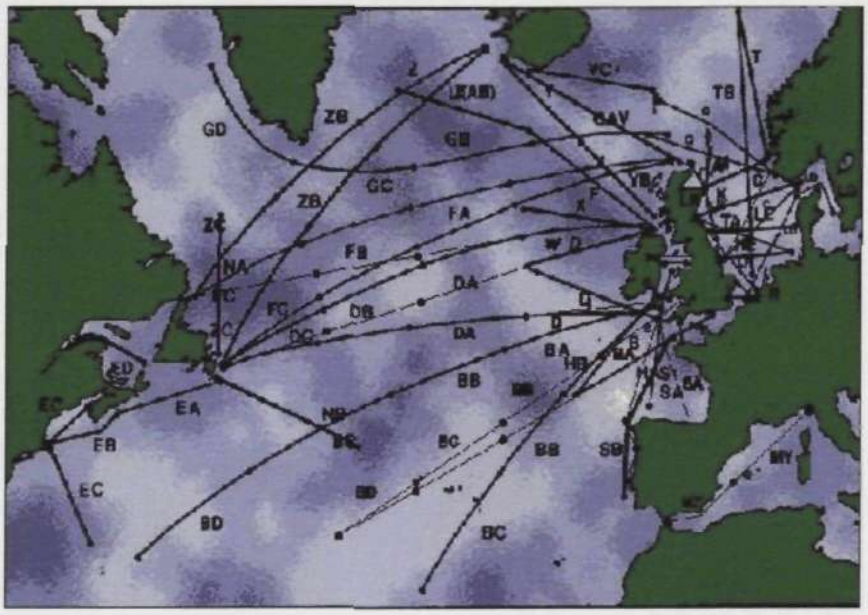

Figure 2.2: CPR sampling routes for the North Sea and Atlantic Ocean (1946-2005), taken from (SAHFOS, 2010)

In 1991 the Southern Ocean CPR (SO-CPR) Survey was established with its primary purpose to map and monitor zooplankton patterns as a means of assessing the status and health of the region (Hosie et al., 2003). Since 1997 an average of 6946 nautical miles of CPR tows have been completed per annum aboard the Australian research vessel "Aurora Australis", and since 1999 a further 3414 nautical miles per annum have been collected aboard Japanese vessels (Hunt and Hosie, 2003).

Theoretically, CPR samples are more effective at filtering microplankton and less effective at filtering nano- or picoplankton, which can slip between the silk mesh. However, species smaller than $10\,\mu m$ have been identified repeatedly in the CPR samples (Hays et al., 1995) which is thought to be a result of plankton clogging up the filter and the capture on the finer threads of silk that constitute the mesh-weave (Raitsos et al., 2006). The proportion of cells captured by the silk has been shown to reflect the major changes in abundance, distribution and community composition of large-celled ($>10\,\mu m$) phytoplankton (Robinson, 1970), and has been shown to be consistent and comparable over time (Batten et al., 2003). Furthermore, molecular analysis of the CPR samples has indicated its use for genotyping smaller phytoplankton sizes (Ripley et al., 2008) at a resolution comparable to traditional sampling techniques (D. Schroeder, pers. comm.).

Recently, the CPR dataset has been used for development and validation of satellite techniques for determining phytoplankton biomass and taxa (Raitsos et al.,

2005, 2006, 2008). Due to the nature and quantity of sampling, the CPR dataset provides is an excellent dataset to compliment satellite measurements.

2.2.3.2 The Atlantic Meridional Transects (AMT)

The Atlantic Meridional Transect (AMT) Programme is a UK National Environmental Research Council (NERC) funded project consisting of a time-series of oceanographic stations along a 13,500 km north-south transect (50°N-52°S) in the Atlantic Ocean, which moved southward in September and northward in April each year from 1995-2004 (Aiken and Bale, 2000; Aiken et al., 2000; Robinson et al., 2006), and more recently moving southward once a year (October to November). AMT began in 1995, with the aim to quantify the nature and causes of biogeochemical and ecological variability in plankton of the Atlantic Ocean, and to assess the effects of this variability on air-sea gas and aerosol exchange and biological carbon cycling (Robinson et al., 2006). It was also designed for the calibration and validation of measurements and products from the Sea-viewing Wide Field-of-view Sensor (SeaWiFS) (Hooker and McClain, 2000).

The AMT transect crosses a range of ecosystems, from the eutrophic subpolar shelf seas and upwelling systems to the oligotrophic gyres of the North and South Atlantic (Figure 2.3). The programme has so far been divided into three phases, 11 cruises were completed in phase 1 (AMT 1-11 for details see Aiken and Bale, 2000) and 6 cruises in phase 2 (AMT 2-17 for details see Robinson et al., 2006). Phase 3 is currently underway having completed 3 cruises (AMT 18-20), which will continue until 2012. Data from phases 1 and 2 are available through the British Oceanographic Data Centre (BODC).

The first two phases of the AMT programme led to several important discoveries concerning the validation of ocean colour algorithms (O'Reilly et al., 1998; Hooker and McClain, 2000; Tilstone et al., 2009), distributions of picoplankton (Zubkov et al., 1998, 2000; Heywood et al., 2006; Tarran et al., 2006) and pigments specific to phytoplankton functional types (Aiken et al., 2009), identification of oceanic provinces (Hooker et al., 2000), the identification of regional sinks of pCO_2 (Lefevre et al., 1998), and variability in rates of primary production (Marañón et al., 2000; Tilstone et al., 2009; Serret et al., 2009) and respiration (Serret et al., 2001; Robinson et al., 2002; Serret et al., 2006; Gist et al., 2009). The dataset is arguably the most coherent set of repeated biogeochemical observations ever made on ocean basin scales.

2.2.3.3 The L4 station

The L4 station was originally founded by the Marine Biological Association (MBA) over 100 years ago (Harris, 2010), and plankton and copepod studies were conducted in the early part of the 20th century (Harvey et al., 1935; Mare, 1940; Digby, 1950).

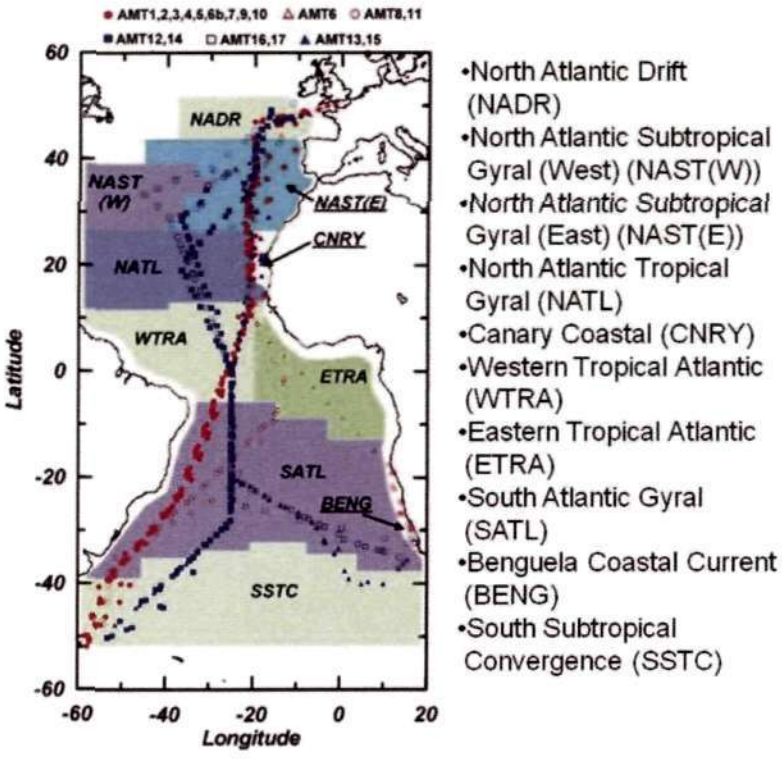

Figure 2.3: Sampling route for AMT transects 1-17, overlain on province boundaries from Longhurst (1998) (adapted from Robinson et al. (2006)).

The L4 time-series was set up by Plymouth Marine Laboratory (PML) in 1988 (10 nautical miles offshore of Plymouth, UK in the English Channel, 50°15'N, 4°13'W, see Figure 2.4) and, since 1992, phytoplankton species, abundance and biomass have been collected on a weekly basis. To mark the 20th anniversary of the L4 time-series a collection of papers were published in the *Journal of Plankton Research* (Harris, 2010), which provide an overview of the L4 station in a physical, biological and chemical context.

The planktonic community has been well studied at L4 over the past 20 years (Llewellyn and Harbour, 2003; Aiken et al., 2004; Llewellyn et al., 2005; Fishwick et al., 2006). Widdicombe et al. (2010) provide a very comprehensive analysis of long-term phytoplankton dynamics at the L4 station. They show long-term decreases in the abundance of diatoms and *Phaeocystis* and long-term increases in coccolithophorids, and some dinoflagellates and ciliates. Phytoplankton data from the L4 station have also been used for global-scale meta-analyses of biodiversity patterns in phytoplankton (Irigoien et al., 2004) and to better understand the spring bloom composition in the English Channel (Irigoien et al., 2005). A recent study by Groom et al. (2009) highlights the optical complexity of the L4 station and conclude that L4 can be considered as case 1 or case 2 (see section 2.3.5 for definition of case 1 and 2 waters) depending on the time period, the optical parameter or even the

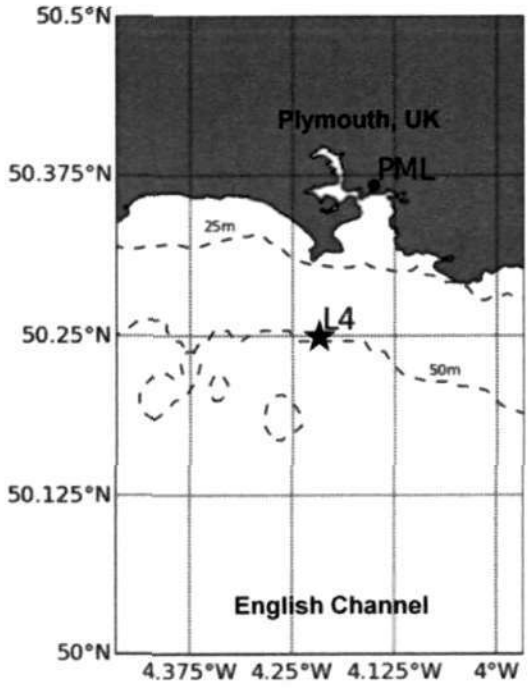

Figure 2.4: The location of station L4 with the bathymetry overlaid (adapted from Litt et al. (2010)).

wavelength in question.

The Western Channel Observatory was set up in 2005 (Harris, 2010), with the aim to draw together long-term *in situ* measurements made at stations L4 and E1 (1903 to the present date), ecosystem modelling studies and EO. Data on phytoplankton cell counts using microscopic analysis is available from the L4 station through the Western Channel Observatory from 1992-2009 (http://www.westernchannelobservatory.org.uk/). Furthermore, the NERC Earth Observation Data Acquisition and Analysis Service (NEODAAS) provide near real time EO data at the L4 site, making the L4 station an ideal site for combining satellite and *in situ* measurements.

2.2.3.4 The Bermuda Atlantic Time-series Study (BATS) and the Hawaii Ocean Time-Series (HOTS)

In 1988, supported by the U.S. National Science Foundation (NSF), as a goal of the US JGOFS time-series research, two ocean time-series stations were set up (Karl and Lukas, 1996). The Bermuda Atlantic Time-series Study (BATS) was established in the North Atlantic Ocean (Michaels and Knap, 1996) and the Hawaii Ocean Time-Series (HOTS) was set up in the subtropical North Pacific Ocean near Hawaii (Karl and Lukas, 1996) (see Figure 2.5). These two stations are operated by the Bermuda Biological Station for Research and the University of Hawaii, respectively.

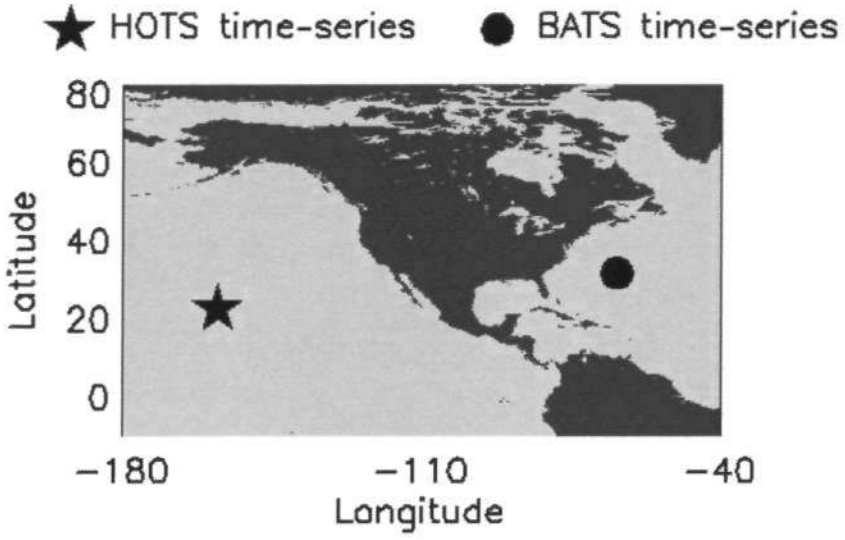

Figure 2.5: The location of the BATS and HOTS stations.

The aim of setting up the BATS and HOTS time-series was to improve our understanding of the processes that control ocean biogeochemistry on both seasonal to decadal timescales (SCOR, 1987). BATS is a long-term time-series study examining biogeochemical cycles in the Sargasso Sea near Bermuda. Monthly measurements are taken of important hydrographic, biological and chemical parameters. Biological measurements taken from BATS include HPLC pigments and fluormetric chlorophyll-a measurements (of which some are available online http://bats.bios.edu/data). The site has been monitored extensively over the past few decades and been at the base of many important discoveries (see Steinberg et al., 2001) including long-term changes in plankton community structure (Karl et al., 2001; DuRand et al., 2001), primary production (Ondrusek et al., 2001; Siegel et al., 2001; Saba et al., 2010), ocean colour (McGillicuddy et al., 2001) and biogeochemical model development (Doney et al., 1996; Hurtt and Armstrong, 1996; Hood et al., 2001).

The primary objective of HOTS was to design, establish and maintain a deep-water hydro-station in the North Pacific oligotrophic gyre, which could be used for observing and interpreting physical and biogeochemical variability (Karl and Lukas, 1996). Repeat measurements of a suite of physical, biological and chemical parameters are taken at monthly intervals and made available online for use by the scientific community (http://hahana.soest.hawaii.edu/hot/). Like BATS, the HOTS time-series has been extensively used in ocean biogeochemistry research and for comparison with EO data (e.g. Campbell et al., 1994; Mitchum, 1996; Lawson et al., 1996; Saba et al., 2010).

2.2.3.5 The National Aeronautics and Space Administration (NASA) biological and bio-optical *in situ* datasets

The NASA Ocean Biology Processing Group (OBPG) maintains *in situ* oceanographic and atmospheric data to support scientific work. When the SeaWiFS sensor was developed, NASA initiated the SeaWiFS Bio-optical Archive and Storage System (SeaBASS), which was designed to catalogue radiometric and phytoplankton pigment data that could be used for calibration and validation activities (Werdell and Bailey, 2002). The database includes measurements of phytoplankton pigment concentrations, apparent and inherent optical properties and other related oceanographic data, such as water temperature and salinity (SeaBASS, 2010), and is freely available online (http://seabass.gsfc.nasa.gov/). The SeaBASS dataset has been extensively used for satellite validation and vicarious calibration, in addition to bio-optical algorithm development (O'Reilly et al., 1998, 2000; Hooker et al., 2000; Maritorena et al., 2002; Schwarz et al., 2002)

Recently NASA developed a subset of the SeaBASS dataset specifically for bio-optical research. The NASA bio-Optical Marine Algorithm Dataset (NOMAD) is a global, high-quality, *in situ*, bio-optical dataset publicly available for algorithm development and validation activities (Bailey and Werdell, 2006; Werdell and Bailey, 2005). NOMAD has been used extensively in the development of bio-optical models, in particular the development and validation of satellite models designed to map PFTs (e.g. Alvain et al., 2006, 2008; Hirata et al., 2008a).

From analysing methods for identifying phytoplankton size class from *in situ* data, and assessing available long-term datasets, it becomes apparent that a wide variety of *in situ* data has been gathered over the past decade on phytoplankton community structure. This data could potentially be used to help scrutinise, validate and improve available methods for detecting phytoplankton size class from EO.

2.3 Light in the aquatic environment

2.3.1 The colour of the ocean

Ocean colour has long been used by scientists to help understand oceanography. For instance, in the 19th and early 20th centuries oceanographers used ocean colour as an indicator of water masses and, indirectly, ocean currents (Robinson, 2004). This was conducted through qualitative methods such as the Forel Scale (Fairbridge, 1966), used to determine the colour of seawater, and the Secchi disk used to quantify the transparency of seawater (Secchi, 1866). Through pioneering developments of the 20th century (Jerlov, 1968, 1976; Preisendorfer, 1976), this principle has since resulted in the discipline of optical oceanography or ocean optics which has extensively been used for a variety of topics from photochemistry to marine pollution

(Robinson, 2004).

2.3.2 The Electromagnetic Spectrum

In order to obtain data from an object through remote sensing it is necessary to measure some parameter that relates directly to the particular scene. This is usually done through measuring the absorption, reflectance, and scattering of electromagnetic radiation. Electromagnetic radiation is made up of a continuum of wavelengths ranging from very short (gamma rays, typically 0.1 nanometres) to very long (radio waves, typically in the order of meters).

Assuming that the speed of light (c) remains constant in a given medium, electromagnetic radiation varies in wavelength (λ) which is inversely related to frequency (v). This can be expressed according to

$$\lambda = \frac{c}{v}. \tag{2.10}$$

The speed of light (c) is $3 \times 10^8\,\mathrm{m\,s^{-1}}$ and the units of wavelength are typically nanometres (nm) (for visible light) and the units of frequency are typically Hertz (Hz) or inverse seconds ($\mathrm{s^{-1}}$).

The sun emits all forms of radiation within the electromagnetic spectrum (EM). The Earth's atmosphere protects the planet by filtering out harmful radiation, thus making the planet fit for habitation. Atmospheric windows (parts of the EM where the atmosphere has a small influence on the transmission of light) dictate which wavebands are available for oceanography.

Between approximately 400-700 nm, referred to as the visible portion of the EM (see Figure 2.6), the atmosphere is particularly transparent to light. In fact, the visible portion of the EM accounts for approximately 45 % of total solar energy (Kirk, 1994). Evolution has resulted in many organisms utilising the visible proportion of the EM whether for sight, as with the case or humans, or for energy, as in the case of photosynthetic organisms (Falkowski and Raven, 1997).

2.3.3 Apparent optical properties and inherent optical properties

Preisendorfer (1961) defines inherent optical properties and apparent optical properties of the water, according to their invariance properties under changes in the radiance distribution about the point at which the property is measured. According to Preisendorfer (1961), if the property is invariant with respect to changes in the radiance distribution, it is said to be an inherent optical property, otherwise it is an apparent optical property (Gordon et al., 1975).

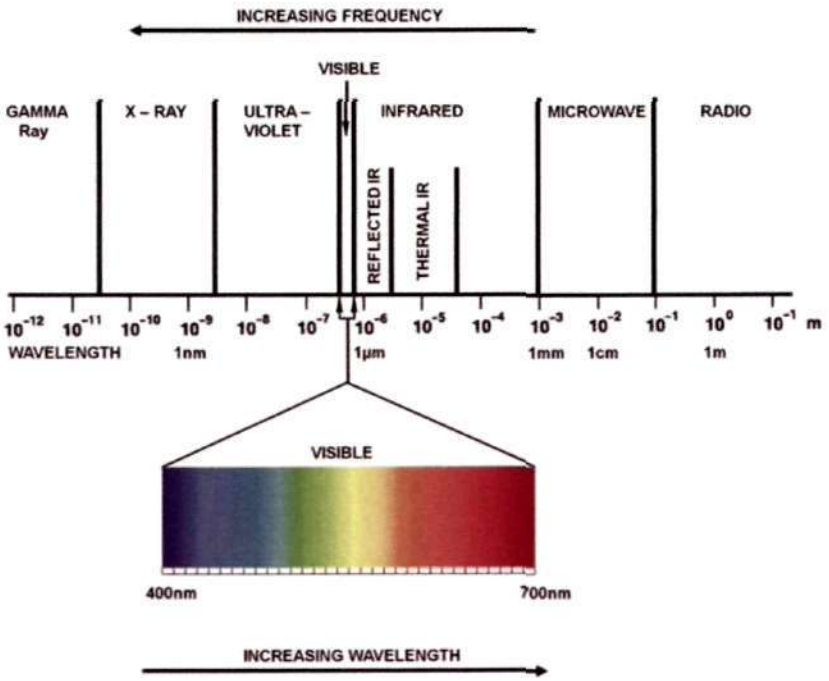

Figure 2.6: The Electromagnetic Spectrum (adapted from Sabins (1987)).

2.3.3.1 Apparent optical properties (AOPs)

Apparent optical properties (AOPs) are optical properties that are influenced by, in addition to the nature and quantity of substances present in the medium, the angular distribution of the light field. They typically encompass the normalised water leaving radiance ($L_{wn}(\lambda)$), the remote sensing reflectance ($R_{rs}(\lambda)$) and the downwelling diffuse attenuation coefficient ($K(\lambda)$). Note that all optical properties of oceanic waters are wavelength (λ) dependent (Kirk, 1994).

Radiance ($L(\lambda)$) is the measure of light energy leaving an extended source (Robinson, 2004). Water leaving radiance ($L_w(\lambda)$) is, therefore, the measure of *light energy leaving the water*. As $L_w(\lambda)$ *depends on both the viewing and sun* geometry, remote sensing scientists have sought to normalise this radiance to a single sun-viewing geometry, forming the normalized water leaving radiance ($L_{wn}(\lambda)$) (Gordon, 2005). Normalized water leaving radiance is the radiance that would be measured leaving the flat surface of the ocean, with the atmosphere absent and the sun directly overhead (i.e. at zenith).

Reflectance is a measure of how much of the downwelling light ($E_d(\lambda)$) is reflected back up from the water below (Robinson, 2004). For the remote sensing reflectance ($R_{rs}(\lambda)$), it is common to use the ratio of the upward normalized water leaving radiance ($L_{wn}(\lambda)$) and the downwelling irradiance ($E_d(\lambda)$) such that

$$R_{rs}(\lambda) = \frac{L_{wn}(\lambda)}{E_d(\lambda)}. \tag{2.11}$$

The downwelling diffuse attenuation coefficient ($K(\lambda)$), dictates the amount of downwelling irradiance ($E_d(\lambda)$) that is lost due to absorption or scattering as it travels through the water column. It can be expressed according to

$$K(\lambda) = -E_d^{-1}(\lambda, z)\frac{dE_d(\lambda)}{dz}, \tag{2.12}$$

where z is depth in metres. The normalised water leaving radiance ($L_{wn}(\lambda)$), the remote sensing reflectance ($R_{rs}(\lambda)$) and the downwelling diffuse attenuation coefficient ($K(\lambda)$), are frequently used in ocean colour research to detect water constituents and for determining inherent optical properties.

2.3.3.2 Inherent optical properties (IOPs)

Inherent optical properties (IOPs) depend only on the substances comprising the aquatic medium and not on the geometric structure of the aquatic light field (Preisendorfer, 1961; Robinson, 2004). This typically relates to how the water constituents present in the medium, absorb and scatter light. These comprise the absorption coefficient ($a_t(\lambda)$), the beam attenuation coefficient ($q(\lambda)$) and the volume scattering function ($\chi(\lambda)$), where the integration of χ over all directions leads to the scattering coefficient (b_t) (Robinson, 2004). Further integration over the forward and backward hemispheres defines the forward and backward scattering coefficients (b_t^f and b_t^b respectively). As stated by Robinson (2004), χ and either $q(\lambda)$ or $a_t(\lambda)$ define completely the optical properties of the water since $b_t = b_t^f + b_t^b$ and $q = a_t + b_t$. Note that, as stated by Kirk (1994), the beam attenuation coefficient (q) is the fraction of the incident flux which is absorbed and scattered, divided by the thickness of the layer.

The inherent optical properties can be further divided according to the different water constituents influencing them. These typically include seawater itself, phytoplankton, suspended particulate matter (SPM) and coloured dissolved organic matter (CDOM). Such that the absorption and scattering coefficients can be expressed according to

$$a_t(\lambda) = a_w + a_{SPM} + a_{CDOM} + a, \tag{2.13}$$

$$b_t(\lambda) = b_w + b_{SPM} + b, \tag{2.14}$$

where, a_w and b_w is absorption and scattering by water, a_{SPM} and b_{SPM} absorption and scattering by suspended particulate matter, a_{CDOM} absorption by coloured dissolved organic matter and a and b are absorption and scattering by phytoplankton. Note that there is no scattering by coloured dissolved organic matter. All these coefficients are bulk inherent optical properties, whereby each constituent in the water column is considered as a composite entity with no regard as to specific component

contributions. Equations 2.13 and 2.14 can be further partitioned according to their specific inherent optical properties, which are attributed to the individual scattering and absorption components, such that

$$a_t(\lambda) = a_w + a^*_{SPM}x_{SPM} + a^*_{CDOM}x_{CDOM} + a^*x_{PHY}, \tag{2.15}$$

$$b_t(\lambda) = b_w + b^*_{SPM}x_{SPM} + b^*_{CDOM}x_{CDOM} + b^*x_{PHY}, \tag{2.16}$$

where x refers to the concentration of a particular constituent (e.g. SPM, CDOM or phytoplankton (PHY)), and the absorption and backscattering coefficients superscripted by an asterisk indicate the absorption and scattering components of each constituent per unit concentration. For phytoplankton, x_{PHY} is often replaced by the chlorophyll-a concentration (C).

From an EO perspective, the bulk backscattering coefficient (b^b_t) from the ocean may be attributed mainly to bubbles, submicron particles and viruses (Stramski and Kiefer, 1991; Zhang et al., 1998), and some larger particles. Phytoplankton groups such as Coccolithophores and *Trichodesmium* can have a particularly strong influence on backscattering of light (Balch et al., 1996; Subramaniam et al., 2002). Absorption, however, has been found to be the main optical property that can be used to identify phytoplankton (Ciotti et al., 2002), as phytoplankton absorb light for photosynthesis. However, recent evidence does suggest the influence of phytoplankton on the backscattering signal may be higher than first thought (see section 2.4.4 for further discussion).

2.3.3.3 Deriving IOPs from AOPs

Satellite sensors cannot measure IOPs of the sea directly, instead they measure AOPs. In order to determine IOPs they must be estimated from AOPs. In order to estimate IOPs from AOPs, assumptions must be made about the directionality of the underwater light field. Radiative transfer equations have been shown to precisely define the incident light field (Preisendorfer, 1961), providing the IOPs and the directionality of the incoming light field are known (Robinson, 2004). However, as these are integral equations they do not permit an easy solution. This has resulted in the development of a variety of numerical and analytical techniques involving approximations in order to produce a solution (Robinson, 2004). Empirical, semi-empirical and analytical techniques have arisen that directly estimate IOPs from AOPs using satellite data (see Garver and Siegel, 1997; Maritorena et al., 2002; Lee et al., 2002; Smyth et al., 2005).

The $R_{rs}(\lambda)$ can be described from the IOPs according to

$$R_{rs}(\lambda) = g\frac{b^b_t(\lambda)}{a_t(\lambda)}, \tag{2.17}$$

as $R_{rs}(\lambda)$ is proportional to $b_t^b(\lambda)$ and inversely proportional to $a_t(\lambda)$ The proportionality factor (g) describes the directional effect at the air-surface interface and forms the basis of IOP modelling (Morel and Gentili, 1993, 1996) In cases where $b_t^b(\lambda)$ is greater than $a_t(\lambda)$ (such as coastal waters with high levels of inorganic particles such as SPM), Gordon et al (1975) suggests that the relationship may be better represented as

$$R_{rs}(\lambda) = g\frac{b_t^b(\lambda)}{a_t(\lambda) + b_t^b(\lambda)}. \quad (2\ 18)$$

2.3.4 Ocean colour sensors

Satellite data of ocean colour first became available in 1978 with the launch of the Coastal Zone Color Scanner (CZCS) instrument onboard the Nimbus-7 satellite (Mitchell, 1994) As part of the Nimbus programme (1964-1972), Nimbus 7 was launched into a 995 km near polar sun-synchronous orbit in 1972 (Gibson et al., 2000). The CZCS obtained reflected radiation in five bands in the 433-800 nm range and had a spatial resolution of 825 m for a 1,556 km wide swath (Gibson et al , 2000) The CZCS saw the beginning of a revolution in ocean colour research, because for the first time biological oceanographers were able to assess synoptic satellite observations over huge geographic areas which was not previously possible with measurement techniques such as buoys, aircraft or research ships

The German Modular Optical Scanner (MOS) was launched in March 1996 on the Indian remote sensing satellite IRS-P3 (Martin, 2004), 28 years after the CZCS became operational It was the first satellite to fly into space with a purely ocean colour measurement role The next marine sensor to be launched was the Japanese Ocean Color and Temperature Sensor (OCTS) onboard the ADEOS-1 satellite (Kawamura and OCTS Team, 1998) This operated from August 1996 to June 1997, in the 412-866 nm range, having a spatial resolution of 700 m (Kawamura and OCTS Team, 1998)

The Sea-viewing Wide Field-of-view Sensor (SeaWiFS) was launched on the ORBVIEW-2 satellite in August 1997 (Robinson, 2004), and has been operating between the 412-865 nm range since September 1997 to the present day (with the exception of a few periods of time when it has not collected data, e.g February-March 2008), providing daily global imagery at a spatial resolution of 1 km and 9 km for over 12 years. A major aim of the SeaWiFS sensor is to examine oceanic factors that affect global change, particularly the role of phytoplankton in the biogeochemical cycle (Hooker et al., 1992) The SeaWiFS sensor is still in operation providing the longest ocean colour dataset on record, and at the time of writing it is the most extensively used satellite dataset for biological oceanography (McClain et al , 1998; McClain, 2009).

The Moderate Resolution Imaging Spectrometer (MODIS) was launched on the TERRA satellite in December 1999 and on AQUA satellite in May 2002 (Martin,

2004). MODIS was NASA's third ocean colour sensor to be sent into space following SeaWiFS and CZCS. Like SeaWiFS, it caters for both ocean colour and atmosphere products, and it continuously supplies daytime data which is supported by a rapid-processing ground segment. The sensors have a spatial resolution of 250 m in the UV band, 500 m in the visible waveband in the red, and 1 km in the ocean colour wavebands (Robinson, 2004). In March 2002 the European Space Agency (ESA) launched its first ocean colour sensor the Medium Resolution Imaging Spectrometer (MERIS), onboard the ENVISAT platform (Rast and Bezy, 1999). Its primary goal was to monitor ocean colour. However, it was also designed to determine atmospheric and land surface information. MERIS has five parallel arrays to gain a swath width of 1150 m, offering ocean colour and geophysical products at a resolution of 1200 m with a capability of 300 m (Robinson, 2004). It is in a descending sun-synchronous orbit with 15 observing bands between 400 and 900 nm (Martin, 2004).

There are a number of ocean colour satellites to be launched in the coming years, including the Visible Infrared Imaging Spectro-Radiometer Suite (VIIRS), set to be launched by NASA under the National Polar-orbiting Operational Environment Satellite System (NPOESS) Preparatory Project Mission, and the Sentinal-3 satellites as part of the European Union-ESA Global Monitoring for Environment and Security (GMES) programme. Recently, research has also focused on merging satellite ocean colour observations, including the GlobColour project (GlobColour, 2010) and the NASA SIMBIOS Program (McClain et al., 2002; Maritorena and Siegel, 2005). The benefits of data merging include the development of unified, consistent ocean colour time-series from multiple sensors, improved spatial and temporal coverage, and a more diverse ocean colour product with lower uncertainties (Maritorena and Siegel, 2005). However, there are disadvantages. As sensors are not identical, there are differences in design, calibration, algorithms and accuracies, which make merging particularly difficult.

As the majority of PFT satellite algorithms have been developed using the SeaWiFS sensor, and as it is the only sensor with over a decade of satellite ocean colour observations, this thesis uses the SeaWiFS dataset for ocean colour observations. In addition to ocean colour, physical parameters such as sea surface temperature (SST), wind stress data and sea-surface height (SSH), can also be observed from satellite. Sea surface temperature is typically recorded using NASA's Advanced Very High Resolution Radiometer (AVHRR), in the thermal wavebands of the EM (although it can also be determined in the microwave waveband, e.g. NASA's Advanced Microwave Scanning Radiometer (AMSR)). Windstress can be derived using scatterometers, such as the European Remote-Sensing Satellites (ERS-2) and NASA's QuikSCAT sensor (QS), and sea-surface height is usually derived using altimetry, such as from NASA's TOPEX/Poseidon satellite mission which determines ocean surface topography. Additional physical data from these satellite missions

can compliment the ocean colour observations (Raitsos et al , 2006, 2008) and are therefore also utilised throughout this thesis

2.3.5 Optical classification of water types

Ocean waters can be partitioned into two classifications based on their optical properties, referred to as case 1 and case 2 waters According to Morel and Prieur (1977), case 1 waters are waters whose variations in optical properties are mainly driven by the abundance of phytoplankton. In case 2 waters, the optical properties are influenced, in addition to phytoplankton, by variable concentrations of CDOM and SPM. Case 1 waters are typically in the open ocean and case 2 waters are typically in coastal areas which are heavily influenced by the terrestrial environment (e g riverine runoff)

2.3.5.1 Chlorophyll-a detection

The phytoplankton pigment total chlorophyll-a (C) absorbs light in the blue and red proportions of the visible spectrum and reflects light at green wavelengths. As the chlorophyll-a concentration increases, light is absorbed more strongly in the blue and red proportions and reflects more strongly in the green Therefore, as chlorophyll-a increases, the reflectance in the blue regions decreases and in the green it increases slightly. Thus a ratio of blue to green water reflectance can be used to derive quantitative estimates of the satellite-derived chlorophyll-a concentration (C^s)

Following the launch of the CZCS onboard the Nimbus-7 satellite, which had spectral bands in the blue and green regions of the visible spectrum, "blue-green" band ratio algorithms were used to estimate the chlorophyll-a concentration from EO (see Gordon et al , 1983) Targeted toward the launch of SeaWiFS, NASA set-up the SeaWiFS Bio-optical Algorithm Mini-workshop (SeaBAM, O'Reilly et al , 1998), designed to identify chlorophyll-a algorithms suitable for operational use by SeaWiFS. A database was developed with simultaneous measurements of *in situ* chlorophyll-a (derived from HPLC data) and *in situ* $R_{rs}(\lambda)$ Based on the results from the workshop, empirical "blue-green" band ratio algorithms were adopted The Ocean Chlorophyll 2 (OC2) algorithm performed with the highest accuracy in the SeaBAM and was chosen as the SeaWiFS operational algorithm It is based on a modified cubic polynomial function which uses $R_{rs}(490)/R_{rs}(555)$ This was later updated to the Ocean Chlorophyll 4 (OC4) algorithm (O'Reilly et al , 1998, 2000), expressed as

$$C^s = 10^{(0\,366-3\,037x+1\,930x^2+0\,649x^3-1\,532x^4)}, \tag{2 19}$$

where

$$x = \log_{10}(R_{rs}443 > R_{rs}490 > R_{rs}510/R_{rs}555) \tag{2.20}$$

Caution must be taken when using band ratio algorithms to derive the chlorophyll-a

concentration as they will only function in waters whose variations in optical properties are mainly driven by the abundance of phytoplankton, i.e. case 1 waters. In more optically complex waters (case 2 waters), where $R_{rs}(\lambda)$ is more heavily influenced by CDOM and SPM, band ratio algorithms are likely to break down. Various authors have attempted to used semi-analytical models to derive the chlorophyll-a concentration in more optically complex waters (e.g. Maritorena et al., 2002). Nonetheless, band ratio algorithms are still the preferred choice for deriving chlorophyll-a using the SeaWiFS sensor.

2.3.6 The absorption coefficient of phytoplankton

The absorption coefficient of phytoplankton ($a(\lambda)$) is a fundamental quantity in marine primary production models because (i) it alters the transmission of light underwater (Morel, 1978, 1988; Sathyendranath and Platt, 1988); (ii) it modifies the photosynthetic response of phytoplankton to available light (Platt and Jassby, 1976; Kiefer and Mitchell, 1983; Platt and Sathyendranath, 1988); (iii) it can be used as a direct indicator of phytoplankton abundance (Smyth et al., 2006; Marra et al., 2007) and phytoplankton size (Ciotti et al., 2002; Devred et al., 2006; Hirata et al., 2008a); and (iv) it can be used as an indicator of environmental variability (Marra et al., 2007; Hirata et al., 2009b).

Several regional and global studies to assess the phytoplankton absorption coefficient have been undertaken in the past few decades (e.g. Prieur and Sathyendranath, 1981; Sathyendranath and Platt, 1988; Cleveland, 1995; Lutz et al., 1996; Bricaud et al., 2004) and it is well established that the phytoplankton absorption coefficient is controlled by changes in both pigment composition and size structure (Morel and Bricaud, 1981; Sathyendranath et al., 1987; Lohrenz et al., 2003; Bricaud et al., 2004). Figure 2.7 shows how different (weight-specific) phytoplankton pigments can have contrasting absorption features. Despite these variations, the influence of both pigment composition and size structure on the phytoplankton absorption coefficient can be linked with the trophic status of the water (as indexed by the chlorophyll-a concentration), and it is generally admitted that from oligotrophic to eutrophic waters there is an increase in phytoplankton cell size and a decrease in the relative concentration of accessory pigments (Malone, 1980; Yentsch and Phinney, 1989; Chisholm, 1992; Bricaud et al., 1995, 2004). Therefore, the phytoplankton absorption coefficient can be estimated directly as a function of the dominant phytoplankton pigment, chlorophyll-a.

Power-law or polynomial expressions have proven useful predictors of the phytoplankton absorption coefficient as a function of the chlorophyll-a concentration (e.g. Prieur and Sathyendranath, 1981; Morel, 1991; Cleveland, 1995; Bricaud et al., 1995, 1998, 2004). Alternatively, models have been proposed based on Michaelis-Menten-type equations (e.g. Sathyendranath and Platt, 1988; Lutz et al., 1996). However,

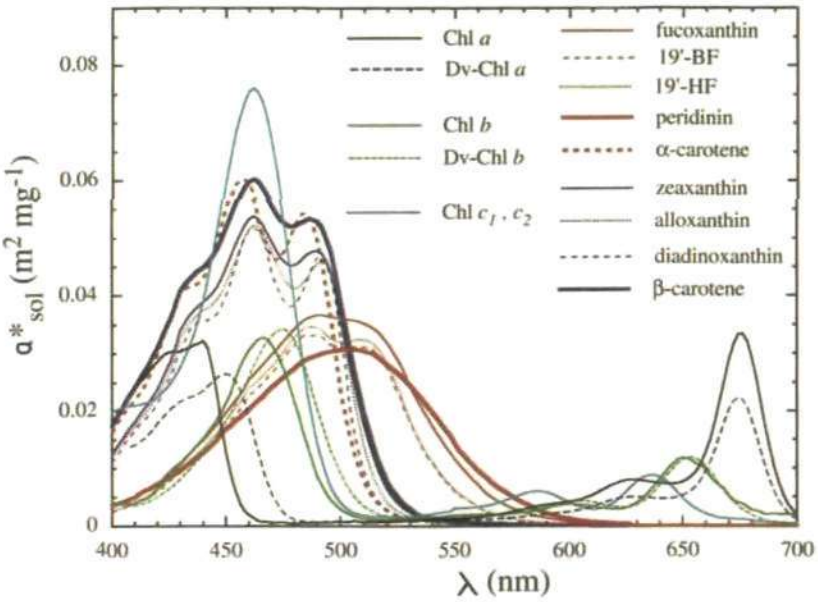

Figure 2.7: The assumed *in vivo* weight-specific absorption spectra of the main pigments, $a^*_{sol}(\lambda)$ (in m^2 mg^{-1}), as derived from absorption spectra of individual pigments in solvent (taken from Bricaud et al. (2004)). Bricaud et al. (2004) calculated $a^*_{sol}(\lambda)$ of the individual pigments by scaling the absorption spectra of individual pigments in solvent (measured in relative values by HPLC), to the weight-specific absorption coefficients proposed by Goericke and Repeta (1993), and then shifting the positions of maxima to their *in vivo* positions, as in the work of Bidigare et al. (1990).

such approaches have limitations at extreme values of chlorophyll-a concentrations and the interpretation of the model parameters is difficult (Lutz et al., 1996; Devred et al., 2006).

Recently, total phytoplankton absorption has been expressed as the contribution of two populations of optically-distinct phytoplankton (e.g. Sathyendranath et al., 2001; Ciotti et al., 2002; Devred et al., 2006). Such approaches ensure realistic values of the specific absorption coefficient of phytoplankton (absorption per unit chlorophyll-a, $a^*(\lambda)$) when applying the model to extreme values of chlorophyll-a concentration, since the range of values of $a^*(\lambda)$ is bounded by the two values associated with the two populations. Furthermore, the parameters of the model have bio-optical interpretation.

Devred et al. (2006) extended the Sathyendranath et al. (2001) model to derive $a^*(\lambda)$ for the two optically-distinct phytoplankton populations. Assuming that $a^*(440)$ of large-celled populations of phytoplankton would be smaller than 0.05 (m^2 $[mg\ C]^{-1}$), Devred et al. (2006) related the large-celled population to microplankton and the small-celled population to combined nano-picoplankton that constitute the remaining autotrophic pool. Brewin et al. (2010c) identified problems in using the two-component model of Sathyendranath et al. (2001), in that it failed to reproduce

the spectral shape of the absorption coefficient at low chlorophyll-a concentrations.

It is well documented that small phytoplankton have a higher specific absorption coefficient and a steeper spectral shape than large phytoplankton (Duysens, 1956; Morel and Bricaud, 1981; Sathyendranath et al., 1987; Ciotti et al., 2002; Uitz et al., 2008). Uitz et al. (2008) calculated $a^*(\lambda)$ of micro-, nano- and picoplankton. In their model, the proportions of the three size classes in the autotrophic pool are determined according to a small number of class intervals in chlorophyll-a concentrations (Uitz et al., 2006), which may introduce unrealistic spatial discontinuities when satellite data are used to map the distribution of these size classes. Nonetheless, the Uitz et al. (2008) model does reproduce the expected spectral shape of the absorption coefficient at low chlorophyll-a concentrations when compared with other laboratory and field studies (see Uitz et al., 2008).

By combining the approach of Uitz et al. (2006), that uses HPLC data to help identify phytoplankton size structure, with the two-component model of Sathyendranath et al. (2001), it may be possible to improve the capability of the two-component model when retrieving the spectral shape of the phytoplankton absorption coefficient at low chlorophyll-a concentrations. Thus having the advantages of the Uitz et al. (2008) model, in that it can accurately retrieving the spectral shape of the phytoplankton absorption coefficient at low chlorophyll-a concentrations, but also like the two-component model of Sathyendranath et al. (2001), be applied to a continuum of chlorophyll-a concentrations.

2.4 Review of current approaches for detecting PFTs and PSCs from EO

In this section a review of the current approaches for identifying and detecting multiple PFTs and PSCs from EO is conducted. Such approaches can be categorised into four groups that: (i) use the spectral response of optical properties to distinguish between different phytoplankton groups; (ii) rely on phytoplankton abundance to infer information on the size structure or taxonomic group; (iii) rely on other information in addition to ocean colour data to distinguish between different phytoplankton groups; or (iv) estimate the particle size spectrum from the satellite derived backscattering signal and associate it with the phytoplankton community.

2.4.1 Spectral-response-based approaches

Spectral-response algorithms utilise differences in the optical signatures of specific phytoplankton groups to distinguish among them. Alvain et al. (2005) (extended in Alvain et al., 2008) developed an AOP-based method that used a large set of *in situ* pigment inventories with coincident ocean colour spectral measurements. The

method is designed to detect satellite pixels that are dominated by nanoeukaryotes (and separately *Phaeocystis* and coccolithophores), two types of picoplankton (*Prochlorococcus*, and *Synechococcus*-like cyanobacteria) and diatoms. The method involved producing a look-up table (LUT) of the mean normalised water leaving radiances $L_{wn}(\lambda)$, for a given chlorophyll-a concentration $L_{wn}(\lambda, C)$. Then the satellite $L_{wn}(\lambda)$ was normalised by $L_{wn}(\lambda, C)$ in order to develop empirical correlations between spectral characteristics and HPLC-based diagnostic pigments The technique was developed using $L_{wn}(\lambda, C)$ measured in case 1 open ocean waters, therefore, it is only applicable to such an area

Ciotti et al (2002) assessed the dominant cell size of phytoplankton and their absorption spectra for a wide variety of surface waters The phytoplankton were characterised according to their dominant cell size and taxonomic group, and the relationship between this classification and the spectral shape of the phytoplankton absorption coefficient ($a(\lambda)$) for the whole assemblage was described Using a two-component mathematical model, a dimensionless "size factor", varying between 0 (100 % microplankton) and 1 (100 % picoplankton), was adopted to specify the complementary contribution to the normalised $a(\lambda)$ of the smallest and largest cells in the dataset It was found that, by classifying the cell size of the dominant organism into pico- (<2 μm), ultra- (2-5 μm), nano- (5-20 μm) or microplankton (>20 μm), more than 80 % of the variability in spectral shape of $a(\lambda)$ from 400 to 700 nm could be explained Ciotti and Bricaud (2006) used the IOP model of Loisel and Stramski (2000) to retrieve total absorption from EO (SeaWiFS reflectances) A non-linear optimisation method was used to decompose the total absorption into phytoplankton and coloured dissolved and detrital matter (CDM) absorption The non-linear optimisation method also retrieved the phytoplankton size factor and the slope of the exponential decrease of the absorption coefficient of CDM with wavelength.

Using a similar approach to Ciotti and Bricaud (2006), Mouw and Yoder (2010) estimated phytoplankton cell size distributions from satellite imagery of SeaWiFS reflectances In their model, the chlorophyll specific absorption spectra for pico- and microplankton are weighted by the percentage of microplankton The percentage of microplankton is then derived using a forward optical model LUT that incorporates the range of absorption and scattering variability due to the chlorophyll-a concentration, the size of the phytoplankton and the influences of dissolved and detrital matter Bracher et al (2009) determined whether satellite pixels were dominated by cyanobacteria or diatoms using the SCIAMACHY sensor which flies onboard the European satellite ENVISAT The technique involves adapting Differential Optical Absorption Spectroscopy (DOAS) to retrieve the absorption and biomass of cyanobacteria or diatoms. Brewin et al (2010c) developed a model that uses the spectral shape of $a(\lambda)$ to determine satellite pixels dominated by pico-, nano- or microplankton. The model is based on the assumption that larger size classes have

a flatter $a(\lambda)$ spectral shape than smaller size classes. The spectral shape of $a(\lambda)$ was estimated using the IOP model of (Lee et al., 2002) (that made no assumptions about the derivation of $a(\lambda)$), and directly from an abundance-based parameter (chlorophyll-a). Therefore, the algorithm can also function as an abundance-based model.

Spectral-response approaches rely on the covariation between some spectral features of optical properties and the dominant PFTs or PSCs. Accurately exploiting the spectral characteristics of different phytoplankton groups to identify and distinguish among them may not always be successful. Previous research into the variability of particulate absorption spectra has suggested that differences in the shape of the phytoplankton absorption spectra for different communities of phytoplankton are too small to detect from satellite (Garver et al., 1994). In the Brewin et al. (2010c) study, it was found that estimating the shape of the absorption coefficient of phytoplankton directly from chlorophyll-a was more accurate than estimating it using the IOP model of Lee et al. (2002). Problems with spectral-response algorithms can also occur when distinguishing among different phytoplankton groups with the same or similar optical signatures. Furthermore, there are difficulties dealing with variations in the spectral characteristics of the same phytoplankton group or species due to growth conditions, nutrient availability and light regimes (Nair et al., 2008). However, unlike abundance-based approaches, spectral-response approaches can detect different phytoplankton groups with the same chlorophyll-a biomass providing they have contrasting optical signatures. For example, coccolithophores produce calcite plates, or coccoliths which are highly reflective (Holligan et al., 1983) and algorithms have been proposed to identify them from other phytoplankton with similar biomass based on their spectral characteristics (Ackleson et al., 1994; Brown and Yoder, 1994; Brown and Podesta, 1997). Other satellite spectral-response algorithms have been proposed for distinct phytoplankton groups, for instance, the cyanobacterium *Trichodesmium* (Subramaniam et al., 1999) and diatoms (Sathyendranath et al., 2004).

2.4.2 Abundance-based approaches

Abundance-based approaches rely on typically-observed relationships between the trophic status of the environment and the type of phytoplankton (Margalef, 1967, 1978). The trophic status can be linked directly to biogeochemical parameters such as chlorophyll-a or related to variables such as the magnitude of $a(\lambda)$.

Devred et al. (2006) extended the two-population absorption model of Sathyendranath et al. (2001) to retrieve $a(\lambda)$ from the chlorophyll-a concentration, assuming the assemblages of the two populations vary as the phytoplankton biomass changes. The model was applied to *in situ* data collected from six regions during 34 cruises. Significant seasonal and regional changes in the spectral form and magnitude of the

specific absorption coefficients of small- and large- celled populations were identified, which were then related to changes in species composition (micro- and combined nano-picoplankton) The model was also found to be consistent with pigment analysis performed on the same datasets The parameters of the model provide direct bio-optical and biological interpretation.

Uitz et al (2006) examined the potential for using near-surface chlorophyll-a to infer the column-integrated phytoplankton biomass, its vertical distribution and its community composition They analysed an extensive set of HPLC determined pigment data collected in open ocean waters Using the detailed pigment composition and specific diagnostic pigments, the chlorophyll contribution and vertical distribution of three size classes (micro-, nano- and picoplankton) were assessed. The results led to an empirical parameterisation enabling vertical chlorophyll-a profiles of each size class to be inferred from the knowledge of satellite-based chlorophyll-a, the euphotic depth (Morel and Maritorena, 2001) and the mixed-layer depth (de Boyer Montégut et al., 2004)

Aiken et al (2007) used ranges in the absorption coefficient and chlorophyll-a to classify phytoplankton into three different size classes in the Benguela upwelling. They used the backscattering characteristics to sub-divide the size classes into functional types. The distributions of the dominant phytoplankton types compared well with the observations from station HPLC data Diatom and dinoflagellate populations were located in shallow, recently upwelled water (cold, with high nutrients) while flagellates (and prokaryotes) occurred in nutrient-poor offshore water The validation demonstrated that an empirical analysis of remotely sensed data can be used to determine the distributions of PFTs

Hirata et al (2008a) used HPLC data to explore the relationship between the direct optical properties of phytoplankton and size class. Phytoplankton were classified into their dominant taxonomic size classes of pico-, nano- and microplankton using diagnostic pigment analysis (Vidussi et al , 2001; Uitz et al , 2006) extended to account for picoeukaryotes. Two models were then developed relating either phytoplankton absorption at 443 nm ($a(443)$) or chlorophyll-a (C) to the spectral slope of absorption in the range 443 -510 nm The models were then validated against *in situ* data and contemporary SeaWiFS 8-day composite data, which indicated good agreement The distributions were found to be consistent with previous basin-scale observations (Aiken et al , 2008) Using a global HPLC dataset, Hirata et al (2011) estimated the fractional contribution to the total chlorophyll-a of three size classes (pico-, nano- and microplankton) which were further partitioned into the contributions of diatoms, dinoflagellates, green algae, picoeukaryotes, prokaryotes and *Prochlorococcus* Pan et al (2010) used polynomial equations to describe the relationship between phytoplankton pigments and remote sensing reflectance (similar to that of O'Reilly et al (1998) for deriving chlorophyll-a from satellite). In total

11 phytoplankton pigments were empirically derived using a ratio of blue to green reflectance (e.g. $R_{rs}(490)/R_{rs}(555)$), and the relationships were applied to MODIS satellite data to map the pigment distributions off the northeast coast of America in 2006.

Abundance-based algorithms assume that a given indicator of abundance, either the surface chlorophyll-a or $a(\lambda)$, covaries with the dominance of, or the fraction of, a particular PFT or PSC. While such approaches can be robust at extremes (high and low), they may be limited in intermediate regions where variations in the proportions of different groups could confound the signal. In such regions, abundance-based algorithms may fail to distinguish between blooms of different PFTs or PSCs that have the same biomass. Furthermore, variability of optical properties within-species or within functional types according to growth conditions could introduce additional classification errors. Despite this, abundance-based approaches have relevance to primary production models that produce estimates based on phytoplankton biomass.

2.4.3 Ecological-based approaches

Ecological approaches blend spatio-temporal and physical data, in addition to bio-optical information, to help detect different phytoplankton groups. Raitsos et al. (2008) developed an approach based on knowledge of the physical and biological regime to infer PFTs in the North Atlantic. The dominance of different groups was determined from 3,732 CPR match-ups based on cell counts, and then compared to spatio-temporal information: SST, chlorophyll-a, photosynthetically-active radiation (PAR), wind stress and $L_{wn}(\lambda)$.

The approach used an Artificial Neural Network (ANN) to discriminate among diatoms, dinoflagellates, coccolithophorids and silicoflagellates. Results showed that 70 % of PFT dominance derived from the CPR was explained by the input data, and that specific PFTs dominate based on a different blend of physical, ecological and biological factors. The chemical regime was not assessed in this study as no satellite offers such data. However, it may have been indirectly tested through wind stress which is partly responsible for vertical mixing of the water column and may be an indication of nutrient availability (Raitsos et al., 2008). Overall, the model indicated that spatio-temporal information (latitude, longitude, and month) and SST were the most important factors determining PFTs.

An advantage of the ecological approach is that it utilises additional information to bio-optics to detect different phytoplankton groups. This could potentially lead to better results. Furthermore, this approach may provide an insight into how different phytoplankton groups react to changing environmental conditions and which environmental parameters have the largest influence on specific phytoplankton groups. However, advanced statistical approaches are intricate, involving hidden layers and complex interactions. Therefore, from an analytical perspective they can be difficult

to interpret and are heavily dependent on the quality and quantity of the input data

2.4.4 Backscattering-based approaches

A number of approaches have recently been introduced that estimate the particle size distribution (PSD) from the satellite derived backscattering signal Hirata et al (2008b) developed a model that retrieves the Junge parameter, which characterises the PSD of total suspended particles, and then links it to the dominant phytoplankton size class. Hirata et al (2008b) showed that the Junge parameter can be derived from a ratio algorithm following the radiative transfer theory of Zaneveld (1995), Hirata and Højerslev (2008) and Hirata et al. (2009a) The model was compared with the abundance-based absorption model of Hirata et al (2008a) and indicated good agreement

Kostadinov et al. (2009) developed a bio-optical algorithm that first involved retrieving the particle backscattering coefficient spectrum ($b_i^b(\lambda)$) following the method of Loisel et al (2006) Kostadinov et al (2009) then used Mie modelling to estimate the parameters of a power law PSD (the PSD slope and the particle differential number concentration for a given reference diameter) as a function of the particulate backscattering spectrum Particle number and volume concentrations were then partitioned into pico, nano and micro size particles and then associated with the same size classes of phytoplankton Kostadinov et al (2010) validated the approach against HPLC data, which indicated considerable discrepancies but reasonable agreement for pico- and microplankton, and applied the approach to 10-years of satellite measurements to investigate seasonal and interannual variations

Methods that estimate the particle size spectrum from the satellite derived backscattering signal and associate it with the phytoplankton make the assumption that the ocean assemblage is biogenic, when in reality it is a mixture of biogenic and non-biogenic material The bulk backscattering coefficient ($b_i^b(\lambda)$) is influenced, in addition to phytoplankton, by viruses, heterotrophic bacteria, microzooplankton, nonliving particles in the colloidal size range, and larger non-living (separately biogenic and minerogenic) particles (Stramski et al , 2004) It has been suggested that within the euphotic layer only between 20-43 % of the particle beam attenuation coefficient can be attributed to phytoplankton, with the remaining fraction attributed to non-vegetal components (Claustre et al , 1999) Therefore, as highlighted by Westberry et al (2010), there has been a reluctance in the past towards using $b_i^b(\lambda)$ to study phytoplankton due to the prevailing paradigm suggesting that small, non-living particles determine the magnitude of backscattering in the open ocean. Methods that use Mie modelling to infer the PSD unrealistically assume particle sphericity, and such approaches are sensitive to deviations from sphericity (Karp-Boss et al , 2007). The parameters used in Mie theory, such as the index of refraction and the maximum particle diameter, can also vary depending on the

phytoplankton community and physiological adaptations.

Despite these disadvantages, recent evidence suggests that the influence of phytoplankton on the backscattering signal is higher than previously thought (Behrenfeld et al., 2005; Westberry et al., 2008; Dall'Olmo et al., 2009), and that phytoplankton may in fact contribute more to $b_t^b(\lambda)$ than is currently apportioned based on Mie theory alone (Kitchen and Zaneveld, 1992; Dall'Olmo et al., 2009). The backscattering-based approaches offer an alternative approach to assess PFTs from EO.

While many approaches have been developed to detect phytoplankton communities from EO, in order to confidently use these satellite products, validation exercises need to be conducted to ascertain accuracy. This is particularly important considering the detection of PFTs from EO is in its early stages of development.

2.5 Contemporary trends in phytoplankton from a decade of satellite observations

2.5.1 Decadal and interannual changes in phytoplankton production and biomass

Armed with over 10-years of SeaWiFS satellite observations, researchers have observed trends in phytoplankton production and biomass on decadal and interannual scales. McClain et al. (2004) examined 8 months (November 1996 to June 1997) of OCTS ocean colour data and 6-years (September 1997 to October 2003) of SeaWiFS ocean colour data. They found that the oligotrophic waters of the North Pacific and North Atlantic gyres had expanded over this period, while those of the South Pacific, South Atlantic, and South Indian Ocean showed much weaker and less consistent tendencies. Gregg et al. (2005) used a 6-year time-series of remotely-sensed global ocean chlorophyll-a measurements to evaluate trends for the 1998 to 2003 period. Using linear regression, Gregg et al. (2005) found that global ocean chlorophyll-a had increased significantly by 4.1 %. Most of this increase was found in coastal areas (<200 m depth) which saw an increase of 10.4 %. However, decreases in chlorophyll-a in 4 out of the 5 mid-ocean gyres were observed and linked to increases in SST.

Behrenfeld et al. (2006) describe changes in global ocean primary production for the 1997 to 2006 period using SeaWiFS data. They found an initial increase in net primary production between 1997 to 1999, associated with the El Niño (La Niña) Southern Oscillation (ENSO), followed by a prolonged decrease between 1999 to 2006. These changes were found to occur mainly in the stratified low-latitude oceans and were tightly coupled to coincident climate variability (changes in stratification and SST). Polovina et al. (2008) analysed 9-years of SeaWiFS data to examine temporal trends in the ocean's most oligotrophic waters. They concluded that globally, the low surface chlorophyll areas have expanded by 6.6 million km^2 or

by about 15.0 % from 1998 through to 2006, and that this expansion exceeds global warming scenarios based on increased vertical stratification in the mid-latitudes

Recently work has also looked at decadal changes in phytoplankton biomass by comparing ocean colour observations from the CZCS and the SeaWiFS sensor, with contrasting results Gregg and Conkright (2002) revised the CZCS chlorophyll-a archive using compatible algorithms with SeaWiFS which were blended with *in situ* data to reduce residual errors This permitted them to compare decadal changes in global ocean chlorophyll from the CZCS (1979 to 1986) and SeaWiFS (1997 to 2000) records. They found that mean global chlorophyll-a had decreased over the two observational segments by 6 %. In contrast to this study, Antoine et al (2005) developed a consistent, reanalyzed, ocean colour time-series from 5-years of CZCS data (1979 to 1983) and 5-years of SeaWiFS data (1998 to 2002), and found an overall increase in the global average chlorophyll-a concentration of ~22 %, associated with large increases in the intertropical areas.

Using the reanalyzed CZCS and SeaWiFS data, developed by Antoine et al (2005), Martinez et al. (2009) linked the decadal changes in chlorophyll-a concentrations with basin-scale oscillations of the physical ocean, specifically the Pacific Decadal Oscillation and the Atlantic Multidecadal Oscillation This coupling between the physical and biological environment is also supported by the recent study of Boyce et al (2010), who combined available ocean transparency measurements and *in situ* chlorophyll-a observations to estimate changes in phytoplankton biomass at local, regional and global scales since 1899 They observed a global rate of decline of ~1 % per year in phytoplankton biomass Like Martinez et al (2009), fluctuations were strongly correlated with basin-scale climate indices However, long-term declining trends were related to increasing SST

Henson et al. (2010) compared recent trends in satellite ocean colour data to longer-term time-series from three biogeochemical models They found detection of climate change-driven trends in the satellite data is confounded by its short time-series and by large interannual and decadal variability in productivity This implies that the recently observed changes in chlorophyll, production and the size of the oligotrophic gyres cannot be unequivocally attributed to the impact of global climate change Henson et al. (2010) suggested a time-series of ~40 years in length is needed to distinguish a global warming trend from natural variability. This is further supported by Yoder et al (2010) who looked at trends in the SeaWiFS chlorophyll time-series (1997-2004) and compared them with an ocean coupled circulation and biogeochemical model covering the period 1958-2004 Results indicated that the trends observed from satellite were not unusual and fell well within the range in magnitude of linear trends observed in other 8-year periods of model output This also suggested that a time-series of 10-years is not long enough to directly observe any long-term changes in surface chlorophyll-a concentrations Caution should be

made when linking changes in ocean colour, over a 10-year period, to long-term changes in ocean biogeochemistry.

2.5.2 Interannual changes in phytoplankton community structure

While a number of approaches have been developed to detect phytoplankton community structure from EO, only a few studies have looked for trends in phytoplankton community structure on interannual scales.

Alvain et al. (2008) applied the PHYSAT algorithm to 9-years of SeaWiFS observations (1998 to 2006). They found large interannual variability in the North Atlantic diatom bloom, and observed large blooms of both diatoms and *Phaeocystis* during the winter in the Southern Ocean. The geographical distribution of diatoms and *Phaeocystis* were shown to be tightly related with the mixed-layer depth, with diatoms dominating in stratified waters. Blooms of diatoms were also observed in the equatorial Pacific during the La Niña phase of the ENSO cycle. Using the ecological provinces classification of Devred et al. (2007), Devred et al. (2009) produced a time-series of ecosystem delineation for the northwest Atlantic Ocean over a 10-year period (1998 to 2007). For each province, data was compiled on SST, chlorophyll-a and occurrence of diatoms (using the model of Sathyendranath et al. (2004)). They found a strong correlation between chlorophyll-a and diatoms. However, the correlations varied depending on province. Furthermore, changes in occurrences of diatom during the 10-year period also varied depending on region.

Uitz et al. (2010) applied a size-specific primary production model to 10-years of global satellite observations. They revealed large interannual variations in size-specific primary production in both the North Atlantic ocean and in the equatorial Pacific. In the equatorial Pacific, microplankton showed the largest range of variability of the three phytoplankton classes which was related to the ENSO cycle. Both Brewin et al. (2010c) and Kostadinov et al. (2010) have also applied their phytoplankton size class models to 10-years of SeaWiFS observations and both found a significant positive correlation between picoplankton and the multivariate ENSO index (MEI), which is used to evaluate the strength of the El Niño to La Niña Southern Oscillation cycle (Wolter, 1987), and a significant negative correlation between nanoplankton and MEI and microplankton and MEI, on global scales. This suggests a strong coupling between the phytoplankton size structure and physical forcing. Nonetheless, all this studies are preliminary and there is clearly potential to further investigate the relationship between phytoplankton size structure and coincident climate variability.

2.5.3 Climatic indices

Climate indices are a useful tool for linking changes in the physical environment with changes in the biological environment on decadal and interannual scales (Behrenfeld et al , 2006, Martinez et al , 2009, Boyce et al , 2010) Over a decade of ocean colour observations are available from the SeaWiFS database that are utilised in this thesis. Martinez et al. (2009) linked changes in phytoplankton biomass with the Pacific Decadal Oscillation (PDO) and the Atlantic Multidecadal Oscillation (AMO) Both these atmosphere-ocean phenomena vary on decadal scales. A decade of SeaWiFS observations alone is inadequate for comparison, ideally 20-30 years of observations would be required (as in the Martinez et al. (2009) study). The North Atlantic oscillation (NAO) describes fluctuations in the difference of atmospheric pressure at sea level between the Arctic and the subtropical Atlantic (Hurrell, 1995). Unlike the PDO, AMO and ENSO, the NAO is a largely atmospheric mode. Two climatic indices that have been used for interannual analysis, and that specifically relate to atmosphere-ocean climatic variability, are the ENSO and the Indian Ocean Dipole (IOD)

2.5.3.1 El Niño (La Niña) Southern Oscillation (ENSO)

The ENSO is a coupled atmosphere-ocean phenomenon It constitutes the largest single source of interannual climatic variability on Earth (Diaz and Markgraf, 1992) and generally occurs at intervals of 2-7 years (Colling, 2001) The ENSO causes large-scale fluctuations in atmospheric mass between the south-eastern tropical Pacific and the Australian-Indonesian region (Garcia-Herrera et al , 2008). El Niño is usually characterised by abnormally warm sea temperatures in the eastern half of the equatorial Pacific, whereas the occurrence of the opposite ENSO phase, La Niña, is usually characterised by abnormally cold SST in the eastern half of the equatorial Pacific (Wolter and Timlin, 1993, 1998)

The MEI is a multivariate measure of the ENSO signal MEI is derived from the COADS dataset (Comprehensive Ocean-Atmosphere Data Set) and is expressed in the first principle component of six variables over the tropical Pacific, sea-level pressure, surface zonal and meridional wind components, sea surface temperature, surface air temperature and cloudiness (Wolter and Timlin, 1993, 1998). Such an index has previously been found to explain major impacts on phytoplankton and fisheries (Barber and Chavez, 1983, Chavez et al , 1999, Behrenfeld et al , 2001) and there is recent evidence it also relates to the phytoplankton size structure (Brewin et al., 2010c, Kostadinov et al., 2010), although further analysis is needed to fully understand this connection.

2.5.3.2 Indian Ocean Dipole (IOD)

The IOD is recognised as a major atmosphere-ocean phenomenon in the Indian Ocean (Saji et al., 1999; Webster et al., 1999). Saji et al. (1999) developed an index to quantify the IOD, which is calculated as the SST gradient between the tropical western Indian Ocean and the tropical south-eastern Indian Ocean (Saji et al., 1999) and referred to as the Dipole Mode Index (DMI). When DMI is positive it can lead to heavy rainfall and flooding over East Africa and droughts in the Indonesian region, when DMI is negative the inverse of this pattern can occur (Ashok et al., 2001).

There is evidence that the IOD can evolve during certain years independent of ENSO forcing (Saji et al., 1999; Webster et al., 1999). However, some researchers argue that, on some occasions, ENSO can force the IOD and it has been shown that positive phases of the IOD tend to co-occur with El Niño, and negative phases with La Niña (Annamalai et al., 2005; Behera et al., 2006; Luo et al., 2010; Izumo et al., 2010). There is recent evidence that the IOD can significantly influence the phytoplankton chlorophyll-a biomass (Vinayachandran et al., 2007), yet it remains to be revealed whether the size structure of the phytoplankton is influenced by the IOD in the Indian Ocean.

2.6 Summary

By analysing literature in the context of the aims and objectives of the thesis, this chapter has indicated that:

- Phytoplankton size class seems a suitable classification of phytoplankton functional types in the context of primary production and the carbon cycle.
- Methods for detecting phytoplankton communities from EO can be partitioned into: spectral response approaches which utilise distinct optical signatures of different phytoplankton communities to distinguish between them; approaches which differentiate between phytoplankton groups based on the trophic status of the waters, approaches which use other ecological data in addition to bio-optical information to distinguish between different phytoplankton communities, and approaches that estimate the particle size spectrum from the satellite derived backscattering signal and associate it with the phytoplankton community. All these methods display advantages and disadvantages.
- A variety of *in situ* data has been gathered over the past few decades on phytoplankton community structure and there are a variety of methods to determine phytoplankton size class *in situ*. By combining satellite and *in situ* data, methods for detecting phytoplankton size structure from EO can be validated and scrutinised, which may raise questions that can guide future efforts in the field.

- The absorption coefficient of phytoplankton ($a(\lambda)$) can be estimated as a function of the dominant pigment chlorophyll-a. There is evidence to suggest that estimates of $a(\lambda)$ could be improved by accounting for the size structure of the phytoplankton at low chlorophyll-a concentrations.

- Recent research indicates that interannual changes in phytoplankton biomass and primary production is linked with climate variability. However, research into the influence of climate variability on phytoplankton size structure is limited

Chapter 3

An intercomparison of bio-optical techniques for detecting dominant phytoplankton size class from Earth Observation*

3.1 Introduction

In the previous chapter, a thorough review of existing work was undertaken. An outcome of this review indicated that approaches for detecting phytoplankton size class (PSC) from satellite data can be partitioned into spectral-response approaches, abundance-based approaches, ecological-based approaches and backscattering-based approaches, and that a variety of *in situ* and satellite data is available that could be used to scrutinise and validate these approaches. This chapter aims to take the first step towards the validation and comparison of different PFT and PSC satellite algorithms by comparing current approaches to six different sources of *in situ* data, spanning from 1997-2007, in order to assess their ability at detecting PSCs. By applying these satellite techniques to the 10-year SeaWiFS ocean colour data series and by comparing the results with *in situ* data, a better understanding of the performance of these algorithms can be gained and issues can be raised which may influence future model development.

*Aspects of this chapter are included in the following paper
Brewin, R.J.W., Hardman-Mountford, N.J., Lavender, S.J., Raitsos, D.E., Hirata, T., Uitz, J., Devred, E., Bricaud, A., Ciotti, A. and Gentili, B. (2011). An intercomparison of bio-optical techniques for detecting dominant phytoplankton size class from satellite remote sensing. Remote Sensing of Environment. 115, 325-339, doi:10.1016/j.rse.2010.09.004.

3.2 Data

3.2.1 *In situ* data

When identifying phytoplankton groups from *in situ* data, HPLC analysis has the advantage to be comprehensive in terms of phytoplankton size range (Claustre, 1994), it is the only method for which a sufficient amount of globally representative data is available, and despite having limitations (see section 3 4), in recent years it has been extensively used as a proxy for size class (e g Vidussi et al , 2001, Bricaud et al , 2004, 2007, Claustre et al , 2005, Devred et al., 2006, Uitz et al , 2006, 2008, 2009, Hirata et al , 2008a, Ras et al , 2008, Aiken et al , 2008, 2009) Analysis from Chapter 2, also noted by Nair et al (2008), highlights that the use of any *in situ* method in isolation could imply identifications of phytoplankton groups that may not be entirely dependable, hence incorporating different *in situ* methodologies would lead to a more accurate diagnosis. Therefore, in addition to four HPLC datasets, two *in situ* cell count datasets were used in this chapter

- AMT HPLC pigment data from 1997 to 2004 (AMT 5-15) were obtained and quality assured by statistical methods according to Aiken et al (2009)
- NASA SeaBASS HPLC pigment data were obtained from the NASA website from 1997 to 2007 (http://seabass.gsfc nasa gov/, Werdell et al , 2003) The data were accessed on the 5th September 2008 after the removal of the CHORS HPLC pigment data [1]
- HOTS HPLC pigment data acquired from between 1997 and 2006 (http://hahana soest.hawaii.edu/hot/, Karl and Lukas, 1996).
- BATS HPLC pigment data acquired from 2002 to 2004 (http //bats.bios edu, Michaels and Knap, 1996)
- Phytoplankton cell count data from the CPR were obtained for the North Atlantic from 1997 to 2003 (Richardson et al., 2006).
- Phytoplankton cell count data were obtained from the Western Channel Observatory for the L4 site during the period of 1997 to 2007 (http://www.westernchannelobservatory org.uk/, Southward et al., 2005)

3.2.1.1 HPLC data

All HPLC data were classified using DPA according to two different methods. the method of Vidussi et al. (2001) extended by Uitz et al. (2006), and the method of Hirata et al (2008a) (see section 2.2.2 3) The dominant size class was established

[1]The CHORS HPLC pigment data were recently found to have average uncertainties exceeding allowed maximums for calibration and validation activities

based on whether a size class (pico-, nano- or microplankton) had a diagnostic pigment to chlorophyll-a ratio (F_p, F_n and F_m) of greater than 0.45, i.e. representing >45 % of the total population in terms of pigment concentration (Hirata et al., 2008a).

Originally 2176 HPLC AMT, 2131 SeaBASS HPLC, 305 HOTS HPLC and 34 BATS HPLC measurements were utilised. This was reduced to 1093 AMT HPLC measurements, 761 HPLC SeaBASS measurements, 96 HPLC HOTS measurements, and 34 HPLC BATS measurements by only including data taken in the top 10 m of the water column. Where there were two or more measurements within the 10 m surface layer, either the dominant size class closest to the surface was selected, or if there were more than two measurements within the surface layer, the most frequent dominant size class was selected. Any HPLC data used to develop and train any of the satellite algorithms used in this intercomparison (see section 3.3.1) were eliminated from the database.

3.2.1.2 CPR data

Despite the CPR approach not sampling small cells (see section 2.2.3.1), samples dominated by large (microplankton) and small (nano- and picoplankton) cells can still be estimated. This method has uncertainty (see section 3.4), but another source of data, other than HPLC, would add value to the intercomparison. For the purposes of this chapter, the CPR dataset was used to infer the dominant microplankton group, and samples were categorised as dominated by microplankton or not. The total number of species per sample for four PFTs (diatoms, dinoflagellates, silicoflagellates and coccolithophores) were determined, and a final category of no-dominance was allocated to samples with no cell counts (see Raitsos et al., 2008, for details). The dominant groups were then determined using the Z-factor standardised method (Raitsos et al., 2008),

$$Z_i = \frac{w_i - \overline{x}_i}{u_i}, \tag{3.1}$$

where, w_i is the cell count for phytoplankton type i in a sample, $\overline{x}_i$ is the overall mean of all cell counts for each type i, and u_i is the standard deviation of all samples for type i. The largest Z_i for each sample was used as the dominant phytoplankton type. The dominant phytoplankton type can be derived from this standardised method because the number of cells between each of the four groups was substantially different (Raitsos et al., 2008). Where either diatoms or dinoflagellates were dominant, samples were allocated as dominated by microplankton, and the rest of the samples (including no-dominance samples) were allocated as not dominated by microplankton. Therefore, it was assumed that the pixels not dominated by microplankton were dominated by either pico- or nanoplankton that constitute the remaining autotrophic pool. Originally 17,061 measurements were used in this chapter spanning 1997-2003.

3.2.1.3 L4 data

The taxonomic groups identified in the quantitative sample analysis conducted at the L4 site include diatoms, dinoflagellates, coccolithophores, flagellates and picoplankton Diatoms and dinoflagellates were classified as microplankton and coccolithophores and flagellates as nanoplankton Paired samples were collected from a depth of 10 m and preserved with 2% Lugol's iodine solution (Throndsen, 1978) and 4% buffered formaldehyde. Between 10 and 100 ml of the sample was settled for about 48 hours, and cells identified by inverted microscopy to the species level (Southward et al , 2005). For picoplankton, however, samples were settled for >6 days and picoplankton enumerated using high magnification (e g × 900 mag) in appropriate numbers of fields-of-view, such as 20 or 50 Data from 1997 to 2007 were downloaded from the Western Channel Observatory website (http //www westernchannelobservatory org uk) The dominant phytoplankton type for each sample was estimated using the Z-factor standardised method as for the CPR data Table 3 1 shows the number of dominant PSC samples in each *in situ* dataset.

Table 3 1: Intercomparison results showing the percentage accuracy of each model when compared with *in situ* datasets using method 1

PFT Technique	HPLC data Vidussi et al (2001) DPA				HPLC data Hirata et al (2008) DPA				L4 data				CPR data	
	Pico %	Nano %	Nano/ Pico %	Micro %	Pico %	Nano %	Nano/ Pico %	Micro %	Pico %	Nano %	Nano/ Pico %	Micro %	Nano/ Pico %	Micro %
Model A	78 6 ±9 0	55 5 ±10 9	98 2 ±2 0	27 8 ±33 9	73 5 ±7 0	71 4 ±27 1	98 2 ±2 0	33 3 ±54 2	–	–	–	–	94 2 ±1 3	12 8 ±2 9
Model B	52 0 ±9 3	87 7 ±6 4	98 8 ±1 5	52 2 ±15 0	38 0 ±7 0	87 5 ±15 4	98 5 ±1 5	52 2 ±15 0	1 4 ±2 8	77 4 ±15 6	68 7 ±11 4	61 3 ±18 2	85 5 ±1 7	51 7 ±3 0
Model C	70 3 ±5 7	61 0 ±6 5	95 0 ±1 9	91 0 ±4 5	69 7 ±4 5	88 2 ±7 8	95 0 ±1 9	91 9 ±4 4	1 3 ±1 8	54 7 ±11 5	58 6 ±7 9	74 3 ±8 4	89 8 ±1 2	58 5 ±2 3
Model D	93 1 ±3 2	22 1 ±5 4	96 0 ±1 8	36 5 ±7 6	90 7 ±2 8	37 3 ±13 1	96 3 ±1 7	37 6 ±7 9	73 4 ±10 0	39 9 ±11 3	81 8 ±6 2	54 8 ±9 6	95 7 ±0 6	23 3 ±2 0
Model E	95 0 ±2 7	65 5 ±6 4	99 2 ±0 8	75 6 ±6 8	95 9 ±1 9	73 6 ±11 3	99 2 ±0 8	75 8 ±7 0	73 4 ±10 0	68 9 ±10 8	98 7 ±1 8	53 8 ±9 6	99 5 ±0 2	87 4 ±1 5
Model F	87 4 ±4 1	37 1 ±6 4	95 1 ±1 9	90 1 ±4 7	88 7 ±3 1	84 5 ±9 3	95 2 ±1 9	91 9 ±4 4	4 5 ±4 6	57 4 ±11 5	63 9 ±7 7	66 7 ±9 1	85 5 ±1 1	49 8 ±2 3
Model G	–	–	98 2 ±1 1	92 9 ±4 1	–	–	98 0 ±1 2	93 3 ±4 1	–	–	42 1 ±7 9	80 5 ±7 6	72 6 ±1 4	60 8 ±2 3
Model H	–	–	94 0 ±2 1	91 0 ±4 5	–	–	93 8 ±2 1	92 6 ±4 2	–	–	44 0 ±8 0	80 5 ±7 6	77 8 ±1 3	60 4 ±2 3
Model I	87 4 ±4 1	34 7 ±6 2	95 1 ±1 9	90 7 ±4 6	89 0 ±1 9	82 7 ±9 8	95 2 ±3 0	92 6 ±4 2	4 5 ±4 6	52 0 ±11 6	56 6 ±8 0	71 4 ±8 7	82 3 ±1 2	54 6 ±2 3
Model J	64 7 ±7 1	45 5 ±9 2	88 4 ±3 7	79 3 ±8 4	61 8 ±5 9	66 7 ±18 3	88 5 ±3 6	78 9 ±8 6	–	–	–	–	–	–
Model B2	77 2 ±8 3	76 5 ±8 3	98 3 ±1 7	84 4 ±11 0	68 4 ±6 7	81 3 ±19 2	98 0 ±1 8	84 4 ±11 0	4 2 ±6 2	37 1 ±17 7	41 0 ±12 0	77 4 ±15 6	74 1 ±1 8	67 0 ±2 8
Number of samples	239 84^A 101^B 173^J	213 82^A 102^B 112^J	452 166^A 203^B 285^J	156 9^A 45^B 92^J	404 155^A 187^B 263^J	55 14^A 16^B 24^J	459 169^A 203^B 287^J	149 6^A 45^B 90^J	77 36^B	74 31^B	151 67^B	105 31^B	3863 1233^A 2228^B	1801 489^A 1061^B

^{A} denotes the number of samples used to test Model A
^{B} denotes the number of samples used to test Models B and B2
^{J} denotes the number of samples used to test Model J

3.2.2 Satellite data

The HPLC and CPR data were matched to Level 3 SeaWiFS daily products acquired from the NASA *Oceancolor* website (*http://oceancolor.gsfc.nasa.gov/*), at 9 km resolution, and plus or minus one pixel (3 × 3 window). This criterion, although less restricting than NASA's 3-hour window for data and algorithm validation, was adopted to maximise the number of match-ups. Mean data for $L_{wn}(\lambda)$ (mW cm^{-2} μm^{-1} sr^{-1}), chlorophyll-a (C^s, mg m^{-3}), PAR (E m^{-2} d^{-1}), and optical aerosol thickness (T865 dimensionless), as well as the associated standard deviations, were calculated across the 9 pixels. The IOP models of Lee et al. (2002) (Quasi-Analytical Algorithm (QAA) v5) and Smyth et al. (2006) were used to calculate the $a(\lambda)$ at these data points. For the Hirata et al. (2008a) approach, we used two IOP models in this chapter to highlight sensitivity of the algorithm to IOP input. The match-ups resulted in 250 HPLC AMT, 305 HPLC SeaBASS, 39 HPLC HOTS, 14 HPLC BATS and 5664 CPR measurements spanning from 1997 to 2007, and shown in Figure 3.1.

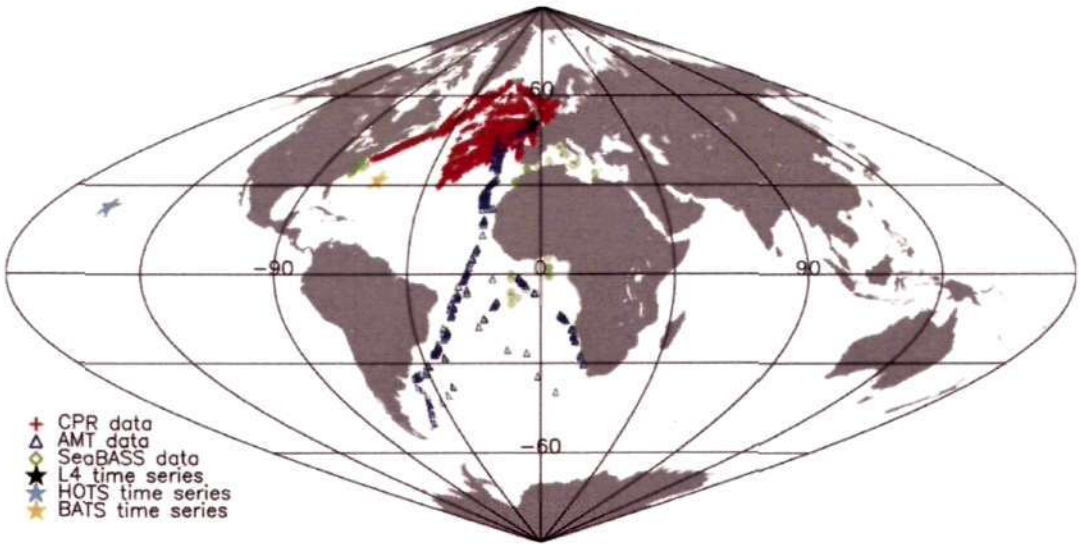

Figure 3.1: Geographic distribution of *in situ* data used in Chapter 3.

AVHRR Pathfinder 5 daily mean SST data at 4 km resolution were obtained from the NASA PO.DAAC website (http://poet.jpl.nasa.gov/) and matched to all the HPLC data points. Night time SST products were used to avoid the solar radiation bias from daily surface heating. Weekly composites of mean wind stress data from ERS-2, and daily mean wind stress data from QS (0.5° by 0.5° spatial resolution) were obtained from CERSAT, IFREMER (http://www.ifremer.fr/cersat/en/index.htm). All SST and wind stress data were interpolated to 9 km resolution and matched to all HPLC data points.

At the L4 station, SeaWiFS daily 1km mapped data ($L_{wn}\,\lambda$, C^s, and T865) were acquired from NEODAAS in order to reduce potential interference from the adjacent land. This data was processed over the L4 station. The $a(\lambda)$ coefficients

were calculated as previously described, and the satellite data were matched to the phytoplankton cell counts which resulted in 256 matching data points between 1997 and 2004 (Figure 3.1). Samples between 2002-2004 were matched to daily satellite data. Because samples collected before 2002 were logged with only the start day of the week as opposed to the sample day, satellite data were extracted on the Monday of every sampling week (usual sampling day), whether the *in situ* were actually sampled on that day or not (see section 3.5.1 regarding the validity of this approach).

3.3 Methods

3.3.1 PFT and PSC techniques

All published spectral-response, abundance-based and ecological-based PFT satellite approaches, designed for global application using the SeaWiFS sensor (Table 3.2), were incorporated into the intercomparison. This section describes how the following PFT and PSC algorithms were reformulated or directly implemented to detect dominant phytoplankton size class (micro-, nano-, and picoplankton) and applied to the satellite *in situ* match-up data:

- Model A: Alvain et al. (2008) spectral-response approach (PHYSAT).
- Model B: Ciotti and Bricaud (2006) spectral-response approach.
- Model C: Uitz et al. (2006) abundance-based approach.
- Model D: Hirata et al. (2008a) abundance-based approach ($a(443)$; Lee et al., 2002).
- Model E: Hirata et al. (2008a) abundance-based approach ($a(443)$; Smyth et al., 2006).
- Model F: Hirata et al. (2008a) abundance-based approach using C^s.
- Model G: Devred et al. (2006) abundance-based approach using regional parameters.
- Model H: Devred et al. (2006) abundance-based approach using global parameters.
- Model I: Brewin et al. (2010c) abundance-based model.
- Model J: Raitsos et al. (2008) ecological-based approach.

Table 3.2: Description of models used in the intercomparison.

Model	Type	Satellite Input variables									Reference
		C^s	$L_{wn}(\lambda)$	$R_{rs}(\lambda)$	$a^1(\lambda)$	$a^2(\lambda)$	T865	PAR	WS	SST	
A	SR	×	×				×				Alvain et al. (2005, 2008)
B	SR	×		×							Ciotti and Bricaud (2006)
C	AB	×									Uitz et al. (2006)
D	AB				×						Hirata et al. (2008a)
E	AB					×					Hirata et al. (2008a)
F	AB	×									Hirata et al. (2008a)
G	AB	×									Devred et al. (2006)
H	AB	×									Devred et al. (2006)
I	AB	×									Brewin et al. (2010c)
J	EB	×	×					×	×	×	Raitsos et al. (2008)

SR = a spectral-response model, AB = an abundance-based model, EB = an ecological-based model, WS = wind stress, $a^1(\lambda)$ refers to $a(\lambda)$ calculated according to Lee et al. (2002) and $a^2(\lambda)$ refers to $a(\lambda)$ calculated according to Smyth et al. (2006).

3.3.1.1 Model A (Alvain et al., 2008)

The PHYSAT method determines six dominant PFTs: diatoms, nanoeukaryotes (separately *Phaeocystis* and coccolithophores), *Prochlorococcus* and *Synechococcus*. In this intercomparison, it was assumed that these major PFTs can be divided into the three phytoplankton size classes: microplankton = diatoms; nanoplankton = nanoeukaryotes (and separately detected *Phaeocystis* and coccolithophores); and picoplankton = *Prochlorococcus* and *Synechococcus*. It is acknowledged that the approach does not identify all the phytoplankton groups within each size class. The PHYSAT algorithm (Alvain et al., 2008) was applied to SeaWiFS data with chlorophyll-a (C^s) ranges between 0.04 and 4 mg m^{-3} and aerosol thickness lower than 0.15. The SeaWiFS $L_{wn}(\lambda, C)$ LUT was then implemented (see Table 1 of Alvain et al., 2005, for details) to determine the dominant group.

3.3.1.2 Model B (Ciotti and Bricaud, 2006)

The Ciotti and Bricaud (2006) approach involved initially running the updated Loisel and Stramski (2000) IOP model (Loisel and Poteau, 2006, Loisel et al. in prep) to derive total absorption $a(\lambda)$ from the remotely sensed reflectance ($R_{rs}(\lambda)$). Once $a(\lambda)$ had been retrieved, a nonlinear optimization technique was used to split $a(\lambda)$ into the contributions from coloured detrital matter ($a_{CDM}(\lambda)$) and phytoplankton ($a(\lambda)$) (see equations 3 and 8; Ciotti and Bricaud, 2006). Using the model of Ciotti et al. (2002), and following the procedure described in Ciotti and Bricaud (2006) (see 'Method 2: nonlinear optimization technique'; Ciotti and Bricaud, 2006), a generalised reduced-gradient nonlinear optimization code was set up to retrieve $a_{CDM}(443)$, the spectral slope of CDM absorption (S_{CDM}) and a size parameter of phytoplankton (S_f).

When running this technique, samples with chlorophyll-a (C^a) ≤ 0 or remote sensing reflectance (Rrs) ≤ 0 at 412, 443, 490 or 510 nm were removed When running the reflectance inversion any samples which gave out-of-range values for the diffuse attenuation coefficient (K) (hence invalid $a(\lambda)$ values) or where the optimisation method did not converge, were removed Samples for which the retrieved S_f was dependent on the initial value (several minima in the function to solve) were also removed. This was determined by comparing three sets of results, with initial values of S_f equal to 0, 0.5 and 1, and discarding the samples for which the standard deviation divided by the mean exceeded 10 %.

The size parameter of phytoplankton (S_f) is fixed to vary continuously between two extremes of 0 and 1, that represent the extremes in size (i.e the largest microplankton and smallest picoplankton) For this intercomparison, it became necessary to establish interval values for S_f that could represent the micro-, nano- and picoplankton To do that, a size value for the two extremes of S_f were first assigned, representative of the smallest picoplankton (referred to as a picovector) and the largest microplankton (referred to as a microvector) An equation was then chosen to interpolate between these two extremes in order to estimate S_f values at 2 and 20 μm which could then be used to determine a dominant micro-, nano- or picoplankton pixel Note that these assumptions ignore that part of the S_f variability was due to pigment packaging independent of cell size (i e variations in intracellular pigment concentrations resulting from photoacclimation)

The selection of a general shape for the curve of the expected decay of S_f with cell size is not a simple choice, as a large amount of noise around any curve will be expected, due to the distinct degrees of packaging possible in a given cell size (Bricaud et al , 2004) that in the field may vary in time and space Based on the theory of Van de Hulst (1957), it is expected that there would be an exponential decay in pigment packaging as the product of the diameter and the internal concentration of the pigments increases Therefore, this would suggest either a log-linear or exponential relationship between packaging and cell size

Table 3 3 shows a range of possible values of S_f at 2 and 20 μm using both log-linear and exponential interpolations. In producing Table 3, a variety of diameter values for the fixed pico- and microvectors were used, ranging from 0 2 to 1 μm for the picovector and 30 to 120 μm for the microvector Each picovector was set to an S_f value of 0.999 and each microvector set to an S_f value of 0 001 when interpolating Depending on the representative sizes for the vectors and mathematical interpolation, the 2 μm S_f value varies between 0 540 and 0.943 and the 20 μm S_f value varies between 0 010 and 0 376. This large variability highlights the importance of assigning extreme cell sizes, and interpolation methods, that are appropriate for a particular region or alternatively, for large scale application, developed using globally representative data

Table 3.3: S_f boundaries at 2 and 20 μm using logarithmic (log) and exponential (exp) interpolations and for a variety of assumed microvectors and picovectors set to the extremes of S_f (0.999 and 0.001 respectively).

Picovector (μm)	Size (μm)	S_f (microvector 30 μm)		S_f (microvector 60 μm)		S_f (microvector 90 μm)		S_f (microvector 120 μm)	
		log	exp	log	exp	log	exp	log	exp
0.2	2	0.540	0.658	0.596	0.812	0.623	0.870	0.640	0.900
0.4	2	0.627	0.688	0.679	0.830	0.703	0.883	0.717	0.910
0.6	2	0.692	0.719	0.738	0.849	0.759	0.897	0.772	0.921
0.8	2	0.747	0.751	0.787	0.868	0.806	0.897	0.817	0.932
1.0	2	0.796	0.788	0.830	0.889	0.845	0.924	0.855	0.943
0.2	20	0.082	0.010	0.193	0.102	0.248	0.217	0.281	0.317
0.4	20	0.095	0.010	0.220	0.103	0.279	0.221	0.314	0.320
0.6	20	0.105	0.010	0.238	0.105	0.301	0.228	0.340	0.324
0.8	20	0.114	0.011	0.255	0.106	0.320	0.224	0.358	0.328
1.0	20	0.121	0.011	0.268	0.108	0.334	0.227	0.376	0.332

For this intercomparison, a picovector of 0.6 μm and a microvector of 60 μm was used (each assigned to S_f values of 0.999 and 0.001 respectively). The picovector was chosen based on *Prochlorococcus* data (see Ciotti and Bricaud, 2006) and the microvector was chosen based on samples taken during a bloom of *Gonyaulax digitale* (Ciotti et al., 2002). A logarithmic interpolation was chosen to calculate S_f values at 2 and 20 μm (0.74 and 0.24 respectively) which were then used to determine a pixel dominated by pico- (<2 μm), nano- (2-20 μm) and microplankton (>20 μm) after retrieving S_f from the inversion. Note that these S_f boundaries must be interpreted with caution and their limitations must be considered when discussing the results from model B.

3.3.1.3 Model C (Uitz et al., 2006)

The Uitz et al. (2006) approach involved dividing global oceanic waters into stratified and mixed environments based on the ratio of the euphotic depth (Z_p) (Morel and Maritorena, 2001) to the mixed-layer depth (Z_m) (de Boyer Montégut et al., 2004). As the satellite signal only penetrates the surface layer of the ocean, for the stratified environment, surface PSC percentages (Figure 6c in Uitz et al., 2006) were used. For the mixed environment, mixed water PSC percentages (Table 6 in Uitz et al., 2006) representing the euphotic layer were used, as according to Uitz et al. (2006) these percentages were found to be uniform with depth.

The Uitz et al. (2006) approach involves partitioning stratified and mixed environments into a small number of trophic classes according to intervals of chlorophyll-a values, and associating each interval with a size structure (PSC%). For the intercomparison, interpolation was conducted between the mean chlorophyll-a values of each trophic class to avoid discontinuities. These percentages were then applied to the satellite chlorophyll-a (C^s) values in order to calculate the percentage contri-

bution of the three size classes for each pixel The percentage of the size class at a given pixel was then converted into a dominant size class if the relative chlorophyll contribution of a particular size class was greater than 45 %, as in the DPA analysis

3.3.1.4 Models D, E and F (Hirata et al., 2008a)

The two approaches of Hirata et al (2008a) use ranges of variation in chlorophyll-a (C^s) (pico $< 0\ 25$, nano $0\ 25$ to $1\ 3$, and micro $> 1\ 3\,\mathrm{mg\ m^{-3}}$, as implemented in Aiken et al , 2008) or in $a(443)$ (pico $< 0\ 024$, nano $0\ 024$ to 0.060, and micro $> 0\ 060\,\mathrm{m^{-1}}$, Aiken et al , 2008) to distinguish dominant size class Both methods were applied to satellite-derived C^s and $a(443)$ in order to determine the dominant size class Model D uses $a(443)$ calculated according to Lee et al (2002), Model E uses $a(443)$ calculated according to Smyth et al (2006) and Model F uses C^s

3.3.1.5 Models G and H (Devred et al., 2006)

The absorption model of Devred et al (2006), based on the work of Sathyendranath et al. (2001), yields information about the two main optically significant phytoplankton populations in a dataset The information derived from fitting the model to the data consists of the specific absorption of both populations ($a_1^*(\lambda)$ and $a_2^*(\lambda)$), the rate of increase of chlorophyll in the small-celled population as a function of total chlorophyll (S_1) and the maximum chlorophyll concentration of the small-cell population (C_1^m) If the dataset used to fit the model covers a wide range of chlorophyll, the two populations of phytoplankton are assumed to be (1) a combination of pico- and nanoplankton and (2) microplankton (Devred et al , 2006)

For a given sample (pixel in our case), the proportion of each population to the total biomass can be derived either by linear combination of the derived specific absorption coefficients of the two populations, which will yield the concentration of *both populations* (spectral-response-based approach), *or by applying* Equation 2 in Devred et al. (2006), using the chlorophyll concentration, the derived rate of increase (S_1) and the maximum concentration of the small-cell population (C_1^m) (abundance-based approach). Ideally, the fitted parameters should be computed for any given dataset (*in situ* or remotely sensed) In this chapter, the second method (abundance-based approach) was used with the regional (Model G) and global (Model H) parameters from Devred et al (2006) which were both derived from data that included pico-, nano- and microplankton, such that the proportion of the large-cell population can be seen as exclusively microplankton The Devred et al (2006) method focused on two size classes, the microplankton size class and the combined nano-picoplankton size class Following the Uitz et al. (2006) technique, when the percentage of microplankton was greater than 45 %, the pixel was allocated as dominated by microplankton, and the rest of the pixels allocated as dominated by combined nano-picoplankton

3.3.1.6 Model I (Brewin et al., 2010c)

The model of Brewin et al. (2010c) uses the spectral shape of the absorption coefficient of phytoplankton to determine satellite pixels dominated by pico-, nano- or microplankton. The model may be implemented into an IOP model that can determine the spectral shape of $a(\lambda)$ (without making any assumptions in its determination, e.g. Lee et al., 2002) or alternatively the spectral shape of $a(\lambda)$ may be determined from an abundance-based parameter (e.g. chlorophyll-a (C^s)). Therefore, like the model of Devred et al. (2006), the Brewin et al. (2010c) model may be used as a spectral-response or abundance-based approach. Using a satellite and *in situ* match-up dataset, Brewin et al. (2010c) found that using C^s to determine the spectral shape of $a(\lambda)$ was considerably more accurate than using the IOP model of Lee et al. (2002), which failed to accurately reproduce the spectral shape of $a(\lambda)$ (see Table 2 and Figure 5 of Brewin et al., 2010c). When implementing the Brewin et al. (2010c) model, the spectral-shape of the absorption coefficient of phytoplankton ($a(\lambda)$) was determined from C^s and it is therefore considered an abundance-based model in this intercomparison.

Using parameters given in Table 3 of Brewin et al. (2010c), the absorption coefficient of phytoplankton ($a(\lambda)$) was calculated at six wavelengths (443, 510, 520, 530, 550 and 555 nm) using C^s. The spectral shape of the absorption coefficient of each sample was then calculated by normalising each wavelength to its value at 443 nm. Then by comparing the spectral shape at 510, 520, 530, 550 and 555 nm, estimated from the satellite data, with derived *in situ* PSC spectral shapes from HPLC data (using NOMAD and data from the Benguela, see Table 1 of Brewin et al., 2010c), and using equations 9-14 in Brewin et al. (2010c), a pixel was assigned to be dominated by pico- nano- or microplankton. Of all the models used in this intercomparison, the Hirata et al. (2008a) and Brewin et al. (2010c) models (Models D, E, F and I) were the only approaches that did not need to be reformulated to detect dominant PSC.

3.3.1.7 Model J (Raitsos et al., 2008)

The Neural Network approach of Raitsos et al. (2008) was run using the spatial (latitude and longitude), temporal (month), bio-optical (C^s, $L_{wn}555$), and physical (PAR, SST, and wind stress) match-up data. The approach is designed to determine the probability of four PFTs (diatoms, dinoflagellates, silicoflagellates, and coccolithophores) occurring in a satellite pixel (probability ranged from 0 to 1, 0 being not present 1 being present) in addition to the probability of none of these PFTs occurring (referred to as 'non-dominance', see Raitsos et al., 2008).

The Raitsos et al. (2008) approach was developed using CPR data. Here an arbitrary assumption is made that the 'non-dominance' category can be referred to as the probability of picoplankton occurring in a satellite pixel. It can be assumed that

the dominant phytoplankton size was smaller than 10 μm when a 'non-dominance' response occurred in the CPR filter (Richardson et al., 2006, Raitsos et al , 2008). While it is acknowledged that nanoplankton can range from 2 to 10 μm, this assumption is based on the fact that silicoflagellate and coccolithophore cells can range from 2 to 10 μm, and that these groups may also be identified using this satellite approach and classified as nanoplankton Nonetheless, it is acknowledged that this assumption has to be used cautiously when analysing the results.

A dominant microplankton satellite pixel was allocated where either the diatom or dinoflagellate group had the highest probability of occurring, a dominant nanoplankton pixel was allocated where either the silicoflagellate or coccolithophore group had the highest probability of occurring, and a dominant picoplankton pixel was allocated where the 'non-dominance' category had the highest probability of occurring.

3.3.2 Comparison with *in situ* data

All methods were applied to the satellite data and compared to the *in situ* HPLC data As a sub-set of the CPR data was used to develop model J, this model was not tested on the CPR data to avoid potential biases in the intercomparison As model A and model J were developed using 9 km as opposed to 1 km resolution SeaWiFS data, they were not applied to the L4 dataset Only pixels that met the selection criteria for models A, B and J were used when testing these approaches in the intercomparison. Furthermore, model A was only tested using pixels where the model detected a dominant phytoplankton group as opposed to including pixels where an unidentified group was determined. This reduced the number of HPLC comparison data points from 608 to 377 for model J, 248 for model B and 180 for model A For the L4 dataset the number of comparison data points was reduced from 256 to 98 for model B, and for the CPR dataset from 5561 to 1724 for model A and 3284 for model B

Two methods were used to compare the satellite approaches with the *in situ* data The first method, referred to as method 1, was designed to provide a robust calculation of the probability of detection of each size for each model This method was designed to account for potential uncertainty in both the satellite and *in situ* measurements The second method, referred to as method 2, was used to test interclass errors and misclassifications in the satellite approaches

3.3.2.1 Method 1: Probability of detection

A method similar to Hirata et al. (2008a) was used to analyse the performance of the satellite-derived PSCs when compared with *in situ* match-ups This method is based on a scoring technique, with a correct classification indicating 2 points, a near-correct classification 1 point, and an incorrect classification indicating 0 points.

For each match-up, the satellite approaches were run on the mean, the mean plus the standard deviation and the mean minus the standard deviation of the 9 pixels using their respective satellite input, yielding three results for each model. If any of the three results matched the dominant *in situ* size class a correct classification (2 points) was assigned. In the few cases where the three results span more than one size class, providing one of these results matched the dominant *in situ* size class, a correct classification (2 points) was still assigned. This was deemed appropriate given uncertainty due to the contrasting observational scales (temporal and spatial) between *in situ* and satellite data, and considering the variability around the *in situ* sample as indexed by the satellite measurements.

For the near-correct classification criteria, if no correct classification was recorded the *in situ* data were re-analysed to assess a more mixed environment where there could be co-dominance of two size classes. For the HPLC DPA data, where the dominant size had a DPA ratio greater than 0.45 the data was also assessed to find if another size class had a DPA ratio of greater than 0.4 (based on an uncertainty estimate of 9.3 % for the ratio of accessory pigment to total chlorophyll, Claustre et al., 2004, i.e. +/− 0.05) at the same point, if so, a second dominant size class was recorded. For CPR and L4 cell counts, if a second size class had a Z-factor within 0.025 of the dominant size class (based on calculated 95 % confidence levels when pooling CPR and L4 data), it was recorded as a second dominant size class. If any of the three satellite results matched the second dominant size class, a near-correct classification (1 point) was recorded. Otherwise, where there were no matches in any of the three satellite results, an incorrect classification (0 points) was recorded. The results were then converted into a percentage for each size class by dividing the number of points calculated for each technique by the maximum possible number of points and multiplying by one hundred. This methodology was applied to all the datasets. A flow chart of the validation procedure is shown in Figure 3.2.

For each model and each size class, 95 % confidence intervals were derived from the standard error of the mean percentage and the *t*-distribution of the sample size. Confidence levels provide a very powerful way of showing differences and similarities between many groups (Dythan, 2003). If the 95 % confidence intervals of two or more models overlapped then it was interpreted that the models performance was statistically similar in the comparison. If the 95 % confidence intervals of two or more models did not overlap, then it was interpreted that the models performance was statistically different in the comparison.

3.3.2.2 Method 2: Misclassification matrices

In order to test inter-class errors in the satellite approaches, misclassification matrices were adopted (Guptil, 1989; Nathanail and Rosenbaum, 1995). Figure 3.3 shows an example of a misclassification matrix. In the matrix (Figure 3.3 a), points

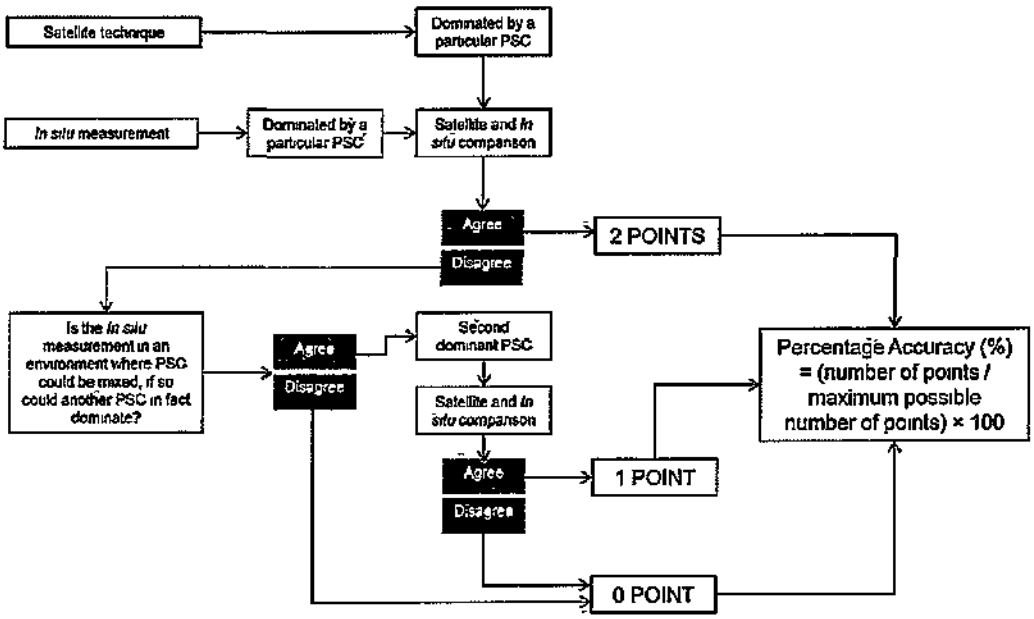

Figure 3.2 Flow chart describing the validation procedure used in method 1 to test the probability of detection by the different satellite approaches

on the leading diagonal have been correctly classified (Nathanail and Rosenbaum, 1995) An error of omissions occurs when a satellite prediction fails to recognize a size class that should have been identified according to the *in situ* sample This is calculated according to the sum of the column less the leading diagonal cell value, divided by the sum of the column and multiplied by one hundred (see Figure 3 3 a) An error of commission occurs when a satellite prediction incorrectly identifies a pixel as a different size class This is calculated according to the sum of the row less the leading diagonal cell value, divided by the sum of the row and multiplied by one hundred (see Figure 3 3 a)

A scatter plot of the errors of omission and commission in the dataset (Figure 3 3 b) allows the size classes that have been poorly defined by the satellite approach to be readily identified (Nathanail and Rosenbaum, 1995) Each size class in the matrix is represented by a single point on the plot with the error of omission as the ordinate and the error of commission as the abscissa Points lying above the 45° line represent classes whose definition is too narrow leading to false exclusion of members of that size class, whereas points lying below the 45° line represent classes whose definition is too broad leading to false inclusion of members of other size classes. Points lying far from the origin reflect higher error, and points lying closer to the origin reflect lower error.

For method 2, only the *in situ* data for which a single dominant size class occurred were used (samples from the near-correct criteria in Method 1 were eliminated from the datasets); this reduced the number of samples to 547 HPLC samples using the

(a)

Satellite estimate	*In situ* database: Pico	Nano	Micro	Σ (row)	Error of commission (%)
Pico	196	20	3	219	10.5
Nano	110	56	14	180	68.9
Micro	14	8	132	154	14.3
Σ (column)	320	84	149		
Error of omission (%)	38.8	33.3	11.4		

Error of commission (%) = {[Σ(row) – (Leading diagonal cell value)] / Σ(row)} × 100

Error of omission (%) = {[Σ(column) – (Leading diagonal cell value)] / Σ(column)} × 100

(b)

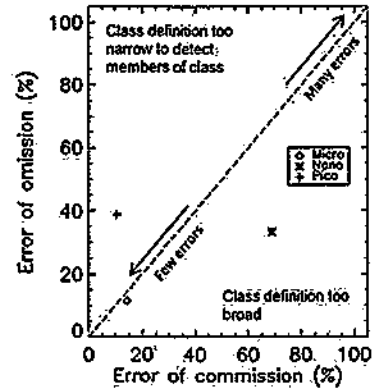

Figure 3.3: Example of a misclassification matrix used in method 2 (a) and a scatter plot of omission against commission for each class in the misclassification matrix (b).

Vidussi et al. (2001) DPA, 571 HPLC samples using the DPA of Hirata et al. (2008a), 5575 CPR samples and 246 L4 samples. For each match-up, a single dominant size class was determined for each model by calculating the most frequent size class from the three match-up results. The satellite approaches were then compared with the *in situ* data using the misclassification matrix.

3.4 Methodological Uncertainties

There are four main areas of methodological uncertainty within the analysis. Firstly, there are measurement errors. In this chapter, the *in situ* data is essentially deemed to be the truth, whereas, in reality *in situ* measurements also have associated errors. Measurement outliers were minimised for the HPLC analysis through robust quality control procedures (see Aiken et al., 2009), however, an intercomparison of HPLC pigment methods indicates instrument error of 7 % for chlorophyll-a (C) and on average 21.5 % for other pigments (ranging from 11.5 % for fucoxanthin to 32.5 % for peridinin; Claustre et al., 2004). When comparing satellite data with *in situ* data, errors can occur due to the observational scales of the two types of measurements. The L4 cell count data was typically analysed using 10 to 100 ml samples, which are then compared with 3 km × 3 km satellite data, assuming the satellite penetrates to 10 m depth; this equates to a volume of water of 0.09 km^3. The HPLC data was typically taken in volumes of sea water in the order of 5 l, whereas satellite measurements used for this chapter were typically representative of 27 km × 27 km, equating to an approximate volume of water of 7.29 km^3. This is quite a contrast in volume when compared with the *in situ* measurements. Furthermore, there are additional errors with the satellite approaches associated with atmospheric correction and the performance of the satellite sensor itself.

Secondly, there are errors associated with the use of pigment concentration to

determine size class The HPLC DPA, as highlighted in section 2 2.2 3, does not strictly reflect the true size of phytoplankton. PFT or PSC techniques that have been developed using a specific *in situ* method, such as HPLC, are expected to perform better when compared to *in situ* data measured in the same way This is the case of all models except B, G, H and J and will need to be taken into account when analysing the results from the HPLC data Due to the size of the CPR mesh silk, and the fact that the CPR samples cannot quantitatively calculate the contribution of each size class, the CPR dataset is essentially a semi-qualitative estimate of dominant microplankton samples, which will also have to be considered when analysing the results Furthermore, with regard to the L4 data, there is expected to be higher uncertainty in the picoplankton cell counts in comparison with nano- and microplankton cell counts, due to the difficulty in counting smaller size classes when using an inverted microscope

Thirdly, with regard to the satellite algorithms, each method is very different in its approach and it is thus very difficult to make a quantitative comparison with the *in situ* data This intercomparison focuses primarily on size class, whereas models A and J look at specific taxonomic groups They do not attempt to account for all the taxonomic groups within a size class that this study is assuming, although model A is based on the same specific diagnostic pigments as in the other HPLC based approaches.

Finally, this intercomparison is assessing dominance of phytoplankton size classes, and some of the approaches have been adapted to fit this criterion in order to make the satellite techniques inter-comparable Therefore, methods 1 and 2 are specifically designed to test dominance based approaches Approaches that derive fractional contributions (e g models C, G and H) may fare differently in an inter-comparison based on fractional contributions. It is important to bear in mind these methodological uncertainties when discussing the performance of the algorithms

3.5 Results

3.5.1 Method 1 results

Table 3.1 and Figures 3 4 to 3.7 show the results from method 1 The error bars in these figures represent the 95% confidence levels In the case of the HPLC results (Figure 3 4), using the Vidussi et al. (2001) DPA procedure and concerning microplankton alone, models C, F, G, H and I were found to perform with higher accuracy (90 1-92 9%) than models A, B, D and E (27 8-75.6%). Model J however, was not significantly different from models C, E, F, G, H and I. Furthermore, models E and J performed with higher accuracy (75 6-79 3%) than models A, B and D (36 5-52.2%), and models A, B and D were not statistically different. Results using the Hirata et al (2008a) DPA procedure (Figure 3.5) and concerning microplankton

alone, indicated that models C, E, F, G, H, I and J were found to perform with higher accuracy (75.8-93.3 %) than models A, B and D (33.3-52.2 %) although they were not significantly different from model A. Concerning combined nano-picoplankton, in both DPA procedures (Figures 3.4 and 3.5), all models were found to perform with similar accuracy (>88.4 %).

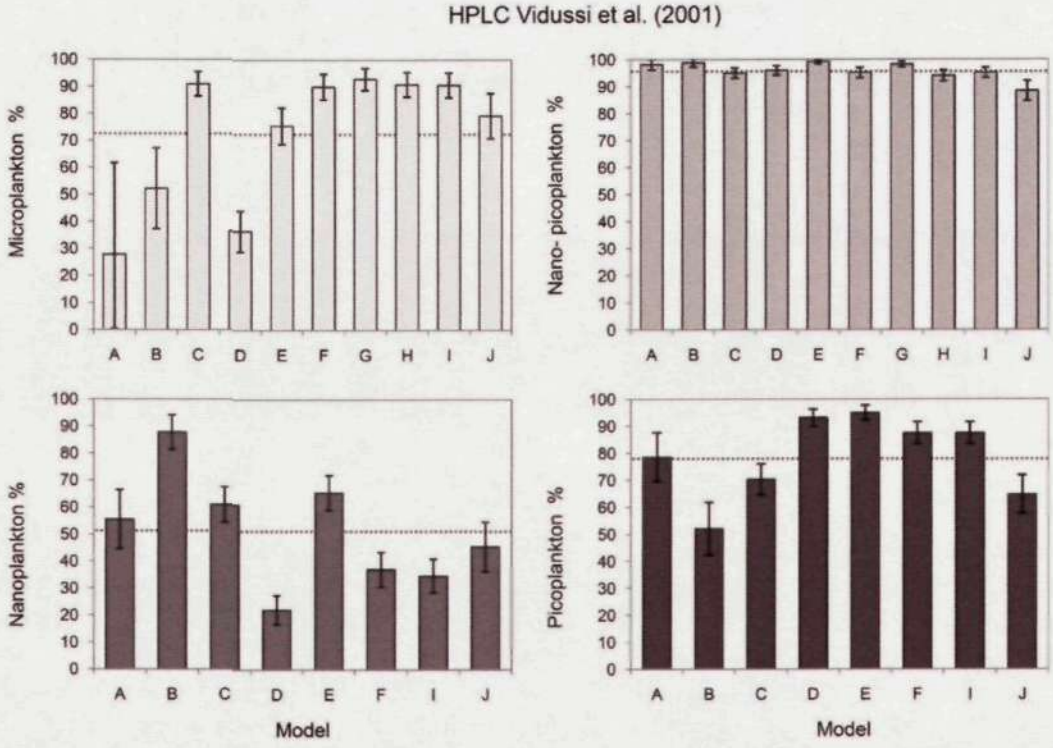

Figure 3.4: Histograms showing the score (%) of satellite-derived versus *in situ* dominant PSCs for several algorithms using method 1 for HPLC data using the Vidussi et al. (2001) DPA procedure. The error bars represent the 95 % confidence intervals and the dotted line represents the mean of all models.

Concerning nanoplankton, in the Vidussi et al. (2001) DPA procedure (Figure 3.4), model B performed with the highest accuracy (87.7 %), followed by models C and E (61.0-65.5 %). However, model A was not significantly different from models C and E, and model J was not significantly different from models A and C. Models A, F, I and J performed with higher accuracy than model D. Concerning nanoplankton, using the Hirata et al. (2008a) DPA procedure (Figure 3.5), models B, C, E, F and I performed with higher accuracy (73.6-88.2 %) than model D. Models A, B, C, E, F, I and J were not statistically different from each other, and models A, D and J were not statistically different from each other. Concerning picoplankton, in both the Vidussi et al. (2001) and Hirata et al. (2008a) DPA procedures (Figures 3.4 and 3.5), models D, E, F and I performed with higher accuracy (87.4-95.9 %) than models A, B, C and J. However, in Vidussi et al. (2001) DPA procedure, models F and I were not significantly different from model A and models C and J were not statistically different. In the Hirata et al. (2008a) DPA procedure (Figure 3.5),

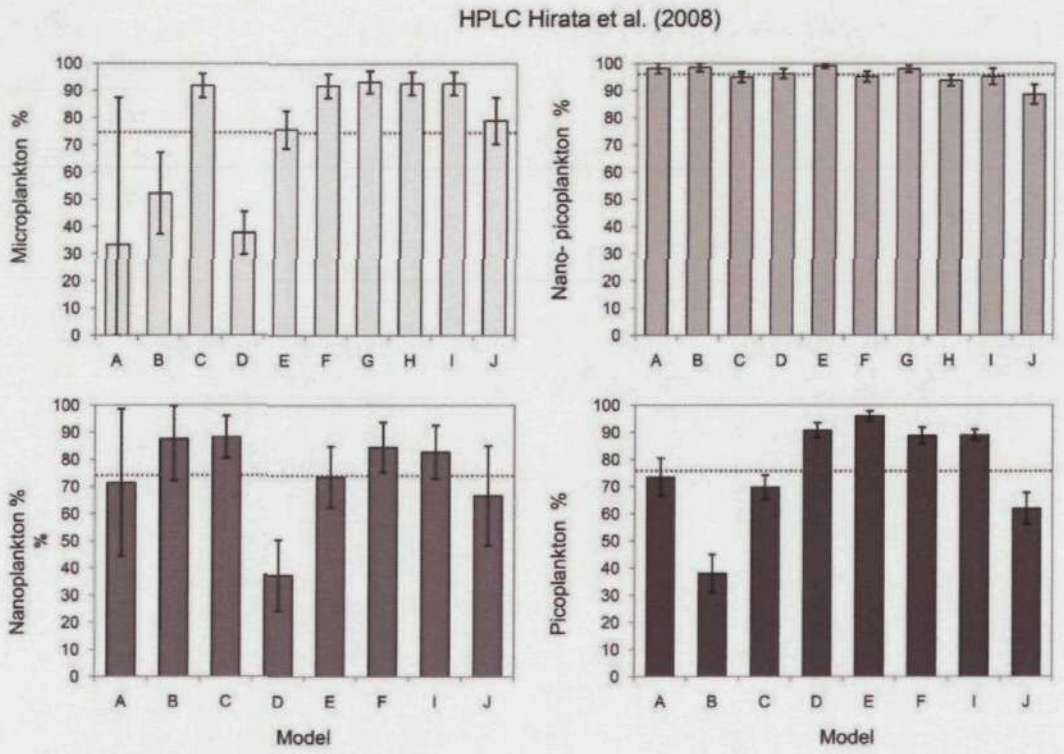

Figure 3.5: Histograms showing the score (%) of satellite-derived versus *in situ* dominant PSCs for several algorithms using method 1 for HPLC data using the Hirata et al. (2008a) DPA procedure. The error bars represent the 95 % confidence intervals and the dotted line represents the mean of all models.

model J performed with higher accuracy than model B. The mean percentage of all the models combined, using the HPLC dataset and the Vidussi et al. (2001) DPA procedure, was 72.7 %, 95.8 %, 51.1 % and 78.1 % for microplankton, combined nano-picoplankton, nanoplankton and picoplankton respectively. The mean percentage of all the models combined, using the HPLC dataset and the Hirata et al. (2008a) DPA procedure, was 74.0 %, 95.8 %, 74.0 % and 75.9 % for microplankton, combined nano-picoplankton, nanoplankton and picoplankton respectively.

Regarding the L4 comparison (Figure 3.6), and concerning microplankton, models C, G, and H performed with slightly higher accuracy than models D and E (74.3-80.5 %). Concerning combined nano-picoplankton, model E was found to perform with higher accuracy than all other models (98.7 $\pm$1.8 %), model D also was found to perform with higher accuracy than models C, F, G, H and I, but was not statistically different from model B. Concerning nanoplankton all models were similar (39.9-77.4 % accuracy) with models B and E performing significantly higher than model D. Regarding picoplankton, models D and E were found to perform with the highest accuracy (73.4 $\pm$10.0 %). The mean percentage of all the models combined, using the L4 dataset, was 67.9 %, 64.3 %, 58.4 % and 26.4 % for microplankton, combined nano-picoplankton, nanoplankton and picoplankton respectively. PSC percentages retrieved pre-2002 were compared with post-2002 percentages and a

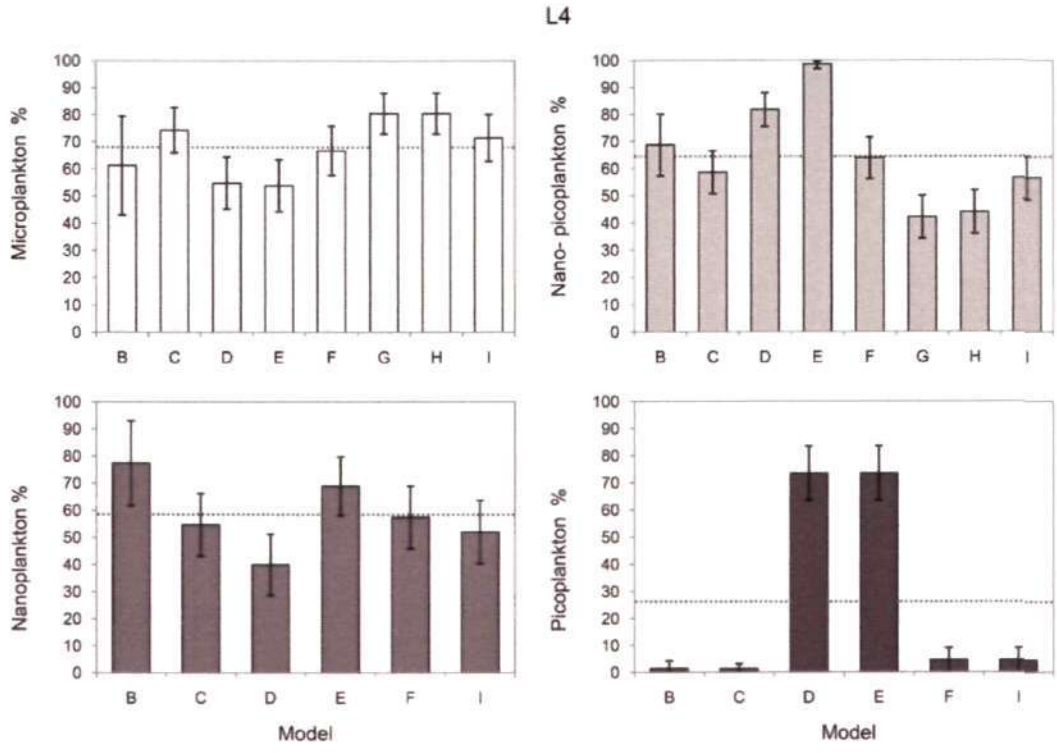

Figure 3.6: Histograms showing the score (%) of satellite-derived versus *in situ* dominant PSCs for several algorithms using method 1 for L4 data. The error bars represent the 95 % confidence intervals and the dotted line represents the mean of all models.

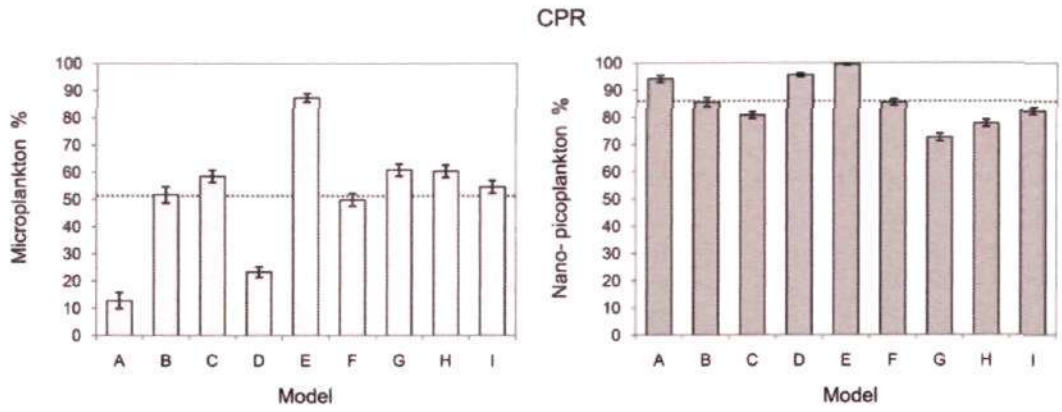

Figure 3.7: Histograms showing the score (%) of satellite-derived versus *in situ* dominant PSCs for several algorithms using method 1 for CPR data. The error bars represent the 95 % confidence intervals and the dotted line represents the mean of all models.

significant statistical correlation was found (p-value <0.05) supporting the pre-2002 L4 match-up procedure described in section 3.2.2.

Regarding the CPR comparison (Figure 3.7), and concerning microplankton, model E performed with the highest accuracy (87.4 ±1.5 %), followed by models G, H, C, I, B, and F which performed with higher accuracy than models A and D.

Model D performed with higher accuracy than model A. Concerning combined nano-picoplankton, model E performed with the highest accuracy (99.5 ±0.2 %) followed by models D and A, then models B and F. Models C, H and I performed with higher accuracy than model G. The mean percentage of all the models combined, using the CPR dataset, was 51.0 % and 86.0 % for microplankton and combined nano-picoplankton respectively.

3.5.2 Method 2 results

Figure 3.8 shows the scatter plots of omission against commission for each size class for (a) HPLC derived using Vidussi et al. (2001), (b) HPLC derived using Hirata et al. (2008a), (c) L4 data and (d) CPR data. Consistent with method 1 the models are generally found to detect combined nano-picoplankton with the highest accuracy as indicated by their representative points lying closer to the origin when compared with other size classes.

When comparing the two DPA procedures (Figure 3.8 a and b), while the results for the micro- and combined nano-picoplankton are similar, the results from the pico- and nanoplankton were different. Figure 3.8a indicates that when using the Vidussi et al. (2001) DPA technique, all the picoplankton data points (with the exception of models B and J) lie below the 45 ° line, implying that the satellite models' detection of this size class is too broad and that they are incorrectly trapping members of other size classes. Alternatively, the nanoplankton data points appear to lie above the 45 ° line, implying that the satellite models' are poorly identifying nanoplankton and that their detection of this size class is too narrow. When using the Hirata et al. (2008a) DPA (Figure 3.8 b) all the nanoplankton data points appear to lie below the 45 ° line implying that all the models' detection of this size class is too broad. Both DPA procedures indicate that the models appear to detect picoplankton with higher accuracy than nanoplankton, as the picoplankton points lie closer to the origin, consistent with the mean percentages of all models shown in method 1 (HPLC data, using Vidussi et al. (2001) DPA).

Regarding the L4 dataset and taking all the results from the models into account, there appears to be no obvious bias with all points lying evenly around the 45 ° line (Figure 5 c). However, individually, models D and E appear to be detecting combined nano-picoplankton too broadly and microplankton too narrowly, conversely, models B, C, F, G, H and I appear to be detecting microplankton too broadly and combined nano-picoplankton too narrowly. Models F and I appears to also classify picoplankton too narrowly. Regarding the CPR dataset (Figure 3.8 d), models A, D, and E appear to classify combined nano-picoplankton too broadly and microplankton too narrowly, and models B, C, F, G, H and I lie evenly around the 45 ° line implying no obvious bias.

With regard to model B, by placing limits on the S_f values the model appeared

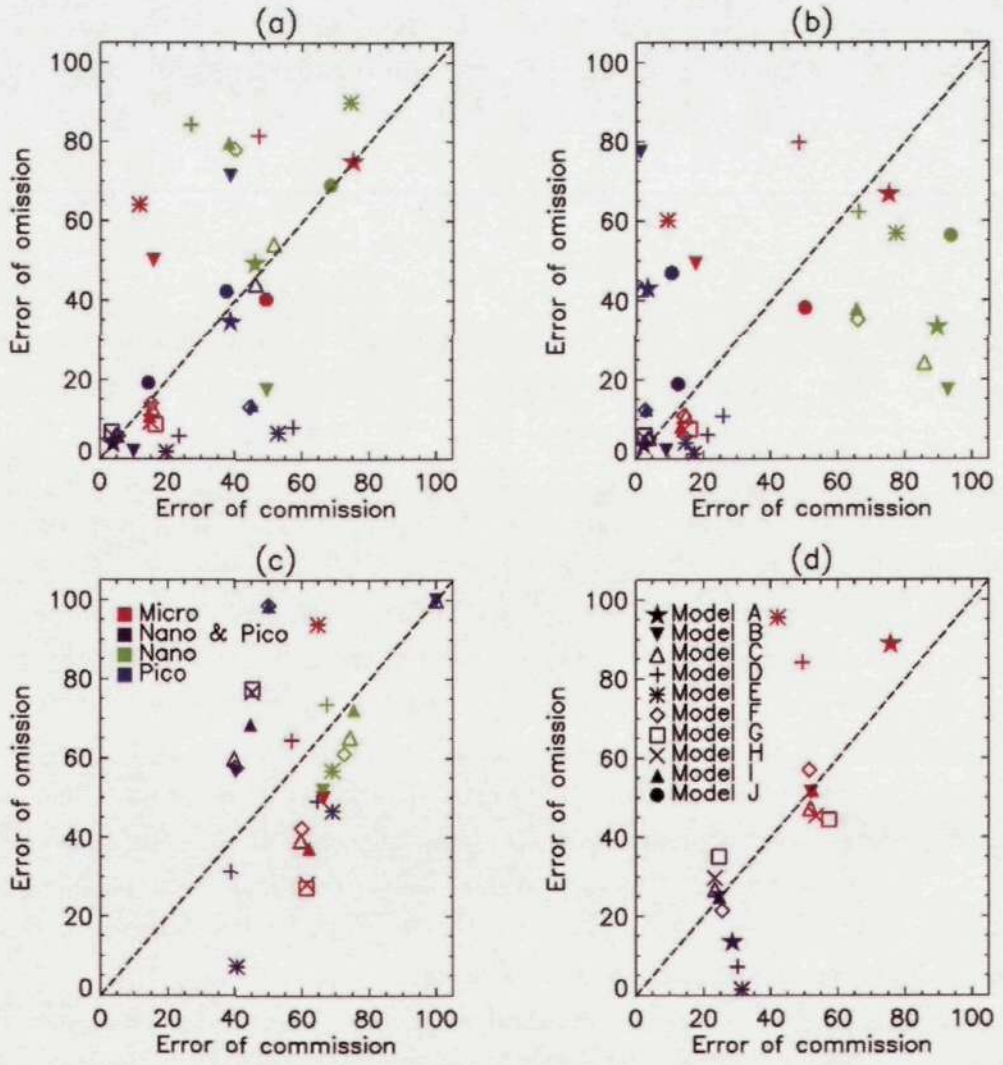

Figure 3.8: Scatter plots of omission against commission for each size class in method 2 for (a) HPLC derived *in situ* using Vidussi et al. (2001), (b) HPLC derived *in situ* using Hirata et al. (2008a), (c) L4 *in situ* data and (d) CPR *in situ* data.

to be detecting pico- and microplankton too narrowly and nano- and combined nano-picoplankton too broadly, when compared with the HPLC data (see Figure 3.8 a and b). Note that this result is reflected in the HPLC data in method 1 (Figures 3.4 and 3.5) as model B performs accurately at detecting nanoplankton (87.5-87.7 %) and combined nano-picoplankton (~98.5 %), and less accurately at detecting picoplankton (38.0-52.0 %) and microplankton (~52.2 %). By detecting nanoplankton too broadly, model B appears to misclassify pico- and microplankton pixels as nanoplankton. S_f values derived from model B were proposed as a continuum for co-varying pigment packaging and cell size, not for detecting dominant PSC, and placing limits was not intended.

Results from Figure 3.8 (a and b) indicate that the S_f value of 0.74 was too large to accurately split the pico- and nanoplankton population (at 2 μm) and the S_f value of 0.24 was too small to accurately split the combined nano-picoplankton

and microplankton population (at 20 μm). Therefore, using the Vidussi et al. (2001) DPA procedure on the HPLC data, the S_f value was consecutively reduced from 0.74 (at 2 μm) by 0.01 in each iteration until the nano- and picoplankton data points converged on the 45 ° line in Figure 3.8 (a) and the S_f value was consecutively increased from 0.24 (at 2 μm) by 0.01 in each iteration until the combined nano-picoplankton and microplankton population data points converged on the 45 ° line in Figure 3.8 (a). This indicated that S_f values of 0.64 at 2 μm and 0.32 at 20 μm were more adequate and prevented model B detecting pico- and microplankton too narrowly and nano- and combined nano-picoplankton too broadly. Furthermore, these values compliment comparisons of S_f to the proportion of micro- and picoplankton >0.45 (using the DPA procedure of Vidussi et al., 2001; Uitz et al., 2006) using a variety of data gathered by the Laboratoire d'Océanographie de Villefranche (see Bricaud et al., 2006).

Model B was re-run in method 1 (referred to as model B2) using the new S_f values at 2 and 20 μm. Results for model B2 are shown in Table 3.1. Regarding the HPLC data, results for picoplankton are shown to improve significantly, increasing from 52.0±9.8 % to 77.2±8.3 % for the Vidussi et al. (2001) DPA procedure and from 38.0±7.0 % to 68.4±6.7 % for the Hirata et al. (2008a) DPA procedure. For both DPA procedures, results for microplankton are also shown to improve significantly from 52.2±15.0 % to 84.4±11.0 % and results for the combined nano-picoplankton and nanoplankton did not change significantly. Such results clearly emphasise how misclassification matrices may be used to improve model designs.

When comparing the results from methods 1 and 2 certain discrepancies arise. In method 1 (Figures 3.4 to 3.7), Model E generally performs above the average of all models and consistently performs better than Model D at detecting nano- and microplankton in the HPLC and CPR datasets. However, according to method 2, Model E performs similarly to Model D across the three size classes and appears to perform less accurately than one would expect after examining results from method 1 (points do not lie very close to the origin in Figure 3.8). Closer analysis revealed that the variability in $a(443)$ around each sample site (9 satellite pixels), when using the Smyth et al. (2006) model, was consistently higher than when using the Lee et al. (2002) model, particularly at higher $a(443)$ values. According to method 1, a correct classification (2 points) was assigned when any of the mean, the mean plus the standard deviation and the mean minus the standard deviation of the 9 pixels matched the *in situ* sample. In method 1, Model E may have benefited from higher variability in $a(443)$ around each sample site, which would explain the discrepancies between the performance of model E in method 1 when compared with the performance of model E in method 2, particularly considering method 2 did not account for model input variability around each sample site.

3.6 Analysis of intercomparison results

The HPLC data used in this chapter was taken from a wide geographical area, incorporating the North and South Atlantic Oceans, the North Pacific gyre and the Mediterranean Sea, and thereby covering a number of trophic regimes. When analysing the HPLC results in methods 1 and 2 from an integrative perspective, it becomes apparent that dominant pico-, combined nano-picoplankton and microplankton pixels are, in general, more easily detected than nanoplankton pixels from satellite, as indexed by the mean percentages of all models using the Vidussi et al. (2001) DPA (95.8 % for combined nano-picoplankton, 72.7 % for microplankton, 78.1 % for picoplankton and 51.1 % for nanoplankton) and considering that nanoplankton data points lie further from the origin in Figure 3.8 (a) and (b) than other size classes. Irigoien et al. (2004) investigated global biodiversity patterns in marine phytoplankton and found their diversity to be a unimodal function of phytoplankton biomass, with maximum diversity at intermediate levels of biomass and minimum diversity at high and low levels of biomass. Assuming nanoplankton prevail at intermediate biomass (Irigoien et al., 2004; Aiken et al., 2008) one may expect higher diversity in nanoplankton than pico- or microplankton, which may result in greater variability in their optical characteristics making them harder to detect, as a community, from satellite.

Conversely, however, at the L4 site micro- and nanoplankton had a higher mean percentage when combining all models (67.9 % and 58.4 %) than picoplankton (26.4 %). This result, to a certain extent, can be attributed to the location of the L4 site which is essentially in a case 2 region (depending on seasonal physical forcing, see Groom et al., 2009). The chlorophyll-based models (C, F and I) performed particularly poorly at detecting picoplankton, lowering the integrative mean percentage. Furthermore, model B, which uses a non-linear relationship between chlorophyll-a and $a(505)$ to normalise the derived absorption spectrum (see equation 10; Ciotti and Bricaud, 2006), also performed poorly at detecting picoplankton. This may be linked to the fact that the satellite estimate of chlorophyll-a, acquired using the OC4 SeaWiFS algorithm, is known to be frequently overestimated in case 2 regions. Considering that the chlorophyll-based models rely on low chlorophyll-a values to detect picoplankton, and that the derived absorption spectrum used in model B is normalised using an $a(505)$ to chlorophyll-a relationship, this would be expected to influence the models' results significantly. Improvements in the two IOP-based models (D and E) at detecting picoplankton could be due to the advantage of using an IOP model in optically complex case 2 regions where it is important to partition and quantify the influence various organic and inorganic water constituents have on the reflectance spectrum. All the models used are designed for open ocean waters (case 1), so their application to case 2 waters has to be handled cautiously.

When comparing spectral-response, ecological and abundance-based models, it

firstly becomes apparent that, in general, models A, B and J (two spectral-response-based models and an ecological-based model) perform with similar accuracy to the abundance-based models (models C through to I) Model J was shown to perform moderately well when compared with the HPLC data This result is encouraging for ecological methods in general, as the Raitsos et al (2008) technique is not a size-class-based approach and it is different from the other models in that it relies on additional information to that of bio-optics Considering that model J is specifically trained for the North Atlantic, it was shown to perform with fair accuracy in areas outside the North Atlantic (Note the Artificial Neural Network failed on latitudes south of the equator). This is particularly interesting considering that Raitsos et al (2008) found spatial and temporal information to be two of the three most important variables for PFT discrimination. When constraining the *in situ* pigment data to the North Atlantic, percentage accuracy did not substantially increase. The accuracy of the neural network algorithm may improve if it was trained on globally representative HPLC and cell count data Results support the conclusions in Raitsos et al. (2008) that by introducing additional information besides bio-optical information, improved satellite PSC detection may be achieved However, further analysis needs to be conducted to verify this assumption Use of advanced statistics such as neural network, self-organising maps and multilayered perceptrons, to identify additional biological information to that of chlorophyll-a from optical measurements, is a developing area of research (see Chazottes et al , 2006, 2007, Bricaud et al., 2007)

Model A performed with moderate accuracy at detecting pico- and nanoplankton, however, with lower accuracy at detecting dominant microplankton pixels It should be noted that the algorithm is designed to detect specific PFTs rather than all the PFTs within a specific size class (e g model A does not detect dinoflagellates in the microplankton size class), the diagnostic pigment fucoxanthin is the primary pigment that was used to identify diatoms in the development of model A, *as with the other HPLC abundance-based satellite approaches for detecting* microplankton. Model B was also seen to perform moderately well throughout the intercomparison, particularly at detecting nanoplankton, and improved at detecting pico- and microplankton when adjusting the S_f boundaries (model B2) This result is encouraging for model B considering that the model was validated on relatively limited data (see Ciotti and Bricaud, 2006) and that the S_f value was proposed as a continuum for co-varying pigment packaging and cell size, not to detect dominant size class.

When comparing the number of samples used to test the algorithms in Table 1 it becomes apparent that the abundance-based models (C to I) were tested against approximately twice the amount of samples tested on models J and B and approximately thrice the amount of samples tested using model A This was a consequence of the two spectral-response algorithms (models A and B) functioning on a specific cri-

terion and the ecological-based approach (model J) limited to its geographical region (Northern hemisphere). The results from method 1 indicated that the abundance-based models performed with high accuracy across the three size classes; models C, E, F, G, H and I all performed with high accuracy at detecting microplankton in the HPLC dataset (75.6-93.3%) and in the L4 and CPR datasets (49.8-87.4%). Models C and E also performed with high accuracy at detecting nanoplankton in both the HPLC and L4 datasets (54.7-88.2%) and models C, D, E, F and I performed with high accuracy at detecting picoplankton in the HPLC dataset (69.7-95.9%). Therefore, it can be concluded from this chapter that abundance-based algorithms generally provide good accuracy in detecting PSC from satellite remote sensing, suitable for wide scale application.

Surrounding the general relationship between size and chlorophyll-a there is biological variability (Bricaud et al., 2004; Uitz et al., 2006), which very likely contains information on the phytoplankton. If abundance-based models are to improve, research needs to focus on understanding the source of this biological variability and accounting for it in PSC predictions. This may include understanding diversity in the phytoplankton within each size class, or alternatively may focus on how these abundance-based relationships vary with photoacclimation to various light conditions (various incident irradiances) or with a decrease in irradiance with depth.

3.7 Summary

Ten models, designed to detect multi-phytoplankton communities from satellite data, were implemented in a phytoplankton community intercomparison exercise. The models were reformulated to detect dominant phytoplankton size class in order to make the approaches comparable and a co-located satellite and *in situ* matchup dataset was developed. Model performance was tested by: firstly, developing a robust procedure to assess the models probability of detecting a dominant phytoplankton size class pixel and, secondly, using misclassification matrices in order to test inter-class errors in the satellite models. Results from the chapter indicate:

- Spectral-response, ecological and abundance-based approaches can all perform with similar accuracy.
- Individual model performance varied according to the size of the phytoplankton, the input satellite data sources and *in situ* validation data types.
- Detection of microplankton and picoplankton were generally better than detection of nanoplankton.
- Abundance-based approaches were shown to provide better spatial retrieval of PSCs.

- The potential use of misclassification matrices as a design aid to modify models for detecting dominant PSC was highlighted
- Uncertainties in the comparison procedure and data sources were considered and indicate that improved availability of *in situ* observations is required to advance research in this field

Chapter 4

A three-component model of phytoplankton size class with applications to Earth Observation*

4.1 Introduction

In the intercomparison of different satellite approaches for detecting phytoplankton size class presented in the previous chapter, spectral-response, ecological and abundance-based approaches were found to all perform with similar accuracy in general. However, abundance-based approaches were shown to provide better spatial retrieval of PSCs. The abundance-based PSC models implemented into the intercomparison in Chapter 3 were designed to detect either the dominant PSC (e.g. Hirata et al., 2008a; Brewin et al., 2010c) or the fractional contribution of each PSC (e.g. Devred et al., 2006; Uitz et al., 2006) at a satellite pixel. Both techniques offer valuable information that can be used to validate multi-phytoplankton ecosystem models or can be used in data assimilation (Anderson, 2005; Hemmings et al., 2008). Models designed to estimate fractional contributions of various size classes, however, can offer the distinct advantage of providing more information than those that treat only the dominant class.

Based on knowledge of the abundance-based approaches implemented in Chapter 3, this chapter aims to develop a new, improved abundance-based model that calculates the fractional contributions of three PSCs for a continuum of chlorophyll-a concentrations. The model is fitted to a large pigment dataset from the Atlantic Ocean using a previously-established diagnostic pigment approach (Vidussi et al., 2001; Uitz et al., 2006) extended to account for small pico-eukaryotes in ultra-oligotrophic environments. The performance of the algorithm is tested against both a global *in*

*Aspects of this chapter are included in the following paper
Brewin, R.J.W., Sathyendranath, S., Hirata, T., Lavender, S.J., Barciela, R. and Hardman-Mountford, N.J. (2010). A three-component model of phytoplankton size class for the Atlantic Ocean. Ecological Modelling 221, 1472-1483, doi:10.1016/j.ecolmodel.2010.02.014.

situ pigment dataset and also a concurrent co-located satellite match-up dataset The model is then adapted to incorporate the effect of optical depth on the model parameters

4.2 Data and Data analysis

4.2.1 Data

To develop the model, a large HPLC pigment dataset from the AMT cruises 5-15 was quality controlled according to Aiken et al. (2009), yielding 2176 measurements The dataset was then split into two: a test dataset and a training dataset (database A and B respectively)

For database A, only data taken in the top 10 m of the water column were selected, which reduced the database to 1085 measurements Samples were then matched to Level 3 SeaWiFS daily products (24 hour window), for a 3 by 3 pixel window, following the procedure adopted in Ciotti and Bricaud (2006) but using 9 km SeaWiFS pixels (as conducted in Chapter 3) Mean satellite-derived chlorophyll-a values (C^s) (NASA OC4 algorithm O'Reilly et al , 1998, 2000) as well as the associated standard deviations were calculated for the nine pixels, as conducted in Chapter 3, yielding 250 samples Any samples for which the standard deviation exceeded three standard deviations with respect to the mean were excluded This was done in order to minimise the effect of mismatch in spatial scales of *in situ* and satellite observations The match-up yielded 241 samples spanning the period 1997-2004 The *in situ* chlorophyll-a concentrations (C) from AMT database A and the corresponding satellite chlorophyll-a concentrations (C^s) values are well correlated ($r = 0\ 71$, Figure 4 1)

Database B contained the original 2176 pigment measurements, from which the 241 match-up data were removed, leaving 1935 measurements. A third database (database C) was used for comparison and model development. This database consisted of simultaneous measurements of phytoplankton absorption coefficients and HPLC data Global pigment data from the NOMAD HPLC dataset (Werdell and Bailey, 2005) were downloaded from the NASA website (http.//seabass gsfc nasa.gov) and quality controlled as for the AMT pigment data This dataset provided surface (0-10 m) pigment and absorption measurements In addition to encompassing samples from the Atlantic Ocean, the dataset included samples from the North Pacific, the California Current, the Scotia Sea, the East China Sea and the Japan Sea Coupled pigment and absorption measurements from AMT 6 were also used in database C.

For model validation purposes, in addition to the NOMAD dataset and database A, a separate HPLC pigment dataset from AMT cruises 2-4 was set aside. This dataset was quality controlled as for database A, B and C, yielding 1158 measure-

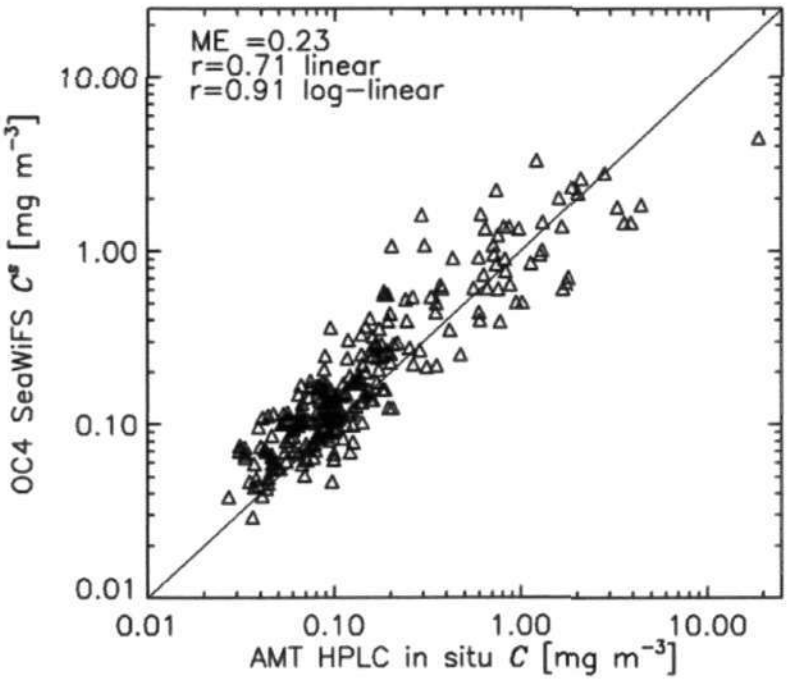

Figure 4.1: Relationship between the HPLC chlorophyll-a concentrations (C) and the satellite derived chlorophyll-a concentrations (C^s, SeaWiFS OC4) from AMT database A, black line represents 1:1 relationship.

ments and is hereafter referred to as database D. Equations 2.1 to 2.9 (section 2.2.2.3) were applied to all data to derive the size-specific fractions and chlorophyll-a concentrations needed to develop and validate the model, using the Vidussi et al. (2001) and Uitz et al. (2006) DPA. A flow chart of the analysis is shown in Figure 4.2 and the sampling locations of the observations are plotted in Figure 4.3. Finally, the model is applied to satellite data and compared with the HPLC dataset used in the intercomparison in Chapter 3.

4.2.2 Empirical adjustment to the use of diagnostic pigments *in ultra-oligotrophic environments*

Figure 4.4 (a-d) shows F_m, $F_{p,n}$, F_n and F_p as a function of the chlorophyll-a concentration (C) from database B. In addition to the raw data (light grey crosses), a 5 point running-mean (dark grey line) is also plotted to highlight the major trends in the data.

In Figure 4.4 (a) and (b) the microplankton and the combined nano- and picoplankton fractions remain relatively stable between 0.01-0.3 mg m^{-3} chlorophyll-a, before the microplankton fraction increases with increasing chlorophyll-a and the combined nano- and picoplankton fraction decreases. In Figure 4.4 (c) and (d), in ultra-oligotrophic environments (<0.04 mg m^{-3} C; Alvain et al., 2005), a distinct

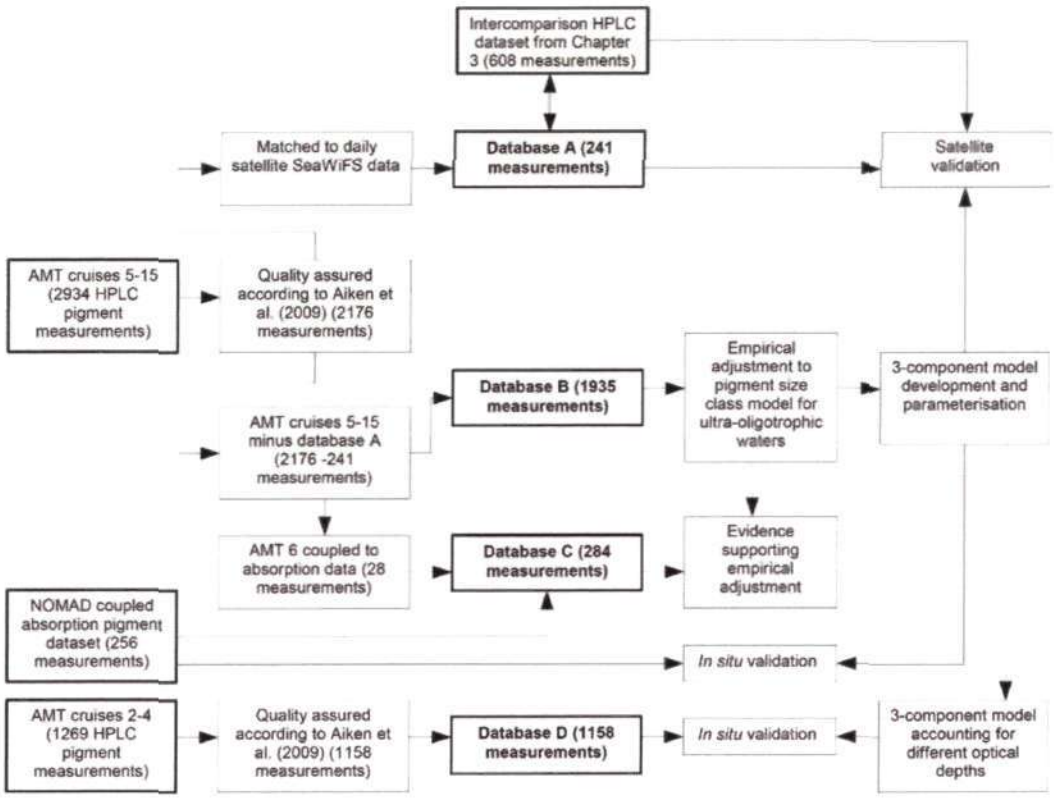

Figure 4.2: A flow chart of the data used and the processing techniques conducted to partition the data into the four databases (A-D).

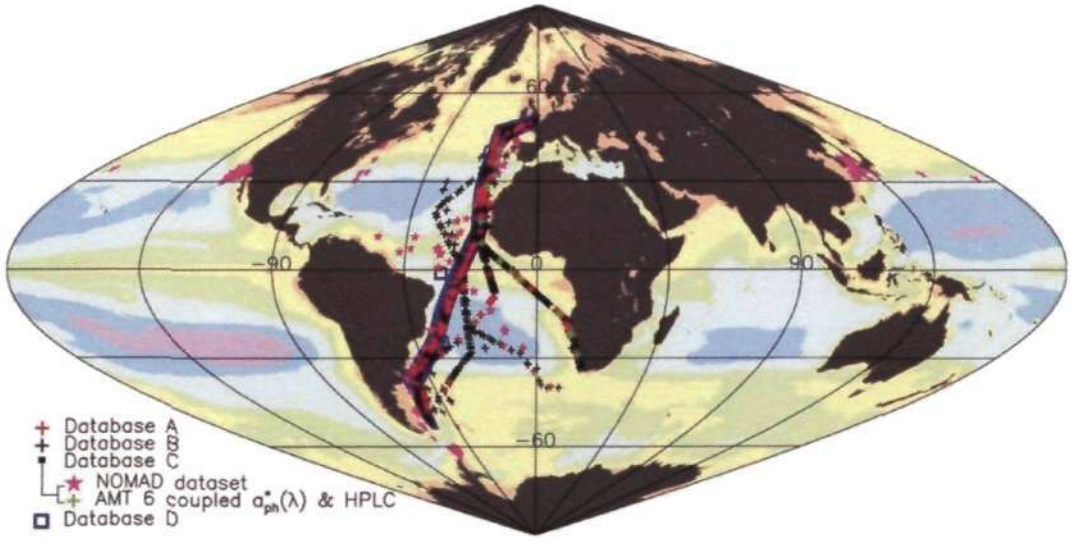

Figure 4.3: Locations of databases A-D, with the Hardman-Mountford et al. (2008) biomes classification superimposed: light orange = *very high*, light yellow = *high*, light green = *intermediate*, light cyan = *low-intermediate*, light blue = *low*, light magenta = *very low*.

and unusual trend is seen in both the nanoplankton and picoplankton fractions. The majority (~70 %) of the measurements below 0.04 mg m^{-3} chlorophyll-a were collected at depths less than 50 m suggesting this unusual trend is predominantly in

surface waters. Here the picoplankton fraction increases with increasing chlorophyll-a (between 0.01-0.04 mg m^{-3} C) and the nanoplankton fraction decreases. This contradicts the common observation that low chlorophyll-a environments in the surface layer of the ocean are essentially dominated by picoplankton (Zubkov et al., 2000; Barlow et al., 2002; Aiken et al., 2008; Hirata et al., 2008a; Aiken et al., 2009). Chisholm (1992) suggested that picoplankton contribute as much as 90 % of the total biomass in extremely oligotrophic waters. Furthermore, recent work on retrieval of particle size distribution from satellite-derived backscattering signal indicates that picoplankton-sized particles dominate in the subtropical gyres where they contribute 60 to nearly 100 % of the total particle volume (Kostadinov et al., 2009).

The data with higher computed nanoplankton fractions for concentrations less than 0.04 mg m^{-3} chlorophyll-a were analysed to see which pigment was responsible for this pattern. It was found that, on average, the ratios of 19'-butanoyloxyfucoxanthin to chlorophyll-a was 0.06, alloxanthin ratio was 0.002, and that of 19'hexanoyloxyfucoxanthin 0.43, clearly indicating that the higher nanoplankton fractions below 0.04 mg m^{-3} chlorophyll-a in Figure 4.4 (c) result from the pigment 19'hexanoyloxyfucoxanthin. Various recent studies have highlighted that at low chlorophyll-a values picoplankton dominate the eukaryotic population (e.g. Not et al., 2004; Fuller et al., 2006; Tarran et al., 2006), so the 19'hexanoyloxyfucoxanthin signal is most probably attributable to pico-eukaryotes rather than nanoplankton (Hirata et al., 2008a). Furthermore, in a recent study into the ultra-oligotrophic centre of the South Pacific Subtropical Gyre, Ras et al. (2008) speculated that 19'hexanoyloxyfucoxanthin could belong to smaller cells of the picoplankton pool, and pointed out that further information was needed to re-assess the definition of size classes relative to the pigment composition in such ultra-oligotrophic waters.

With this in mind and to test the assertion of Hirata et al. (2008a), coupled absorption and pigment data from database C were used to evaluate if the anomalously high 19'hexanoyloxyfucoxanthin signal below 0.04 mg m^{-3} of chlorophyll-a could be from picoplankton rather than nanoplankton. It is well known that picoplankton have a higher specific absorption coefficient (absorption per unit C) at the blue wavelength of 443 nm ($a^*(443)$) than nanoplankton (Sathyendranath et al., 1987; Ciotti et al., 2002; Ciotti and Bricaud, 2006) due to changes in cellular pigment composition and pigment packaging (Kirk, 1975; Morel and Bricaud, 1981). Database C was divided into dominant size classes using pigment data (Equation 2.1-2.4) and assigned a dominant size class based on a size class fraction (F_p, F_n or F_m) >0.45, as in Hirata et al. (2008a). Data points below 0.04 mg m^{-3} chlorophyll-a are identified as ultra-oligotrophic and though only two points were identified both these data points exhibited very high $a^*(443)$ values (0.22-0.31 [m^2 (mg C)$^{-1}$]), indicating that they are not nanoplankton, as suggested by the pigment analysis (Figure 4.5).

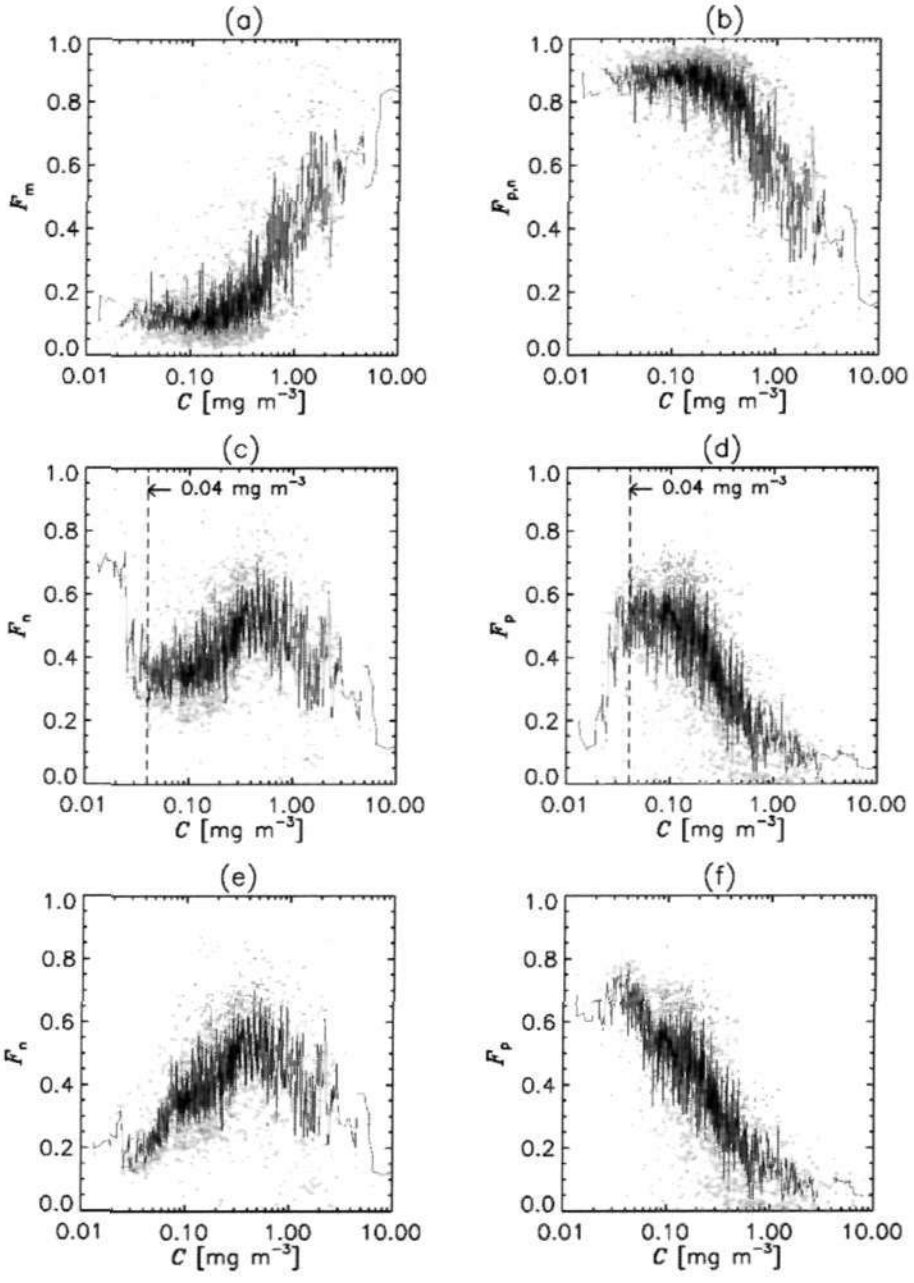

Figure 4.4: Fractions of the microplankton (a), combined nano- and picoplankton (b), nanoplankton (c) and picoplankton (d) as a function of chlorophyll-a from database B (1935 measurments). The nanoplankton (e) and picoplankton (f) fractions are re-plotted using the empirical adjustment (equations 4.1 and 4.2). Light grey crosses represent raw data and the thin dark grey line represents the 5 point running mean.

Evidence from database C, coupled to the unusual and unexplainable patterns in the nanoplankton and picoplankton fractions (database B) and supporting evidence from the literature previously cited, suggest that the use of diagnostic pigments for identifying phytoplankton size classes requires refinement in ultra-oligotrophic waters.

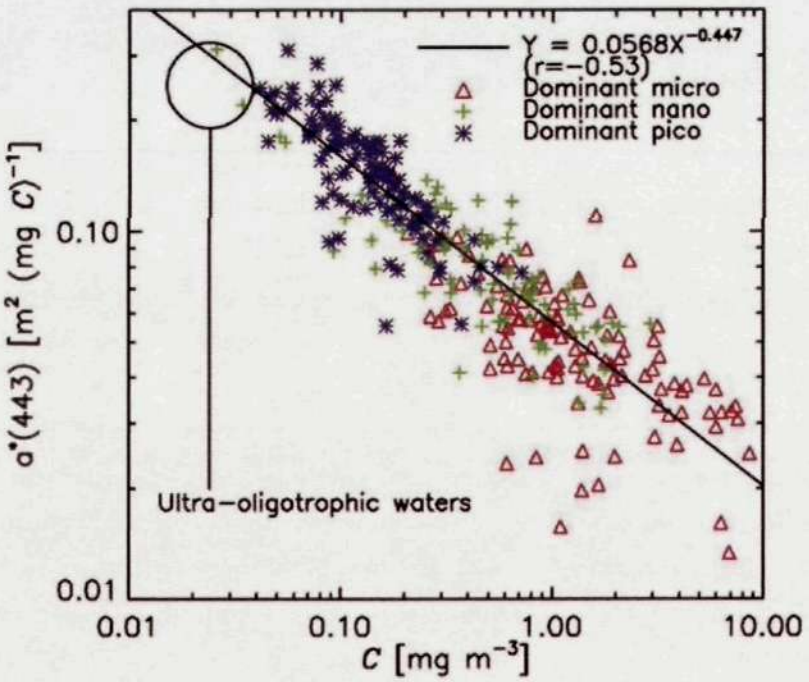

Figure 4.5: The specific absorption coefficients at 443 nm ($a^*(443)$) from database C plotted as a function of chlorophyll-a. The size class classification is from the HPLC DPA of Vidussi et al. (2001) and Uitz et al. (2006).

A linear adjustment is therefore proposed, according to which, the 19'hexanoyloxyfucoxanthin signal is attributed half to nanoplankton and half to picoplankton when the concentration of chlorophyll is $0.04\,\mathrm{mg\,m^{-3}}$, with the picoplankton fraction increasing to one at $0.001\,\mathrm{mg\,m^{-3}}$ (value used as a model endpoint) and the nanoplankton fraction increasing to one at $0.08\,\mathrm{mg\,m^{-3}}$, such that equations 2.3 and 2.4 are adjusted as follows:

$$F_n = \begin{cases} \frac{12.5CW_3P_3}{C_w} + \frac{\sum_{i=4}^{5} W_iP_i}{C_w} & \text{if } C < 0.08\,\mathrm{mg\,m^{-3}} \\ \frac{\sum_{i=3}^{5} W_iP_i}{C_w} & \text{if } C > 0.08\,\mathrm{mg\,m^{-3}}, \end{cases} \tag{4.1}$$

$$F_p = \begin{cases} \frac{(-12.5C+1)W_3P_3}{C_w} + \frac{\sum_{i=6}^{7} W_iP_i}{C_w} & \text{if } C < 0.08\,\mathrm{mg\,m^{-3}} \\ \frac{\sum_{i=6}^{7} W_iP_i}{C_w} & \text{if } C > 0.08\,\mathrm{mg\,m^{-3}}, \end{cases} \tag{4.2}$$

Figure 4.4 (c) and (d) are re-plotted in Figure 4.4 (e) and (f) using equations 4.1 and 4.2. When compared with the original pigment analysis (Figure 4.4 c-d) the adjusted results show higher pico- and lower nanoplankton fractions below $0.04\,\mathrm{mg\,m^{-3}}$ chlorophyll-a, which appear more realistic when compared with the previously cited literature. However, it is acknowledged that the proposed *ad hoc* adjustment merits re-evaluation and refinement as more data from the ultra-oligotrophic waters become available.

4.3 Methodology

4.3.1 Model development

It has been unequivocally established that the fractional contribution of small cells to the total standing crop decreases as the total chlorophyll-a concentration increases (Chisholm, 1992). Furthermore, Raimbault et al. (1988) showed that chlorophyll is added to a system by the addition of larger size classes of phytoplankton. An example of a model that accounts for these two ecological theories was published for two populations of phytoplankton by Sathyendranath et al. (2001). Devred et al. (2006) showed that the Sathyendranath et al. (2001) model may be used to estimate two phytoplankton size classes (micro- and combined nano-picoplankton).

In this section, we extend the two-component model of Sathyendranath et al. (2001) to a three-component model of phytoplankton size class. Here the total chlorophyll-a concentration (C) is assumed to be the sum of the pico- (p), nano- (n) and microplankton (m) concentrations such that

$$C = \sum_{i=1}^{3} C_i, \tag{4.3}$$

where, $i = \{p, n \text{ and } m\}$. Here, as in Devred et al. (2006), we assume that the large-celled population belongs to microplankton (C_m), and the small-celled population ($C_{p,n}$) is the sum of the nano- and picoplankton population, such that the model of Sathyendranath et al. (2001) may be written as

$$C_{p,n} = C_{p,n}^{m}[1 - \exp(-S_{p,n}C)], \tag{4.4}$$

where, $C_{p,n}^{m}$ is the asymptotic maximum value for $C_{p,n}$ and $S_{p,n}$ is the initial slope. Therefore, it follows that C_m can be calculated according to

$$C_m = C - C_{p,n}. \tag{4.5}$$

Furthermore, Figure 4.4 (b) and Figure 4.4 (f) indicate that both the picoplankton and the combined nano- and picoplankton fractions decrease with increasing chlorophyll-a. The fractions have a similar form so can be expressed by the same mathematical formulation, such that the change in C_p as C increases can also be represented as

$$C_p = C_p^{m}[1 - \exp(-S_pC)], \tag{4.6}$$

where, C_p^{m} is the asymptotic maximum value for C_p and S_p is the initial slope. Once $C_{p,n}$ and C_p are known, C_n can be calculated as:

$$C_n = C_{p,n} - C_p. \tag{4.7}$$

The fractions of each phytoplankton size class (F_p, F_n and F_m) can then be calculated by dividing the size-specific chlorophyll-a concentrations (C_p, C_n and C_m) by the total chlorophyll-a concentration (C).

To derive the unknown parameters, equations 4.4 and 4.6 were fitted to C, $C_{p,n}$ and C_p from database B. The fitting procedure used a standard, nonlinear least squares method (Levenberg-Marquardt (Press et al., 1992), IDL Routine MPFITFUN). To avoid the undue influence of large chlorophyll-a values on the parameterisation of the model, the fitting procedure was applied to log-transformed data. The performance of the model was quantified using the Mean absolute Error (ME) between the modelled and measured values (size-specific chlorophyll-a concentrations and fractions). The ME was computed according to

$$\mathrm{ME} = \frac{1}{N}\sum_{i=1}^{N}|X_E - X_M|, \tag{4.8}$$

where, X is the variable (either the size-specific chlorophyll-a concentration or the size-specific fraction) and N is the number of samples. The subscript E denotes the estimated variable and the subscript M denotes the measured variable. Values of parameters C_p^m, $C_{p,n}^m$, S_p and $S_{p,n}$ are given in Table 4.1, together with ME calculated by comparing sample values of $C_{p,n}$ and C_p in database B with the corresponding values estimated using the model.

Table 4.1: Parameter values obtained for the three-component model from database B.

Population	Maximum C	Initial Slope	Mean error
Combined nano-picoplankton	1.057 mg m^{-3} ($C_{p,n}^m$)	0.851 ($S_{p,n}$)	0.063 mg m^{-3}
Picoplankton	0.107 mg m^{-3} (C_p^m)	6.801 (S_p)	0.039 mg m^{-3}

4.3.2 Comparison with independent data

To test the accuracy of the three-component model described in section 4.3.1, two independent datasets were used; database A and the NOMAD dataset. For the *in situ* comparison, the three-component model was applied to total chlorophyll-a (C) values from the NOMAD dataset to estimate C_p, C_n and C_m. These values were compared with C_p, C_n and C_m values estimated from diagnostic pigments.

For the satellite comparison, the three-component model was applied to C^s from database A to derive C_p^s, C_n^s and C_m^s. For further comparison, the approach of Uitz et al. (2006) was also applied to C^s to derive C_p^s, C_n^s and C_m^s. The Uitz et al. (2006) approach was implemented as in Chapter 3. The results were then compared with the concurrent *in situ* size-specific chlorophyll-a concentrations (C_p, C_n and C_m) from database A.

In addition, coupled satellite chlorophyll-a and *in situ* pigment data (HPLC) from Chapter 3 (see Figure 3.1) were partitioned into biogeochemical biomes following the classification of Hardman-Mountford et al. (2008) (see Figure 4.3). The three-component model was applied to C^s from database A (to derive C_p^s, C_n^s, C_m^s, F_p^s, F_n^s and F_m^s) and results were then compared with the concurrent *in situ* values.

4.4 Results

4.4.1 Model results

Figure 4.6 (a) shows the change in percentage contribution of the three size classes of phytoplankton with increasing chlorophyll-a calculated according to the model presented in section 4.3.1. It can be seen that picoplankton dominates the total population when chlorophyll is small; as the chlorophyll increases beyond $0.20\,\mathrm{mg\,m^{-3}}$ nanoplankton begin to dominate; as chlorophyll increases beyond $1.3\,\mathrm{mg\,m^{-3}}$ microplankton begin to dominate. These boundaries are consistent (within $0.05\,\mathrm{mg\,m^{-3}}$) with boundaries calculated by Hirata et al. (2008a). Figure 4.6 (b) illustrates the change in C_p, C_n and C_m as a function of total chlorophyll-a.

To examine how well the three-component model fits database B with which it was parameterised, the model is plotted in Figure 4.7 (a-d) against C_p, C_n, $C_{p,n}$ and C_m from database B and Figure 4.7 (e-h) shows the model plotted against the fractional contributions (F_p, F_n, $F_{p,n}$ and F_m) smoothed with a 5-point running-mean. It can be seen that the model fits the observations well, indicated by low mean errors for both the chlorophyll concentrations (Figure 4.7 a-d) and the fractional contributions (Figure 4.7 e-h). AMT database B suggests a continuum from picoplankton dominated waters to nanoplankton and then to microplankton domination with increasing chlorophyll.

4.4.2 *In situ* comparison

Figure 4.8 (a-c) shows the results from the comparison with the independent NOMAD dataset. Considering that the three-component model is parameterised with pigment data taken at a variety of different optical depths, it compares well with NOMAD surface pigment measurements. This is highlighted by reasonable ME differences between the model and the NOMAD data for the three size classes (Figure 4.8 a-c). Furthermore, when comparing the modelled size-specific fractions with the NOMAD *in situ* size-specific fractions, mean errors ranged from 11.7-13.3 %, which are comparable to fractional mean errors between the model and database B (Figure 4.7 e-h). As the NOMAD dataset includes observations from a variety of global locations, this also supports the application of the three-component model to areas outside the Atlantic Ocean.

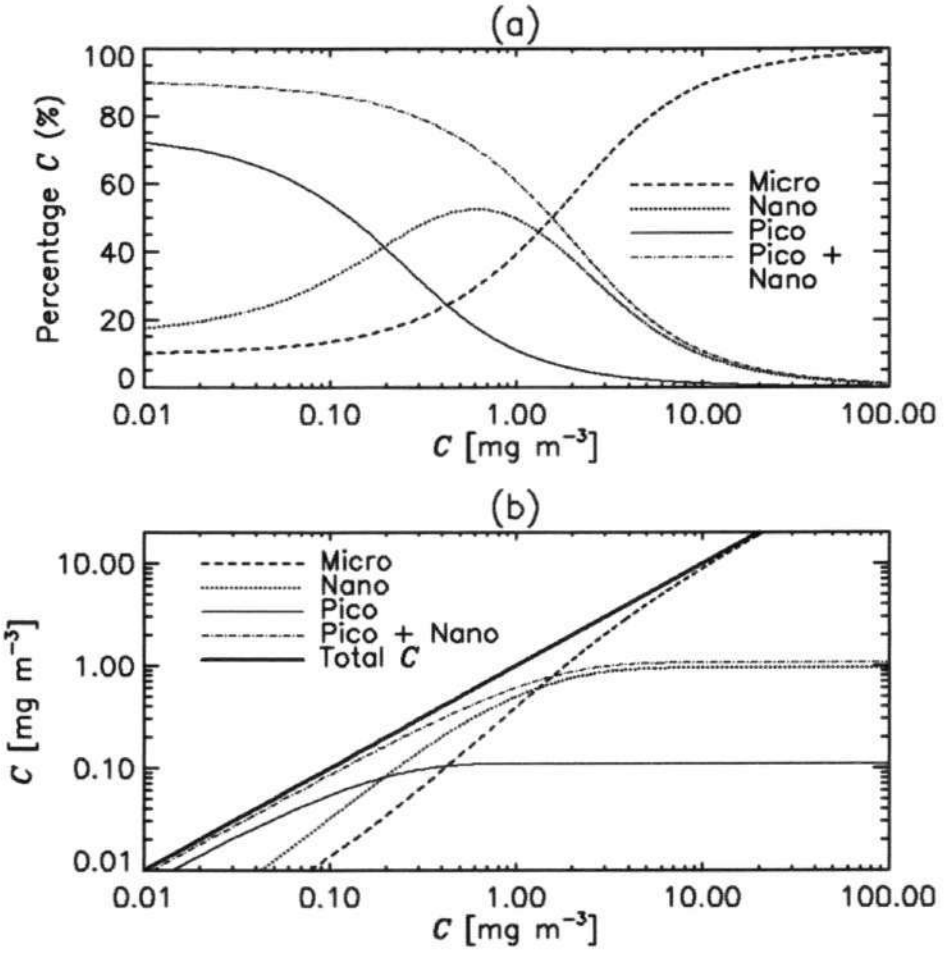

Figure 4.6: (a) The change in percentage of the three size classes of phytoplankton with increasing chlorophyll-a on a log x-axis (b) illustration of changes in chlorophyll-a of the three size classes in the model (log y-axis) as a function of the total chlorophyll-a concentration (log x-axis).

4.4.3 Satellite comparison

Results from the satellite comparison are shown in Figure 4.8 (d-f). When compared with the statistical approach of Uitz et al. (2006), the three-component model is shown to perform similarly in deriving C_p^s, C_n^s and C_m^s, with mean errors of $0.039\,\mathrm{mg\,m^{-3}}$ compared with $0.042\,\mathrm{mg\,m^{-3}}$ (Figure 6 f), $0.076\,\mathrm{mg\,m^{-3}}$ compared with $0.074\,\mathrm{mg\,m^{-3}}$ (Figure 4.8 e) and $0.149\,\mathrm{mg\,m^{-3}}$ compared with $0.154\,\mathrm{mg\,m^{-3}}$ (Figure 4.8 d). Furthermore, the model can be applied to a continuum of chlorophyll concentrations without having to deal with discrete trophic classes and the parameters of the three-component model offer direct biological interpretation.

The three-component model developed in section 4.3.1 is based on exponential equations that were chosen as they provide a good description of the shape of the experimental data (e.g. Figure 4.7). Therefore, it could be referred to as an "empirical" model, considering that the function is not derived directly from arguments based on the 1st principles of population ecology. However, based on the theory that

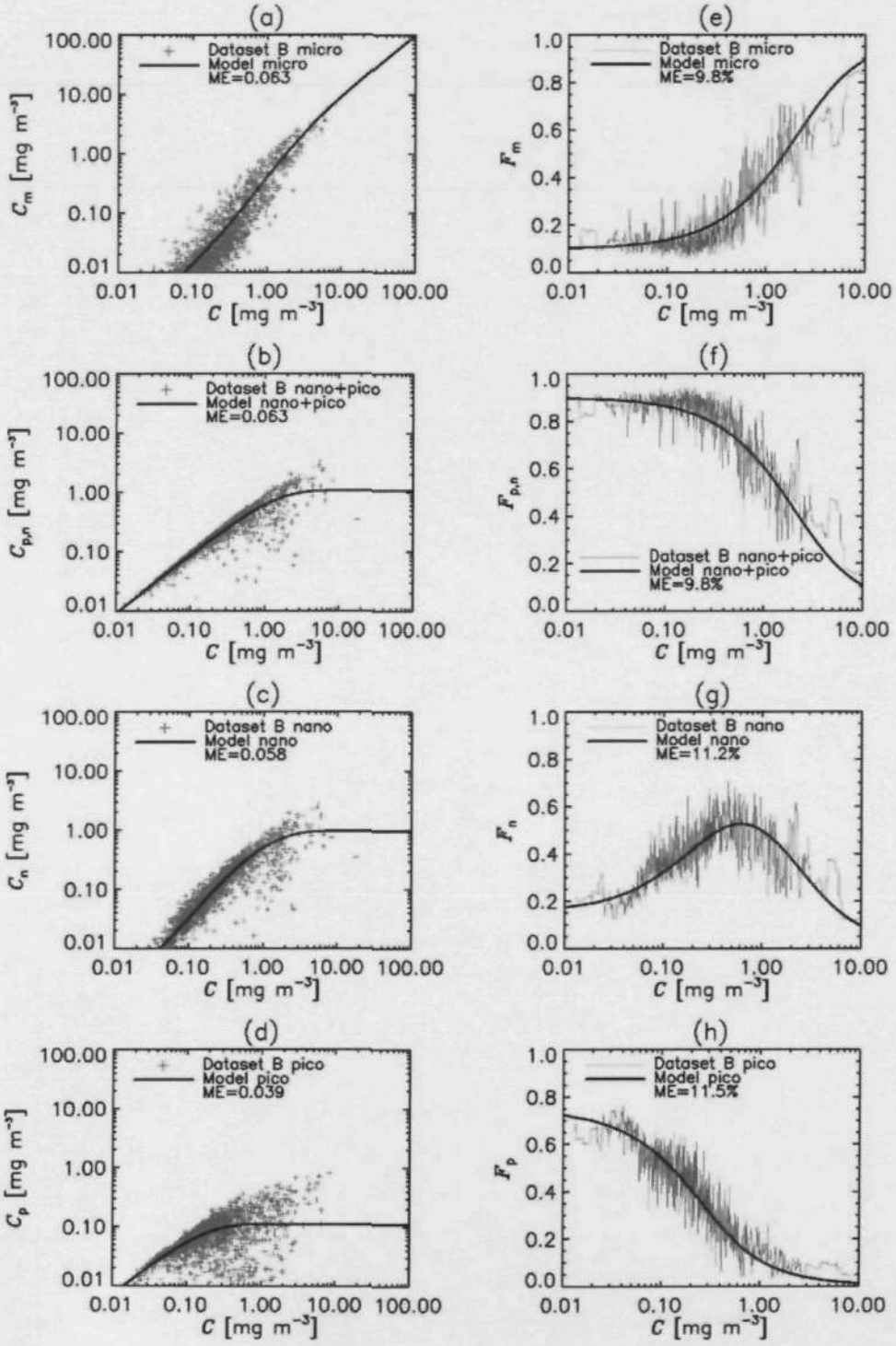

Figure 4.7: (a-d) shows the three-component model plotted against the raw size-specific chlorophyll-a values from database B, (e-h) shows the size-specific fractional contributions calculated according to the model plotted against the size-specific fractional contributions from database B as a function of total chlorophyll-a (smoothed with a 5 point running mean).

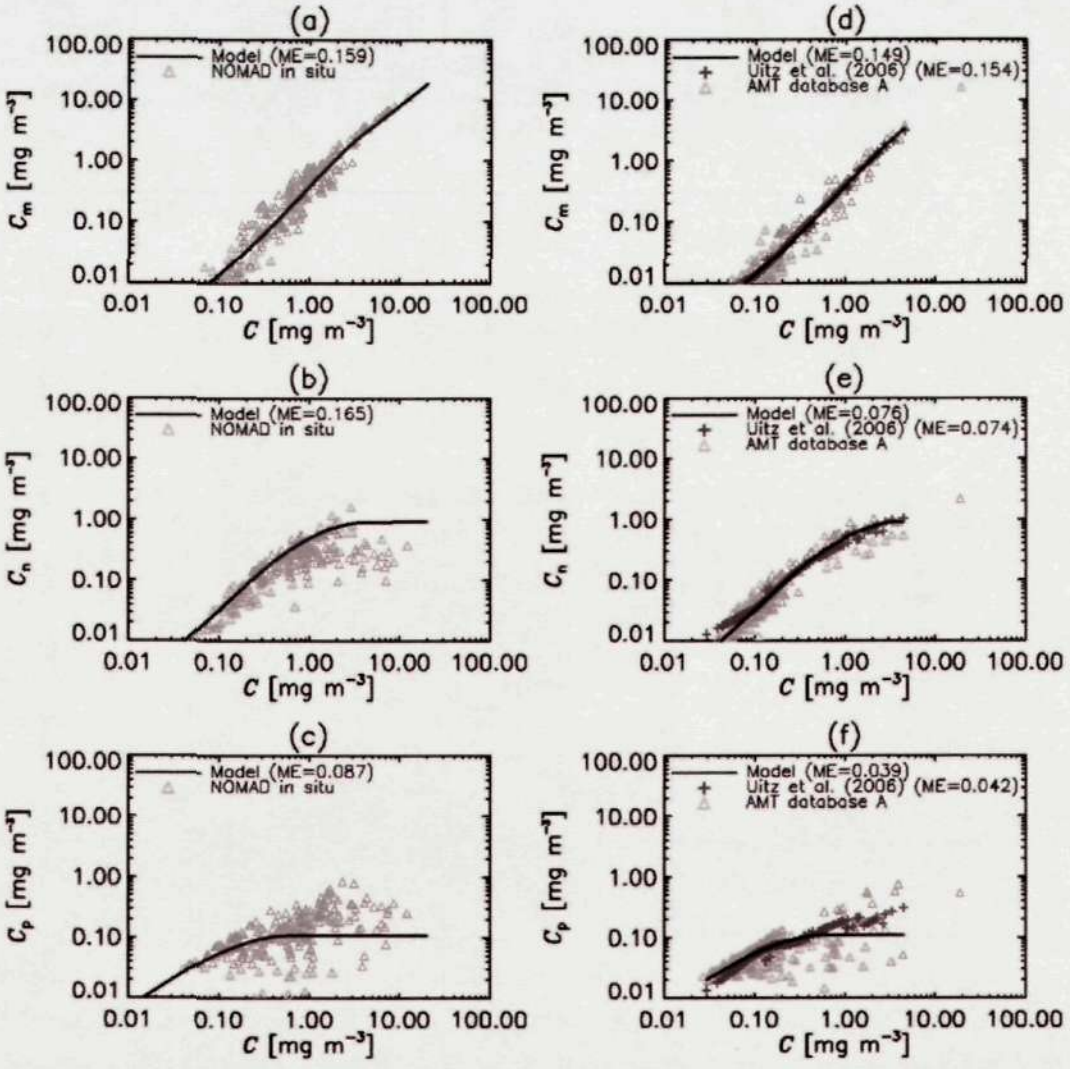

Figure 4.8: (a-c) shows the three-component model plotted against the size-specific chlorophyll-a concentrations from the NOMAD pigment dataset. (d-f) shows the relationship between the AMT *in situ* size-specific chlorophyll-a concentrations from dataset A (grey triangles), and those calculated according to Uitz et al. (2006) (dark grey crosses) and the three-component model (black line) from C^s.

small cells are incapable of growing beyond a certain concentration, and that chlorophyll is added to a system by the addition of larger size classes of phytoplankton, as suggested by Raimbault et al. (1988), Chisholm (1992) and Sathyendranath et al. (2001), the parameters of the three-component model have simple biological interpretation. The parameter C^m corresponds to the maximum chlorophyll-a concentration a given size class can grow to (picoplankton or combined nano-picoplankton) and S describes the rate of increase in the chlorophyll-a concentration of a particular size class (picoplankton or combined nano-picoplankton) as a function of the total chlorophyll-a concentration. So for this reason the three-component model could be referred to as a "semi-empirical" model, in comparison with the purely "empirical" approach of Uitz et al. (2006).

Table 4.2: Mean Error (ME) values from applying the three-component model to satellite chlorophyll-a data and validating against *in situ* data from the HPLC dataset used in Chapter 3 (608 measurements). Errors are given for each Hardman-Mountford et al. (2008) biome. In addition, typical values for each biome are provided in square brackets which were derived from applying the three-component model to 10-years of satellite data (see Chapter 6) and extracting the average values for each biome from a 10-year climatology.

Biome	C_m^s	C_n^s	C_p^s	F_m^s (%)	F_n^s (%)	F_p^s (%)	n
Very low	– [0.003]	– [0.007]	– [0.019]	– [11.0]	– [20.9]	– [68.1]	–
Low	0.005 [0.007]	0.012 [0.014]	0.017 [0.031]	8.0 [11.9]	22.3 [24.7]	19.3 [63.4]	20
Low intermediate	0.007 [0.015]	0.020 [0.036]	0.025 [0.051]	6.7 [13.7]	13.7 [31.6]	14.5 [54.7]	153
High intermediate	0.011 [0.030]	0.027 [0.067]	0.028 [0.065]	7.1 [16.3]	14.6 [38.5]	14.6 [45.2]	69
High	0.243 [0.096]	0.102 [0.132]	0.047 [0.071]	13.6 [21.7]	20.8 [44.8]	17.4 [33.5]	192
Very High	6.137 [0.242]	0.650 [0.114]	0.511 [0.027]	19.7 [38.5]	10.6 [44.6]	16.1 [16.9]	174

*Units in $\mathrm{mg\,m^{-3}}$
n refers to number of samples.

Results from the comparison with coupled satellite chlorophyll-a and *in situ* pigment data (HPLC) from Chapter 3 are shown in Table 4.2 and Figure 4.9. On average over the global ocean, mean errors (ME) were estimated to be $0.260\,\mathrm{mg\,m^{-3}}$ for C_m^s, $0.062\,\mathrm{mg\,m^{-3}}$ for C_n^s, $0.046\,\mathrm{mg\,m^{-3}}$ for C_p^s, 9.2 % for F_m^s, 17.1 % for F_n^s and 16.1 % for F_p^s. These errors were shown to vary among biogeochemical regions of the ocean (see Table 4.2 and Figure 4.9) and are vulnerable to uncertainty as highlighted in Chapter 3 (see section 3.4).

4.4.4 Application of the model to satellite derived chlorophyll-a fields

Results from the *in situ* and satellite comparison shown in Figure 4.8 and 4.9 support the model's global application to satellite-derived chlorophyll fields (C^s). Figure 4.10 shows the phytoplankton size class percentages (fractions multiplied by 100) and chlorophyll-a concentrations calculated according to the three-component model for a SeaWiFS composite of May 2005. Theoretically, as the three-component model is based on non-linear equations, the model needs to be applied directly to daily satellite chlorophyll-a images and then averaged to produce a monthly composite. Results from Appendix A however, indicate that the three-component model can be applied directly to monthly SeaWiFS chlorophyll-a composites as the mean error (ME) differences between procedures are below 1 % and 0.015 $\mathrm{mg\,m^{-3}}$ for the per-

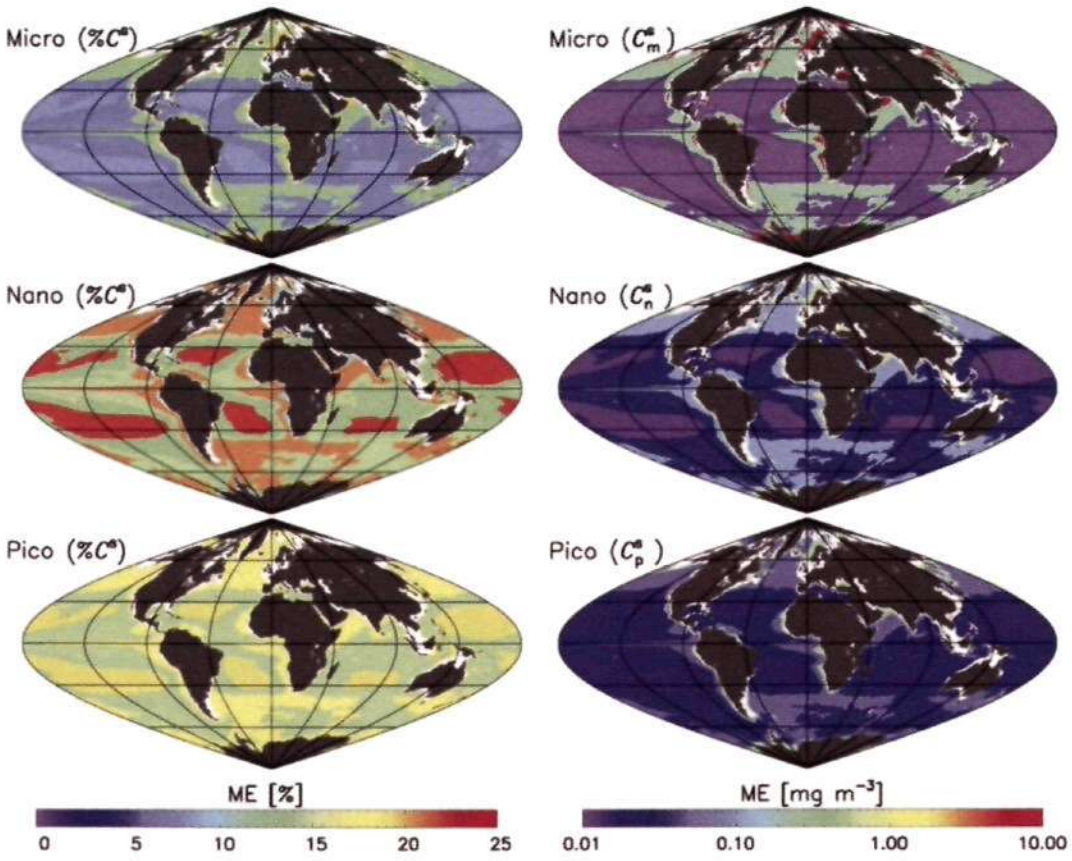

Figure 4.9: Estimated errors (ME) for the three-component model mapped on an entire SeaWiFS chlorophyll-a composite (1997-2007). Size-specific fractions (%) are shown on the left and chlorophyll-a concentrations ($mg\,m^{-3}$) on the right. White pixels represent coastal and inland waters (<200 m depth) in order to eliminate areas where the C^s OC4 algorithm has been found to overestimate chlorophyll due to the presence of SPM and / or CDOM.

centage total chlorophyll-a and the absolute chlorophyll-a of the three size classes respectively.

The general geographic pattern in the surface layer shown in Figure 4.10 is consistent with current knowledge about the distributions of species (e.g. Malone, 1980; Chisholm, 1992) and biogeochemical provinces (e.g. Longhurst et al., 1995; Hardman-Mountford et al., 2008). For the month of May 2005 microplankton are shown to dominate the subarctic and the major upwelling zones. Percentage of microplankton reduces to around 20 % along the equator, and down to as low as 10 % in the subtropical gyres. Nanoplankton seem to be more stable globally, ranging from about 17 % in the subtropical gyres to 55 % in the more eutrophic zones such as upwelling areas. Picoplankton are the dominant group within the subtropical gyres with their abundance reaching over 70 % in oligotrophic zones. This reduces to approximately 40 % along the equator and at the subantarctic convergence, and decreases to as low as 1 % in the subarctic and upwelling zones. Regarding the size-specific chlorophyll-a concentrations, picoplankton appear to act as a background

population with nano- and microplankton displaying larger spatial variability and higher concentrations in mid to high latitudes, coastal areas and areas of upwelling (e.g. Benguela upwelling).

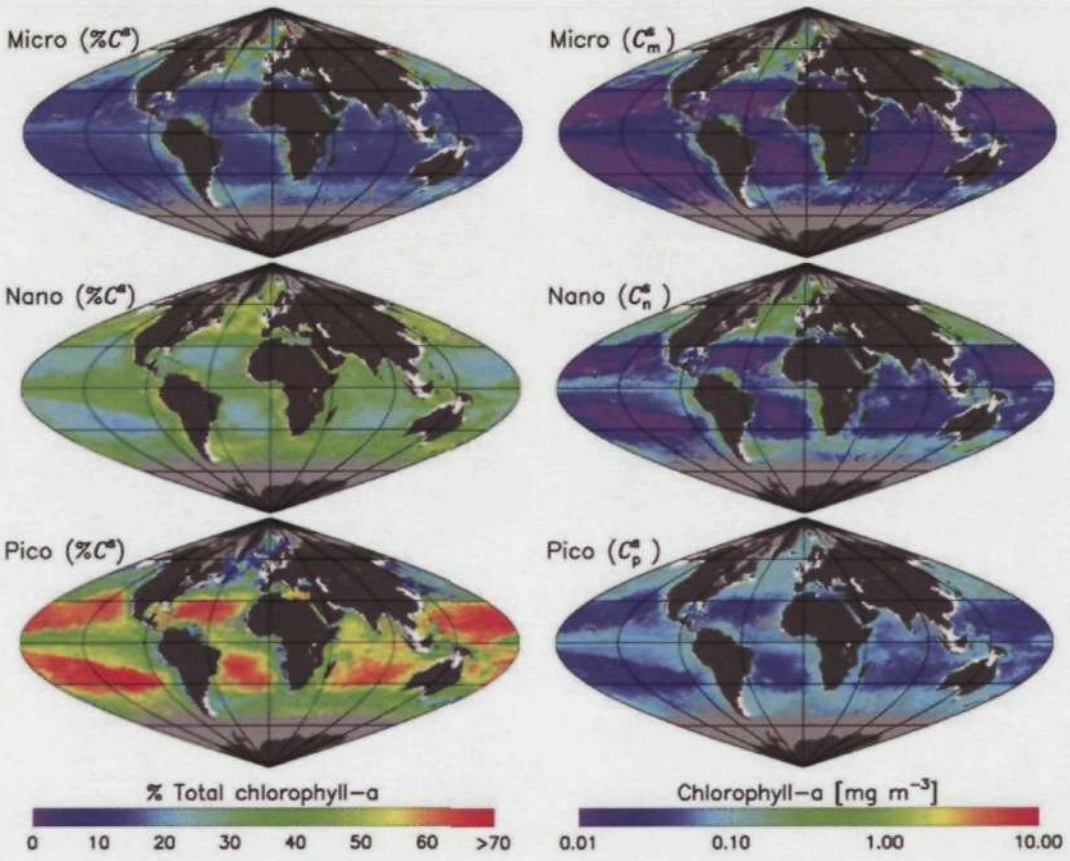

Figure 4.10: Phytoplankton size class percentages and chlorophyll-a concentrations calculated according to the three-component model for the monthly SeaWiFS composite of May 2005. Light grey pixels refer to unidentified pixels either due to cloud coverage or high sun zenith angles. White pixels represent coastal and inland waters (<200 m depth) in order to eliminate areas where the C^s OC4 algorithm has been found to overestimate chlorophyll due to the presence of SPM and / or CDOM.

4.4.5 Comparison with previous satellite PSC models

Figure 4.11 shows the differences between the technique of Uitz et al. (2006) and the three-component model for the same SeaWiFS composite of May 2005. The mean percentage difference for the global ocean between the two techniques regarding the fractions (three-component model minus the Uitz et al. (2006) model) is -0.3 % for microplankton, -4.5 % for nanoplankton, and 4.8 % for picoplankton. The corresponding chlorophyll-a concentrations are 0.0002 mg m^{-3} for microplankton, -0.001 mg m^{-3} for nanoplankton, and 0.001 mg m^{-3} for picoplankton. Considering the satellite error estimates of the three-component model (Figure 4.9), these differences appear insignificant. However, in the oligotrophic gyres the three-population model

predicts over 20 % more picoplankton and 20 % less nanoplankton (Figure 4.11), which is higher than the error estimates of the three-component model, implying significant differences. This can be attributed to the contrasting pigment criteria used in the three-component model that accounts for picoeukaryotes, in comparison with the Uitz et al. (2006) pigment criteria. Regarding the size-specific chlorophyll-a concentrations, larger differences are seen in more eutrophic environments, with the Uitz et al. (2006) model predicting relatively higher picoplankton chlorophyll-a concentrations.

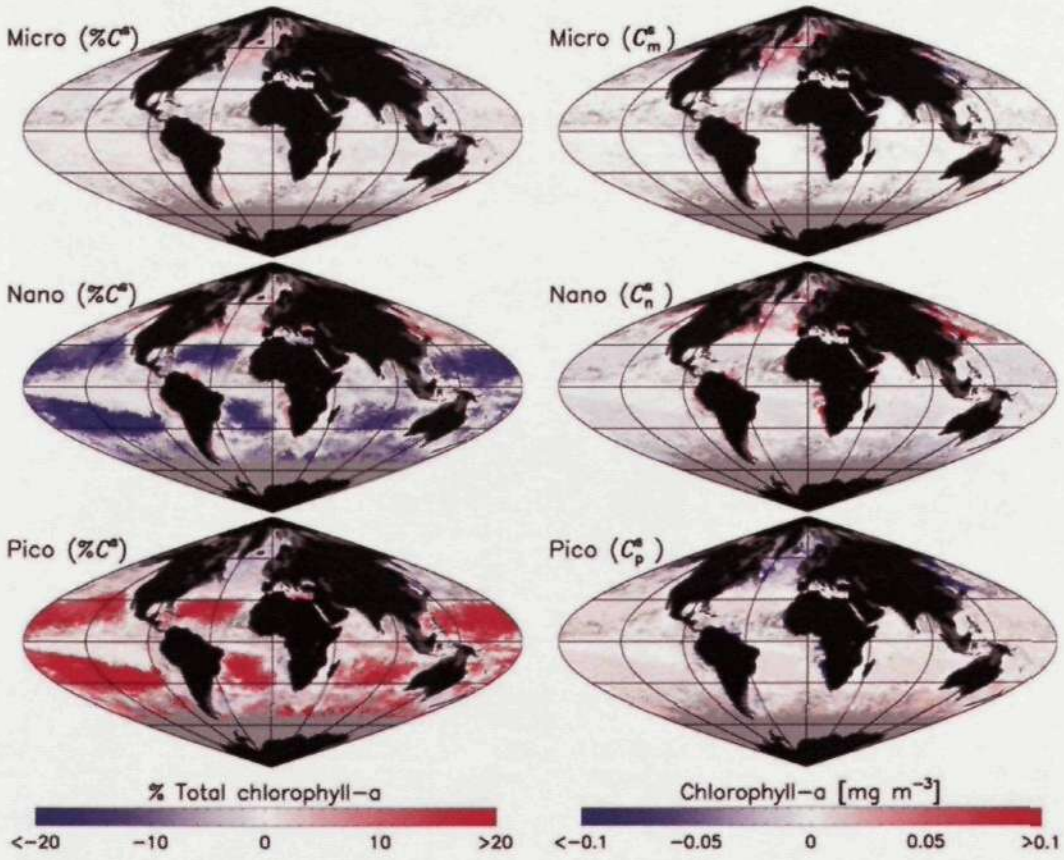

Figure 4.11: Comparison between the phytoplankton size class percentages and chlorophyll-a concentrations calculated according to the three-component model and the model of Uitz et al. (2006) for the monthly SeaWiFS composite of May 2005 (three-component model minus Uitz et al. (2006)). Dark grey pixels represent coastal and inland waters (<200 m depth) in order to eliminate areas where the C^s OC4 algorithm has been found to overestimate chlorophyll due to the presence of SPM and / or CDOM.

To compare the three-component model and the model of Hirata et al. (2008a), the Hirata et al. (2008a) chlorophyll-a model was adopted with the adjusted boundaries from Aiken et al. (2008) (pico < 0.25; nano 0.25 to 1.3; and micro > 1.3 mg m^{-3}). The three-component model was then converted into a dominant size class model by allocating dominance according to the highest percentage contribution of the three size classes. Both these techniques were then applied to the SeaWiFS May

2005 monthly chlorophyll-a (OC4) composite for comparison, shown in Figure 4.12.

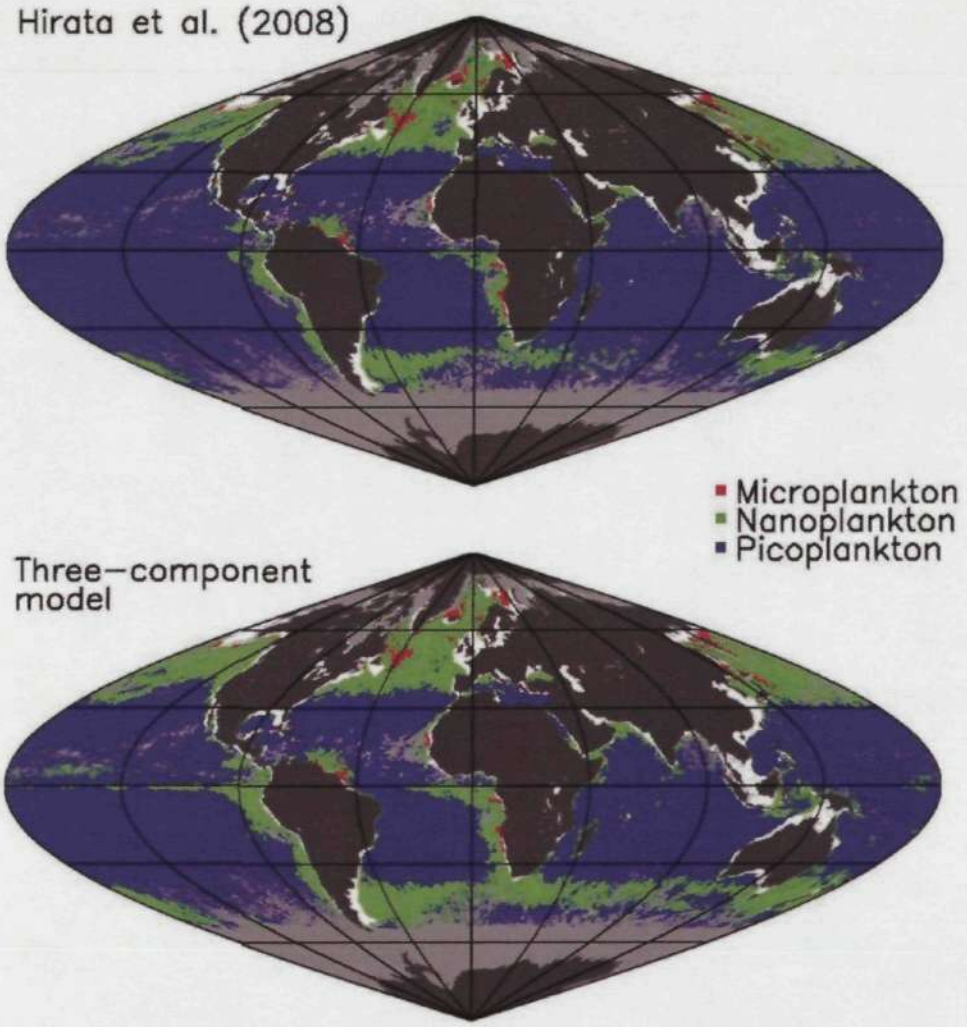

Figure 4.12: The Hirata et al. (2008a) chlorophyll-a-based model (top image) applied to a SeaWiFS May 2005 monthly composite and three-component model adapted to show dominant size class and applied to the same SeaWiFS May 2005 monthly composite. White pixels represent inland and coastal waters (<200m), dark grey represents land, and light grey represents unidentified pixels due to either cloud or low sun zenith angles.

Figure 4.12 indicates strong similarity between the three-component model and the model of Hirata et al. (2008a). In both cases picoplankton are shown to dominate the majority of the oceans, followed by nanoplankton and microplankton. The geographic distribution of the three size classes between the two models is also very similar. The dominant microplankton pixels are almost identical between approaches, both allocating microplankton pixels as $>1.3\,\mathrm{mg\,m^{-3}}$ chlorophyll-a. The Hirata et al. (2008a) model partitions dominant nanoplankton pixels at 0.25-1.3 $\mathrm{mg\,m^{-3}}$, and the three-component shows the nanoplankton to be dominant between 0.2-1.3 $\mathrm{mg\,m^{-3}}$. Therefore, when compared with the Hirata et al. (2008a) model, the

three-component model seems to predict slightly more dominant nanoplankton pixels at lower chlorophyll-a concentrations at the expense of dominant picoplankton pixels. This is seen in Figure 4.12 as equatorial and southern oceanic waters show a larger dominance of nanoplankton when using the three-component model. At such boundaries, the three-component model is still predicting very similar percentages of nano- and picoplankton, highlighting that these areas are essentially very mixed waters. This supports the use of models that estimate the fractional contribution of each size class as opposed to using dominance based models which partition groups at distinct boundaries.

4.4.6 Effect of optical depth on model parameters

As the AMT data were taken at a range of depths within the euphotic zone, depth-dependent variations could be investigated. Database B was organised according to depth. Using the approach of Morel et al. (2007c), the diffuse attenuation coefficient (K) was calculated from the surface chlorophyll-a value for each profile. The optical depth (τ) for each sample was then computed according to $\tau = zK$, where z represents the geometrical depth. We restricted database B to τ ranging from 0 to 9.2 (dimensionless), similar to Uitz et al. (2006). This whole procedure reduced the number of samples to 1335. The data were split into arbitrary ranges of τ, and Equation 4.4 and 4.6 were fitted to data from the different layers to derive model parameters for each layer, shown in Table 4.3.

Table 4.3: Parameter values obtained for the three-component model for a variety of optical layers (n refers to number of samples.)

Range τ	**Mean τ**	$C^m_{p,n}$ *	$S_{p,n}$	C^m_p *	S_p	**C range** *	n
0.0-0.6	0.388	1.001	0.931	0.098	8.271	0.022-5.643	522
0.6-1.2	0.860	1.108	0.777	0.089	8.302	0.037-8.299	268
1.2-2.0	1.507	1.320	0.651	0.142	3.741	0.040-4.589	119
2.0-3.5	2.754	1.279	0.685	0.129	4.313	0.044-6.564	174
3.5-6.0	4.547	1.450	0.630	0.237	1.744	0.035-6.537	188
6.0-9.2	7.059	2.521	0.345	0.223	1.795	0.022-0.880	64

*Units in $\mathrm{mg\,m^{-3}}$

Figure 4.13 shows the four parameters (C^m_p, $C^m_{p,n}$, S_p and $S_{p,n}$) plotted as a function of the mean τ. All the parameters are significantly correlated with τ, with p-values less than 0.05 and high r values (>0.89) for the fitted curves. To account

for the relationship between the model parameters and optical depths, equations 4.4 and 4.6 were reformulated such that,

$$C_{p,n} = [C^m_{p,n} \exp(\beta_a \tau)][1 - \exp(-[S_{p,n} \exp(\beta_b \tau)]C)], \tag{4.9}$$

$$C_p = [C^m_p \exp(\beta_c \tau)][1 - \exp(-[S_p \exp(\beta_d \tau)]C)], \tag{4.10}$$

where, β_a, β_b, β_c and β_d represent the change in $C^m_{p,n}$, $S_{p,n}$, C^m_p and S_p respectively with increasing τ. Parameters of equations 4.9 and 4.10 are given in Table 4.4.

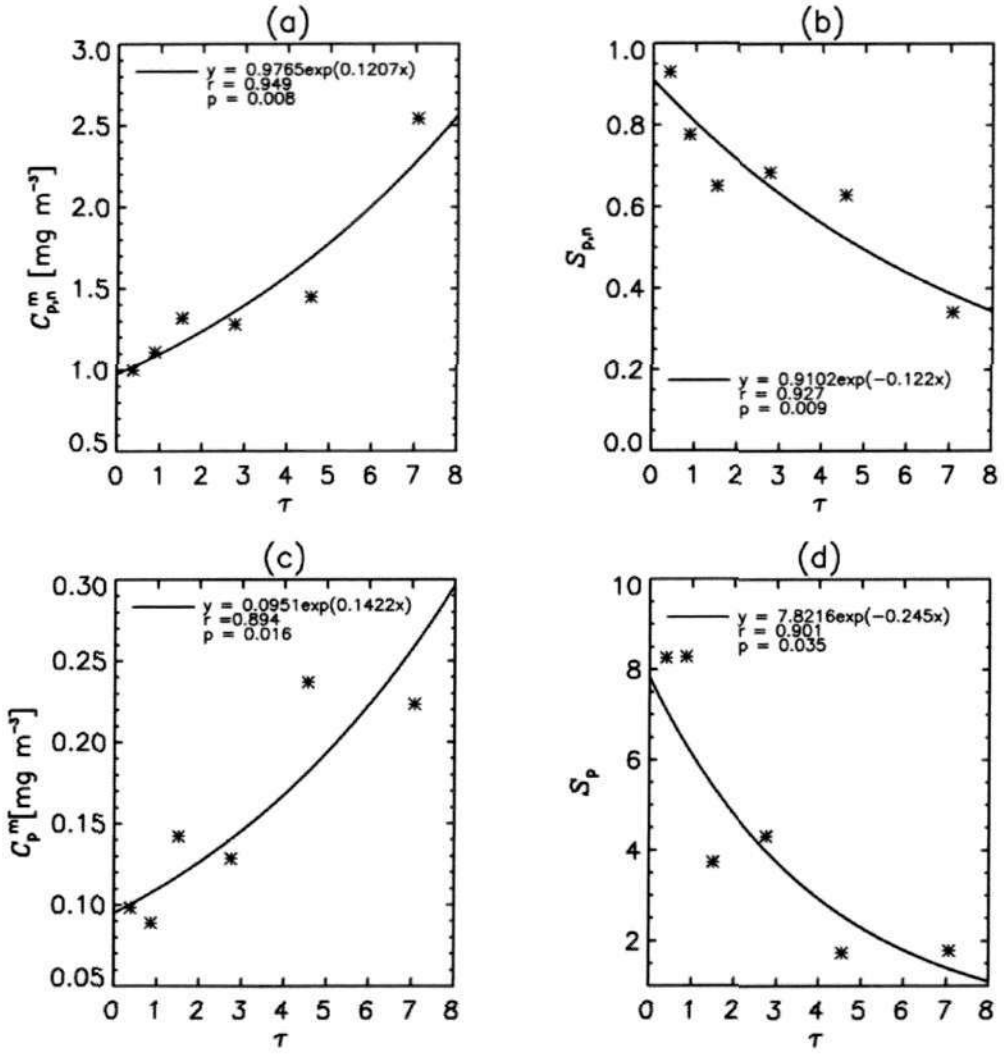

Figure 4.13: Variations in the three-component model parameters as a function of the optical depth (τ).

Equations 4.9 and 4.10 (in addition to equations 4.5 and 4.7) were applied to total chlorophyll-a values and derived optical depths (Morel et al., 2007c) from database D to estimate C_p, C_n and C_m. These values were then compared with C_p, C_n and C_m values derived from diagnostic pigments from the same dataset (Figure 4.14) and low ME differences between the model and all the observations were calculated for each

Table 4.4: Model parameters for the three-component model accounting for optical depth (Equations 4.9 and 4.10). Parameters are given with and without the empirical adjustment described in section 4.2.2.

Parameter	With empirical adjustment	Without empirical adjustment
$C_{p,n}^{m}$ *	0.977	0.977
$S_{p,n}$	0.910	0.910
C_{p}^{m} *	0.095	0.075
S_{p}	7.822	9.268
β_a	0.121	0.121
β_b	-0.122	-0.122
β_c	0.142	0.322
β_d	-0.245	-0.438

*Units in $\mathrm{mg\,m^{-3}}$

size class (~0.05 mg $\mathrm{m^{-3}}$). Additionally, database D was divided according to the Hardman-Mountford et al. (2008) biome classification (see Figure 4.3). The relative mean error of each size class fraction was calculated per biome (Table 4.5). This was seen to remain relatively stable for each size class from the *low* to the *high* biome, indicating the three-component model is performing with similar accuracy across the trophic range. However, for the *very high* biome the relative error increases for F_n and F_m indicating a reduction in model performance for these size classes. A smaller amount of samples in the *very high* biome, in comparison with the other biomes, could be influencing these results, or alternatively, it could be due to the *very high* biome being located in case 2 regions.

When applying the three-component model to a continuum of chlorophyll-a concentrations and optical depths (Figure 4.15), at low chlorophyll-a concentrations (0.01 -0.3 $\mathrm{mg\,m^{-3}}$) the picoplankton chlorophyll-a fractions decrease with increasing τ, whereas the nanoplankton chlorophyll-a fraction increases. At chlorophyll-a concentrations >0.3 $\mathrm{mg\,m^{-3}}$ the nano- and picoplankton fractions increase with increasing τ, whereas the microplankton fractions decrease.

Uitz et al. (2006) highlighted possible deviations in the pico- and nanoplankton size fractions when comparing the surface layer with the integrated euphotic zone. At less than 0.1 $\mathrm{mg\,m^{-3}}$ (see Figure 6 of Uitz et al., 2006) an enhanced picoplankton contribution near the surface was noted at the expense of the nanoplankton. This feature is also evident in our model and suggests that at low chlorophyll-a concentrations in low-light environments, nanoplankton prevail as the dominant size class, whereas in high-light environments picoplankton dominate. However, it is acknowledged that as the majority of measurements below 0.04 $\mathrm{mg\,m^{-3}}$ of chlorophyll were

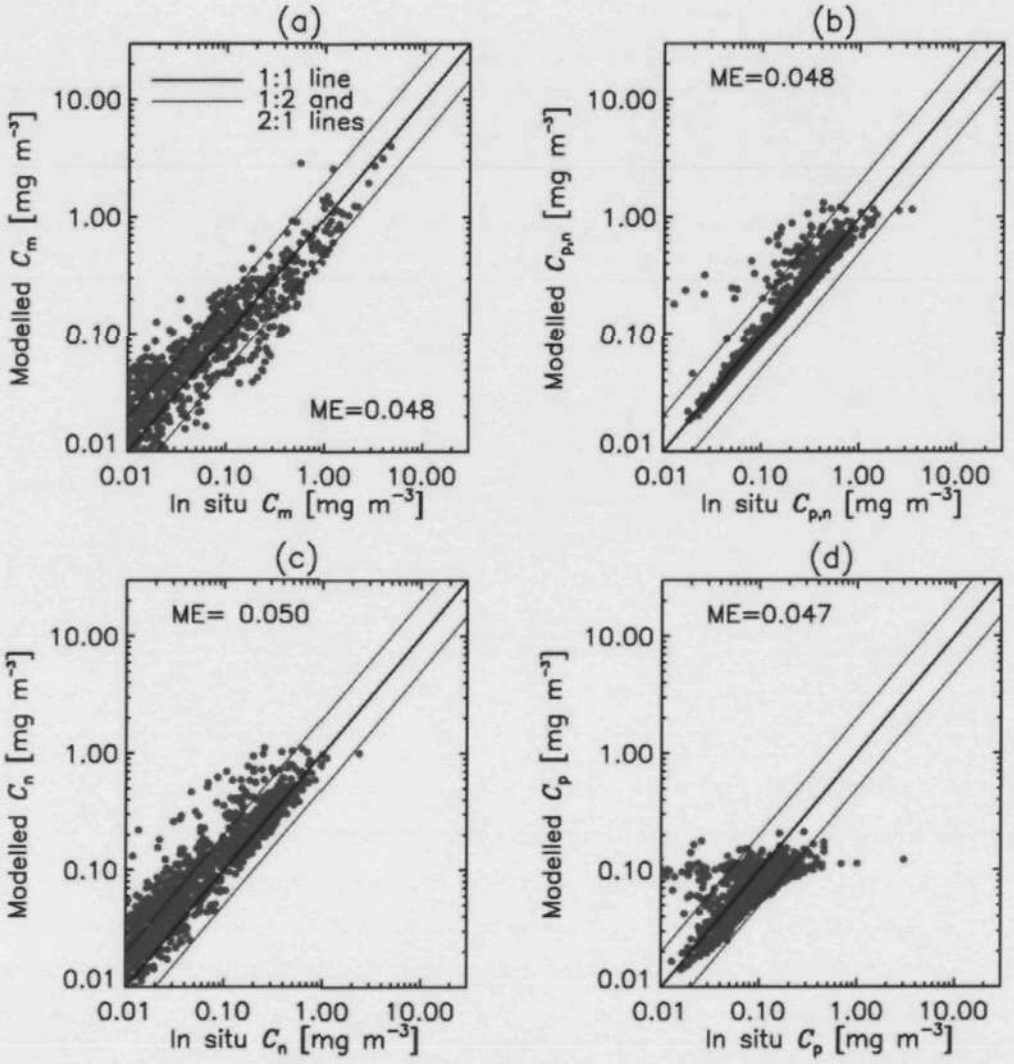

Figure 4.14: Independent validation of the three-component model (equations 4.9 and 4.10) using database D. The modelled and *in situ* size-specific chlorophyll-a concentrations are shown for (a) microplankton, (b) combined nano-picoplankton, (c) nanoplankton and (d) picoplankton.

obtained within the first optical depth (~70 %), where $\tau<1$, such relationships could be an artifact of the uneven sample distribution.

4.4.7 Estimation of the vertical phytoplankton size structure from EO

The three-component model may be used in conjunction with procedures designed to estimate the vertical chlorophyll profile from the surface concentration (Morel and Berthon, 1989; Sathyendranath et al., 1995; Uitz et al., 2006). In order to achieve this, researchers have partitioned the ocean into mixed and stratified waters, typically by using the ratio of the euphotic depth (Z_p) to the mixed-layer depth (Z_m) (e.g. Uitz et al., 2006). When the mixed-layer depth is shallower than the euphotic

Table 4.5: Mean error (ME) values in percentages for the size-specific fractions (F_p, F_n and F_m) calculated from validating the three-component model (Equations 4.9 and 4.10) using database D for each Hardman-Mountford et al. (2008) biome.

Biome	F_p	F_n	F_m	n
Very low	–	–	–	–
Low	25.3	14.3	11.8	98
Low intermediate	19.1	12.6	9.5	329
High intermediate	22.9	15.0	9.4	211
High	16.6	15.1	11.8	468
Very high	15.4	26.3	29.9	52

n refers to number of samples

depth one may assume the waters are stratified and when the euphotic depth is shallower than the mixed-layer depth one may assume the waters are mixed. In mixed waters, it is generally assumed that the vertical chlorophyll profile is homogeneous (Morel and Berthon, 1989; Uitz et al., 2006). For stratified waters, a shifted Gaussian curve has typically been used for which the parameters vary widely with region (Platt and Sathyendranath, 1988; Sathyendranath and Platt, 1989; Morel and Berthon, 1989).

For stratified conditions, Morel and Berthon (1989) and Uitz et al. (2006) quantify the change in the shape of the vertical chlorophyll-a profile as a function of the surface chlorophyll-a concentration (C_{sur}). In the Morel and Berthon (1989) study, the average dimensionless profile of each trophic category was modelled using a generalized Gaussian profile (Lewis et al., 1983). Uitz et al. (2006) extended this theory and developed a slightly modified version which accounted for the fact that surface chlorophyll-a concentrations generally exceed the deepest values beyond the euphotic depth, which is incompatible with a constant background. In the Uitz et al. (2006) model, the constant background is replaced by a linear decrease in slope, s, starting from the surface value (D_b).

To illustrate how the three-component model may be integrated into a model that estimates the vertical chlorophyll profile from the surface concentration, the Uitz et al. (2006) model has been adapted slightly. Firstly, instead of using the dimensionless depth ($\zeta = z/Z_p$) as in Uitz et al. (2006), the optical depth (τ) was used for consistency with the three-component model. Note that these two are entirely compatible as $Z_p = 4.6/K$, $\tau = zK$ and hence $\tau = z4.6/Z_p$ (Kirk, 1994). The Uitz et al. (2006) model can therefore be reformulated such that the

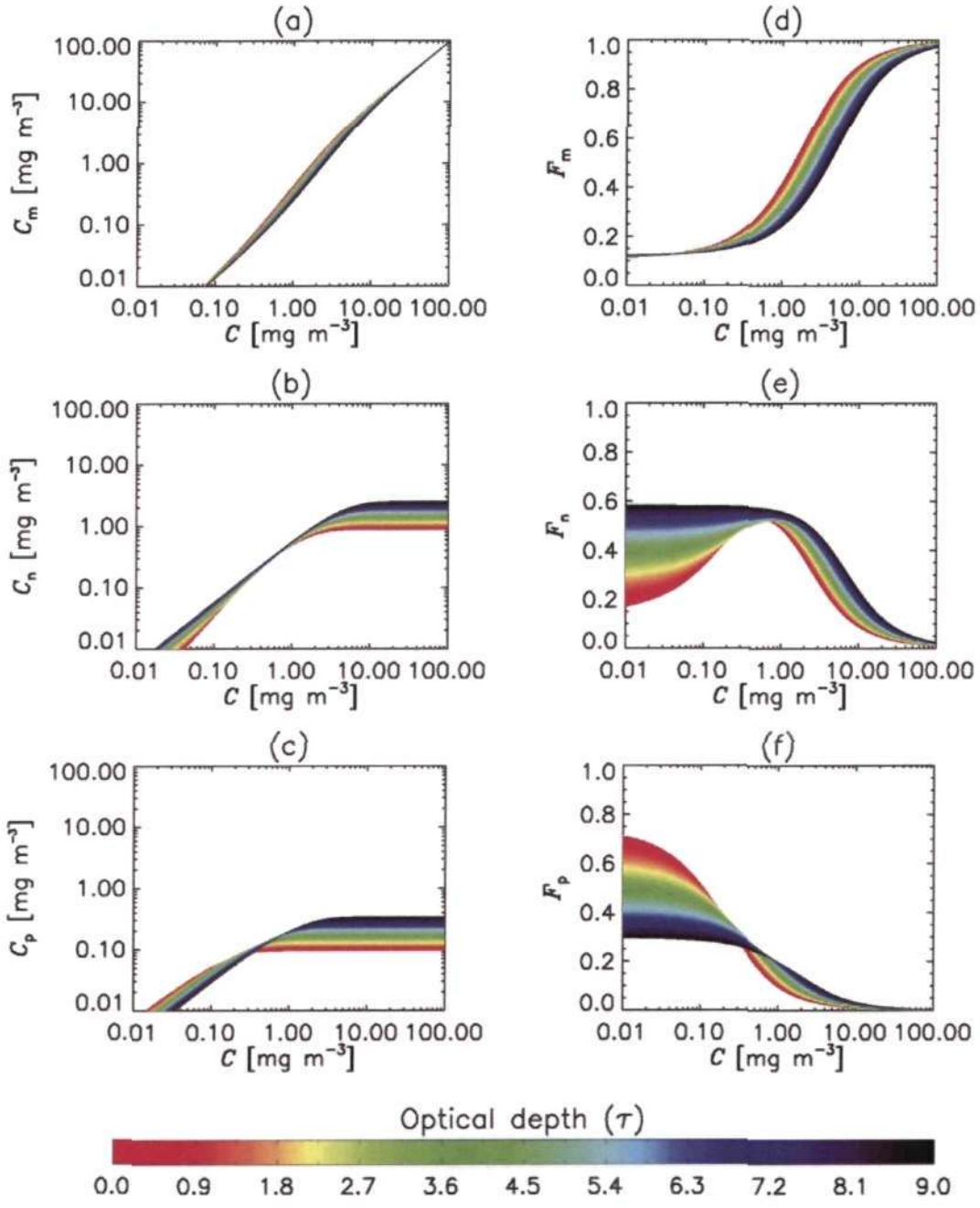

Figure 4.15: (a-c) shows the size-specific chlorophyll-a values and (d-c) the size-specific fractions all plotted as a function of the total chlorophyll-a concentration according to the three-component model for a variety of optical depths (τ) (equations 4.5, 4.7, 4.9 and 4.10).

dimensionless chlorophyll-a concentration (C_{DIM}) can be calculated according to

$$C_{DIM} = C_\zeta / \overline{C_{Zp}}, \tag{4.11}$$

where, $\zeta = \tau/4.6$, C_ζ is the chlorophyll-a concentration at a specific ζ and $\overline{C_{Zp}}$ is the average concentration within the euphotic layer. According to Uitz et al. (2006),

and assuming $\zeta = \tau \times 4.6$, C_{DIM} can be inferred according to

$$C_{DIM} = D_b - s\zeta + C_{max} \exp\left\{-\left[\left(\zeta - \zeta_{max}\right)/\Delta\zeta\right]^2\right\}, \tag{4.12}$$

where, C_{max} represents the maximum chlorophyll-a concentration, ζ_{max} is the depth at which C_{max} occurs, and $\Delta\zeta$ depicts the width of the peak.

Uitz et al. (2006) parameterised the above equation for nine different stratified classes, with each class varying based on their C_{sur} value and thus their trophic status. Values for these parameters, for the nine separate trophic classes, are given in Table 5 of Uitz et al. (2006). These parameters were interpolated using the average C_{sur} values for the nine trophic classes (Table 6 of Uitz et al., 2006) which resulted in a continuously changing vertical profile for a continuum of surface chlorophyll-a concentrations. These dimensionless profiles have been plotted in Figure 4.16 (a). The dimensionless profiles can easily be restored to their physical values by rescaling in concentration and depth (Figure 4.16 b). To rescale in concentration and depth, Z_P was calculated according to Morel et al. (2007c) as a function of C_{sur}, and $\overline{C_{Zp}}$ was calculated by interpolating the average $\overline{C_{Zp}}$ values for the nine trophic classes (Table 3 of Uitz et al., 2006) which resulted in an estimate of $\overline{C_{Zp}}$ for a continuum of C_{sur} values.

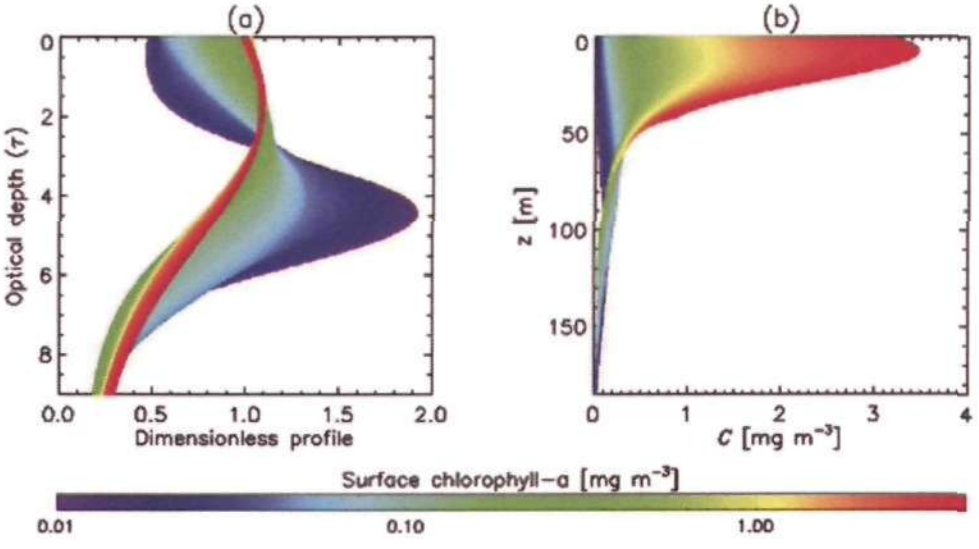

Figure 4.16: (a) dimensionless vertical profiles from Uitz et al. (2006) interpolated between each of the nine trophic classes. (b) show the rescaled profiles in (a).

Using a SeaWiFS monthly climatological mean (1997-2010) of chlorophyll-a, for October, the euphotic depth (Z_p) was calculated according to Morel et al. (2007c) and the mixed-layer depth (Z_m) was derived from the de Boyer Montégut et al. (2004) mixed layer climatology (Figure 4.17). Then using the Z_p/Z_m ratio, pixels were classified into mixed and stratified waters (Figure 4.17).

For comparison with this approach, fluorometric chlorophyll-a data from Conductivity Temperature and Depth casts (CTD) were accessed from the BODC for

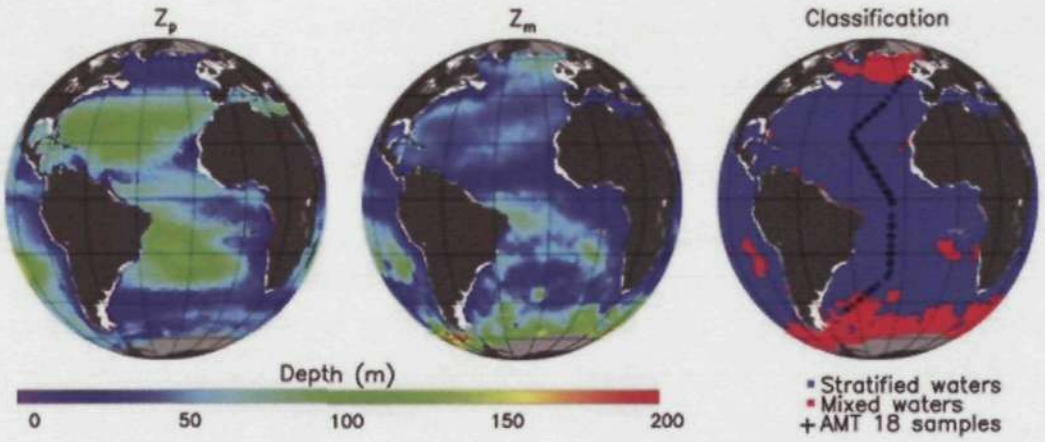

Figure 4.17: Estimates of the euphotic depth, mixed-layer depth, stratified and mixed waters for a SeaWiFS monthly climatological mean (1997-2010) of October focusing on the Atlantic Ocean.

October 2008 (AMT 18). The stations are shown in Figure 4.17 and consisted of 96 casts. These data were interpolated in order to view the vertical chlorophyll-a concentrations along the AMT transect. For comparison with the satellite approach, pixels were extracted from the October SeaWiFS climatology along the AMT 18 transect and the vertical profiles were predicted using the adapted Uitz et al. (2006) model and assuming $C_{sur} = C^s$ (Note that the October SeaWiFS climatology was used rather than the October 2008 SeaWiFS monthly composite, as extensive cloud coverage rendered many satellite pixels unusable in the October 2008 SeaWiFS monthly composite along the AMT 18 transect).

Figure 4.18 shows a comparison between the AMT 18 transect and the satellite model. There are significant differences between the two plots. In general the satellite model overestimates chlorophyll-a when compared with the AMT 18 transect. Furthermore, the deep chlorophyll-a maximum is quite broad in comparison with the AMT 18 estimate. At the surface of the gyres the AMT 18 transect predicts lower chlorophyll-a concentrations and the deep chlorophyll-a maximum is lower in the Southern Hemisphere gyres when compared with the satellite model. This suggests that the Uitz et al. (2006) model may need refinement for the Atlantic Ocean. However, the Uitz et al. (2006) model is based on HPLC pigment data that incorporated AMT cruises 1-11.

Considering that each cast was taken at a different time, that the data has been interpolated along the AMT transect using only 96 casts, and that Figure 4.18 is a comparison between AMT data taken during October 2008 and an October SeaWiFS climatology, the two plots do show similarities. Both show elevated chlorophyll-a concentrations near the surface at -40°, 45° and around the equator. Furthermore, the structure of the chlorophyll-a maximum follows a similar pattern with a deeper chlorophyll-a maximum in the gyres. Based on these similarities, it appears that the adapted Uitz et al. (2006) model is suitable for the purpose of illustrating how

the three-component model may be applied to EO data, in order to view changes in phytoplankton community structure with depth.

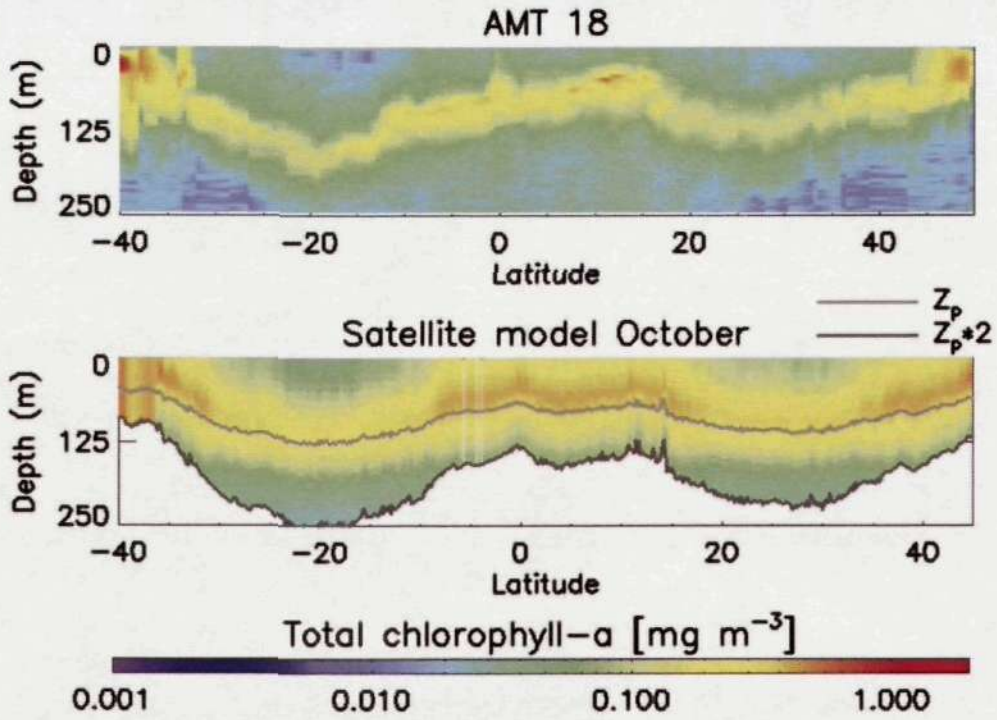

Figure 4.18: A comparison of AMT 18 fluorometric chlorophyll-a data along a vertical Atlantic Ocean transect, with the estimated vertical chlorophyll-a concentrations along the same transect using the adapted model of Uitz et al. (2006) and a SeaWiFS climatology of October.

To investigate phytoplankton size structure with depth, the adapted Uitz et al. (2006) model was applied to the SeaWiFS climatology image of October and then the three-component model was applied to the vertical chlorophyll-a concentrations to estimate the size-specific chlorophyll-a concentrations and the fractional contributions. Figure 4.19 shows the vertical structure in phytoplankton size class estimated using the three-component model along a meridional-time transect (30° W) in the Atlantic Ocean, and Figure 4.20 shows depth slices though the Atlantic Ocean of the total chlorophyll-a concentration and fractional contributions (shown in $\%C^s$) of the three size-classes, both for the SeaWiFS climatology of October.

In eutrophic areas (e.g. -40°, 45° and around the equator), where the water is generally well mixed, higher chlorophyll-a concentrations and fractional contributions (shown in $\%C^s$) of microplankton are seen. The microplankton $\%C^s$ generally declines with depth in the subtropical gyres. Brown et al. (1991) showed that at the equator some patches may be dominated by larger cells if upwelling currents reach the surface, but if they do not then the structure from the gyres will be maintained, but compressed at shallower depths. This is again replicated in Figure 4.19 as above 100 m, in certain equatorial areas, higher micro- and nanoplankton chlorophyll-a concentrations occur. Furthermore, in areas where this is not apparent

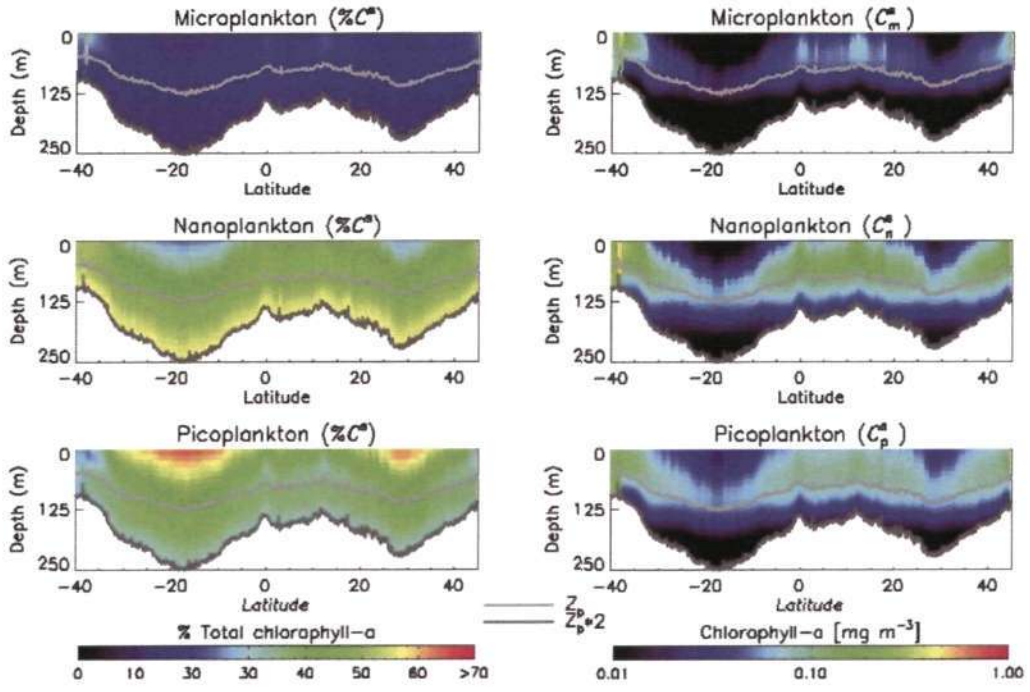

Figure 4.19: Estimates of the size-specific chlorophyll-a concentrations and fractional contributions along a meridional-time transect (30° W) in the Atlantic Ocean, extracted from the SeaWiFS climatology of October.

the structure from the gyres seems to be maintained but compressed at a shallower depth (Figure 4.19). In and around the subtropical gyres, there appears to be a significant change in the composition of pico- and nanoplankton with depth (Figure 4.19 and 4.20). At the surface (0 m) picoplankton are highly dominant (>65 %), whereas at 200 m nanoplankton appear to be the dominant size class (∼60 %).

4.5 Summary

In this chapter, a new abundance-based model has been developed that calculates the fractional contribution of three phytoplankton size classes (micro-, nano- and picoplankton) to the overall chlorophyll-a concentration. The model has the advantage in that it can be applied to a continuum of chlorophyll concentrations so avoids discontinuities introduced by partitioning chlorophyll values into discrete trophic classes. Based on the theory that small cells are incapable of growing beyond a certain concentration, and that chlorophyll is added to a system by the addition of larger size classes of phytoplankton, as suggested by Raimbault et al. (1988), Chisholm (1992) and Sathyendranath et al. (2001), the model parameters provide direct biological interpretation. Therefore, the model reconciles the Uitz et al. (2006) and Sathyendranath et al. (2001) approaches.

The model was fitted to a large pigment dataset from the Atlantic Ocean using a previously-established diagnostic pigment approach (Vidussi et al., 2001; Uitz

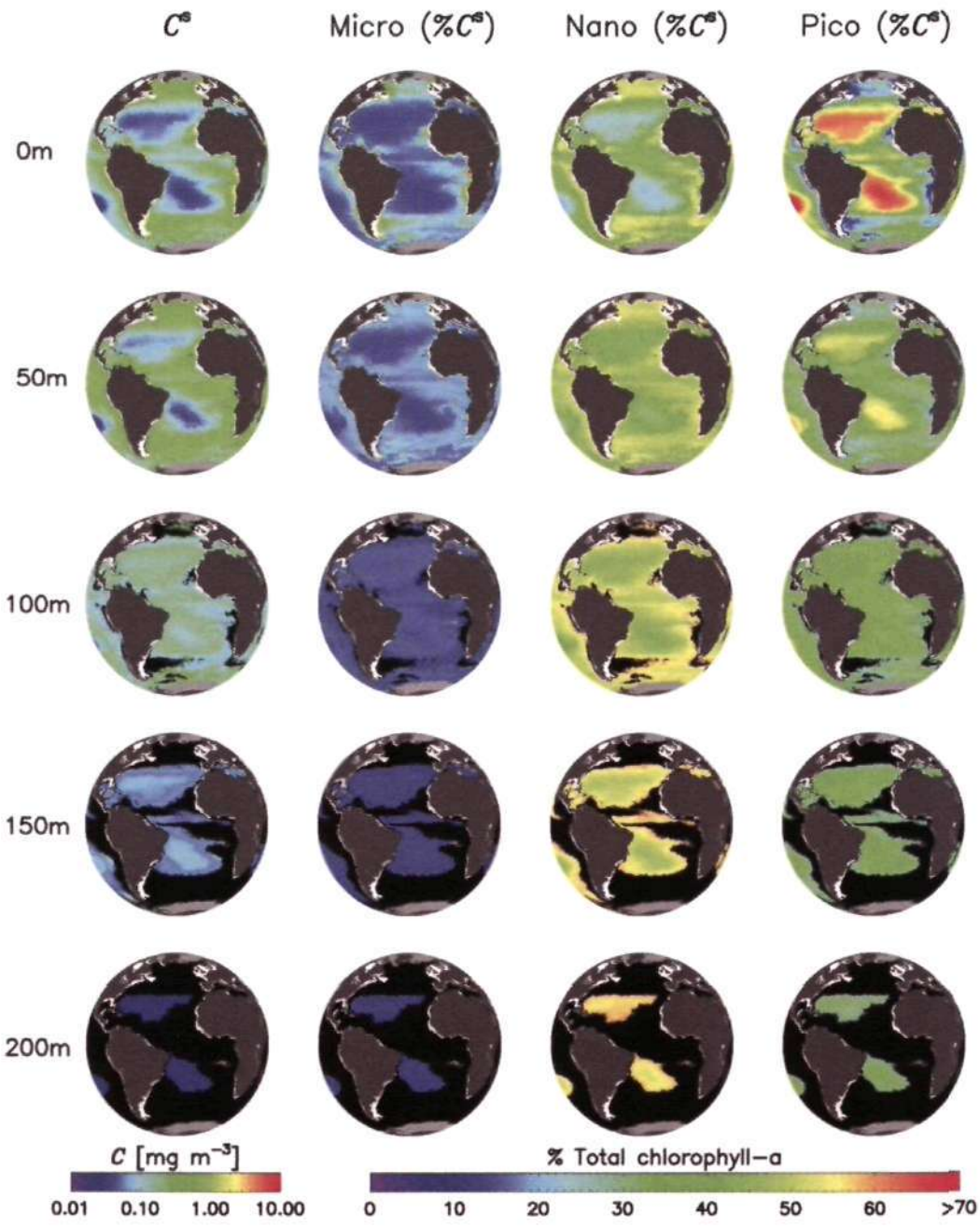

Figure 4.20: Depth slices though the Atlantic Ocean of the chlorophyll-a concentration and fractional contributions (shown in $\%C^s$) of the three size-classes, extracted from the SeaWiFS climatology of October. Black pixels represent depths below twice the euphotic depth.

et al., 2006) extended to account for small picoeukaryotes in ultra-oligotrophic environments. The performance of the algorithm was tested against a global *in situ* pigment dataset, a concurrent co-located satellite match-up dataset and compared with previously published algorithms. The model was then adapted to incorporate the effect of optical depth on the model parameters. Results from the chapter indicate:

- The proposed empirical adjustment to account for the picoeukaryote signature in ultra-oligotrophic waters provides an improvement on the diagnostic pigment procedure developed in Vidussi et al. (2001) and Uitz et al. (2006).

- Using the three-component model, size-specific chlorophyll-a concentrations in the surface layer of the global ocean can be retrieved from EO to within $0.260\,\mathrm{mg\,m^{-3}}$ for microplankton, $0.062\,\mathrm{mg\,m^{-3}}$ for nanoplankton and $0.046\,\mathrm{mg\,m^{-3}}$ for picoplankton.

- Using the three-component model, size-specific chlorophyll-a fractions in the surface layer of the global ocean can be retrieved from EO to within 9.2 % for microplankton, 17.1 % for nanoplankton and 16.1 % for picoplankton.

- These errors were shown to vary among biogeochemical regions of the ocean.

- The three-component model may be used as a tool for understanding subsurface phytoplankton size structure in the Atlantic Ocean. Results indicate a change in the composition of pico- and nanoplankton with optical depth at chlorophyll-a concentrations below $0.3\,\mathrm{mg\,m^{-3}}$. Picoplankton appear to dominate at the surface of the subtropical gyres and nanoplankton at the base of the euphotic layer.

Chapter 5

Improving estimates of the phytoplankton absorption coefficient by introducing size structure*

5.1 Introduction

In the previous chapter, a three-component model was developed which calculates the fractional contribution of three PSCs to the overall chlorophyll-a concentration. The phytoplankton absorption coefficient is a fundamental quantity in marine primary production models (see section 2.3.6). Furthermore, deriving size-specific phytoplankton absorption coefficients from EO can ultimately be used to help improve our understanding of primary production in the global ocean (Claustre et al., 2005; Mouw and Yoder, 2005; Uitz et al., 2008, 2009, 2010; Silió-Calzada et al., 2008; Hirata et al., 2009b). It is well known that the phytoplankton absorption coefficient can be described as a function of the dominant phytoplankton pigment, chlorophyll-a, and that this relationship can be ascribed to changes in both pigment composition and size structure (Morel and Bricaud, 1981; Sathyendranath et al., 1987; Lohrenz et al., 2003; Bricaud et al., 2004). This chapter explores the use of the three-component model to improve estimates of the phytoplankton absorption coefficient, as a function of the chlorophyll-a concentration. Using the three-component model developed in Chapter 4, the two-component absorption model of Sathyendranath et al. (2001) and Devred et al. (2006) is extended to three size classes of phytoplankton. The new three-component absorption model yields the specific absorption coefficients of three size-classes (micro-, nano- and picoplankton) and, furthermore, it can be applied to a continuum of chlorophyll-a concentrations. The performance of the model, when used to retrieve total phytoplankton absorption

*Aspects of this chapter are included in the following paper
Brewin, R.J.W., Devred, E., Sathyendranath, S., Hardman-Mountford, N.J. and Lavender, S.J. (In revision) A model of phytoplankton absorption based on three size classes. Applied Optics.

for a given chlorophyll-a concentration, is compared with a power-law model and the Devred et al. (2006) model fitted to the same dataset. The specific absorption coefficients of the three size classes derived using the new model are also compared with the results of Ciotti et al. (2002) and Uitz et al. (2008). Finally, absorption coefficients obtained by applying the model to remotely-sensed chlorophyll-a are compared with corresponding *in situ* data.

5.2 Methodology

5.2.1 *In situ* absorption and pigment data

The NOMAD dataset (Werdell and Bailey, 2005) was used for model development and inter-comparison. A subset of NOMAD made of contemporary, co-located $a(\lambda)$ (20 wavelengths between 405 and 683 nm) and pigment concentration derived from HPLC, was downloaded from the NASA website (Version 1.3.h, 22/02/2007 HPLC evaluation data set). This consisted of 269 measurements collected in various oceans. The pigment and $a(\lambda)$ dataset was quality controlled according to Aiken et al. (2009), reducing the number of measurements to 260, and is hereafter referred to as database E.

The model was used to calculate phytoplankton absorption as a function of chlorophyll-a concentration estimated from remote-sensing reflectances (O'Reilly et al., 1998), and the results compared with *in situ* data from the NASA NOMAD dataset (Version 2.0w APLHA, 18/07/2008, OOXIX IOP Algorithm Workshop evaluation dataset, Werdell and Bailey, 2005; Werdell, 2009) from which data points that were common to Database A were eliminated, such that the comparison might be regarded as an independent test of the performance of the model in a remote-sensing context. The resulting dataset consisted of 648 matched remote-sensing reflectances at SeaWiFS visible wavelengths, *in situ* absorption coefficient of phytoplankton, $a(\lambda)$, and chlorophyll-a concentration. This validation dataset is hereafter referred to as database F. Diagnostic pigments were used to compute the size-specific chlorophyll-a concentrations and the fractions of a given size-class in the total chlorophyll-a biomass for each sample in database E following equations 2.1, 2.2, 4.1, 4.2, and 2.5 to 2.9.

5.2.2 Phytoplankton absorption model development

In this section, using the three-component model, the two-component absorption model of Sathyendranath et al. (2001) is extended to a three-component absorption model of phytoplankton size class. The phytoplankton absorption coefficient can be expressed as:

$$a(\lambda) = a^*(\lambda)C. \tag{5.1}$$

According to the three-component model, the fractions of each size class (F_p, F_n and F_m) can be derived according to

$$F_p = \frac{C_p^m[1 - \exp(-S_p C)]}{C}, \tag{5.2}$$

$$F_n = \frac{C_{p,n}^m[1 - \exp(-S_{p,n} C)] - C_p^m[1 - \exp(-S_p C)]}{C}, \tag{5.3}$$

$$F_{p,n} = \frac{C_{p,n}^m[1 - \exp(-S_{p,n} C)]}{C}, \tag{5.4}$$

and

$$F_m = \frac{C - C_{p,n}^m[1 - \exp(-S_{p,n} C)]}{C}. \tag{5.5}$$

The unknown parameters C_p^m, $C_{p,n}^m$, S_p and $S_{p,n}$ were obtained by performing a non-linear least square regression (Levenberg-Marquardt (Press et al., 1992), IDL Routine MPFITFUN) of F_p and $F_{p,n}$ on C from database E using equations 5.2 and 5.4. The retrieved parameters are given in Table 5.1. Here the phytoplankton absorption coefficient ($a(\lambda)$) is assumed to be the sum of the pico- ($a_p(\lambda)$), nano- ($a_n(\lambda)$) and microplankton ($a_m(\lambda)$) contributions such that

$$a(\lambda) = \sum_{i=1}^{3} a_i^*(\lambda) C_i, \tag{5.6}$$

where $i = \{p, n \text{ and } m\}$. Expanding Equation 5.6 by inserting Equations 4.4 to 4.7 yields the expression:

$$\begin{aligned} a(\lambda) \;=\; & a_p^*(\lambda) C_p^m[1 - \exp(-S_p C)] + \\ & a_n^*(\lambda)\{C_{p,n}^m[1 - \exp(-S_{p,n} C)] - C_p^m[1 - \exp(-S_p C)]\} + \\ & a_m^*(\lambda)\{C - C_{p,n}^m[1 - \exp(-S_{p,n} C)]\}. \end{aligned} \tag{5.7}$$

Having retrieved C_p^m, $C_{p,n}^m$, S_p and $S_{p,n}$, Equation 5.7 was then fitted to C and $a(\lambda)$ from database E to derive $a_p^*(\lambda)$, $a_n^*(\lambda)$ and $a_m^*(\lambda)$ at each of the 20 wavelengths shown in Table 5.2.

The performance of the three-component absorption model (as well as of other models tested later) was quantified using the Mean absolute Error (ME) between the retrieved and measured absorption coefficients. Following analysis of absorption data by Ciotti and Bricaud (2006), the ME was computed in relative values so as to give equal weight to all measurements and expressed in percentages according to

$$\mathrm{ME}\% = \left[\frac{1}{N}\sum_{i=1}^{N}\left|\frac{(a_{i,E}(\lambda) - a_{i,M}(\lambda))}{a_{i,M}(\lambda)}\right|\right] \times 100, \tag{5.8}$$

where, $a(\lambda)$ is the variable (phytoplankton absorption coefficient) and N is the num-

ber of samples. The subscript E denotes the estimated variable and the subscript M denotes the measured variable. The ME% values as well as the Pearson correlation coefficients (r) between the model and database E are given in Table 5.2.

Table 5.1: Parameter values derived from fitting equations 5.2, 5.4 and 5.10 to database E.

	$C^m_{p,n}$ [mg m^{-3}]	$S_{p,n}$	C^m_p [mg m^{-3}]	S_p
Three-component model (Equation 5.7)	0.771	1.162	0.146	5.154
Two-component model (Equation 5.10)	0.768	1.302	-	-

Table 5.2: Size-specific absorption coefficients (m^2 [mg C]$^{-1}$) retrieved from database E using the three-component model (Equation 5.7), the Devred et al. (2006) model (Equation 5.10) as well as parameters for the power-law model (Equation 5.9). Mean Error percentages (ME%) and Pearson correlation coefficients (r) are provided for each model.

	Three-component model (Equation 5.7)					**Two-component model (Equation 5.10)**				**Power-law model (Equation 5.9)**			
λ (nm)	a^*_p	a^*_n	a^*_m	ME%	r	$a^*_{p,n}$	a^*_m	ME%	r	A	B	ME%	r
405	0.153	0.031	0.021	23.7	0.826	0.082	0.018	29.8	0.832	0.046	0.364	23.1	0.835
412	0.161	0.036	0.021	23.3	0.840	0.087	0.019	29.2	0.844	0.049	0.370	22.4	0.846
443	0.191	0.040	0.025	22.3	0.889	0.098	0.022	28.7	0.893	0.057	0.368	21.8	0.894
455	0.179	0.034	0.023	22.5	0.895	0.089	0.020	29.2	0.899	0.052	0.378	22.1	0.900
465	0.159	0.041	0.020	22.2	0.900	0.086	0.018	27.8	0.903	0.049	0.374	21.2	0.905
490	0.123	0.029	0.016	22.5	0.898	0.066	0.014	28.3	0.902	0.038	0.372	21.8	0.904
510	0.076	0.017	0.012	22.6	0.905	0.040	0.011	27.7	0.907	0.025	0.324	22.3	0.909
520	0.055	0.015	0.011	22.3	0.911	0.031	0.010	25.8	0.912	0.019	0.288	21.9	0.913
530	0.040	0.013	0.009	23.1	0.912	0.024	0.009	25.3	0.913	0.016	0.250	22.7	0.912
550	0.026	0.008	0.007	26.8	0.896	0.016	0.006	29.3	0.896	0.010	0.226	26.6	0.896
555	0.024	0.007	0.006	27.3	0.891	0.014	0.006	29.8	0.891	0.009	0.233	27.1	0.890
560	0.022	0.006	0.005	27.5	0.887	0.013	0.005	29.9	0.887	0.008	0.240	27.3	0.886
565	0.020	0.006	0.005	27.9	0.884	0.012	0.005	30.2	0.884	0.008	0.244	27.6	0.883
570	0.018	0.005	0.004	28.5	0.887	0.011	0.004	30.7	0.887	0.007	0.237	28.1	0.886
590	0.017	0.007	0.005	29.7	0.913	0.011	0.005	31.3	0.913	0.007	0.210	29.4	0.913
619	0.017	0.006	0.006	27.3	0.934	0.011	0.006	28.4	0.934	0.008	0.161	26.9	0.934
625	0.017	0.006	0.006	26.3	0.938	0.011	0.006	27.3	0.937	0.008	0.159	25.9	0.937
665	0.032	0.015	0.014	23.5	0.955	0.023	0.014	24.8	0.955	0.017	0.117	23.6	0.955
670	0.038	0.021	0.017	21.5	0.957	0.029	0.017	22.7	0.957	0.022	0.128	21.5	0.957
683	0.029	0.021	0.012	21.4	0.956	0.026	0.013	22.9	0.956	0.018	0.155	21.2	0.957

5.2.3 Comparison with other phytoplankton absorption models

5.2.3.1 Models that relate phytoplankton absorption coefficients to the chlorophyll-a concentration

The absorption model developed in the previous section was compared with a variety of existing phytoplankton absorption models. Power-law expressions have proven useful descriptors of the phytoplankton absorption coefficient as a function of the chlorophyll-a concentration (e.g. Prieur and Sathyendranath, 1981; Morel, 1991; Yentsch and Phinney, 1989; Bricaud et al., 1995, 1998, 2004). The power-law model

can be expressed as:

$$a(\lambda) = A(\lambda)C^{(1-B(\lambda))}, \tag{5.9}$$

where, $A(\lambda)$ and $B(\lambda)$ are positive, wavelength-dependent parameters (of the same formulation as in Table 2 of Bricaud et al., 1995). Equation 5.9 was fitted to $a(\lambda)$ as a function of C from database E to derive the parameters of A and B (shown in Table 2 together with correlation coefficients (r) and ME%).

The Sathyendranath et al. (2001) model is expressed as:

$$a(\lambda) = C^m_{p,n}[a^*_{p,n}(\lambda) - a^*_m(\lambda)][1 - \exp(-S_{p,n}C)] + a^*_m(\lambda)C. \tag{5.10}$$

Their model was not based on pigment composition. Instead, it was designed to classify the phytoplankton component into two optically-distinct classes. Nevertheless, Devred et al. (2006) showed, using data from a variety of ecosystems, that when $a^*_m(440) < 0.05$ ($\mathrm{m}^2\,[\mathrm{mg}\ C]^{-1}$), the corresponding component was well correlated with the microplankton fraction estimated independently by HPLC pigment analysis. Conversely, the component with the higher specific absorption coefficient corresponded to the combined nano- and picoplankton. Therefore, when dealing with the Sathyendranath et al. (2001) model, the model parameters $C^m_{p,n}$ and $S_{p,n}$ in Equations 5.7 and 5.10 are treated analogous to each other, despite differences in the method by which they are determined. Whereas in the model presented here, HPLC data are used to determine the parameters, in the Sathyendranath et al. (2001) model, Equation 5.10 is fitted directly to absorption and chlorophyll data to retrieve model parameters.

Equation 5.10 was fitted to $a(\lambda)$ as a function of C to samples in database E following the procedure described in section 2.4 of Devred et al. (2006). First, the Sathyendranath et al. (2001) model was fitted to the wavelengths from 411 to 489 nm to derive $U(\lambda)$, $S_{p,n}$ and $a^*_m(\lambda)$, where $U(\lambda)$ refers to the composite parameter $C^m_{p,n}[a^*_{p,n}(\lambda) - a^*_m(\lambda)]$. The computed $S_{p,n}$ values were then averaged and used to compute $U(\lambda)$ and $a^*_m(\lambda)$ over the entire spectral range. The parameters $C^m_{p,n}$ and $a^*_{p,n}(\lambda)$ were then computed using equations 5 and 10 in Devred et al. (2006). This procedure assumes that as C tends to zero, C_m (the chlorophyll concentration associated with microplankton) tends to zero and as a consequence $S_{p,n}C^m_{p,n}$ tends to 1. The computed parameters are given in Tables 5.1 and 5.2 together with r and ME% values. Note that the retrieved $a^*_m(443)$ value is less than 0.05 ($\mathrm{m}^2\,[\mathrm{mg}\ C]^{-1}$), therefore, according to Devred et al. (2006), the small-celled component can be assumed to be combined nano-picoplankton and the large-celled component microplankton.

5.2.3.2 Models that derive size-class-dependent specific phytoplankton absorption

The Ciotti et al. (2002) model is expressed in terms of $a^*(\lambda)$:

$$a^*(\lambda) = S_f a_p^*(\lambda) + (1 - S_f) a_m^*(\lambda), \tag{5.11}$$

where, $a_p^*(\lambda)$ and $a_m^*(\lambda)$ represent the specific absorption coefficients of picoplankton and microplankton respectively (Table 3 Ciotti et al., 2002), and S_f represents the fractional contribution of picoplankton to the specific absorption coefficient, accounting for both pigment composition and cell size. In deriving S_f, Ciotti et al. (2002) physically separated phytoplankton samples into size classes using filtration and determined the absorption spectra associated with each size class. The specific absorption coefficients derived by Ciotti et al. (2002, see their Table 3) were used for comparison with the specific absorption coefficients derived using the three-component model (Equation 5.7).

The Uitz et al. (2008) model is expressed as:

$$a^*(\lambda) = \frac{1}{C} \sum_{i=1}^{3} C_i a_i^*(\lambda) \exp\left(-R_i \frac{z}{Z_p}\right), \tag{5.12}$$

where $i = \{p,\ n \text{ and } m\}$ and R_i represent the slopes describing the variations in $a_i^*(\lambda)$ along the vertical z/Z_p axis (z = depth and Z_p = euphotic depth). Note that R_i has the notation S_{micro}, S_{nano} and S_{pico} in Uitz et al. (2008) for the different size classes and their notation has been changed here to avoid confusion with the parameters $S_{p,n}$ and S_p used in the three-component model. Because the study is limited to the surface layer of the ocean, z/Z_p was set to zero and therefore Equation 5.12 reduces to:

$$a^*(\lambda) = \frac{1}{C} \sum_{i=1}^{3} C_i a_i^*(\lambda). \tag{5.13}$$

The parameters of Equation 5.13 are given in Uitz et al. (2008) Web Appendix 1 and were used for comparison with the specific absorption coefficients derived using the three-component model (Equation 5.7).

5.3 Absorption model results

5.3.1 Three-component absorption model

To examine how well the three-component model fits the pigment observations from database E, the model is plotted against the observations in Figure 5.1. It can be seen that the model captures the general trend in both the size-specific chlorophyll-a concentrations (Figures 5.1 a-d) and the fractional contributions (Figures 5.1 e-

h). The retrieved coefficients $a_p^*(\lambda)$, $a_n^*(\lambda)$ and $a_m^*(\lambda)$, derived by fitting the three-component model to database E, are plotted in Figure 5.2 (a) and the same spectra are shown in Figure 5.2 (b) after normalisation at 443 nm to highlight differences in their spectral form. The specific absorption coefficients of all three size classes have typical peaks around 443 nm and 670 nm associated with chlorophyll-a absorption.

Microplankton exhibit the lowest $a^*(\lambda)$ at all wavelengths (Table 5.2), and the flattest spectral shape (Figure 5.2 b) which is consistent with previous studies (Stuart et al., 1998, 2000; Sathyendranath et al., 2004; Devred et al., 2006; Uitz et al., 2008) and can be linked to the strong package effect occurring in large-celled phytoplankton (Morel and Bricaud, 1981; Sathyendranath et al., 1987; Bricaud et al., 2004).

The nanoplankton absorption spectrum ($a_n^*(\lambda)$) is higher than $a_m^*(\lambda)$ but lower than $a_p^*(\lambda)$ at all wavelengths (Table 5.2). In agreement with previous studies (e.g. Uitz et al., 2008), the nanoplankton spectrum exhibits a distinct peak at 465 nm characteristic of the pigments 19'-hexanoyloxyfucoxanthin and 19'-butanoyloxyfucoxanthin (Jeffrey and Mantoura, 1997). Picoplankton display the highest specific absorption, consistent with their small size. This is enhanced in the blue wavelengths, probably due to the presence of non-photosynthetic cartenoids such as zeaxanthin or β-carotene that absorb in this region of the spectrum. The picoplankton spectrum also exhibits a small shoulder at 490 nm which may be attributed to the photoprotective pigment zeaxanthin (Barlow et al., 2002).

Figure 5.3 (a) shows the absorption spectrum of phytoplankton for chlorophyll-a concentration (C) ranging from 0.01 to 5 mg m^{-3}, and Figures 5.3 (b-d) show the fractional contributions to the absorption coefficient from the three size classes at the different wavelengths. The picoplankton contribution is the highest when the total phytoplankton absorption coefficient is low (i.e. 0.00 to 0.06 m^{-1} at 443 nm). As the total phytoplankton absorption coefficient increases (0.06 to 0.10 m^{-1} at 443 nm) the nanoplankton contribution becomes higher, and as the total phytoplankton absorption coefficient increases beyond 0.10 m^{-1} at 443 nm, the microplankton contribution becomes the highest. Superimposed on this first-order relationship associated with concentrations are the spectral characteristics of each size class shown in Figure 5.2. When the nano- and picoplankton fractions are high, their effects on the shape of the total absorption spectra become pronounced (Figure 5.3 b and c). When total absorption is high, the microplankton contribution is more pronounced in the green and red portions of the absorption spectrum as a consequence of the relatively flat shape of its absorption spectrum (Figure 5.3 d). By decomposing the total phytoplankton absorption spectra one can begin to appreciate how the spectrum is influenced by varying phytoplankton composition.

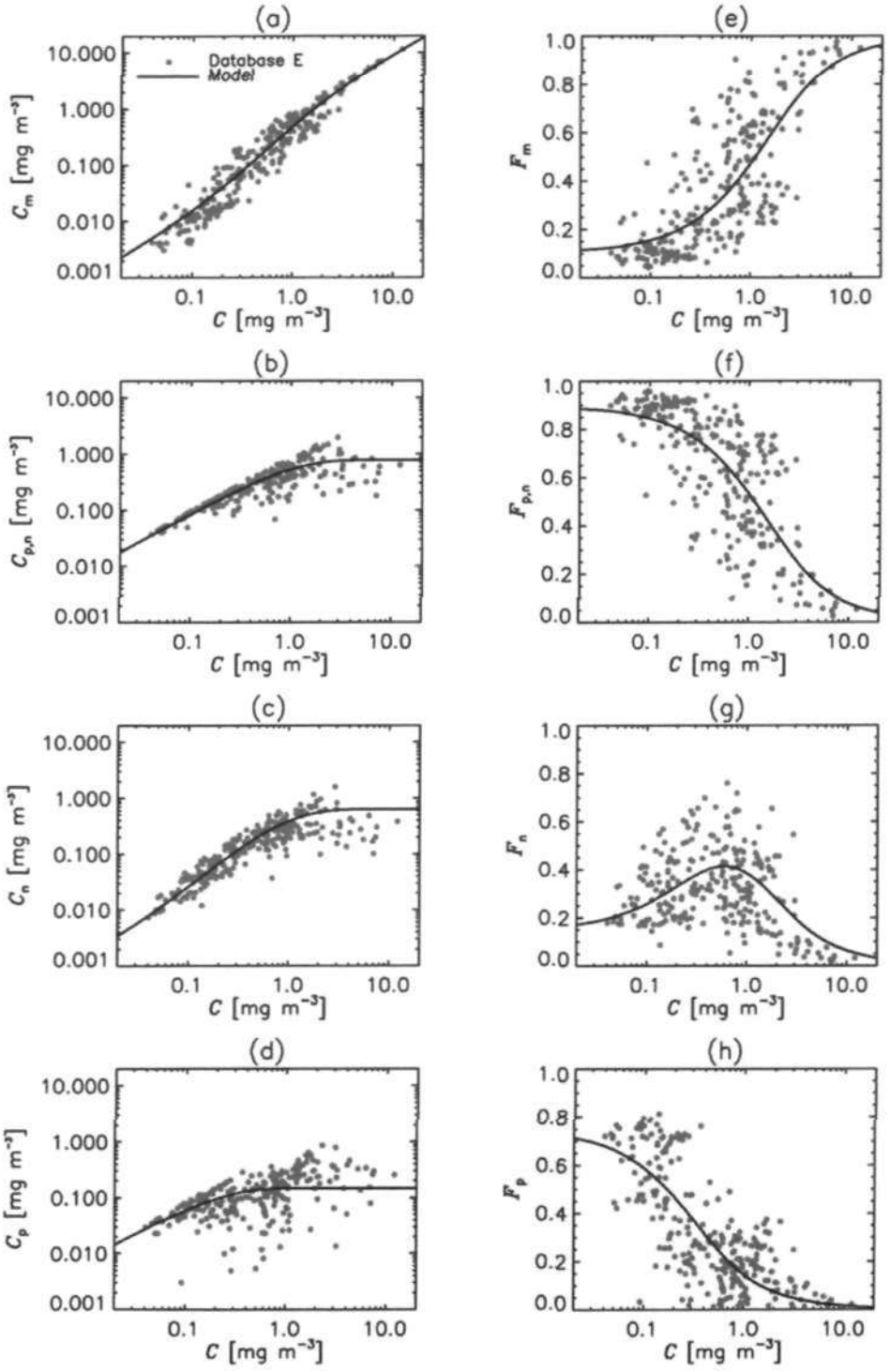

Figure 5.1: The three-component model fitted to pigment data from database E, (a-d) shows the model plotted against the size-specific chlorophyll-a concentrations and (e-h) shows the model plotted against the size-specific fractional contributions to the total chlorophyll-a concentration.

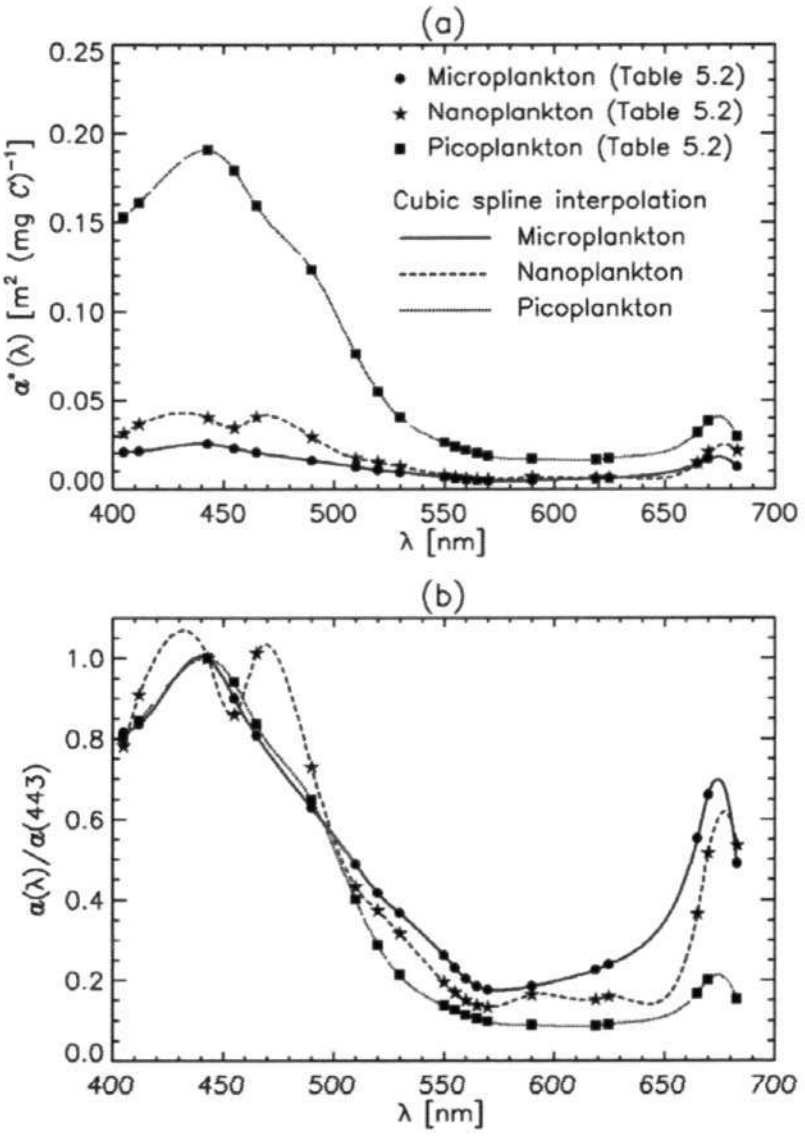

Figure 5.2: Specific absorption curves retrieved from database E using the three-component absorption model: (a) magnitude and (b) shape normalised at 443 nm.

5.3.2 Comparison with other approaches

5.3.2.1 Phytoplankton absorption coefficients as a function of the chlorophyll-a concentration

The power-law model

Figure 5.4 (a-c) shows *in situ* absorption of phytoplankton from database E versus chlorophyll-a at 443 nm, 555 nm, and 670 nm, on which the three-component model and the power-law model fitted to the same database (Table 5.2), are superimposed. Figure 5.4 (d) shows the ME% (given in Table 5.2) as a function of wavelength for the two models. In comparison with the power-law model, the three-component absorption model yielded statistically similar ME% over the 20 wavelengths (t-test p=0.66). The r values in Table 5.2 are generally comparable between the two ap-

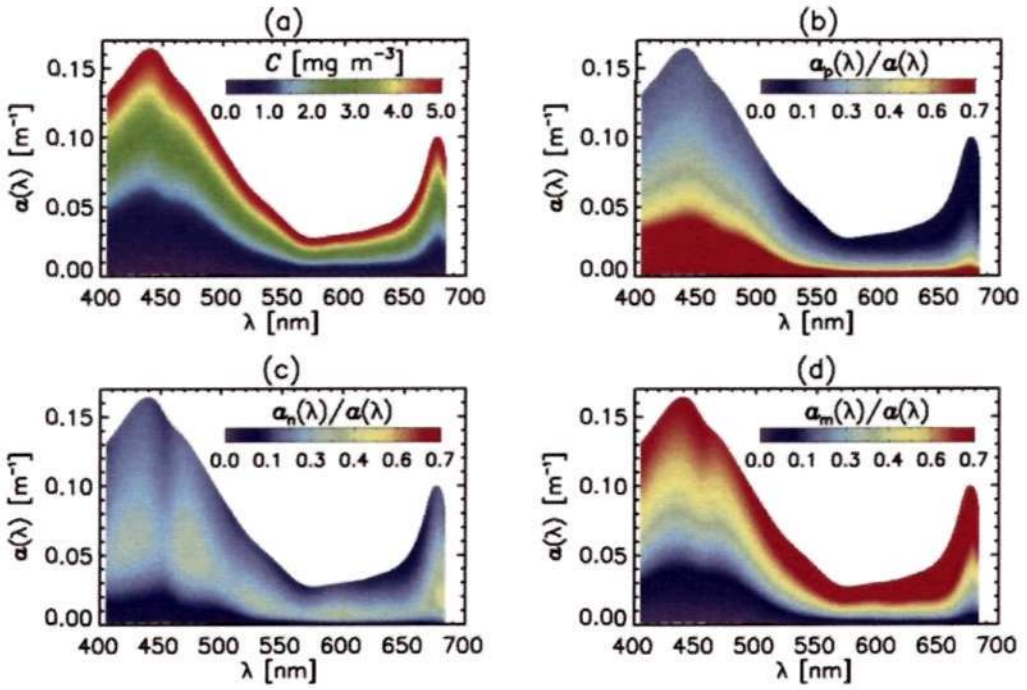

Figure 5.3: (a) The phytoplankton absorption coefficient reconstructed from the chlorophyll-a concentration according to the three-component absorption model, (b-d) shows the fractional contribution from the pico-, nano- and microplankton size classes respectively (Cubic spline used to interpolate between wavelengths in Table 5.2).

proaches (>0.84).

At low chlorophyll-a concentrations in the blue region (Figure 5.4 a) the power-law model predicts higher $a(\lambda)$ values than the three-component model. To investigate this further the specific absorption coefficients ($a^*(\lambda)$) were plotted as a function of the chlorophyll-a concentration according to both the three-component absorption model (Figure 5.5 a) and the power-law model (Figure 5.5 b) using parameters in Tables 1 and 2. The mean dominant specific absorption coefficients for micro-, nano- and picoplankton in database E were also computed using only those samples in database E for which F_p, F_n or F_m were >0.65. The specific absorption coefficients for each size class were then averaged and are superimposed in Figure 5.5 together with their confidence levels.

Whereas the three-component model represents the variability in the specific absorption coefficient between the three size classes, the power-law model overestimates the specific absorption coefficient in the blue-green region (400-550 nm) at low chlorophyll-a concentrations. The three-component model, following the theory of Sathyendranath et al. (2001) and Devred et al. (2006), constrains the specific absorption coefficients to realistic values based on phytoplankton size structure. Furthermore, the parameters of the three-component model not only offer biological interpretation (see Chapter 4), but also direct optical interpretation, as the specific

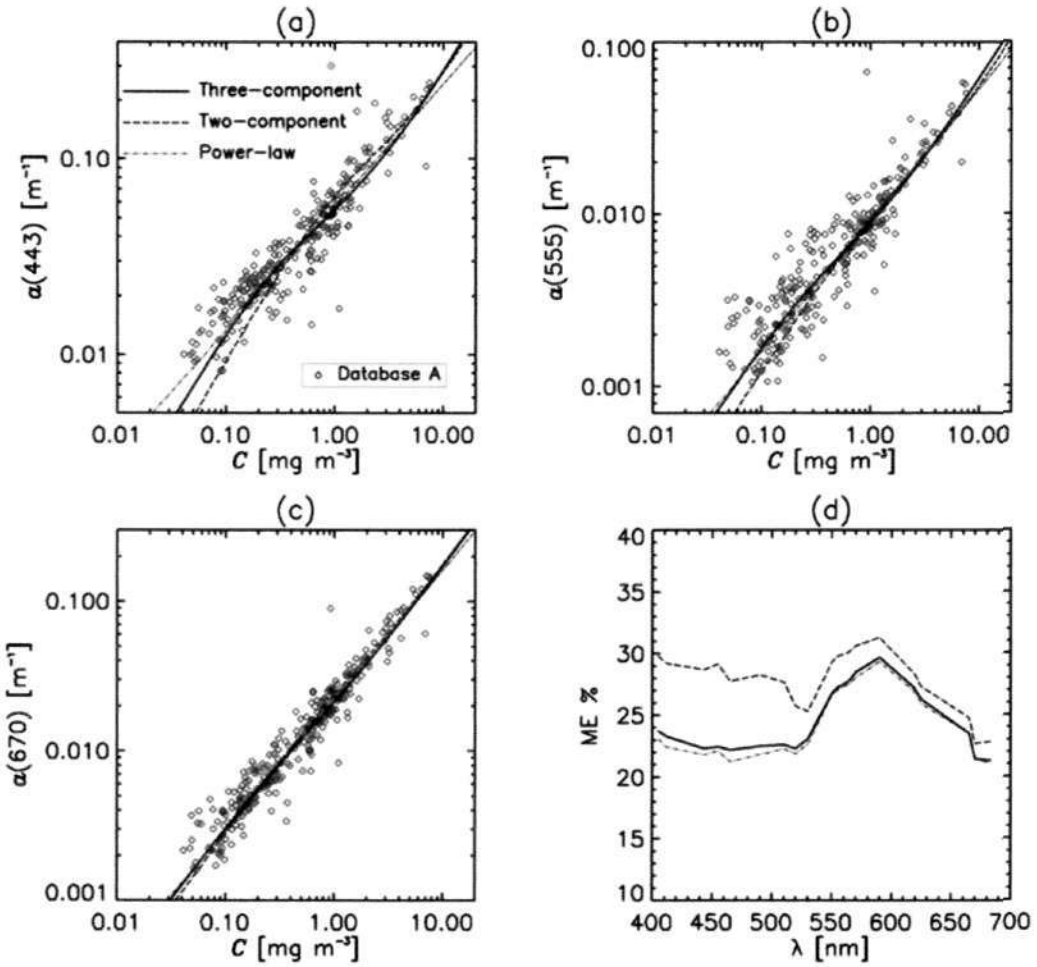

Figure 5.4: The three-component model, the two-component model (Devred et al., 2006) and the power-law model plotted against database E, with which they were parameterised, for the wavelengths (a) 443 nm, (b) 555 nm and (c) 670 nm. Figure 4 (d) shows the mean error percentages from Table 5.2 as a function of wavelength for the three models.

absorption coefficients of each size class are expressed within the model.

The model of Devred et al. (2006)

The specific absorption coefficients calculated using the three-component model and the two-component model (Devred et al., 2006, with the model parameters fitted to the database E), given in Table 5.2, and the specific absorption coefficients calculated in the Devred et al. (2006) study for global applications are plotted in Figure 5.6 (a). At all wavelengths, $a^*_{p,n}(\lambda)$ calculated using the two-component model is shown to lie between the $a^*_p(\lambda)$ and $a^*_n(\lambda)$ spectra calculated using the three-component model, as expected.

Both the $a^*_{p,n}(\lambda)$ and $a^*_m(\lambda)$ derived from database E using the two-component model are slightly higher at all wavelengths when compared with the spectra derived from the global dataset used in the Devred et al. (2006) study. The microplankton

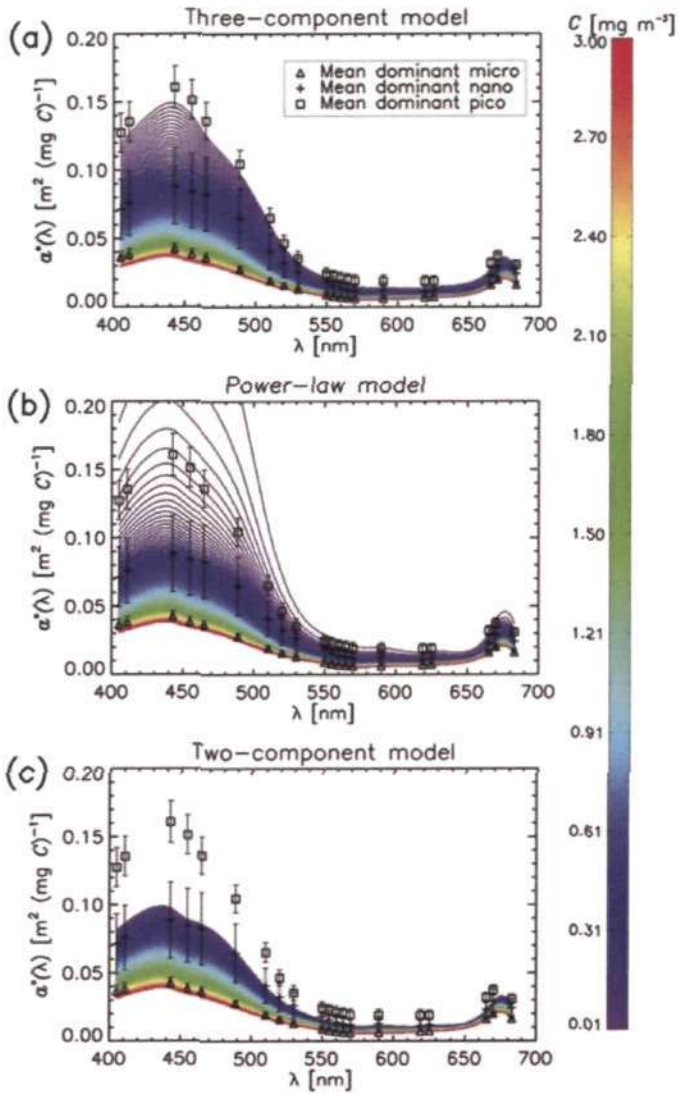

Figure 5.5: (a) $a^*(\lambda)$ calculated from the three-component model for a range of chlorophyll-a concentrations, (b) $a^*(\lambda)$ calculated from the power-law model for a range of chlorophyll-a concentrations and (c) $a^*(\lambda)$ calculated from the two-component model (Devred et al., 2006) for a range of chlorophyll-a concentrations. All models were fitted to database E, with parameters given in Tables 5.1 and 5.2 and a cubic spline used to interpolate between wavelengths in Table 5.2. Superimposed are the mean dominant size-specific $a^*(\lambda)$ spectra from database E and their 95 % confidence levels.

specific absorption coefficients, $a_m^*(\lambda)$, calculated using the three-component model are slightly higher than for the two-component model using database E in the blue part of the spectrum.

Figure 5.4 (d) compares the ME% of the two models. Over all the 20 wavelengths the three-component model produced statistically lower ME% indicating a better fit to the data when compared with the two-component model (t-test $p<0.05$). The values of r (Table 5.2) are generally similar (>0.84) between models.

In Figure 5.4 (a) and (b), for chlorophyll-a concentrations less than $0.6\,\mathrm{mg\,m^{-3}}$,

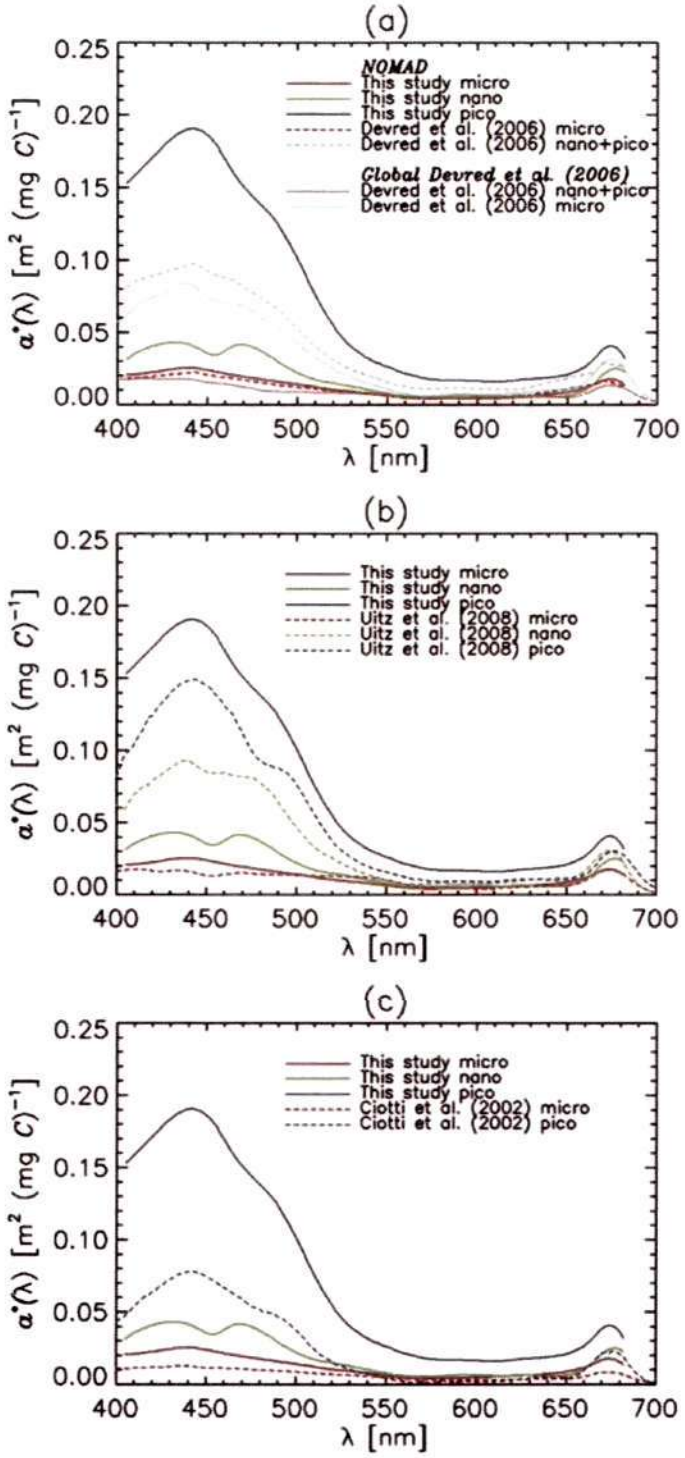

Figure 5.6: Size-specific $a^*(\lambda)$ coefficients calculated from the three-component model plotted against (a) the two-component model (Devred et al., 2006), (b) the model of Uitz et al. (2008) and (c) the model of Ciotti et al. (2002) (Cubic spline used to interpolate between wavelengths in Table 2 for three-component model and the two-component model fitted to database E).

the two-component model yields lower $a(\lambda)$ values than both the power-law model and the three-component model. Figure 5.5 (c) shows $a^*(\lambda)$ calculated according to the two-component model, using parameters in Table 5.2, for a range of chlorophyll-a concentrations. The two-component model constrains its $a^*(\lambda)$ between its $a^*_{p,n}(\lambda)$ and $a^*_m(\lambda)$ values (Figure 5.6 a). As a consequence, it fails to reproduce the high magnitude of $a^*(\lambda)$ in a picoplankton-dominated environment (i.e. at very low chlorophyll-a concentration), seen when superimposing the dominant mean size class spectra onto Figure 5.5 (c).

5.3.2.2 Specific absorption coefficients of the three size classes of phytoplankton

The model of Uitz et al. (2008)

Figure 5.6 (b) compares the specific absorption coefficients calculated using the three-component model with those of Uitz et al. (2008). The picoplankton coefficients from this study are consistently higher than those of Uitz et al. (2008) and the inverse holds for nanoplankton. The two approaches yield similar spectral shapes, with peaks at 490 nm in the picoplankton spectra attributable to zeaxanthin and peaks in the nanoplankton spectra at around 465 nm, thought to be linked to the presence of 19'-hexanoyloxyfucoxanthin and 19'-butanoyloxyfucoxanthin (Jeffrey and Mantoura, 1997). The microplankton spectra also differ between the two approaches (Figure 5.6 b).

The $a^*_m(\lambda)$ values are higher in the three-component model in the blue region of the spectrum and lower in the green region compared with Uitz et al. (2008) and they are similar elsewhere. When applying the Uitz et al. (2008) model to globally-derived chlorophyll-a fields, it is necessary to partition the values into a number of trophic classes before estimating fractions of chlorophyll-a associated with each size class (Uitz et al., 2006). In contrast, the mathematical formulation of the three-component absorption model presented here is a continuous function of chlorophyll-a concentration.

The model of Ciotti et al. (2002)

Figure 5.6 (c) shows the specific absorption coefficients calculated using the three-component model and those calculated by Ciotti et al. (2002). There are large differences between the two $a^*_p(\lambda)$, with the three-component model giving consistently higher $a^*_p(\lambda)$ values at all wavelengths. For the microplankton, $a^*_m(\lambda)$ from the three-component model is slightly higher at all wavelengths compared with that of Ciotti et al. (2002). The Ciotti et al. (2002) model is not designed to predict how the specific absorption coefficient would change as the pigment concentration varies (Figure 5.5), unlike the two-component or three-component models or the power-law function.

5.3.3 Remote-sensing validation

Remote-sensing reflectances ($R_{rs}(\lambda)$) from database F were used to derive the near surface chlorophyll-a concentration (C^s) using the OC4 algorithm (O'Reilly et al., 1998). Figure 5.7 (g) shows a comparison between the *in situ* HPLC chlorophyll-a concentrations (C) and the derived C^s concentrations in database F. The two are well correlated (r=0.69) with a ME% of 62.6 %. Larger differences are associated with samples in more optically-complex waters where simple band-ratio algorithms are known to break down (O'Reilly et al., 1998).

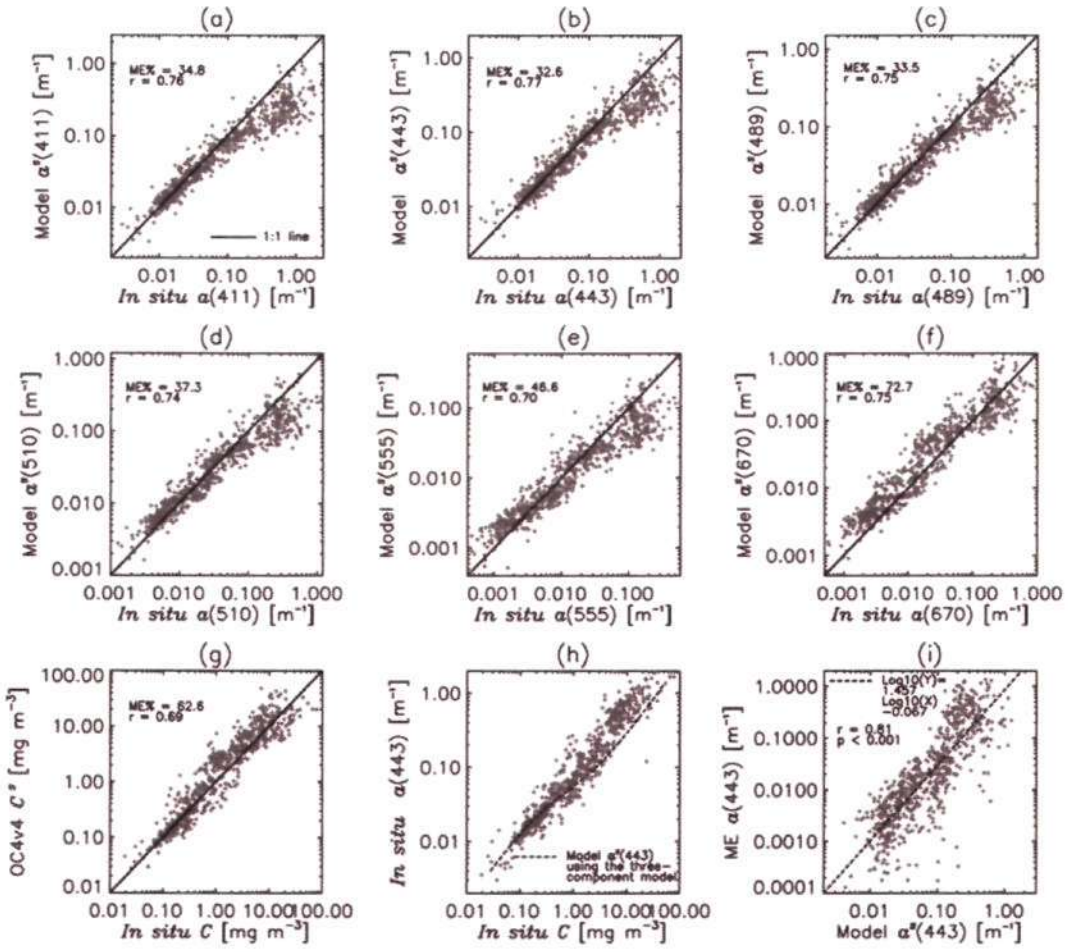

Figure 5.7: The $a^s(\lambda)$ values using the three-component absorption model compared with the *in situ* $a(\lambda)$ values in database F at the wavelengths of (a) 411 nm, (b) 443 nm, (c) 489 nm, (d) 510 nm, (e) 555 nm and (f) 670 nm respectively. The relationship between the *in situ* chlorophyll-a concentrations (C) and C^s (OC4 O'Reilly et al., 1998) from database F is shown in (g), (h) shows *in situ* $a(443)$ plotted against *in situ* C in database F with $a^s(443)$ calculated using the three-component model superimposed, and (i) shows the absolute ME between $a^s(443)$ and $a(443)$ plotted as a function of $a^s(443)$.

The three-component model (Equation 5.7) was applied to C^s using the parameters in Tables 5.1 and 5.2 to derive $a^s(\lambda)$ (total phytoplankton absorption from $R_{rs}(\lambda)$). Comparisons between remotely-sensed and *in situ* phytoplankton absorp-

tion values at the six SeaWiFS wavelengths are shown in Figures 5.7 (a-f) and indicate good agreement at blue and green wavelengths. The ME% is 32.6 to 34.8 % in the blue region of the absorption spectrum (411-489 nm), 37.3 to 46.6 % in the green region (510-555 nm) and 72.7 % in the red region (670 nm). Furthermore, all wavelengths are well correlated ($r > 0.70$). Between 411-555 nm, the three-component model underestimates a^s at high values (e.g. $> 0.2\,\mathrm{m}^{-1}$ see Figure 5.7 a, b, c, d, e and h).

The lowest ME% and the highest r coefficient in the validation was for 443 nm (Figure 5.7 b), which may be a result of this wavelength corresponding to the highest value of absorption for a given spectra and therefore the lowest signal to noise ratio. The ME between *in situ* $a(443)$ and $a^s(443)$ were computed for each sample in database F according to:

$$\mathrm{ME}_i\ [\mathrm{m}^{-1}] = |(a_{i,E}(443) - a_{i,M}(443)|\,, \tag{5.14}$$

where, $a(443)$ is the variable (phytoplankton absorption coefficient at 443 nm). i denotes the sample, subscript E denotes the estimated variable ($a^s(443)$) and the subscript M denotes the measured variable ($a(443)$). Figure 5.7 (i) shows the absolute ME at 443 nm plotted as a function of $a^s(443)$. Using a log-linear fit, a strong correlation was found between the absolute ME at 443 nm and $a^s(443)$ ($r = 0.81$, $p < 0.001$).

5.3.4 Global application

The three-component absorption model was applied to daily, Level 3, SeaWiFS chlorophyll-a composites for May 2005 to produce a monthly composite of total phytoplankton absorption and the absolute and relative estimated error (Figure 5.8). Any values greater than $12.2\,\mathrm{mg\,m}^{-3}$ chlorophyll-a were masked (as the three-component model was fitted to database E which ranged from 0.04 to $12.2\,\mathrm{mg\,m}^{-3}$). The wavelength of 443 nm was chosen for the example as it was found to have the highest correlation with the *in situ* data (Figure 5.7 b). The absolute error was estimated according to the log-linear fit described in Figure 5.7 (i), and the relative error percentage was estimated by dividing the absolute error by $a^s(443)$ and multiplying by 100.

For May 2005, high levels of $a^s(443)$ are seen in the sub-Arctic associated with the boreal Spring blooms, and in coastal upwelling zones such as the Benguela, southern North Sea and the around the Amazon outflow (Figure 5.8). Lower $a^s(443)$ values are found in the sub-tropical oligotrophic gyres. Assuming accurate atmospheric correction, the estimated absolute error is seen to increase with increasing $a^s(443)$ according to the log-linear fit (Figure 5.7 i). The estimated relative error is shown to be less than 20 % in the majority of the global ocean increasing to > 40 % in the

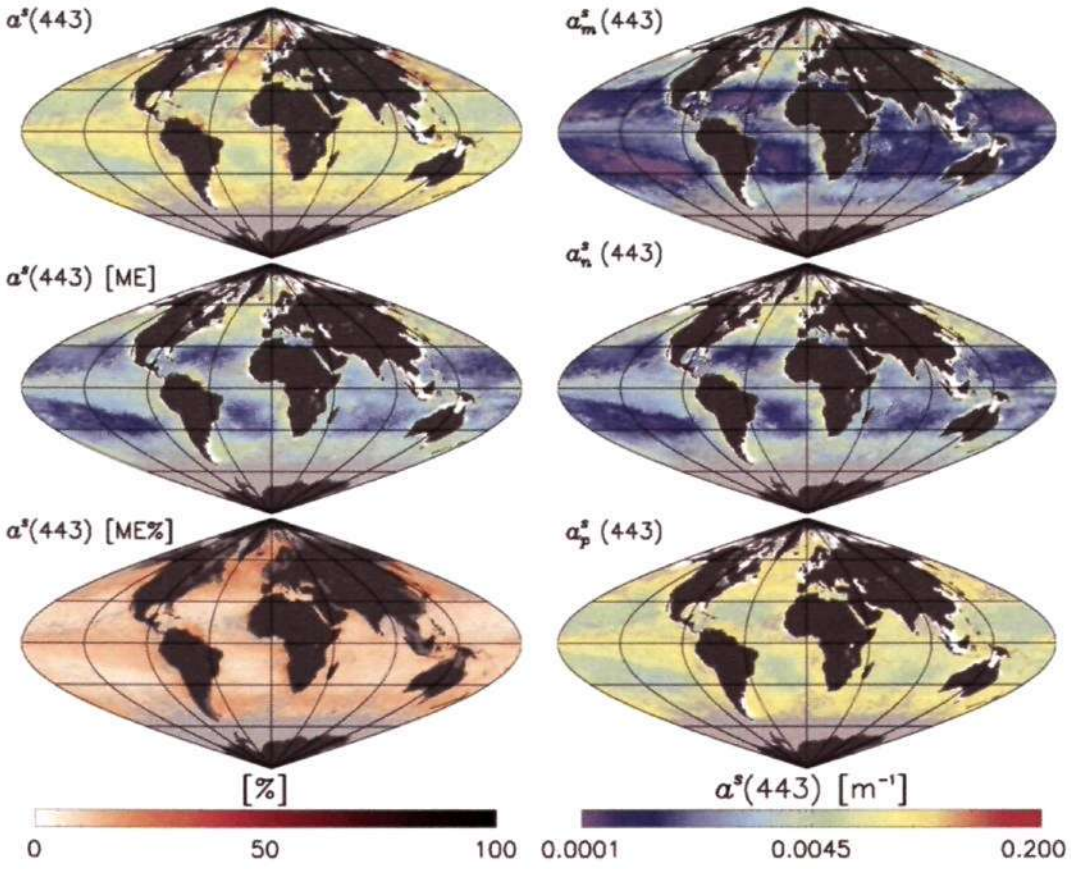

Figure 5.8: The total $a^s(443)$ values for May 2005, using SeaWiFS daily composites, with the estimated absolute and relative errors, and the micro-, nano- and picoplankton $a^s(443)$ values calculated according to the three-component absorption model. Dark grey pixels represent land, and light grey pixels represent missing data due to cloud coverage, high sun zenith angles or chlorophyll-a concentrations >12.2 mg m^{-3}. White pixels represent inland and coastal waters <200m (medium grey for $a^s(443)$ [ME%]).

highly eutrophic regions. On average over the global ocean, the estimated absolute error is 0.002 [m^{-1}] and the estimated relative error is 9.5 %.

Figure 5.8 also shows the estimated absorption coefficient of the three size classes for May 2005. Absorption by microplankton ($a^s_m(443)$) is high in the sub-Arctic and upwelling zones associated with blooms of diatoms and dinoflagellates; elsewhere $a^s_m(443)$ is low. Similar to microplankton, nanoplankton absorption ($a^s_n(443)$) contributes mainly to the eutrophic and mesotrophic regions. However, when compared with $a^s_m(443)$, their contribution extends offshore of the coastal upwelling zones and higher $a^s_n(443)$ values are found in the South and North Atlantic convergence and in equatorial regions. Picoplankton are seen to act as a background component with small variability in $a^s_p(443)$ globally. In comparison with micro- and nanoplankton, $a^s_p(443)$ is higher in the sub-tropical oligotrophic gyres.

A thorough discussion of the results in this chapter are provided in Chapter 7 (section 7.2.3.2) and the potential applications of the three-component absorption

model are also described in Chapter 7 (section 7.3.1).

5.4 Summary

A model has been developed that calculates the phytoplankton absorption coefficient at various wavelengths based on three-component populations of phytoplankton which can be linked to three size classes of phytoplankton (pico-, nano- and microplankton). The model was fitted to a database containing HPLC pigment and $a(\lambda)$ measurements and compared with a power-law model and the two component model, which were also fitted to the same database. Results from this chapter indicate:

- The new three-component absorption model provided a better fit to absorption and chlorophyll-a data than the two component model, as indicated by retrieving lower mean errors when fitting the three models to the same dataset.
- The new three-component model is an improvement on traditional power-law models in that the parameters of the model offer direct biological and bio-optical interpretation, and that the specific absorption coefficients are constrained between limits set by the values of those of picoplankton and microplankton.
- The new three-component absorption model extends the model of Sathyendranath et al. (2001) and Devred et al. (2006) by introducing a third component and this implementation yields a better representation of both $a^*(\lambda)$ and $a(\lambda)$ at low chlorophyll-a concentrations.
- The computed size-specific $a^*(\lambda)$ values were compared with those derived by Ciotti et al. (2002) and Uitz et al. (2008). Unlike the model of Ciotti et al. (2002), the three-component model can be used to predict how $a^*(\lambda)$ would change with varying pigment concentrations. Unlike the model of Uitz et al. (2008), when applying the three-component model to globally-derived chlorophyll-a fields, the model can be applied to a continuum of chlorophyll-a concentrations without having to rely on a small number of class intervals indicative of trophic regimes.
- The three-component model was applied to remotely-sensed chlorophyll-a fields and validated using independent *in situ* data which indicated good agreement (ME% is 32.6 to 34.8 % from 411-489 nm).
- Assuming accurate atmospheric correction, the new three-component absorption model can estimate the absorption coefficient of phytoplankton from satellite with an average mean error of 0.002 $[m^{-1}]$ (ME% of 9.5 %) over the global ocean at 443 nm.

Chapter 6

Seasonal and interannual variability in phytoplankton size class from 10-years of satellite observations: The intrinsic link between physics and biology

6.1 Introduction

The SeaWiFS sensor has provided satellite ocean colour observations for over a decade (McClain, 2009). This has led to a variety of studies assessing both temporal and spatial changes in phytoplankton distributions and biological production (Gregg and Conkright, 2002; Antoine et al., 2005; Behrenfeld et al., 2006; Polovina et al., 2008; Martinez et al., 2009). Whereas there are a number of satellite-based PFT algorithms available, there are a limited number of studies that have attempted to determine seasonal and interannual variability in phytoplankton communities over a 10-year period (Alvain et al., 2008; Devred et al., 2009; Uitz et al., 2010). Yet such information is of paramount importance if we are to improve our understanding of the ocean's role in the carbon cycle needed to help predict future changes in our climate.

In this chapter, the three-component model (developed in Chapter 4) is applied to ocean colour observations from a 10-year period (1997-2007) to estimate the chlorophyll-a concentration and fractional contribution to total chlorophyll-a from three phytoplankton size classes (micro-, nano- and picoplankton) within the global ocean. Seasonal and interannual variations in phytoplankton size class are investigated, with the aim of revealing a greater understanding of the evolved community composition, its spatial and temporal pattern and its relation to the underlying physics.

6.2 Methodology

6.2.1 Interannual variability in the NASA satellite chlorophyll-a algorithm

As the three-component model uses the total chlorophyll-a concentration as an input to calculate the fractional contributions of three phytoplankton size classes, when applying the three-component model to satellite-derived total chlorophyll-a data over a 10-year period, it is essential to test the satellite chlorophyll-a algorithm for any systematic interannual variability. Any small systematic deviations in the input may propagate through the calculations, particularly considering the three-component model is non-linear

In Appendix B, the NASA OC4 algorithm (O'Reilly et al , 1998, 2000) was tested for systematic interannual variability using 822 co-located remote-sensing reflectances, at SeaWiFS visible wavelengths, and *in situ* chlorophyll-a measurements from the NOMAD dataset, over the period of 1995-2007 Results indicate that given the regional and seasonal variability in the NOMAD dataset, one cannot discern any systematic interannual variability in the performance of the NASA algorithm, and that in the years where there were plenty of measurements, that were evenly distributed over the chlorophyll-a range, the OC4 algorithm appears to perform without any systematic bias Considering the three-component model has been fitted to, and verified against, data from 1997 to 2007, results suggest that the three-component model can be applied to the 10-year dataset, and interannual variability in the results can be analysed without concern of systematic bias in the input

6.2.2 Comparison of the three-component model output when using the OC4 chlorophyll-a algorithm and the GSM chlorophyll-a algorithm as input

Various algorithms have been proposed to detect the total chlorophyll-a concentration from satellite data, hence choosing an appropriate satellite algorithm for input to the three-component model is of paramount importance Two of the most common algorithms currently used for global application are the OC4 algorithm (O'Reilly et al , 1998, 2000), currently in operational use by NASA, and the semi-analytical Garver-Siegel-Maritorena (GSM) algorithm (Maritorena et al , 2002) In Appendix C, the three-component model is applied to monthly chlorophyll-a images in 2003, derived from SeaWiFS reflectance data, using both the GSM and the OC4 algorithm

Over the 12 months of 2003, results from Appendix C indicate that using the OC4 algorithm as input to the three-component model, microplankton chlorophyll-

a is 0.020 $mg\,m^{-3}$ higher (microplankton percentage 1.5 % higher), nanoplankton chlorophyll-a is 0.022 $mg\,m^{-3}$ higher (nanoplankton percentage is 1.9 % higher) and picoplankton chlorophyll-a is 0.005 $mg\,m^{-3}$ higher (picoplankton percentage is -3.4 % lower) globally, in comparison with using the GSM algorithm as input to the three-component model. These differences are primarily pronounced in the meso-eutrophic regions as opposed to the oligotrophic areas, which exhibit smaller differences. Additional spatial differences were observed depending on season and trophic level. Despite these differences, the two algorithms yield temporal patterns that are highly correlated for pico- nano- and microplankton ($r \sim 0.87$). Therefore, conclusions drawn by either input algorithm, regarding phytoplankton seasonal and interannual cycles, are generally insensitive to this choice of satellite chlorophyll-a product.

As the OC4 chlorophyll-a algorithm is in operational use by NASA, and has been extensively studied and validated to within ±35 % accuracy in case 1 waters (Gregg and Casey, 2004; Bailey and Werdell, 2006; McClain, 2009), it was chosen as input to the three-component model to investigate seasonal and interannual variability in phytoplankton size class.

6.2.3 Sensitivity analysis of the three-component model

Chlorophyll-a retrievals from ocean colour sensors are thought to be representative of the first optical depth. Within the first optical depth, parameters of the three-component model have been shown to vary between datasets (see Chapters 4 and 5). When applying the three-component model to satellite chlorophyll-a retrievals, it is essential to grasp how sensitive the model is to changes in its parameterisation. In Appendix D, a sensitivity analysis was conducted on the three-component model in order to quantify how sensitive the model is to realistic variations in its parameterisation, within the first optical depth.

The results from the sensitivity analysis indicate that nanoplankton are the most sensitive size class to variations in model parameters, as four parameters are needed to predict the chlorophyll-a concentration ($mg\,m^{-3}$) and the percentage contribution to the chlorophyll-a concentration of nanoplankton (C_p^m, $C_{p,n}^m$, S_p and $S_{p,n}$), in comparison with only two for pico- (C_p^m and S_p) and microplankton ($C_{p,n}^m$ and $S_{p,n}$). Percentage differences indicate pico- and nanoplankton are most sensitive in oligotrophic and mesotrophic areas. Absolute chlorophyll-a differences for the three size classes increase with total chlorophyll-a up to a saturation point. On average, over the global ocean, microplankton percentage difference (+ or - around the mean) was found to be 4.3 % (0.016 $mg\,m^{-3}$ absolute chlorophyll-a), nanoplankton 10.9 % (0.029 $mg\,m^{-3}$ absolute chlorophyll-a) and picoplankton 6.6 % (0.013 $mg\,m^{-3}$ absolute chlorophyll-a). These percentages differences lie within, and may partly correspond with, the errors in the three-component model when applied to

satellite data and compared with *in situ* measurements (see section 4 4.3).

6.2.4 Application of the three-component model to the Global Ocean

In Chapter 4 the three-component model was developed using an extensive dataset from the Atlantic Ocean (AMT cruises 5 to 15) The model was also validated against *in situ* data from the Atlantic Ocean (AMT cruises 2 to 4) and the NOMAD dataset, which incorporated, in addition to samples from the Atlantic Ocean, samples from the North Pacific, the California Current, the Scotia Sea, the East China Sea and the Japan Sea Furthermore, using a co-located satellite and *in situ* dataset developed in Chapter 3, the model was validated against samples incorporating the North and South Atlantic Oceans, the North Pacific gyre and the Mediterranean Sea

Using a separate *in situ* dataset from the equatorial Pacific, Brewin et al. (2010a) found the three-component model to perform with a 4 4 to 9.4 % error in phytoplankton size class percentage chlorophyll-a estimates (9 4 % for picoplankton, 4 4 % for nanoplankton and 7.2 % for microplankton), which is comparable to the validation results in Chapter 4. Furthermore, using a large global pigment database, incorporating samples from the Pacific and Indian Oceans, Hirata et al (2011) also found the total chlorophyll-a concentration and phytoplankton size classes to be highly correlated Its also worth noting that, when applied to satellite data and validated with *in situ* data, the three-component model compares well with the model of Uitz et al (2006) (sections 4 4 3 and 4 4 5), which was developed using a case 1 database with a larger geographic coverage than used in this thesis Therefore, based on this evidence the three-component model appears suitable for global application in case 1 waters

6.2.5 Satellite data and computational processing

6.2.5.1 Seasonal analysis

A total of 3633 daily Level 3 mapped chlorophyll-a SeaWiFS global images, encompassing the time period from the 1st October 1997 to the 30th September 2007, were used for analysis. The spatial resolution of each image was 1/12° by 1/12° at the equator The three-component model (Equations 4 4 to 4 7) was run on each daily image, on a pixel by pixel basis, to derive the chlorophyll-a concentration ($mg\,m^{-3}$) and the percentage contribution to the chlorophyll-a concentration of the three size classes (pico-, nano- and microplankton) resulting in six images for every single SeaWIFS image Parameter values from Table 4.1 were used, as these were found to compare well with *in situ* measurements when applied to satellite data (see section 4 4 3). All the daily images were then pooled into their respective month and 120

monthly average composites, from October 1997 to September 2007, were produced for each of the six products and total chlorophyll-a.

Global climatological seasonal maps of size-specific chlorophyll-a and the percentage contribution of each size class to total chlorophyll-a were produced, by averaging the same month of each year for the 10 year period, on a pixel by pixel basis (12 monthly climatological images for each product). To discern phytoplankton class-specific spatial variability, the 120 monthly average composites for the six products, from October 1997 to September 2007, were rescaled to 1/3° by 1/3° resolution in order to keep computing time at a reasonable level. Then for each pixel, the coefficient of variation, defined as the ratio of the standard deviation to the mean value, was calculated over the entire time-series. Two latitudinal-times transects along 30° W in the Atlantic Ocean (approximately following the AMT cruises) and 140° W in the Pacific Ocean were also used for analysis.

6.2.5.2 Interannual analysis

For interannual analysis, monthly anomalies of total chlorophyll-a, size-specific chlorophyll-a and the percentage contribution of each size class to total chlorophyll-a were produced, by subtracting each monthly climatology from the corresponding month of the time-series, on a pixel by pixel basis (120 anomaly images for each product). For comparison with physics, for the same time period (1997-2007), AVHRR Pathfinder 5 monthly mean SST data at 4 km resolution were obtained from the NASA PO.DAAC website (http://poet.jpl.nasa.gov/). In addition, monthly mean values of the Sea Surface Height Anomaly (SSHA) were downloaded from the Archiving, Validation and Interpretation of Satellite Oceanographic Data website (AVISO, http://www.aviso.oceanobs.com/). The gridded SSHA data are calculated by combining Topex/Poseidon altimetry data.

Monthly stratification estimates were calculated using monthly global density data, from the Simple Ocean Data Assimilation (SODA) database (http://www.atmos.umd.edu/~ocean). This database assimilates available field observations. Following the method of Behrenfeld et al. (2006), the density difference between the surface and a depth of 200 m was used as a measure of stratification. In comparison with the other products, monthly stratification estimates were only available from 1997 to 2004.

Global climatological seasonal maps of SST, SSHA and stratification were produced, by averaging the same month of each year for the 10 year period (7 years for stratification), on a pixel by pixel basis (12 monthly climatological images for each product). Monthly anomalies of SST, SSHA and stratification were calculated by subtracting each monthly climatology from the corresponding month of the time-series, on a pixel by pixel basis (120 anomaly images for each product). All SST, SSHA and stratification anomalies were rescaled to 1/3° by 1/3° resolution.

Two climate indices were used to compare interannual variations in size class The multivariate ENSO index (MEI) was downloaded from the National Oceanic and Atmospheric Administration (NOAA) website (http //www esrl noaa gov/) to be used to compare with the size class anomalies Furthermore, the Indian Ocean Dipole Mode Index (DMI) was also downloaded from the Japanese Agency for Marine-Earth Science and Technology (JAMSTEC) website (http //www.jamstec go jp/frsgc/research/d1/iod/) This DMI is based on output from the HadISST model The HadISST model is a set of SST data in monthly 1° area grids, from 1870 to present

6.3 Results

6.3.1 Seasonal climatoligies

Figures 6 1 though to 6 6 show climatological maps of microplankton chlorophyll-a, microplankton % total chlorophyll-a, nanoplankton chlorophyll-a, nanoplankton % total chlorophyll-a, picoplankton chlorophyll-a and picoplankton % total chlorophyll-a, respectively Microplankton chlorophyll-a is the highest in coastal upwelling systems all year round and exhibits high values in the temperate and subpolar latitudes during spring and summer (Figure 6.1), elsewhere microplankton chlorophyll-a is generally quite low The distribution is reflected in their percentage contribution to total chlorophyll-a (Figure 6.2) where microplankton contribute highly in coastal upwelling systems, and temperate and subpolar latitudes during spring and summer (~40-70 %) Percentage of microplankton declines to ~20 % along the equatorial Pacific and as low as ~10 % in the subtropical gyres Microplankton appear to be highly influenced by season in the Northern and Southern latitudes

Nanoplankton chlorophyll-a (Figure 6 3) exhibit similar patterns to microplankton, except their contribution appears to extend further offshore and nanoplankton chlorophyll-a is higher in the South and North Atlantic convergence and in equatorial regions (~0.3 $mg\,m^{-3}$) Furthermore, nanoplankton appear less influenced by season in comparison with microplankton The percentage contribution to total chlorophyll-a of nanoplankton (Figure 6 4) does not reflect the nanoplankton chlorophyll-a distribution Instead, nanoplankton are shown to maintain a background population of between 20-50 % of the total chlorophyll-a concentration, with relatively lower contributions (~20 %) in the subtropical gyres and relatively higher contributions in the coastal upwelling systems, and temperate and subpolar latitudes (~50 %). Where the microplankton % chlorophyll-a is very high (e g the Congo River Plume and the Arabian Sea in August and September, see Figure 6 2), the nanoplankton % chlorophyll-a is relatively low (~20 %) Note that regions such as the Congo River Plume are considered case 2 environments which may influence the results considering the OC4 chlorophyll-a algorithm was used as input

Picoplankton chlorophyll-a (Figure 6.5) exhibit a relatively homogeneous pattern ranging from ($\sim$0.01-0.10 mg m^{-3}) and appear less influenced by season in comparison with micro- and nanoplankton. Lower picoplankton chlorophyll-a ($\sim$0.01-0.04 mg m^{-3}) is observed in the subtropical gyres and relatively higher values in mesotrophic and eutrophic regions ($\sim$0.10 mg m^{-3}). However, the percentage contribution to total chlorophyll-a of picoplankton (Figure 6.6) displays large spatial variability with very high values in the subtropical gyres ($\sim$70 %), reducing to $\sim$40 % in equatorial regions and decreases to as low as $\sim$1 % in the coastal upwelling systems, and temperate and subpolar latitudes during spring and summer. Furthermore, the picoplankton % total chlorophyll-a appears highly influenced by seasonality, reflecting the inverse pattern to microplankton % total chlorophyll-a in Figure 6.2.

On average over the 10-year period in the global ocean (case 1 waters) picoplankton were found to contribute $\sim$48.9 % (average C_p^s value $\sim$0.05 mg m^{-3}), nanoplankton $\sim$34.9 % (average C_n^s value $\sim$0.06 mg m^{-3}) and microplankton $\sim$16.2 % (average C_m^s value $\sim$0.05 mg m^{-3}) of the total chlorophyll-a concentration.

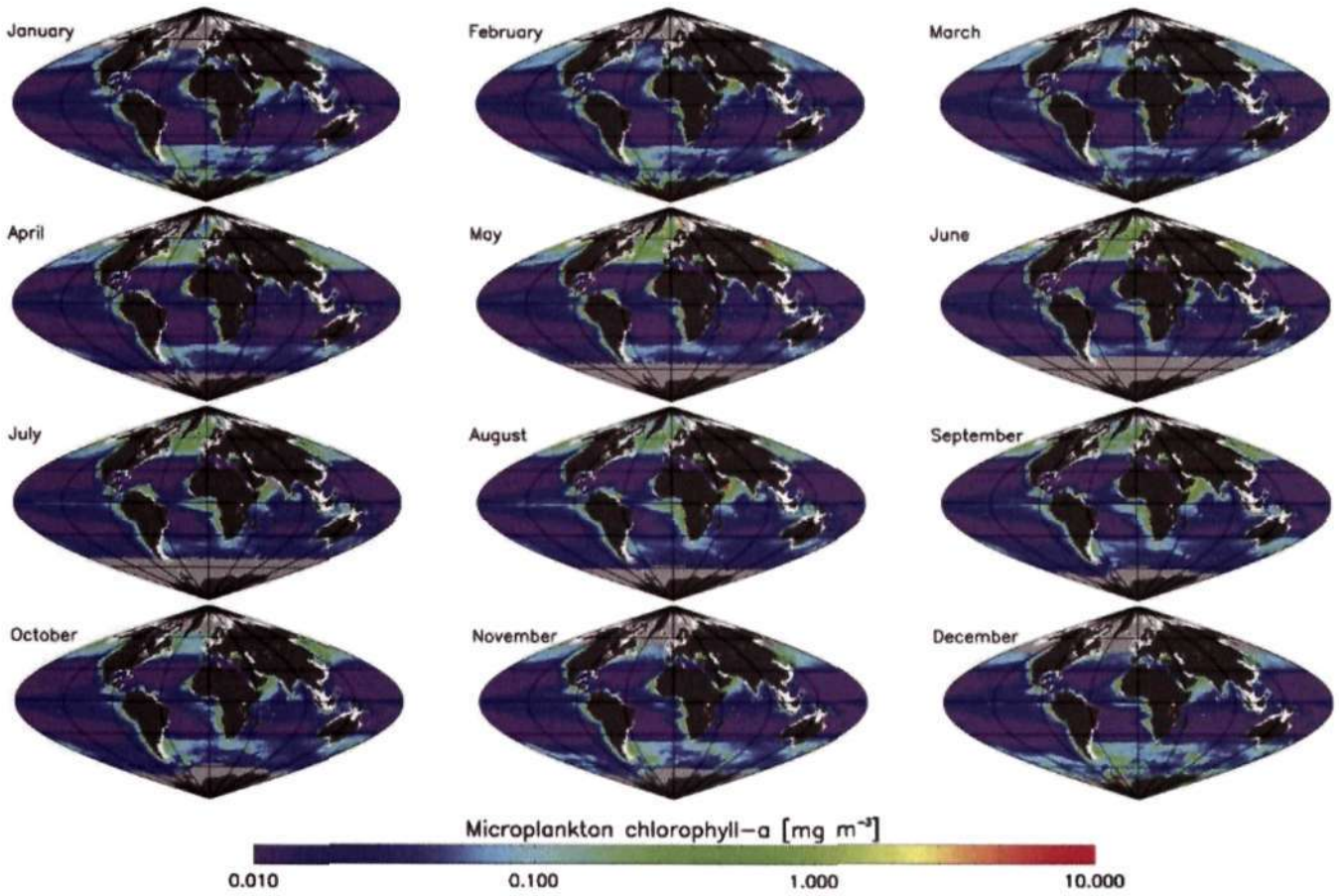

Figure 6.1: Seasonal climatology of microplankton chlorophyll-a in the global ocean. White pixels refer to bathymetry <200 m, dark grey refer to land and light grey refer to pixels not sampled due to high sun zenith angles or cloud coverage.

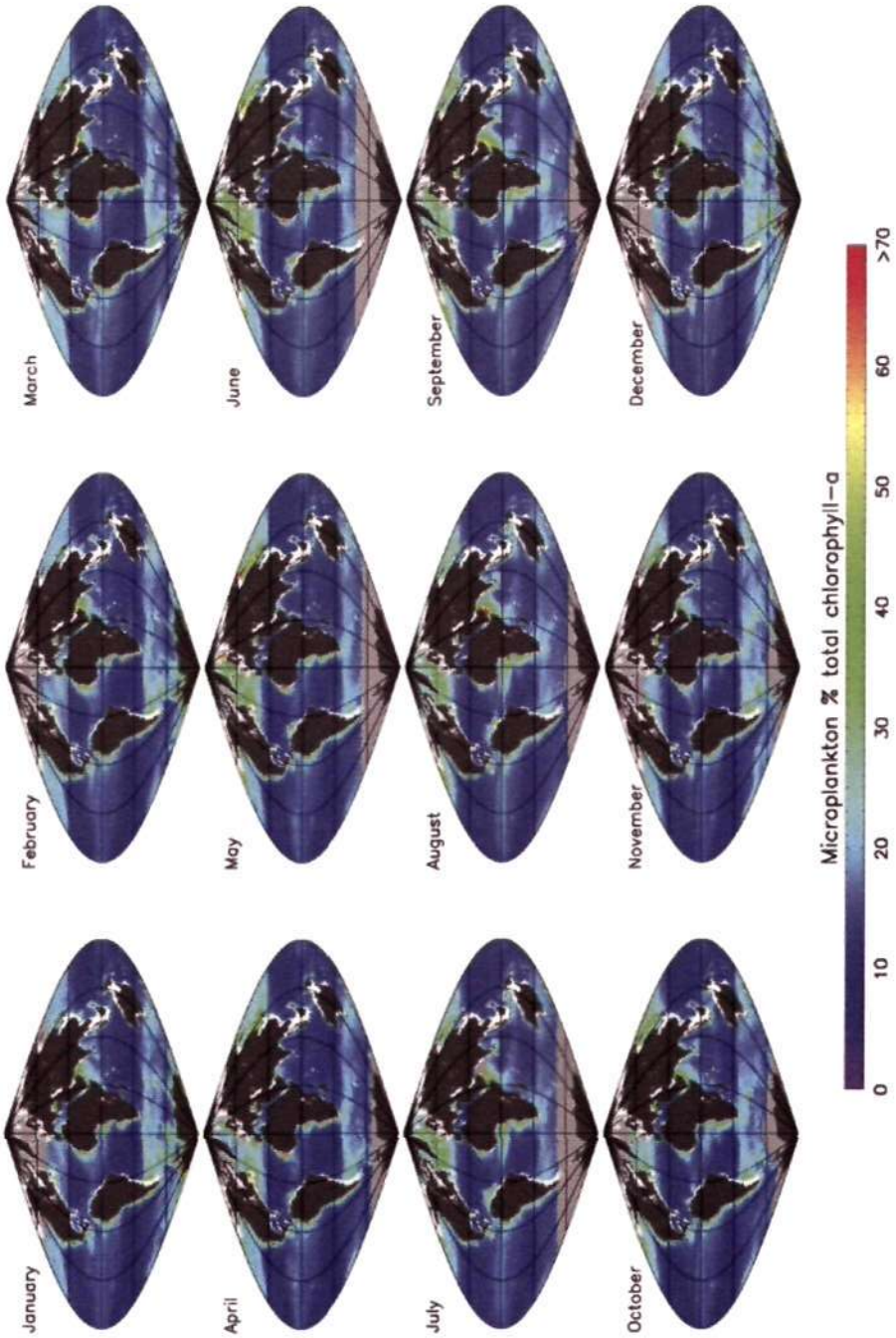

Figure 6.2: Seasonal climatology of microplankton % total chlorophyll-a in the global ocean. White pixels refer to bathymetry <200 m, dark grey refer to land and light grey to pixels not sampled due to high sun zenith angles or cloud coverage.

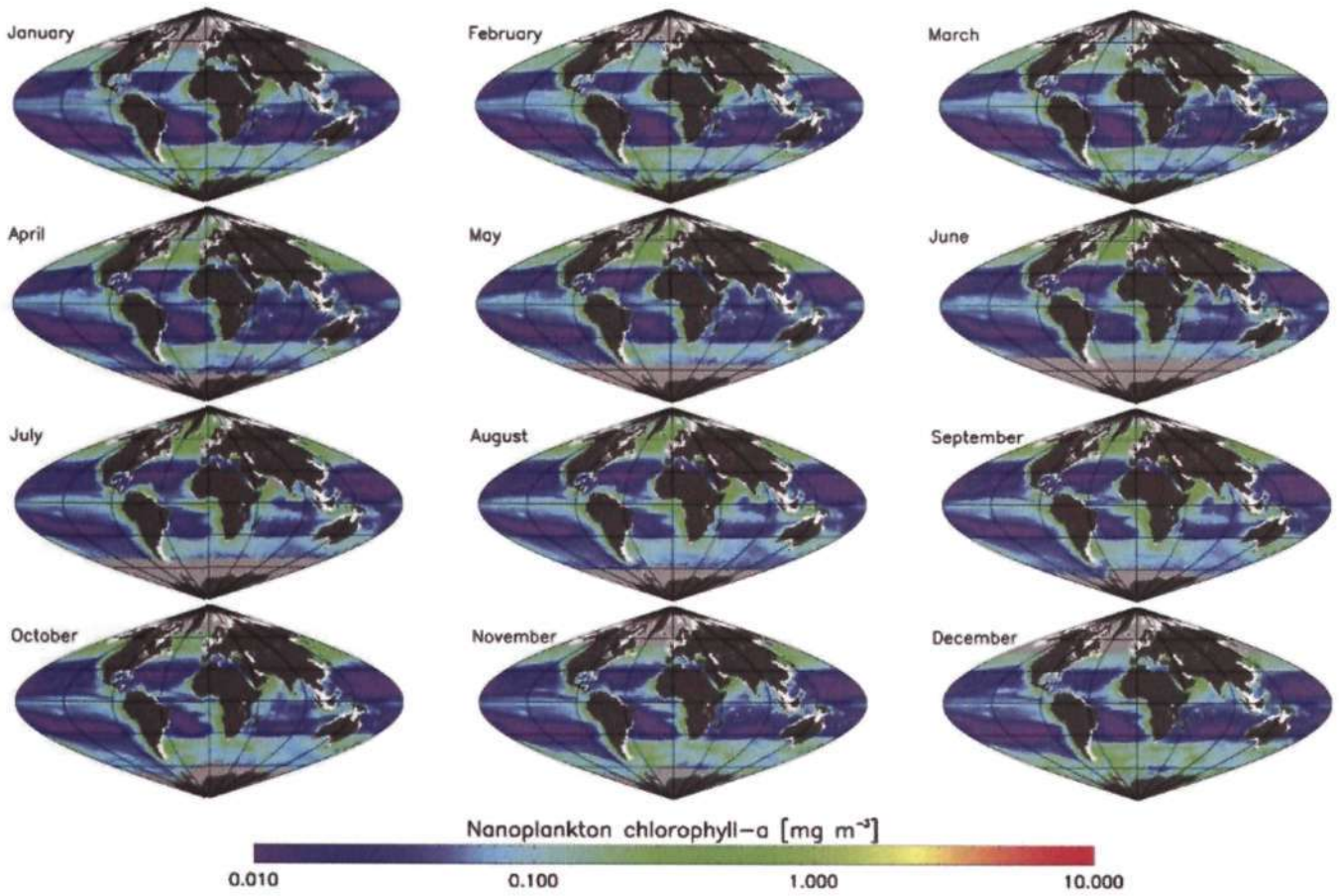

Figure 6.3: Seasonal climatology of nanoplankton chlorophyll-a in the global ocean. White pixels refer to bathymetry <200 m, dark grey refer to land and light grey refer to pixels not sampled due to high sun zenith angles or cloud coverage.

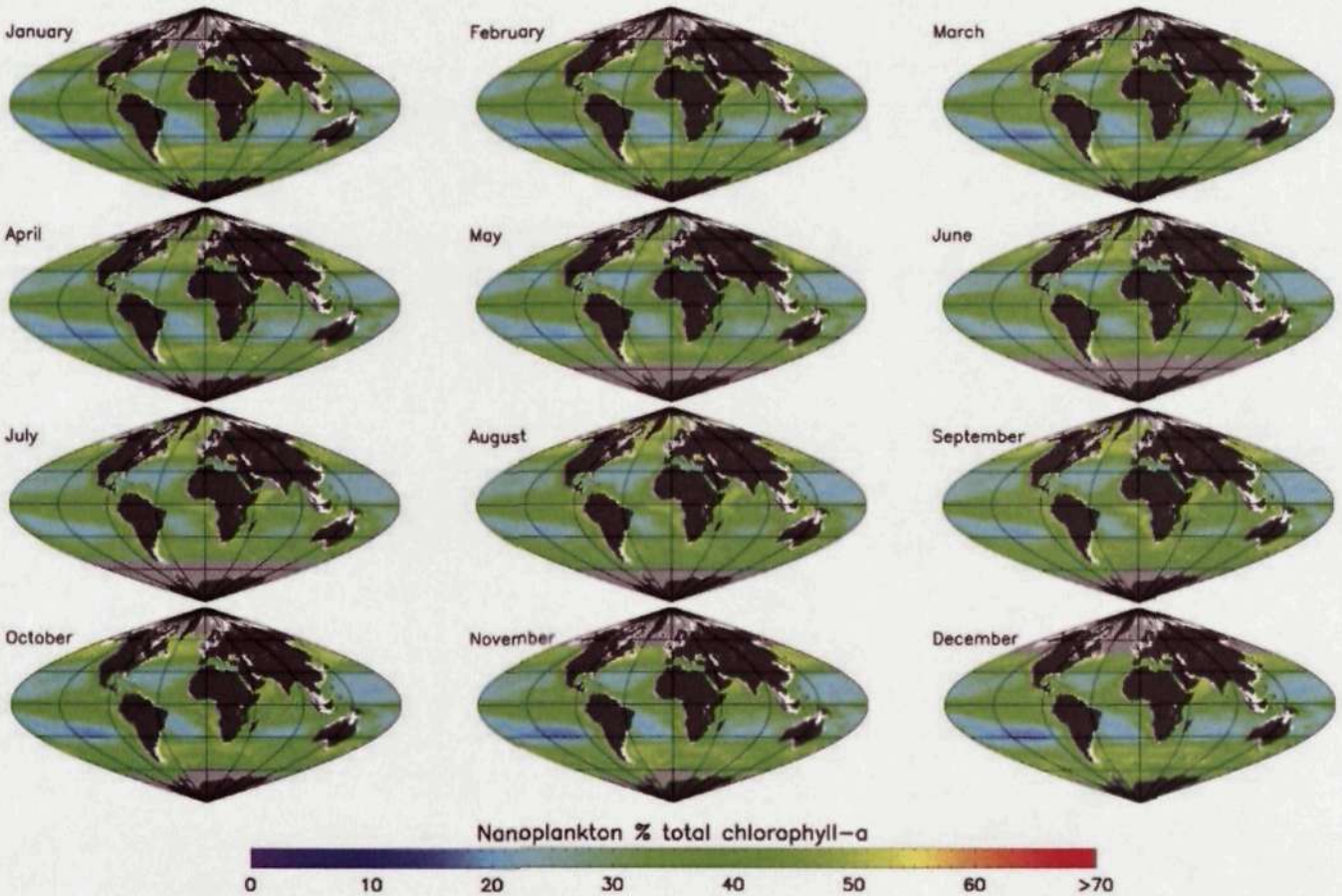

Figure 6.4: Seasonal climatology of nanoplankton % total chlorophyll-a in the global ocean. White pixels refer to bathymetry <200 m, dark grey refer to land and light grey refer to pixels not sampled due to high sun zenith angles or cloud coverage.

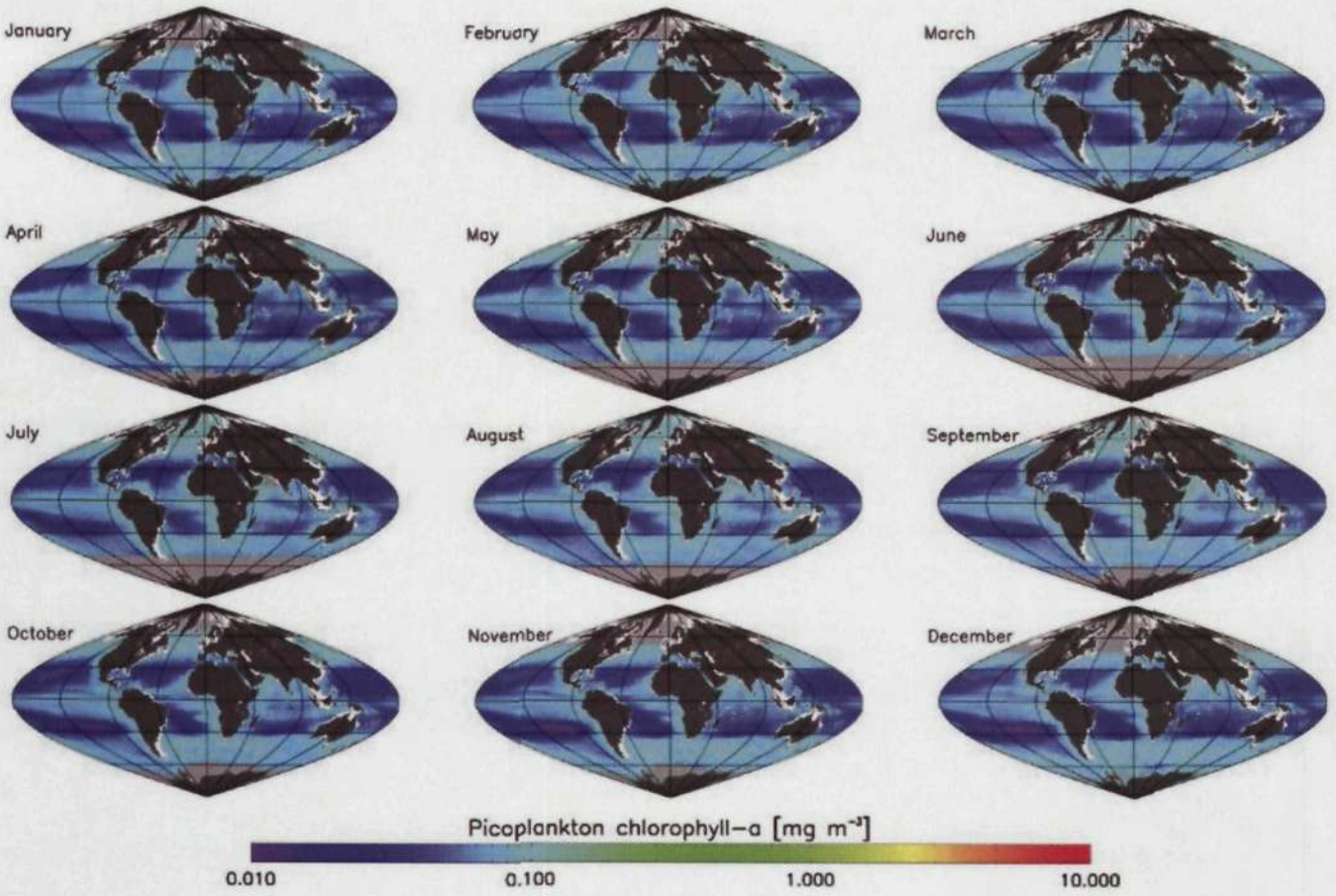

Figure 6.5: Seasonal climatology of picoplankton chlorophyll-a in the global ocean. White pixels refer to bathymetry <200 m, dark grey refer to land and light grey refer to pixels not sampled due to high sun zenith angles or cloud coverage.

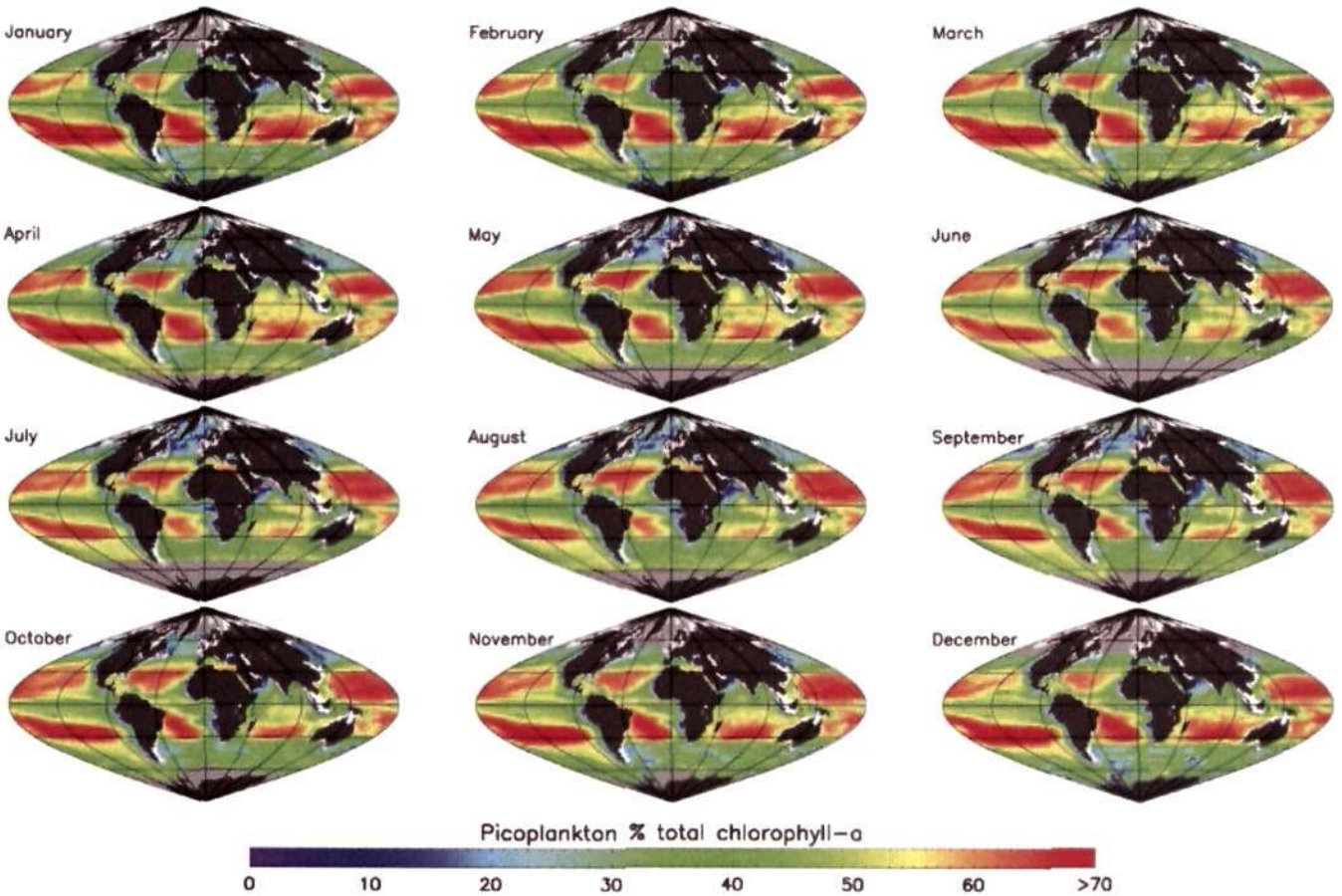

Figure 6.6: Seasonal climatology of picoplankton % total chlorophyll-a in the global ocean. White pixels refer to bathymetry <200 m, dark grey refer to land and light grey refer to pixels not sampled due to high sun zenith angles or cloud coverage.

6.3.2 Phytoplankton size class-specific spatial variability

Figure 6.7 shows the geographic distribution of the coefficient of variation of the three size classes for size-specific chlorophyll-a and % total chlorophyll-a. Figure 6.7 illustrates the temporal variability of the three size classes. The coefficient of variation is strongly influenced by the seasonal cycles of the three size class of phytoplankton. Regarding the size-specific chlorophyll-a concentrations, microplankton show maximum coefficients of variation in subpolar regions, coastal upwelling areas and around the Amazon outflow. Also noted is some degree of variability along the equatorial Pacific at 0° latitude. Microplankton are generally stable in the subtropical gyres. Nanoplankton size-specific chlorophyll-a show lower levels of variation, with higher levels around the Amazon outflow and in convergence zones between oligotrophic and mesotrophic regions. Picoplankton size-specific chlorophyll-a shows little variation globally.

Regarding the % contributions of the three size classes to total chlorophyll-a, both microplankton and picoplankton display large variations in comparison with nanoplankton. Maximum coefficients of variation, for pico- and microplankton, are found in the subpolar regions, coastal upwelling areas and in Arabian Sea. This is consistent with the seasonal cycles in such regions, associated with nutrient and light regimes, monsoonal cycles and river seasonality. Such cycles control the accumulation of large phytoplankton blooms, associated with the microplankton size class, and as a result influence not only the % total chlorophyll-a of microplankton, but also the % total chlorophyll-a of picoplankton which, due to the formulation of the three-component model, maintain a maximum level of chlorophyll-a in eutrophic environments.

Results from Figure 6.7 are consistent with the analysis of the climatological maps. Regarding size-specific chlorophyll-a, picoplankton display a relatively homogeneous pattern (background level), however, in terms of % total chlorophyll-a it is the nanoplankton that are relatively homogeneous. Microplankton clearly exhibit large temporal dynamics in both size-specific chlorophyll-a and % total chlorophyll-a.

6.3.3 Latitudinal transects

Atlantic latitudinal transect

Figure 6.8 shows Hovmöller diagrams of a latitudinal-time transects along 30° W in the Atlantic Ocean for pico-, nano- and microplankton % chlorophyll-a, in addition to their associated anomalies. The oligotrophic gyres are clearly evident as indexed by high % contribution of picoplankton to the total chlorophyll-a concentration. The more productive areas are found around latitudes higher than 40° N, lower than 40° S and in equatorial regions ~0°. Strong seasonality is observed poleward

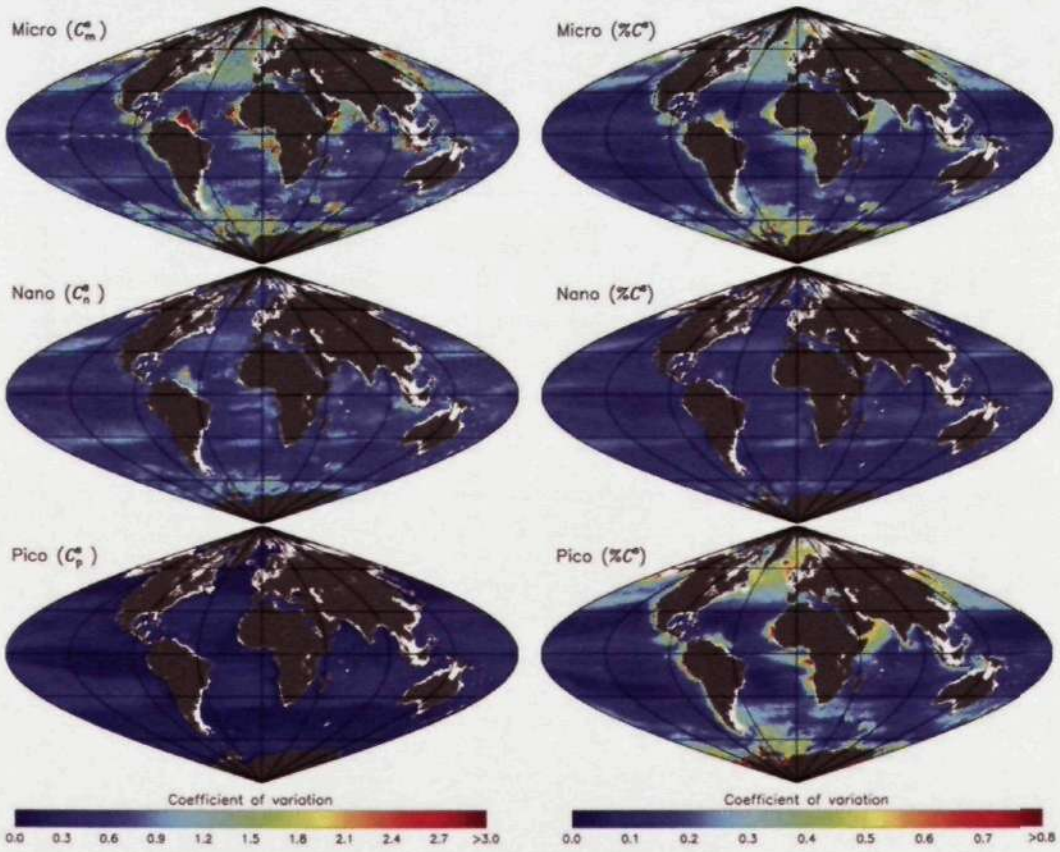

Figure 6.7: Geographic distribution of the coefficient of variation of the three size classes (the standard deviation divided by the mean) for size-specific chlorophyll-a and % total chlorophyll-a. White pixels refer to bathymetry <200 m, dark grey refer to land and light grey refer to pixels not sampled due to high sun zenith angles or cloud coverage.

of 40° latitude and the progressively later timing of the North Atlantic blooms, with increasing latitude, can be observed between 35-45° N. However, the Intertropical Convergence Zone (ITCZ) and high latitude cloud cover mask large areas.

The anomaly maps (Figure 6.8) indicate higher interannual variability at the boundaries between the oligotrophic and mesotrophic regions (i.e. ~40° latitude (N and S)). At 40° N, higher picoplankton anomalies are observed between 1998-2001 and again from 2006-2007. Lower picoplankton anomalies are observed between 2001-2005. The inverse of this is shown for the nano- and microplankton in this region. At ~40° S, a large positive picoplankton anomaly is observed in 2002 (negative for nanoplankton) where the South Atlantic oligotrophic gyre appeared to have migrated further south than usual.

Pacific latitudinal transect

Figure 6.9 shows Hovmöller diagrams of a latitudinal-time transects along 140° W in the Pacific Ocean for pico-, nano- and microplankton % chlorophyll-a, in addition to their associated anomalies. Similar patterns are observed to that of the Atlantic

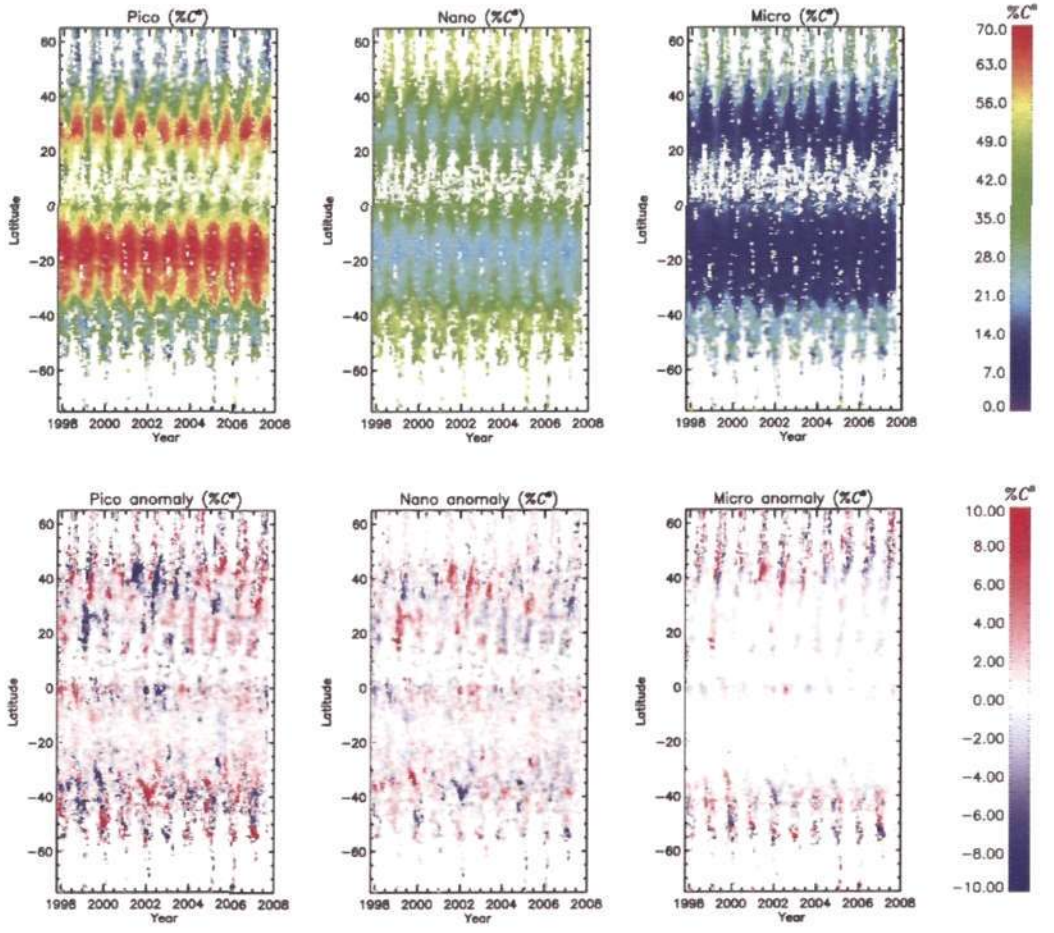

Figure 6.8: Hovmöller diagrams showing latitudinal transects along 30° W of pico- nano- and microplankton (top three images) and their associated anomalies (bottom three images) over the 10-year period (October 1997 to September 2007)

latitudinal transect, with the north and south Pacific gyres dominating at between 15-40° latitude (as indexed by high picoplankton % chlorophyll-a) and the more productive areas found around latitudes higher than 40° and in equatorial regions ~0°. However, certain differences do rise. In both of the gyres, slightly higher picoplankton % chlorophyll-a values are observed in the Pacific gyres when compared with the Atlantic gyres. Regarding the Pacific latitudinal transect, the productive zone at the equator is larger in latitudinal extent than the corresponding Atlantic region (Figure 6.8). The equatorial Pacific shows minimal seasonal variability in comparison to the Atlantic and there is also an enhanced level of microplankton % chlorophyll-a found at the equator and at ~10° S. To a lesser extent, when compared to the Atlantic transect (Figure 6.8), the ITCZ and high latitude cloud cover still mask large areas of the transect.

The major feature of the corresponding anomaly maps (Figure 6.9) is in the equatorial region of the Pacific transect. In this region (-20 to 10° latitude) large interannual variations are observed. Between 1997-1999, large positive picoplankton

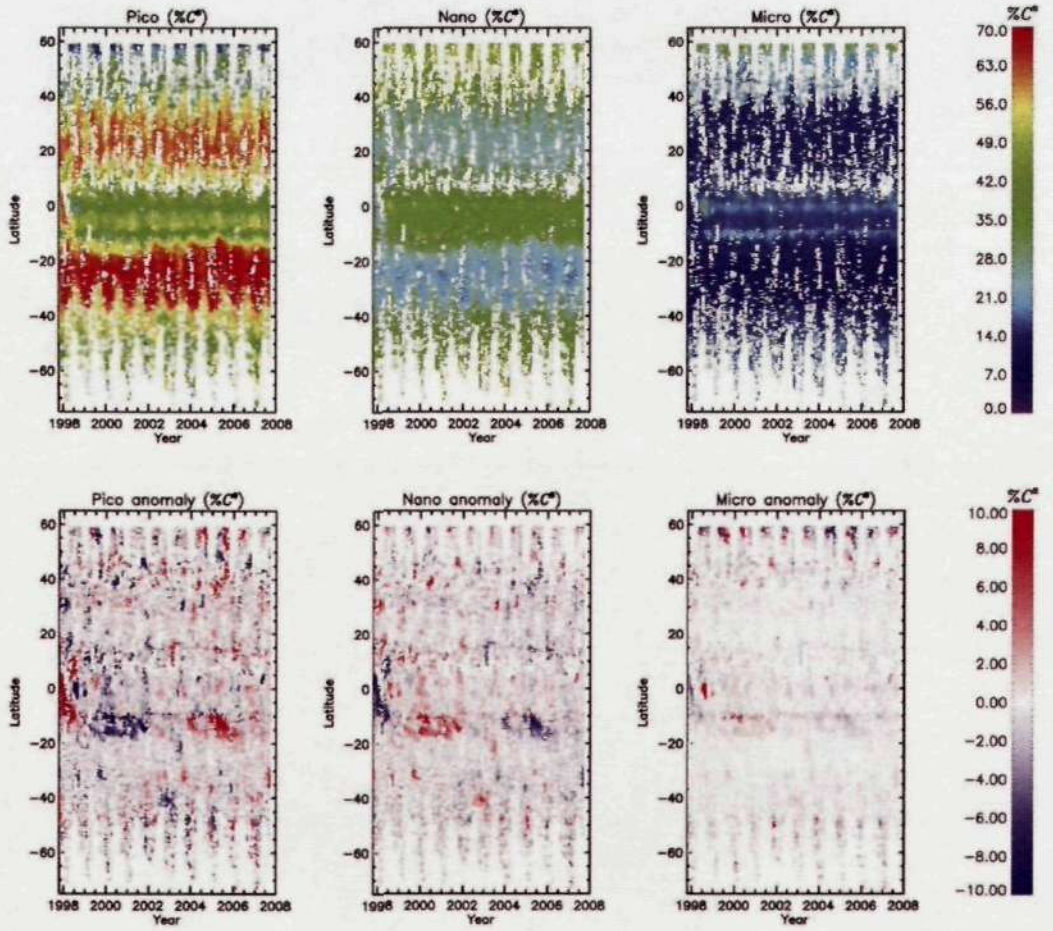

Figure 6.9: Hovmöller diagrams showing latitudinal transects along 140° W of pico- nano- and microplankton (top three images) and their associated anomalies (bottom three images) over the 10-year period (October 1997 to September 2007)

anomalies are seen (negative for nano- and microplankton), then from 1999-2004 negative picoplankton anomalies are seen (positive for nano- and microplankton) and then between 2005-2006 large positive picoplankton anomalies are again seen (negative for nano- and microplankton). This signature is clearly linked to variations in the ENSO cycle, with large picoplankton anomalies (negative for nano- and picoplankton) occurring during El Niño events of 1997-1998 and 2005-2006 at this longitude. This implies a strong correlation between the ENSO cycle and phytoplankton community in this equatorial region of the Pacific.

6.3.4 Interannual influences on phytoplankton size class

Figure 6.10 show a comparison between the DMI and MEI for the time period of October 1997 to September 2007. Between October 1997 and December 1998 the two are well correlated (r=0.82) between January 1999 and September 2007 this correlation is weaker (r=0.24).

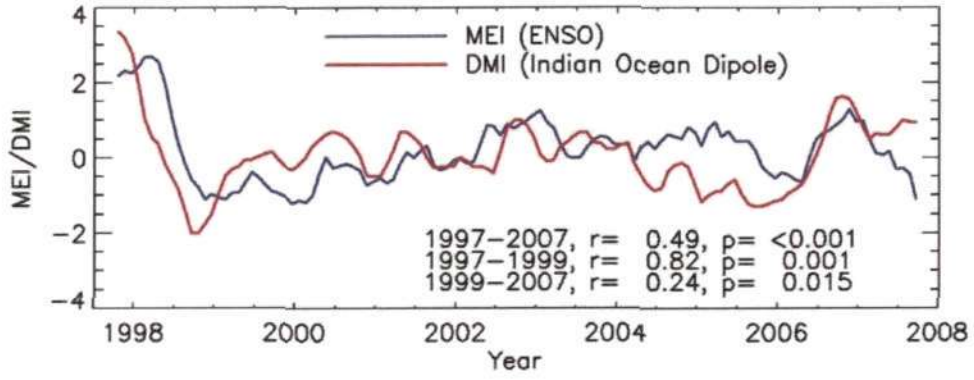

Figure 6.10: Comparison between the DMI and MEI for the time period of October 1997 to September 2007

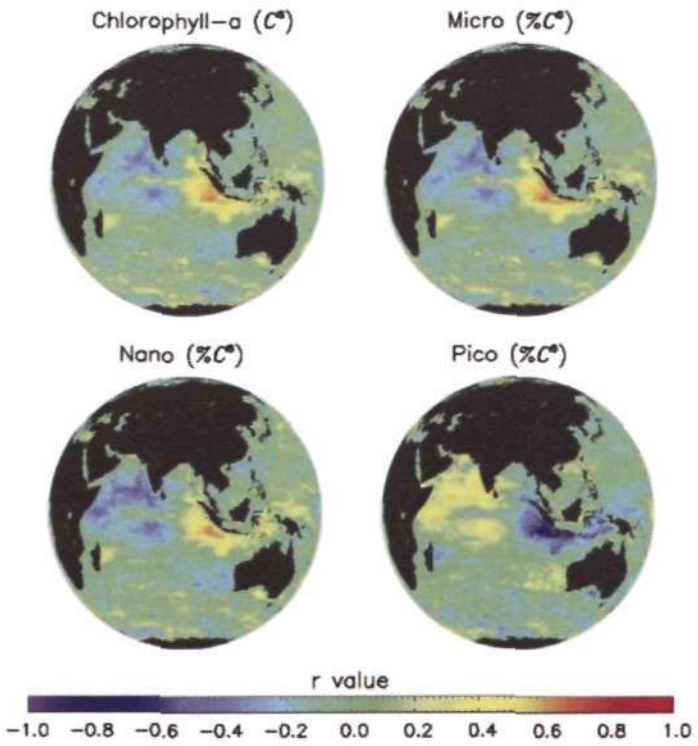

Figure 6.11: Pixel by pixel correlation between the DMI and the total chlorophyll-a anomaly as well as the DMI and phytoplankton size percentage chlorophyll-a anomaly in the Indian Ocean

Figure 6.11 shows a pixel by pixel correlation between the DMI and the total chlorophyll-a anomaly as well as the DMI and phytoplankton size percentage chlorophyll-a anomaly ($\%C^s$) in the Indian Ocean. Over the 10-year period, strong positive correlations are observed between DMI and total chlorophyll-a, DMI and microplankton $\%C^s$ and DMI and nanoplankton $\%C^s$ just off the Java Trench near the coast of Indonesia in the Indian Ocean. An inverse correlation is observed be-

tween DMI and picoplankton $\%C^s$ in the same region. In contrast, in the Arabian Basin, strong negative correlations are observed between DMI and total chlorophyll-a, DMI and microplankton $\%C^s$ and DMI and nanoplankton $\%C^s$. In the same area, strong positive correlations are observed between DMI and picoplankton $\%C^s$.

Figure 6.12 shows a pixel by pixel correlation between MEI and total chlorophyll-a anomaly as well as MEI and the phytoplankton size class $\%C^s$ anomaly in the Global Ocean. Over the 10-year period, weaker correlations are observed in the Atlantic Ocean in comparison with the Pacific and Indian Oceans. Along the equatorial region of the Pacific and Indian Oceans, strong correlations are observed between MEI and total chlorophyll-a anomaly as well as MEI and the phytoplankton size percentage chlorophyll-a anomaly (as highlighted in Figure 6.9). Similar patterns observed in the Indian Ocean (Figure 6.11) are reflected in Figure 6.12 which may be linked to the positive correction between MEI and DMI observed in Figure 6.10. The bottom of Figure 6.12 shows a global image of the number of data point used in each pixel's correlation between the two variables. In general, below 60° latitude the majority of pixels have over 50 data points (out of a possible 120), above 60° the number of data points drop below 50. However, there is a small area off the west coast of Africa (Gulf of Guinea region) where a number of the pixels have below 50 data points. This is likely to be linked with the ITCZ rendering many pixels unusable due to cloud cover.

In order to partition pixels that are strongly correlated with MEI from those that are not, a classification scheme was setup. Any pixels that did not meet the following criteria were removed.

- A correlation coefficient greater than or equal to 0.4 and less then or equal to -0.4 (a modest to very strong correlation, see Fowler et al., 1998).
- A statistically significant correlation ($p<0.05$).
- More than 50 data points (out of a possible 120).

Figure 6.13 shows the results from the classification scheme. Stage 1 (Figure 6.13 a) shows the results from the initial classification scheme. It can be seen that the vast majority of pixels are in the equatorial region of the Pacific and Indian Oceans. Pixels outside this region are sparse and scattered geographically. Therefore, an additional step was introduced which only retained pixels greater than -30° latitude, less than 40° latitude, and between 50 to 180° longitude and -180 to -70° longitude. Results from this additional step are shown in Figure 6.13 (b).

In order to test the robustness of the correlation between MEI and phytoplankton size percentage chlorophyll-a anomaly, for the allocated pixels (Figure 6.13 b), a sensitivity analysis was conducted. Using the sensitivity procedure developed in Appendix D, Appendix E tests this correlation by varying the parameters of the three-component model and running a model ensemble on a test case scenario. The

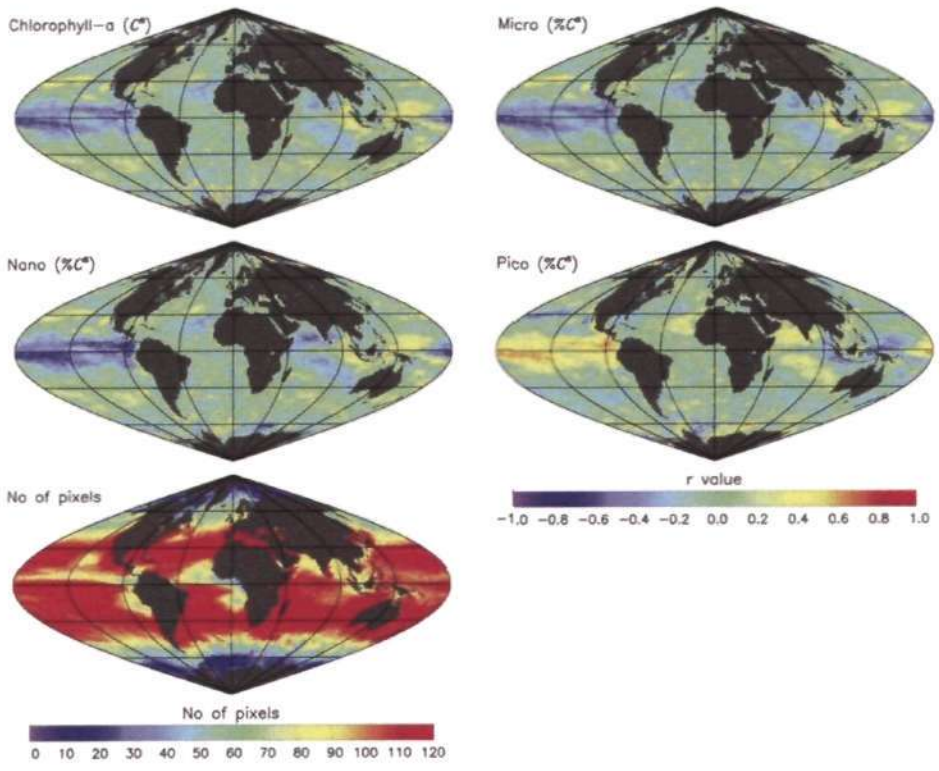

Figure 6.12: Pixel by pixel correlation between the MEI and the total chlorophyll-a anomaly as well as the MEI and phytoplankton size percentage chlorophyll-a anomaly in the Global Ocean

results from the sensitivity analysis indicate that, even when varying the parameters of the three-component model beyond the measured parameter variations shown in Chapters 4 and 5 (see Appendix D), the very strong correlation between phytoplankton size class $\%C^s$ anomaly and the MEI in the equatorial region of the Pacific and Indian Oceans (Figure 6.13 b) was maintained, regardless of parameter variations (see Appendix E).

In order to investigate further which physical parameters are influencing the strong correlation between MEI and phytoplankton size class $\%C^s$, using only the pixels from the classification (Figure 6.13 b), mean anomalies were calculated for phytoplankton size class $\%C^s$, SST, SSHA and stratification over the area of interest for the period October 1997 to September 2007. These anomalies are plotted in Figure 6.14. The biology and the physics are highly correlated in these regions. Table 6.1 shows a correlation table between $\%C^s$ phytoplankton size class anomalies and the physical parameters shown in Figure 6.14. Microplankton $\%C^s$ and nanoplankton $\%C^s$ anomaly are negatively correlated with SST, SSHA and stratification. Picoplankton $\%C^s$ anomaly is positively correlated with SST, SSHA and stratification. These correlations are high throughout the decade but extremely high between October 1997 and December 1998.

Figure 6.12 indicates that the correlation between MEI and the phytoplankton

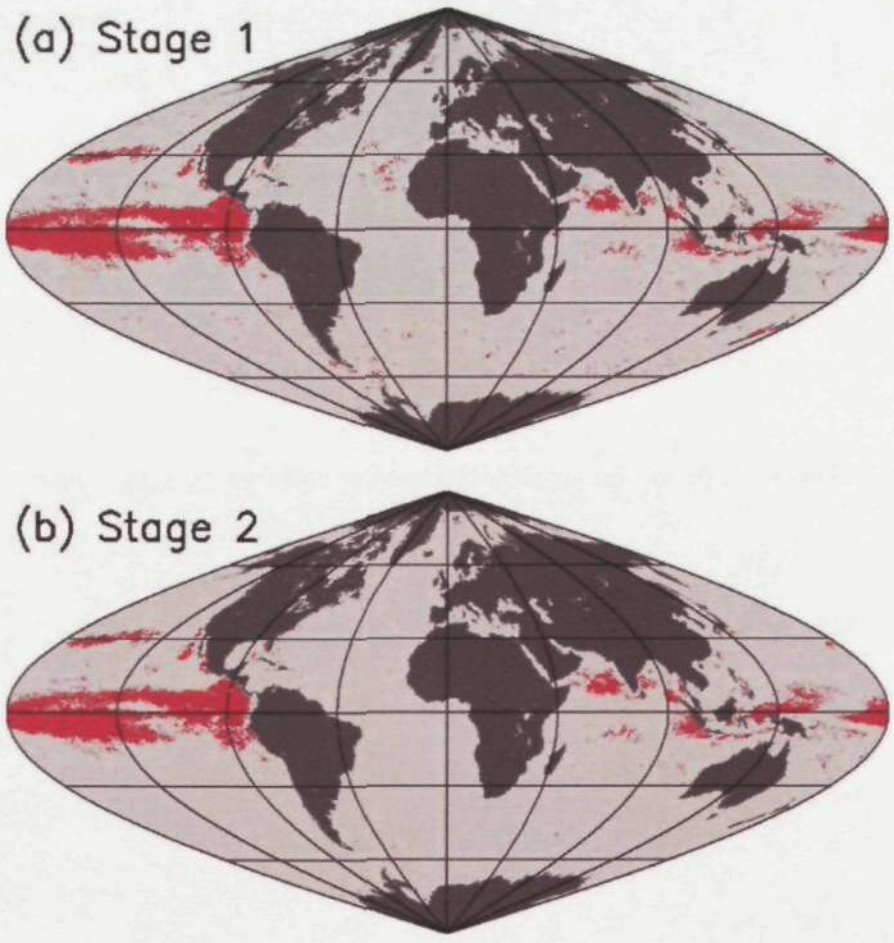

Figure 6.13: Classification scheme to partition pixels that were strongly correlated with MEI and those that were not. Pixels that were retained are shown in red.

Table 6.1: Pearson correlation coefficients (r values) showing the correlation between phytoplankton size class anomalies and physical anomalies for the pixels correlated with MEI (Stage 2 Figure 6.13)

Anomalies	1997 to 2007$^{\varpi}$	1997 to 1998$^{\iota}$	1999 to 2007$^{\gamma}$
Micro $\%C^s$ vrs SST	-0.88	-0.93	-0.82
Nano $\%C^s$ vrs SST	-0.87	-0.98	-0.81
Pico $\%C^s$ vrs SST	0.89	0.98	0.82
Micro $\%C^s$ vrs SSHA	-0.65	-0.94	-0.69
Nano $\%C^s$ vrs SSHA	-0.56	-0.94	-0.69
Pico $\%C^s$ vrs SSHA	0.59	0.95	0.70
Micro $\%C^s$ vrs stratification	-0.92*	-0.96	-0.83$^{\psi}$
Nano $\%C^s$ vrs stratification	-0.94*	-0.99	-0.82$^{\psi}$
Pico $\%C^s$ vrs stratification	0.94*	0.99	0.84$^{\psi}$

$^{\varpi}$Time series from Oct 1997 to Sep 2007
$^{\iota}$Time series from Oct 1997 to Dec 1998
$^{\gamma}$Time series from Jan 1999 to Sep 2007
*Time series from Oct 1997 to Sep 2004
$^{\psi}$Time series from Jan 1999 to Sep 2004

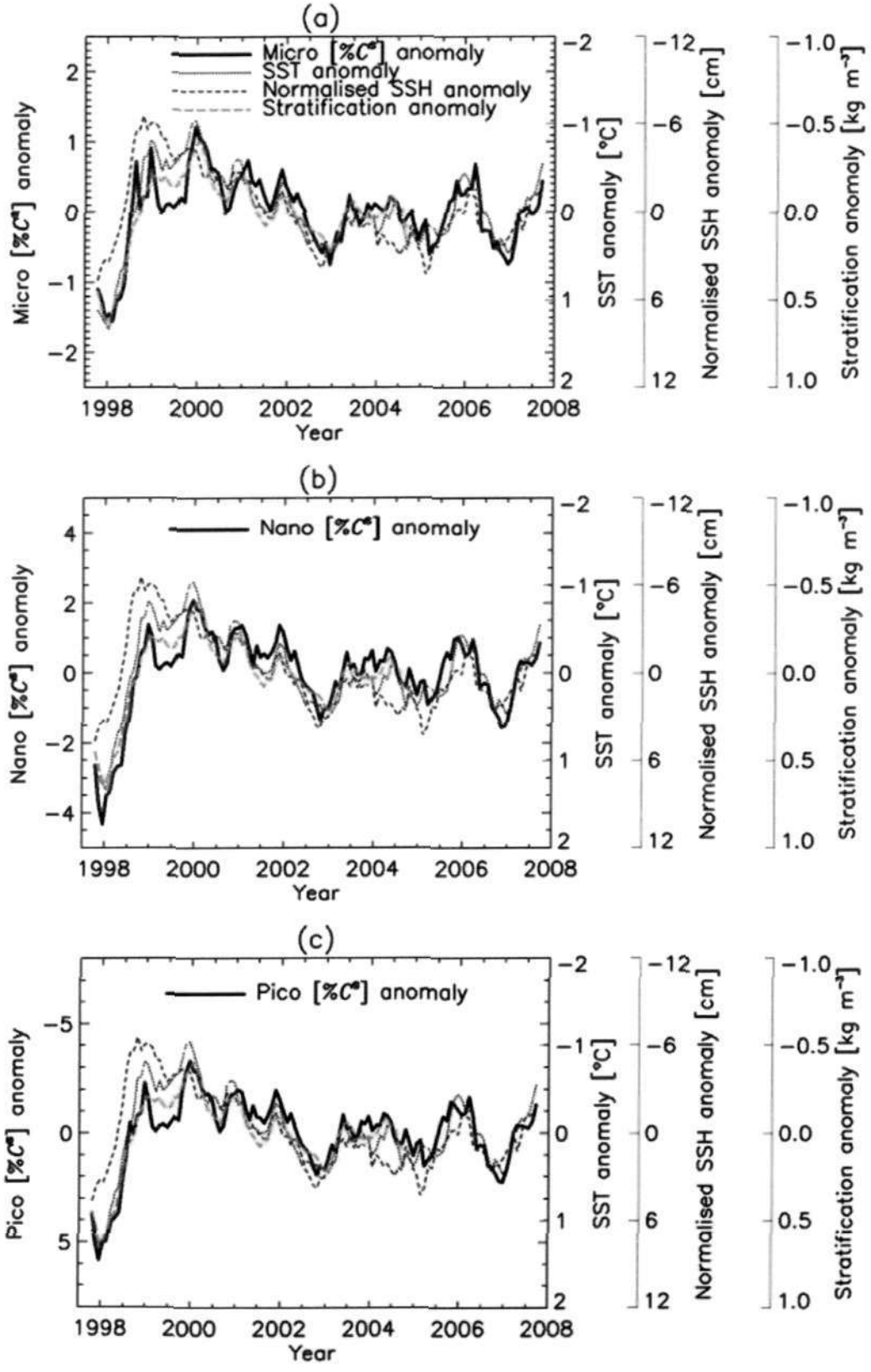

Figure 6.14: Plots of phytoplankton size class anomaly and the anomalies of SST, SSHA and stratification for the pixels classified as well correlated with MEI (Stage 2). *Note that for the picoplankton anomaly (c) the y-axis is reversed in comparison* with the nano- and microplankton y-axis (a and b)

size $\%C^s$ anomaly varies depending on geographical region. Further analysis indicates that the majority of pixels in the classification (Figure 6.13 b) can be split into two separate regions according to the relationship between MEI and phytoplankton size class $\%C^s$ anomalies, each of which can be divided further according to geographical region. Figure 6.15 highlights these four regions. In two particular regions (orange pixels), in the equatorial Pacific (between -15° to 15° latitude and between 160° to 180° longitude and -180° to 80° longitude) and the Arabian Basin (between -15° to 20° latitude and between 52° to 88° longitude), as MEI increases there is an observed decrease in microplankton $\%C^s$ and nanoplankton $\%C^s$ and an increase in picoplankton $\%C^s$, SST, SSHA and stratification. In the two regions shown in blue pixels, around Indonesia and Papua New Guinea (on both the Indian Ocean side and the Pacific, between -15° to 15° latitude and between 90° to 158° longitude) and in the central North Pacific (between 17° to 40° latitude and between 170° to 180° longitude and -180° to -130° longitude), the inverse is seen and with increasing MEI there is an observed increase in microplankton $\%C^s$ and nanoplankton $\%C^s$ and a decrease in picoplankton $\%C^s$, SST, SSHA and stratification. On large scales, MEI reflects both changes in chlorophyll-a (and hence phytoplankton size structure) and the underlying physics, consistent with known processes of equatorial upwelling (Chavez et al., 1999).

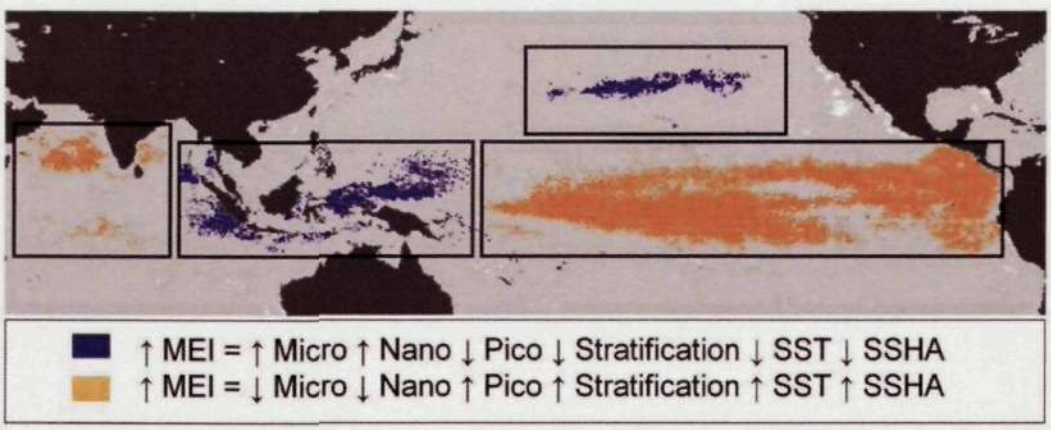

Figure 6.15: Two separate regions of the equatorial Pacific and Indian Oceans that respond differently during ENSO transitions. These regions can be further split according to geographical region.

Results from Table 6.1 highlight that the phytoplankton size structure is well correlated with the physical parameters (SST, SSHA and stratification) but that this correlation is particularly strong during October 1997 and December 1998. In order to investigate whether the same applies to the relationship between MEI and size class, separate correlation maps for the October 1997 to December 1998 period and the January 1999 to September 2007 period were produced (Figure 6.16). Similar to Table 6.1, very high correlations between MEI and size class were observed between the October 1997 to December 1998 period in comparison with moderate

correlations during the January 1999 to September 2007 period (Figure 6.16). This suggest that large ENSO events (e.g. 1997-1998 period, see Figure 6.10) have a prominent influence on the phytoplankton size class composition.

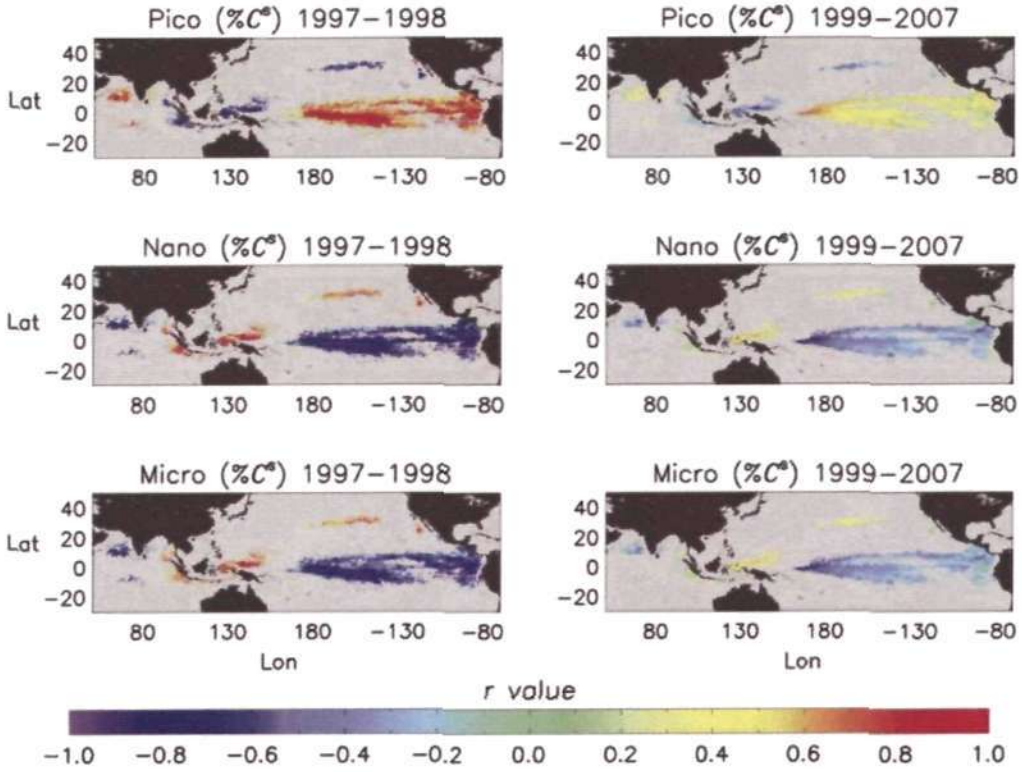

Figure 6.16: Pixel by pixel correlation between the MEI and phytoplankton size percentage chlorophyll-a anomaly in the classified pixels (Stage 2 Figure 6.13) for both the October 1997 to December 1998 period and the January 1999 to September 2007 period.

Figure 6.17 shows the slope and intercepts for the linear correlations between MEI and size class for the October 1997 to December 1998 period. These slope and intercepts have geographical variations depending on pixel location. In addition, mean errors (ME) are provided (Figure 6.17) on a pixel by pixel basis between the satellite estimate (three-component model) and the MEI model estimate. The majority of the pixels have a ME of less than 8 % for all size classes, with the exception of a few small regions in the central equatorial Pacific, off the Java Trench and around the coast of North and South America where pico- and microplankton have a ME as high as 10 %. By using the slope and intercepts, on a pixel by pixel basis, phytoplankton size $\%C^s$ anomalies can be modelled as a function of MEI during large ENSO events similar to the 1997-1998 event (Figure 6.10)

Figure 6.18 shows phytoplankton size $\%C^s$ anomaly maps for January 1998 from the three-component model for the classified pixels (Figure 6.13 b) in addition to the modelled anomaly map estimates using the linear relationship between MEI and phytoplankton size $\%C^s$ (Figure 6.17). In general the two estimates are very similar.

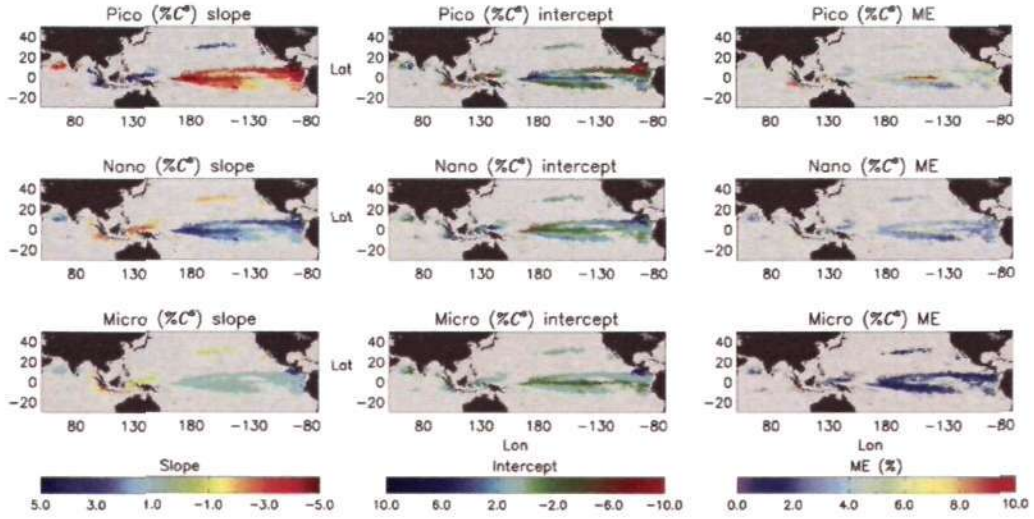

Figure 6.17: The slope and intercept of the pixel by pixel linear correlations between MEI and phytoplankton size percentage chlorophyll-a anomaly for the classified pixels (Stage 2 Figure 6.13). The mean absolute errors (ME) are also provided on a pixel by pixel basis between the satellite estimate (three-component model) and the MEI model estimate of the phytoplankton size percentage chlorophyll-a anomaly.

The patterns in the anomalies derived from the MEI model reproduce those derived from satellite by the three-component model. The MEI model estimates cover a larger spatial area than the satellite estimates, as the MEI model is not constrained by cloud or atmospheric conditions that may render pixels unusable in the satellite estimates.

A further advantage of the MEI model estimates, in comparison with the satellite-based three-component model estimates, is that MEI is available for the past 50 years whereas the SeaWiFS sensor is only available from 1997 to the present day. Therefore, by searching back through the MEI time-series (Figure 6.19) and looking for similar events to that of the El Niño to La Niña 1997-1998 transition, past events can be inferred when there was no available satellite measurements. Figure 6.19 shows MEI model estimates of phytoplankton size class $\%C^s$ anomalies from two months July 1972 and December 1973, when a similar ENSO transition to that of the 1997-1998 event occurred. Over this 15 month period, according to the MEI model estimates, large changes in the community structure of the phytoplankton occurred, due to large changes in physical forcing driven by the ENSO transition.

6.3.5 Summary

In this chapter, the three-component model developed in Chapter 4 has been applied to ocean colour observations from a 10-year period (1997-2007) using the SeaWiFS database. Seasonal and interannual variations in phytoplankton size class were investigated with the aim of understanding of the evolved community composition,

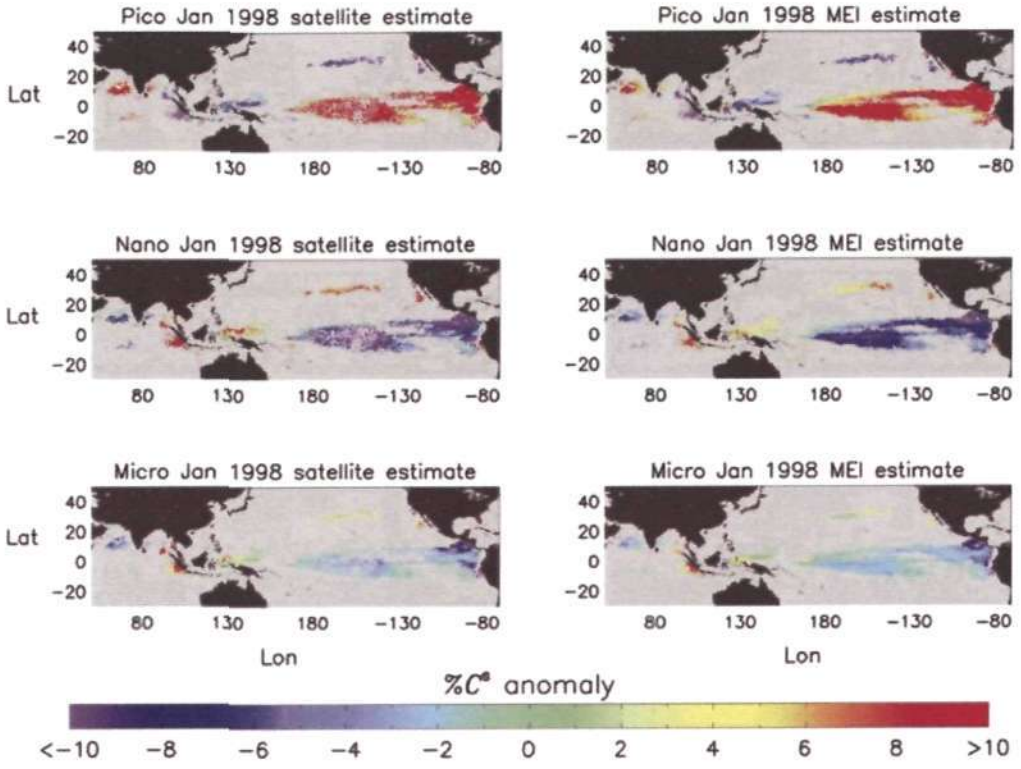

Figure 6.18: Phytoplankton size percentage chlorophyll-a anomaly maps for January 1998 from the satellite-based three-component model for the classified pixels (Figure 6.13 b) in addition to the modelled anomaly map estimates using the linear relationship between MEI and phytoplankton size percentage chlorophyll-a (Figure 6.18).

its spatial and temporal pattern and its relation to the underlining physics. Results from this chapter indicate:

- On average over the 10-year period in the global ocean (1997-2001), picoplankton were found to contribute ~48.9 % (average C_p^s value ~0.05 mg m^{-3}), nanoplankton ~34.9 % (average C_n^s value ~0.06 mg m^{-3}) and microplankton ~16.2 % (average C_m^s value ~0.05 mg m^{-3}) of the total chlorophyll-a concentration in surface waters.

- Microplankton exhibit large temporal and spatial differences in both size-specific chlorophyll-a and % total chlorophyll-a.

- Nanoplankton absolute chlorophyll-a is more variable than picoplankton but less than microplankton. Regarding their fractional contribution to total chlorophyll-a (% range), nanoplankton display a relatively stable pattern.

- Regarding the absolute chlorophyll-a concentrations, picoplankton act as a background population, although higher concentrations are observed in eu-

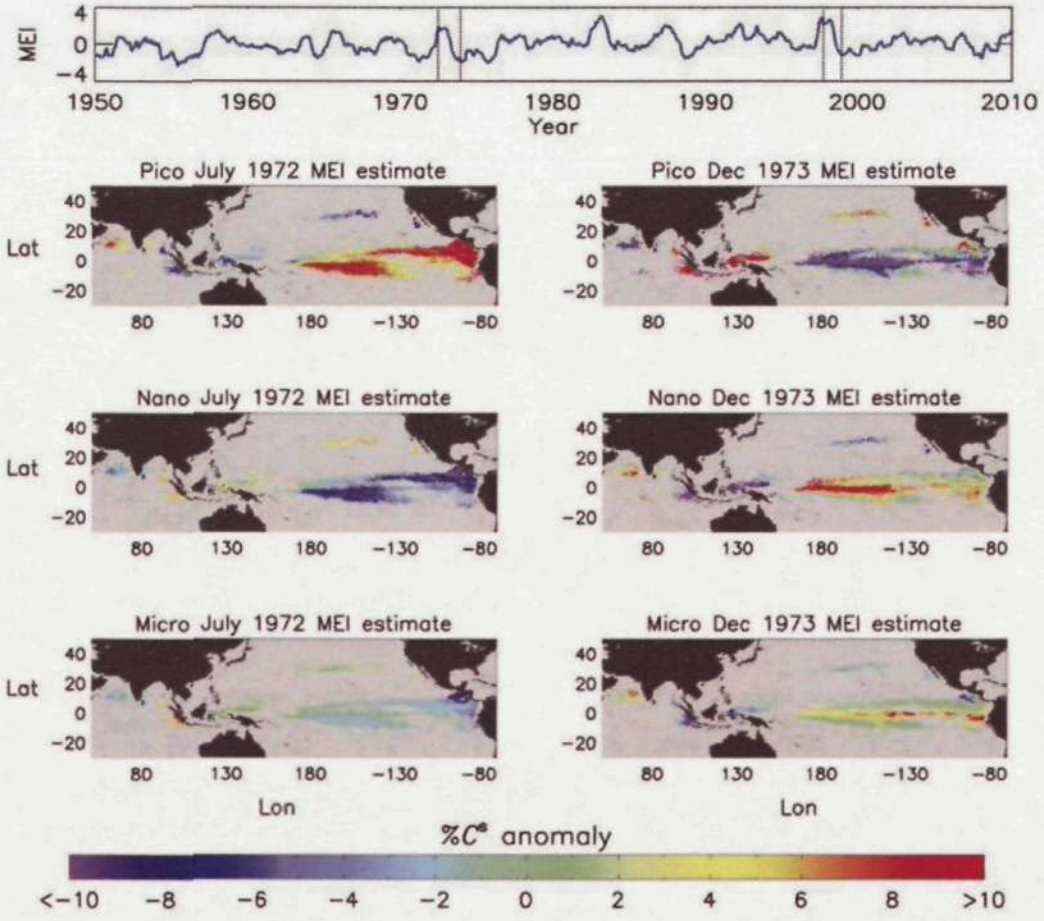

Figure 6.19: Phytoplankton size percentage chlorophyll-a anomaly maps for July 1972 and December 1973 for the classified pixels (Stage 2 Figure 6.13) derived using the linear relationship between MEI and phytoplankton size percentage chlorophyll-a (Figure 6.17). Top graph show the 50 year MEI time-series and the locations of the two large ENSO transitions (1972-1973 and 1997-1998).

trophic waters when compared with oligotrophic waters. Their fractional contribution to total chlorophyll-a is, however, highly variable.

- In the equatorial regions of the Pacific and Indian Oceans, phytoplankton size class anomalies are highly correlated with the ENSO.

- In the equatorial regions of the Pacific and Indian Oceans, interannual changes in phytoplankton size class are highly correlated with changes in SST, SSHA and stratification. Microplankton $\%C^s$ and nanoplankton $\%C^s$ are negatively correlated with SST, SSHA and stratification and picoplankton $\%C^s$ is positively correlated with SST, SSHA and stratification.

- The MEI appears a useful tool for inferring changes in phytoplankton size structure during past El Niño to La Niña events, that pre-date ocean colour sensors.

Chapter 7

Discussion and future research

7.1 Introduction

In this thesis, different PFT satellite algorithms, reformulated to detect dominant phytoplankton size class, were compared and validated using satellite and *in situ* data (Chapter 3). Based on the results, a new algorithm was developed designed to detect the fractional contribution of three phytoplankton size classes to the total chlorophyll-a concentration (Chapter 4). The new algorithm was then implemented into a phytoplankton absorption model in order to estimate size-fractionated phytoplankton absorption as a function of the total chlorophyll-a concentration (Chapter 5). The new algorithm was applied to 10-years of satellite observations to investigate the evolved community composition, its spatial and temporal pattern and its relation to the underlying physics (Chapter 6). This chapter discusses the results in Chapters 3 to 6 in the context of the general body of knowledge in phytoplankton community satellite detection and in marine ecosystem modelling, focusing on the limitations of the work and its current capabilities. This chapter also addresses the impact of the work in other research fields and future projects are outlined. Finally the conclusions of the thesis are stated in context of its aims and objectives.

7.2 General Discussion

7.2.1 Discussion of the satellite phytoplankton size class intercomparison

Results from the intercomparison in Chapter 3 (Figures 3.4 to 3.8) show that abundance-based models performed well across datasets and trophic levels, indicating that information on the size structure of the phytoplankton may in fact be latent in the satellite-derived biomass fields. This result supports a variety of *in situ* evidence also suggesting that the trophic status of a pelagic ecosystem may be indicative of the phytoplankton community (Yentsch and Phinney, 1989; Chisholm,

1992; Bouman et al., 2005; Platt et al., 2005). Aiken et al. (2008) postulated that the bioenergetic status (BE), i.e. the transformation of light energy (photosynthesis) through intermediate stages to the synthesis of cells, is the definitive phytoplankton functional process that determines the composition of phytoplankton taxa, size classes and ecosystem trophic status. According to Aiken et al. (2008), this bioenergetic status is quantitatively linked to phytoplankton bio-optical traits (BOTs) that are specific properties of phytoplankton size and taxa (BE-BOT hypothesis). Aiken et al. (2008) go on to suggest that chlorophyll-a and the slope of the phytoplankton absorption spectrum between 443 and 510 nm (directly linked to chlorophyll-a) are two principle phytoplankton bio-optical traits that are indicative of phytoplankton size, and from a remote sensing perspective, in the open ocean, represent the dominant organic influence on the visible light spectrum. The results from the abundance-based algorithms in the intercomparison support such a theory.

Whereas it is difficult to compare the ecological model (model J) with abundance-based and spectral-response models, as it is based on a complex interaction of ecological as well as bio-optical input, commonalities in the other approaches can be investigated. The abundance-based models (model C, E, F, G and H) generally performed well at detecting dominant microplankton. All these models assume that high levels of chlorophyll-a or $a(443)$ (which are well correlated; Bricaud et al., 2004) are indicative of microplankton. Models I and B2 also detect microplankton well. These two models rely on the assumption that microplankton have a flatter spectral shape (i.e. normailised spectrum) to nano- or picoplankton. It is well known that, with increasing chlorophyll-a, the spectral shape of $a(\lambda)$ becomes flatter due to changes in pigment packaging (Morel and Bricaud, 1981) and from a decrease in the relative concentration of accessory pigments (Bricaud et al., 1995). This feature is at the basis of the development of Model I and B, therefore, similarities between these approaches were expected.

Abundance-based approaches attribute lower magnitudes of chlorophyll-a to the determination of nano- and picoplankton, whereas models B and I attribute a steepening in the spectral shape of $a(\lambda)$ in this regard. Again these two features can be linked, as with decreasing chlorophyll-a the spectral shape of $a(\lambda)$ is expected to become steeper due to an increase in the relative concentration of accessory pigments, again a feature at the basis of the development of Model I. This is also consistent with a number of studies suggesting that the absorption efficiency of pigments increases in the blue wavelengths with decreasing chlorophyll-a (Duysens, 1956; Kirk, 1975; Morel and Bricaud, 1981; Sathyendranath et al., 1987; Hoepffner and Sathyendranath, 1991), which would ultimately steepen the spectral shape of $a(\lambda)$. Regarding model A, a study by Brown et al. (2008) into the origin and global distribution of second order variability in satellite ocean color, suggests that model A is indirectly attributing lower backscattering anomalies to the determination of

smaller sizes (i e nanoeukaryotes) in comparison to higher backscattering anomalies for larger size classes (diatoms) Similar arguments may apply to models B to I considering that nano-picoplankton generally prevail in stratified, stable environments which exhibit low heterogeneity, where one may expect lower backscattering anomalies, lower levels of chlorophyll-a and a steeper spectral shape of $a(\lambda)$. Alternatively, higher backscattering anomalies may be expected in more dynamic heterogeneous regions, characteristic of eutrophic environments, of higher levels of chlorophyll-a and a flatter spectral shape of $a(\lambda)$.

The robustness of abundance-based approaches appears to be a result of their utilisation of the first order variability in the satellite ocean colour signal, whereas spectral-response-based algorithms use the second order variability which is weaker, in some respects harder to infer (Garver et al , 1994) and more vulnerable to errors in atmospheric processing, despite arguably containing additional information on phytoplankton accessory pigments (Alvain et al , 2005) However, with improved sensors and atmospheric correction algorithms, spectral-response-based algorithms may become more robust

Comparing and validating different PFT and PSC satellite algorithms in both case 1 and case 2 regions using *in situ* data is a critical issue with regard to improving synoptic estimates of these groups. Chapter 3 attempted to validate different PFT and PSC satellite algorithms on a global scale, a procedure which is of particular importance for a novel field of study such as the detection of PFTs from satellite data This is especially relevant when other researchers seek to use such synoptic information in different areas of biogeochemical research, including validating other models.

Throughout Chapter 3 the assumption was made that the *in situ* data is the truth, when in fact (as stated in section 3 4) there is uncertainty in the *in situ* observations, which are not direct measurements of phytoplankton size class In order to produce a more robust intercomparison, future efforts need to focus on gathering more *in situ* data over larger spatial scales and clarify uncertainty in using *in situ* proxies to infer phytoplankton size. With extensive field measurements that combine both biological and optical measurements, more quantitative development, testing and validation of the satellite PFT algorithms can be achieved. Future comparisons may benefit from focusing on specific functional groups, in addition to size class, and by comparing the satellite results with the output from a variety of biogeochemical models, which may give an indication into how well PFT biogeochemical models are performing in comparison with the satellite approaches Furthermore, in this rapidly expanding field, novel methods are constantly being developed to identify PFTs from remote sensing (e g Bracher et al , 2009, Kostadinov et al , 2009, Mouw and Yoder, 2010) which should also be incorporated into future comparisons The intercomparison in Chapter 3 neglected backscattering-based approaches as they

were not publicly available (published or known about) when running the intercomparison. Such approaches should be included in the future. This will ultimately result in improved approaches and a better understanding of the role of different phytoplankton groups in the global carbon cycle.

7.2.2 Discussion of the three-component model

7.2.2.1 Using diagnostic pigments to infer size class

The use of diagnostic pigments to infer size-specific chlorophyll-a values relies heavily on two points: 1) the multiple regression analysis from which Equation 2.1-2.4 originate; 2) the validity of using diagnostic pigments to infer phytoplankton cell size. With regard to the multiple regression analysis, confidence can be gained from the extensive *in situ* dataset used in Uitz et al. (2006) to derive the coefficients used in equations 1-4 and also a comparison with an independent statistical approach which found the two approaches to coincide almost exactly (see section 6.1 Uitz et al., 2006).

Regarding the validity of using diagnostic pigments to infer phytoplankton cell size, Chapter 3 highlighted that different diagnostic pigment models can provide contrasting results when determining size class. In Chapter 4, the diagnostic pigment procedure was improved by accounting for the distinctive picoeukaryote signature seen in ultra-oligotrophic waters. There are still certain discrepancies, and as stated by Vidussi et al. (2001), some diagnostic pigments such as fucoxanthin (the main indicator of diatoms) may also be found in some flagellates. Therefore, the pigment grouping does not strictly reflect the true size of phytoplankton communities; and phytoplankton size class derived from pigments are indicative and not definitive. However, pigment composition and cell size are two strong phytoplankton descriptors that co-vary with each other.

Recently, efforts have been made to apply a fucoxanthin adjustment for low chlorophyll-a waters, to improve the diagnostic pigment to size class procedure (e.g. Hirata et al., 2011; Devred et al., In revision). Such adjustments could easily be applied to the three-component model. However, a quantitative validation of such methods is still warranted before doing so. By conducting coupled cell count, size-fractionated chlorophyll measurements, phytoplankton absorption measurements and HPLC pigment measurements, consensus could be reached regarding the limitations of using diagnostic pigments to infer cell size.

Laboratory studies have shown phytoplankton pigment ratios to vary with environmental stimuli (such as nutrient forcing and light). For *in situ* studies, a much clearer relationship between phytoplankton community structure and pigment composition exists. Specifically that the strong relationship between the ratio of chlorophyll-a to accessory pigments (Trees et al., 2000) co-varies with the abun-

dance of different phytoplankton size classes (Fishwick et al , 2006, Aiken et al , 2007, 2008, Hirata et al , 2008a) Nonetheless, future work should focus on understanding the effect photoacclimation may have on pigment ratios in the field, in order to improve the diagnostic pigment to size class procedure

7.2.2.2 Three-component model applicability

The three-component model presented in Chapter 4 is designed for basin-scale application in the open ocean The model is based on an extensive dataset collected in case 1 waters in the Atlantic Ocean Analyses in Chapters 4, 5 and 6 clearly indicate that the model is also applicable to case 1 environments outside the Atlantic Ocean From a satellite perspective, it would seem unwise to use such an approach in case 2 coastal areas, as the accuracy of chlorophyll-a algorithms are known to break down in such environments The poor performance of the chlorophyll-based models at the L4 site in Chapter 3 also emphasises this point Furthermore, it remains to be revealed whether the relationship between size and chlorophyll-a concentration, demonstrated for case 1 waters, also holds in various case 2 waters.

It is also recognised that, whereas the model is designed for large-scale application, model parameters may vary between biogeochemical provinces (Devred et al , 2006, 2009) The three-component model presented in Chapter 4 is expected to break down in cases where there is no clear correlation between the size structure of the phytoplankton and the chlorophyll-a biomass, this may include cyanobacterial blooms in the North Atlantic and Baltic, and mixed *Phaeocystis*-diatom blooms which are known to co-occur in the Labrador Sea (Sathyendranath et al , 2001)

7.2.2.3 Size class depth variations

The vertical structure in phytoplankton size, estimated using the three-component model (Figure 4 19 and 4 20), coincides with previous AMT studies The higher chlorophyll-a concentrations and fractional contributions of microplankton in eutrophic areas (Figure 4 19 and 4 20) are consistent with AMT observations that such waters are dominated by large-celled dinoflagellates and diatoms (Aiken et al , 2004, Gibb et al , 2000) Barlow et al (2002) found that in communities dominated by diatoms or nanoflagellates, pigment absorption was generally uniform with depth and attenuating irradiance, supported by uniform microplankton and nanoplankton percentages with depth in these eutrophic waters

Within the oligotrophic gyres, *Prochlorococcus* are likely to dominate in the surface mixed layer along with some *Synecococcus* (Barlow et al., 2002), indicated by high percentages of picoplankton (Figure 4 19 and 4 20) in these regions at the surface According to field studies in the oligotrophic gyres, below the surface layer at the nutrient pycnocline (i e the region of nutrient and density change between the oligotrophic surface mixed layer and nutrient replete deeper water), a community

dominated by nanoflagellates can be expected (Gibb et al., 2000; Zubkov et al., 2000; Barlow et al., 2002). This change in community composition is seen in Figure 4.19 and 4.20, as the percentage of picoplankton is shown to decrease with depth down to the chlorophyll-a maximum, and the nanoplankton percentage contribution is shown to increase down beyond the chlorophyll-a maximum. Ras et al. (2008) found a similar pattern in the oligotrophic gyre of the South Pacific, with proportions of nanoplankton greater than 60 % below 200 m. Furthermore, this feature has also been observed in other subtropical gyre systems. A deep nanoflagellate population has been observed previously in the North Altantic gyre (Claustre and Marty, 1995) and North Pacific gyre (Monger et al., 1999).

The reason for the existence of nanoplankton deep below the chlorophyll-a maximum are still unclear (Ras et al., 2008). Beaufort et al. (2008) found the deep-layer of the oligotrophic gyre in the South Pacific to be rich in coccoliths and, during the same cruise, Twardowski et al. (2007) observed a high backscattering ratio suggesting that this population may correspond to the coccolithophorid *Florispharea profunda*. It has been suggested that chrysophytes (which contain 19'-butanoyloxyfucoxanthin) are better adapted to existence at the base of the deep chlorophyll maximum layer (Letelier et al., 1993).

Claustre and Marty (1995) have suggested that a deep nanoflagellate population can develop close to the nutricline and that their presence at very low light levels may be governed by nitrate availability as opposed to photoadaption. Claustre and Marty (1995) suggest reasons for flagellates at this deep layer may include a decoupling between NO_3 assimilation and CO_2 fixation, possibly from vertical migration (although doubtful due to their small size), or alternatively, heterotrophic growth may also account for the flagellate maintenance at very low light intensities. Other causes could be related to light utilisation, with conditions in surface waters more favourable for phytoplankton which utilise the blue region of the visible EM for photosynthesis (e.g. picoplankton) and conditions in deep waters more favourable for phytoplankton which utilise longer wavelengths. Further research is needed to ascertain the causes of this deep nanoplankton population, particularly whether or not it is controlled by photoadaption.

7.2.2.4 Comparison with previous abundance-based models

The three-component model relies on the assumptions that the phytoplankton size structure covaries with the total phytoplankton chlorophyll-a biomass, and that chlorophyll is added to a system by the addition of larger size classes of phytoplankton (Raimbault et al., 1988; Chisholm, 1992; Gin et al., 2000). This supports the common consensus regarding the distributions of marine phytoplankton communities, in that there is a background population of smaller cells on which, when certain environmental conditions pertain, larger cells are superimposed (Yentsch and Phin-

ney, 1989, Ciotti et al , 2002; Uitz et al., 2006; Kostadinov et al , 2009) The model provides distinct advantages over existing abundance-based models, extending the Sathyendranath et al. (2001) and Devred et al (2006) models to three size classes and to a wider geographical area It also improves on the model of Hirata et al (2008a) by computing the fractional contribution of each size class Furthermore, the three-component model is an improvement on the model of Uitz et al. (2006) as its parameters have simple biological interpretation.

Abundance-based models build on existing remote-sensing algorithms for retrieving total phytoplankton abundance (as indexed by its chlorophyll biomass) (e g. O'Reilly et al , 1998). However, abundance-based models may fail on occasions where there is no clear correlation between size structure and total chlorophyll-a biomass The relationship between size structure and total chlorophyll-a biomass, seen in database B, generally remained stable over the 7-year period (1997-2004). However, as with all abundance-based approaches, such relationships could change over time For instance, physiological changes in the phytoplankton due to environmental changes may necessitate a regular recalibration of the three-component model over time An advantage of the three-component model over a purely statistical approach (such as Uitz et al., 2006) in this regard, is that it is strongly supported by theory so may be considered more robust

7.2.2.5 The biological interpretation of the three-component model

The three-component model is based on the theory that small cells ($<20\,\mu$m) are incapable of growing beyond a certain concentration (represented by the parameters $C^m_{p,n}$ and C^m_p in the three-component model, where m refers to the maximum concentration, for cells less than $<20\,\mu$m and $<2\,\mu$m respectively) As noted in Chapters 4 and 5, $C^m_{p,n}$ is consistently larger than C^m_p, suggesting that the maximum chlorophyll-a concentration for a specific size-fractionation (e g $<2\,\mu$m, $<5\,\mu$m, $<10\,\mu$m and $<20\,\mu$m) may become larger with increasing size Similar results were observed in the Mediterranean (Raimbault et al , 1988) and in the coastal waters of Singapore (Gin et al , 2000) for other size fractions (e g $<1\,\mu$m, $<5\,\mu$m and $<10\,\mu$m).

Gin et al. (2000) postulated that an upper limit to the different size classes lies in the metabolic constraints of size This was linked to the work of Thingstad and Sakshaug (1990), who found that as nutrient concentrations increase, under constant light intensity, the growth rate of a particular size class of phytoplankton increases until eventually some maximum is reached according to Michaelis-Menten kinetics (or alternatively a Holling type 2 functional response). Gin et al (2000) suggest that, as maximum growth rates are known to be inversely related to size (Eppley and Sloan, 1966, Peters, 1983; Schlesinger et al , 1981; Geider et al , 1986), once the growth rates of small cells are saturated, ambient nutrient concentrations can increase enough to allow larger phytoplankton, which generally have larger half-

saturation constants (e.g. Aksnes and Egge, 1991), to grow. This provides a simple explanation why oligotrophic environments are dominated by small cells, whereas eutrophic environments are dominated by large cells.

7.2.3 Discussion of the three-component absorption model

7.2.3.1 Comparison with laboratory studies

The size-specific $a^*(443)$ values retrieved from the three-component absorption model (Figure 5.2) are consistent with previous laboratory studies on microplankton (e.g. diatoms ~0.015-0.048 $m^2\,[mg\,C]^{-1}$; Sathyendranath et al., 1987; Sakshaug et al., 1989; Finkel, 2001) and nanoplankton (e.g. ~0.032-0.092 $m^2\,[mg\,C]^{-1}$; Morel and Bricaud, 1981). For picoplankton, the specific absorption coefficient at 443 nm ($a_p^*(443)$) obtained ($0.19\,m^2\,[mg\,C]^{-1}$) is comparable to that derived from laboratory monospecific cultures of *Prochlorococcus* (e.g. $0.19\,m^2\,[mg\,C]^{-1}$, Partensky et al., 1993), although slightly higher than other laboratory studies on picoplankton (e.g. 0.14-0.16 $m^2\,[mg\,C]^{-1}$, Morel et al., 1993; Moore et al., 1995). Turning to field studies, $a_p^*(443)$ obtained for picoplankton in this study is again slightly higher than that observed *in situ* by Babin et al. (1996) at the surface in a picoplankton-dominated site in the North Atlantic ($0.16\,m^2\,[mg\,C]^{-1}$). However, at very low chlorophyll-a concentrations (characteristic of picoplankton-dominated sites) the contribution to the specific absorption coefficient is not solely attributed to picoplankton in the three-component absorption model (as may also be the case in the Babin et al. (1996) dataset). There is still some marginal influence from nano- and microplankton (Figure 5.1), such that the estimation of $a^*(443)$ when chlorophyll-a concentration is $0.01\,mg\,m^{-3}$ is closer to $0.15\,m^2\,[mg\,C]^{-1}$ using the three-component absorption model (Figure 5.5 a), which coincides with the Babin et al. (1996) estimate of $0.16\,m^2\,[mg\,C]^{-1}$.

7.2.3.2 Discussion of the comparison with other absorption models

The power-law model

Lutz et al. (1996) and Devred et al. (2006) have highlighted that a model based on the power-law can fail at extremely low chlorophyll-a concentrations as the specific absorption coefficient tends to infinity. However, it is acknowledged that the use of a power-law model when constrained to the range of measurements to which it is fitted may still be reasonable. When fitted to the same dataset, the errors in the power-law model and the three-component model were found to be statistically similar (Figure 5.4). The power-law model only requires two parameters in its calculation of $a(\lambda)$, whereas the three-component model requires seven. Nonetheless, the parameters of the three-component absorption model provide biological and bio-optical interpretation and, unlike a power-law model, the three-component model

can be used to estimate size-specific $a(\lambda)$

The model of Devred et al. (2006)

The higher $a^*_{p,n}(\lambda)$ and $a^*_m(\lambda)$ values derived from the database E using the two-component model, when compared with the global dataset used in the Devred et al (2006) study (Figure 5 6 a), are likely to be due to differences in the composition of the two datasets. The global dataset used in Devred et al. (2006) ranged in chlorophyll-a concentrations between 0 05 to 28 0 mg m^{-3}, whereas the values in database E ranged between 0.04 and 12 2 mg m^{-3}. It might be expected that the higher chlorophyll-a concentrations in the Devred et al. (2006) study would yield lower $a^*_m(\lambda)$ values, and that the slightly lower chlorophyll-a concentrations in database E could yield higher $a^*_{p,n}(\lambda)$ values, as smaller or larger phytoplankton cells are sampled at these very low or very high chlorophyll-a concentrations. The differences could also be indicative of regional or temporal variations in the phytoplankton composition

The higher microplankton specific absorption coefficients in the blue part of the spectrum calculated using the three-component model, when compared with the two-component model, can be related to the contrasting model formulation Table 5 1 compares the parameters $S_{p,n}$ and $C^m_{p,n}$ derived from the two models Whereas $C^m_{p,n}$ is practically identical in the two approaches, $S_{p,n}$ is slightly higher in the two-component model When fitting the two-component model to database E, the assumption is made that as C tends to zero, C_m tends to zero and as a consequence $S_{p,n}C^m_{p,n}$ tends to 1 This assumption is not required for the three-component model as implemented in Chapter 5. As highlighted earlier, certain discrepancies can arise when using diagnostic pigments as indicators of phytoplankton size class The higher percentages of microplankton at low chlorophyll-a concentrations (shown in Figure 5.1 e) may be an artifact of using diagnostic pigments to infer size class

Extending the absorption model from two to three-populations (representative of three size classes) improved accuracy and representation of the variability in the specific absorption coefficient at low chlorophyll-a concentration An advantage of the two-component model is that it can be fitted to any chlorophyll-a and absorption dataset, whereas the three-component model was fitted in Chapter 5 using additional information on the size structure of the phytoplankton in the dataset (HPLC data)

The model of Uitz et al. (2008)

When comparing the specific absorption coefficients derived using the three-component absorption model with those derived by Uitz et al (2008), the picoplankton specific absorption coefficients using the three-component model are consistently higher and for nanoplankton consistently lower (Figure 5 6 b) This might be explained to a certain extent by the refinement to the diagnostic pigment procedure of Uitz et al (2006) that was used in the three-component model to account for

small picoeukaryotes in ultra-oligotrophic environments (see Equations 4.1 and 4.2). Discrepancies in the microplankton specific absorption coefficients, between the two models are likely to be related to contrasting *in situ* datasets. A majority of data in the Uitz et al. (2008) study were from the Pacific and Mediterranean Oceans, whereas, the majority of samples in database E were from the Atlantic Ocean. Therefore, diversity in microplankton species would be expected between the two datasets which could cause variations in $a_m^*(\lambda)$. Furthermore, the data used in Uitz et al. (2008) varied from 0.02 to 28.7 mg m^{-3} chlorophyll-a (see Table 1 of Uitz et al., 2008) whereas, the data used in this study varied from 0.04 to 12.2 mg m^{-3} chlorophyll-a which could also have contributed to the differences.

The model of Ciotti et al. (2002)

Discrepancies between derived specific absorption coefficients of the three-component model and Ciotti et al. (2002) model (Figure 5.6 c) are also likely to be related to contrasting *in situ* datasets. In comparison with the data used by Ciotti et al. (2002), the database E incorporates very oligotrophic, tropical waters such as the North and South Atlantic gyres. This could explain the higher $a_p^*(\lambda)$ values obtained using the three-component model (see also a similar discussion on the effects of regional representation in Uitz et al., 2008).

The Ciotti et al. (2002) database incorporated data with chlorophyll-a concentrations as high as 135 mg m^{-3} (see Table 2 Ciotti et al., 2002). It is possible that, at such large chlorophyll-a concentrations (particularly during an intense bloom of *Gonyaulax digitale* in the Bedford Basin), the sampled microplankton component may well have been different from those encountered at lower concentrations in the open ocean, which could account for the differences in the magnitude of $a_m^*(\lambda)$, also highlighted by Devred et al. (2006). Another point to note is that the Ciotti et al. (2002) model was parameterised using filtration, whereas the three-component model (as well as the Uitz et al. (2008) model) was parameterised using HPLC data. Differences in size-specific absorption coefficients between the two models may have been caused by discrepancies between the size class classification using HPLC and that using filtration (see section 2.2.2).

The use of the three-component absorption model in biogeochemical modelling

With regard to biogeochemical modelling studies, and based on suggestions made repeatedly for over a decade (e.g. Perry, 1994), Cullen and Fennel (2010) recently proposed a modelling framework that is directly based on fundamental bio-optical processes that influence phytoplankton physiology and the rate of photosynthesis in the sea. Cullen and Fennel (2010) suggest using the absorption coefficient for photosynthetic pigments as a state variable and modelling photosynthesis with absorption-based functions. A movement towards using direct bio-optical properties,

such as $a(\lambda)$, in modelling studies, coupled with introducing additional phytoplankton groups (such as size classes), requires phytoplankton group-specific bio-optical observations, in order to help constrain, improve and verify model estimates The three-component absorption model can provide synoptic scales observations of the bulk absorption coefficient of three size classes and would therefore be useful for such purposes. It is an advance on previous models (e g Bricaud et al , 1995, 2004, Ciotti et al , 2002, Devred et al , 2006; Uitz et al., 2008) as it is based on ecological theory and can estimate absorption properties of three size classes for a continuum of chlorophyll-a concentrations

7.2.3.3 Discussion of the validation of the three-component absorption model

When validating the three-component absorption model using database F, between 411-555 nm the three-component model appears to underestimates a^s at high values. This is likely to be linked to differences in the composition of database E compared with database F Database E, with which the three-component model was parameterised, has chlorophyll-a concentrations ranging from 0.04 to 12.2 mg m^{-3} with only 10 % of the database having chlorophyll-a concentrations greater than 2.0 mg m^{-3}. The corresponding values in database F are from 0 02 to 77 8 mg m^{-3}, with 38 % of the database greater than 2.0 mg m^{-3} Therefore, the parameters in Tables 5 1 and 5.2 are not strictly applicable to chlorophyll-a concentrations greater than 12 2 mg m^{-3} and the three-component model appears to underestimate $a^s(443)$ at chlorophyll-a concentrations greater than 2 0 mg m^{-3} when compared with database F (Figure 5.7 h) Additional HPLC and $a(\lambda)$ data may be required to improve the parameterisation of the three-component absorption model at high chlorophyll-a concentrations.

In Figure 5.7 (f), there appears to be a systematic over-estimation of $a^s(670)$ when verifying the three-component absorption model using database F When assessing the specific absorption coefficients of the three-size classes (Figure 5 6) retrieved from database E, the magnitude at 670 nm is quite high for all three size classes (0.038, 0 029, 0 024 for pico-, nano- and microplankton respectively, see Table 5 2), and notably higher for picoplankton when compared with Ciotti and Bricaud (2006) and Uitz et al (2008) Discrepancies between $a^s(670)$ and $a(670)$ in Figure 5.7 (f) are likely to be related to high specific absorption coefficients retrieved at 670 nm using database F.

Considering that database F includes data from a diversity of locations not present in database E (e g Beaufort Sea, Indian Ocean and Australia-Antarctic Basin) and considering the ME% between C^s and the *in situ* chlorophyll-a concentrations in Figure 5 7 (g) ($\sim$ 62 6 %), the ME% shown in Figures 5.7 (a-f) are quite encouraging and support the application of the three-component absorption model

to satellite $R_{rs}(\lambda)$ fields. It is envisaged that, with improvements in remotely-sensed chlorophyll-a retrievals, this error would reduce.

7.2.3.4 Discussion of the application of the three-component absorption model to EO

Results from applying the three-component model to global satellite data indicate picoplankton act as a background component with small variability in $a_p^s(443)$ globally. This supports the theory first proposed in Yentsch and Phinney (1989) that a constant background component of small optically active cells is always present, on which larger-celled phytoplankton may be sporadically superimposed.

When comparing $a_p^s(443)$ to $a^s(443)$ in Figure 5.8, it can be seen that picoplankton contribute highly to total $a^s(443)$, in comparison to nano- and microplankton. In fact, when calculating the global mean fractional contribution of picoplankton to the total phytoplankton absorption in the surface layer for May 2005 ($a_p^s(443)/a^s(443) \times 100$), the three-component absorption model (parameters from Tables 5.1 and 5.2) estimates picoplankton contribute ~74.7% to the total phytoplankton absorption coefficient, whereas it is estimated that picoplankton contribute ~38.0% to the chlorophyll-a concentration (global average for May 2005). As picoplankton have a higher specific absorption coefficient than nano- and microplankton (Figure 5.2), they are more efficient in absorbing light and hence have a larger influence on $a^s(443)$ globally than on the chlorophyll-a concentration. It remains to be revealed whether this relationship, found in surface waters, is also applicable to deeper depths in the euphotic zone, and it is also likely to be wavelength dependent.

Figure 5.8 shows estimates of total and size-specific phytoplankton absorption based on the three-component model fitted to globally representative data (database E). However, it is acknowledge that a global parameterisation may not fully capture the wide scale variability in phytoplankton physiology. Devred et al. (2006) highlighted regional and seasonal variability in the parameters of their two-component model. Future work may need to focus on such temporal and spatial differences, possibly partitioning data into biogeochemical provinces and dealing with each province independently (Hardman-Mountford et al., 2008; Devred et al., 2009).

7.2.4 Discussion of the seasonal and interannual variations in phytoplankton size class

7.2.4.1 Seasonal analysis of phytoplankton size class

In Chapter 6, using the three-component model, seasonal distributions of phytoplankton size class were presented. The patterns highlighted in Figures 6.1 to 6.7 are consistent with the current state of knowledge of pelagic ecosystems (Chisholm,

1992, Aiken et al , 2008) In terms of their contribution to total biomass, the oligotrophic gyres are dominated by small size classes that thrive due to their high surface-to-volume ratio (Raven, 1998) absorbing nutrients with high efficiency under nutrient limited conditions Such communities support regenerated production and have small sinking rates, so are recycled within the euphotic layer (Marañón, 2009) The seasonal cycle of picoplankton fractional biomass ($\%C^s$) is relatively dynamic from month to month (Figure 6 6 and 6 7) However, considering the seasonal cycle of picoplankton chlorophyll-a (C_p) is relatively stable throughout the world's oceans (Figure 6 5 and 6 7), supporting the idea that small picoplankton are ubiquitous and form a stable background (Yentsch and Phinney, 1989; Uitz et al , 2006, Kostadinov et al., 2009), this is likely attributed to the effect on the picoplankton fractional biomass through changes in larger size classes

The contribution to total chlorophyll-a biomass from nanoplankton throughout the world's ocean displays a homogeneous pattern, with low seasonal variability (Figure 6.4 and 6 7) Even the nanoplankton chlorophyll-a distributions, while displaying larger spatial variability than picoplankton, are relatively similar from month to month (Figure 6.5 and 6 7). Prymnesiophytes, which form a major part of the nanoplankton pool, have been associated with transition zones between different environmental conditions (Ondrusek et al , 1991, Claustre, 1994, Jordan and Chamberlain, 1997, Uitz et al , 2010) They appear to persist in a large variety of environments, from stratified stable environments such as the oligotrophic gyres to dynamic environments such as the North Atlantic in winter (Figure 6.4) Liu et al. (2009) linked the persistent presence and biomass of prymnesiophytes to their extreme, but unsuspected, biodiversity. Furthermore, Uitz et al. (2010) suggest that the taxonomic and ecological diversity of prymnesiophytes, in particular their mixotrophic character, is likely to explain the success of this group in the world's open oceans.

Microplankton, in comparison with the nano- and picoplankton size classes, display high spatial and seasonal variability both in terms of their contribution to total chlorophyll-a biomass and their individual chlorophyll-a concentration (Figure 6 1, 6.2 and 6.7). Again these emerging patterns are consistent with current knowledge that microplankton, primarily diatoms, prevail in dynamic environments where plenty of nutrients and light are available For instance, spring in the austral and boreal hemispheres (Figure 6 1 and 6.2), where deep winter mixing replenishes nutrient to the surface and irradiance increases with the onset of summer, or alternatively coastal upwelling systems where nutrients are constantly supplied through the upwelling of cool nutrient rich waters (Malone, 1980, Goldman, 1993, Longhurst, 1998). Low microplankon $\%C^s$ values and microplankton chlorophyll-a concentrations (C_m) are observed in the oligotrophic gyres, consistent with the assumption that their lower surface-to-volume ratio results in them being out-competed by smaller size

classes in nutrient limited conditions (Raven, 1998; Marañón, 2009).

7.2.4.2 Latitudinal-time transects

The latitudinal-time transects (Figure 6.8 and 6.9) demonstrate the utility of applying the three-component model to EO data. Information on the timing of the blooms can be observed, in addition to the seasonal cycles of the size classes and interannual variations. This can compliment available *in situ* data, for instance complementing AMT data by providing information on the whole seasonal cycle (note that the AMT transects have only taken place in March-April and September-October-November).

The distributions in Figure 6.8 are consistent with Aiken et al. (2009), with more productive areas at latitudes higher than 40° N, lower than 40° S and in equatorial regions. Seasonality in the equatorial regions are likely linked to seasonal influences from the Amazon outflow on productivity (DelVecchio and Subramaniam, 2004; Subramaniam et al., 2008) and the influence of the North Equatorial Counter current (Kostadinov et al., 2010).

In Figure 6.8, at 40° N, the larger anomalies in micro- and nanoplankton from 2001-2005 (lower 1998-2001 and 2006-2007) were found not to be related to the NAO. Hypothetically, the larger anomalies in micro- and nanoplankton would be expected to be linked with increasing mixing of the water column (note the strong inverse correlation between stratification and micro- and nanoplankton in Table 6.1). Physical forcing by cyclones has been found to contribute to changes in taxonomic composition of phytoplankton, with an increase in larger size classes of phytoplankton (e.g. diatoms) due to the re-suspension of nutrients (Platt et al., 2005; Son et al., 2007). NOAA use the Accumulated Cyclone Energy (ACE) as an index of the intensity of tropical cyclone seasons. Considering that in the North Atlantic the years of 2001, 2003, 2004 and 2005 were above-normal hurricane seasons with 2003, 2004 and 2005 being in the top 10 most active seasons in the past 50 years, all regarded as hyperactive seasons (Trenberth, 2005; Webster et al., 2005; Sun et al., 2008), there may be a link between PSC anomalies and interannual changes in cyclone activity in the North Atlantic. Further investigation would need to be conducted to verify this link.

The higher picoplankton % chlorophyll-a values observed in the Pacific gyres, when compared with the Atlantic gyres (Figure 6.8 and 6.9), are consistent with previous work suggesting the Pacific gyres constitute the most oligotrophic regions of the ocean (Morel et al., 2007a,b, 2010). The low seasonal variability in the equatorial region can be linked to the constant and stable equatorial solar irradiance pattern and, unlike the Atlantic, is not as influenced by riverine output. The enhanced level of microplankton $\%C^s$ at the equator in the Pacific Ocean, when compared with the Atlantic transect, can be linked to the equatorial undercurrent which provides cooler nutrient rich waters (Chavez et al., 1999; Feely et al., 1999). At 10° S (140° W) the

Pacific transect interacts with the Marquesas Islands and the higher microplankton $\%C^s$ may be linked to the island mass effect (Signorini et al , 1999, Kostadinov et al , 2010) The major feature of the anomaly maps in Figure 6 9 is the strong influence of the ENSO cycle

7.2.4.3 ENSO dynamics in relation to satellite observations in the equatorial Pacific

The equatorial Pacific is a unique region of our oceans It can act as a large source of CO_2 to the atmosphere through the upwelling of CO_2-rich waters along the equator and advection of CO_2-rich waters from the South American coast (Etcheto et al , 1999, Feely et al , 1999), and also a sink though primary production and export (Takahashi et al , 2002) It is one of only three open-ocean areas that, despite having high nitrate and phosphate nutrient concentrations, display moderately low phytoplankton chlorophyll-a biomass (Martin, 1991, Behrenfeld et al , 1996) and has been referred to as exhibiting High Nutrients-Low Chlorophyll characteristics (HNLC, Thomas, 1979) This enigma has been linked to either the lack of iron that limits the growth of the phytoplankton (Martin and Fitzwater, 1988, Behrenfeld et al , 1996, Coale et al , 1996) or to a large amount of grazing from higher trophic levels that limits phytoplankton growth (Walsh, 1976, Cullen, 1991) Results from Chapter 6 highlight a strong interannual influence from the ENSO on this region

Under non-El Niño conditions, easterly trade winds create a channel of cold surface water along the equator, referred to as the Eastern Equatorial Undercurrent (EUC) The EUC flows eastward across the equator at a depth of 20 to 200 m (Toggweiler and Carson, 1995) Studies in the equatorial Pacific have suggested that diatoms do not contribute more than 20 % of phytoplankton biomass during non-El Niño conditions (Blanchot et al , 2001, Kobayashi and Takahashi, 2002, Dandonneau et al , 2004), with the majority of the phytoplankton biomass comprising of small size classes (Chavez et al , 1999) The results using the three-component model are consistent with such observations under non-El Niño conditions (for instance see Figure 4 10)

During an El Niño event (Figure 7 1), a weakening or reversal of the trade winds occurs, which weakens the EUC and hence subdues the upwelling of cold nutrient rich waters and deepens the thermocline in the eastern part of the equatorial Pacific. Surface waters become warmer and nutrient poor and picoplankton thrive due to their competitive advantage In the west equatorial Pacific, the thermocline rises, resulting in cooler waters with higher nutrient concentrations reaching the surface This results in an increase in larger size classes of phytoplankton (nano- and microplankton) in comparison with non-El Niño conditions

During a La Niña event (Figure 7 1), there is a strengthening of the trade winds, which strengthens the EUC, enhancing the upwelling of cold nutrient rich waters

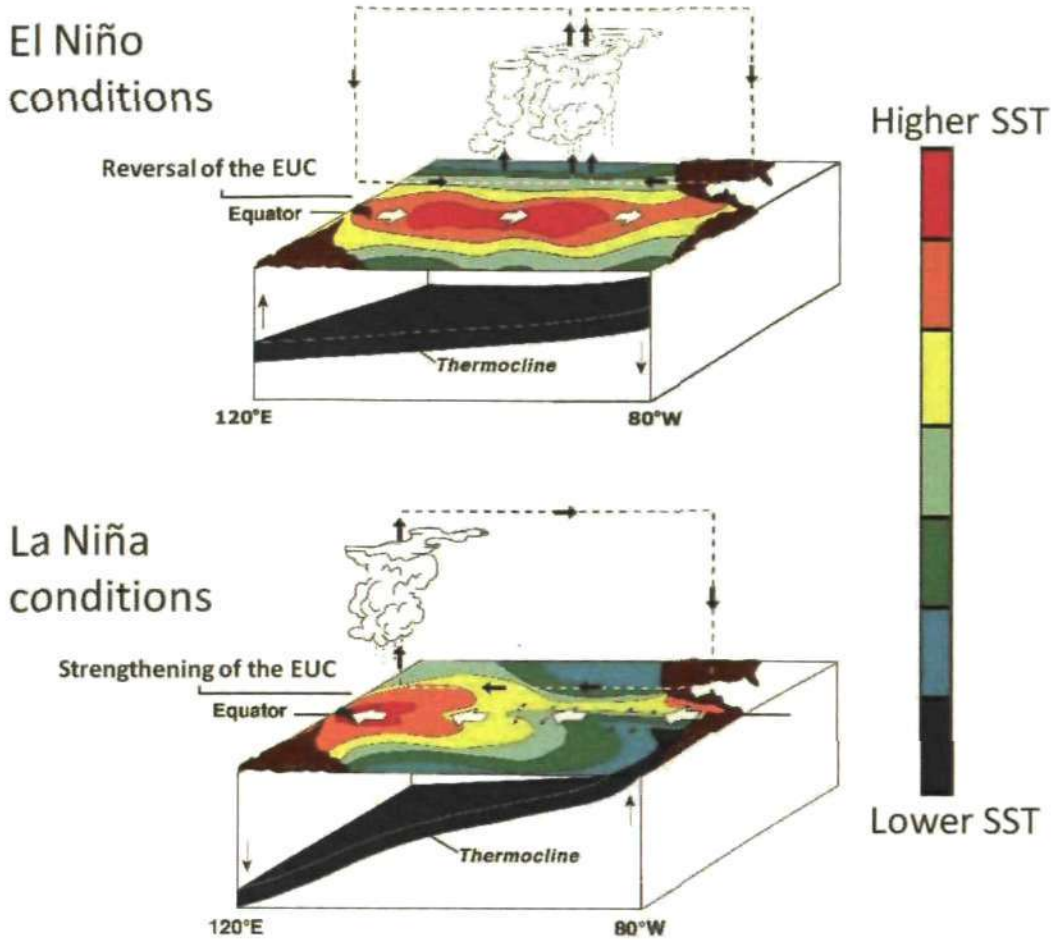

Figure 7.1: The influence of ENSO dynamics on the equatorial Pacific (adapted from NOAA (2010))

and a rising of the thermocline in the eastern part of the equatorial Pacific occurs (deepening in the western Pacific). The higher nutrient waters promote an increase in larger size classes of phytoplankton (nano- and microplankton) in the eastern equatorial Pacific (also noted by Chavez et al., 1999; Strutton and Chavez, 2000; Ryan et al., 2002; Alvain et al., 2008). In the western equatorial Pacific, the thermocline deepens promoting stratification in the surface waters. Such warm low nutrient waters promote an increase in picoplankton.

7.2.4.4 The link between physics and biology in the equatorial Pacific and Indian Oceans

The DMI index for the Indian Ocean Dipole was found to be significantly correlated to the ENSO index MEI (Figure 6.10) during 1997-2007, with a stronger correlation between 1997-1998 than 1999-2007. It has been well established that positive phases of the Indian Ocean Dipole tend to co-occur with El Niño, and negative phases with La Niña (Annamalai et al., 2005; Behera et al., 2006; Luo et al., 2010; Izumo et al.,

2010), supporting this finding as well as the similarities between Figure 6.11 and 6 12 in the Indian Ocean The high correlations between phytoplankton size class anomalies and the physics in the Pacific and Indian Ocean (Figure 6 14) have two implications.

Firstly, considering that microplankton $\%C^s$ and nanoplankton $\%C^s$ are negatively correlated with SST, SSHA and stratification, and that picoplankton $\%C^s$ is positively correlated with SST, SSHA and stratification, provides an indirect validation of the three-component model. As early as the 1960's, Ramón Margalef showed results of community changes of phytoplankton based on physical-chemical-ecological interactions using his proposed Mandala (Margalef, 1967, 1978) Smaller size classes dominate in stratified nutrient limited conditions, due to their high surface-to-volume ratio (Raven, 1998) absorbing nutrients with high efficiency Such conditions are associated with higher SST and SSH (indicative of stratification) Larger size classes (nano- and microplankton) prevail in dynamic environments where plenty of nutrients are available, associated with lower SST, lower stratification and lower SSH, all characteristic of well mixed waters. The strong correlations between size class and physics, using the three-component model, compliments Margalef's Mandala

Secondly, the tight coupling between the biology and physics in the equatorial Pacific supports the idea that all the components of a system, physical, biological and chemical, are intertwined, and that each component of the system is intrinsically linked with another (Lovelock, 1992) Under a global warming scenario, where one may expect increases in SST, SSH and stratification (Behrenfeld et al., 2006, Doney, 2006), in the equatorial Pacific and Indian Oceans one may expect increases in smaller size classes of phytoplankton at the expense of larger phytoplankton size classes Considering that phytoplankton are at the base of the food web, and that zooplankton and fish can have selective feeding preferences for phytoplankton of different sizes and types (Hansen et al , 1994, Scharf et al , 2000; Jennings et al , 2002), under a global warming scenario, this may have a huge impact on higher trophic levels in the future, potentially restructuring the food web in these areas

7.2.4.5 Using MEI to hindcast phytoplankton size class

On large scales, the positive correlations between MEI and picoplankton, and negative between MEI nano- and microplankton, support similar conclusions made by Brewin et al (2010c) and Kostadinov et al. (2010) using contrasting models (a spectral-response model and a backscattering-based model) Furthermore, the sensitivity analysis conducted in Appendix E emphasises the degree to which these correlations are robust

Wara et al (2005) suggest that in a warmer climate state there may be a potential transition to permanent El Niño conditions and, under such circumstances, consid-

ering the large scale correlations between MEI and phytoplankton size class, this may lead to an increase in picoplankton at the expense of nano- and microplankton under a global warming scenario. Furthermore, there is striking evidence to suggest this has already been occurring. During the late 1970's there was an abrupt change of the climate state in the trophical Pacific and in mid-latitude areas (Trenberth and Hurrell, 1994; An et al., 2006). When assessing MEI values from 1950 to the present, before 1979 (1950-1979) the average MEI value is below the entire average of the time-series (i.e. in a negative phase) and post 1979 the average MEI value is above the entire average of the time-series (i.e. in a positive phase). Considering picoplankton are positively correlated with MEI on large scales, there may have already been a shift from large to smaller size classes of phytoplankton over the past 50-years. As smaller size classes are associated with lower chlorophyll-a concentrations, this result would also compliment a recent study by Boyce et al. (2010) which found global phytoplankton concentrations to be declining over the past century.

On regional scales, the correlation between MEI and phytoplankton size class can, however, be very different. In Figure 6.15 the correlations between MEI and phytoplankton size class are vastly different for different regions. In the North Pacific gyre and around Indonesia and Papua New Guinea, MEI is positively correlated with nano- and microplankton and negatively correlated with picoplankton, in contrast to the large scale relationships. By conducting regressions on a pixel by pixel basis, regional variations in the relationship between MEI and phytoplankton size class can be investigated (Figure 6.16 and Figure 6.17), and while, under a transition to permanent El Niño conditions, some areas may see an increase in picoplankton at the expense of nano- and microplankton, it may be expected that other areas would see the inverse. Further investigation into the relationship between ENSO mechanisms and teleconnections would need to be conducted in order improve understanding of regional variations.

Figure 6.18 emphasises how MEI alone can be used to generate very similar phytoplankton size class anomaly maps to those derived from satellite, reproducing the regional scale variations. Over seasonal timescales this appears robust. However, its limitation is that such regressions cannot reproduce small temporal scale anomaly blooms. For instance, Brewin et al. (2010a) used the three-component model to detect a large microplankton bloom in July/August 1998, which resulted from short term changes in the EUC as a consequence of the La Niña transition. This short event cannot be fully reproduced using the MEI model estimate (see Figure 7.2, also note higher ME in Figure 6.17 for pico- and microplankton around the equatorial regions). More complex non-linear regressions may be more appropriate for such circumstances, possibly using additional input variables (e.g. SST, SSHA).

MEI appears a useful tool for simulating changes in phytoplankton size class structure during past El Niño to La Niña events, that pre-date ocean colour sensors

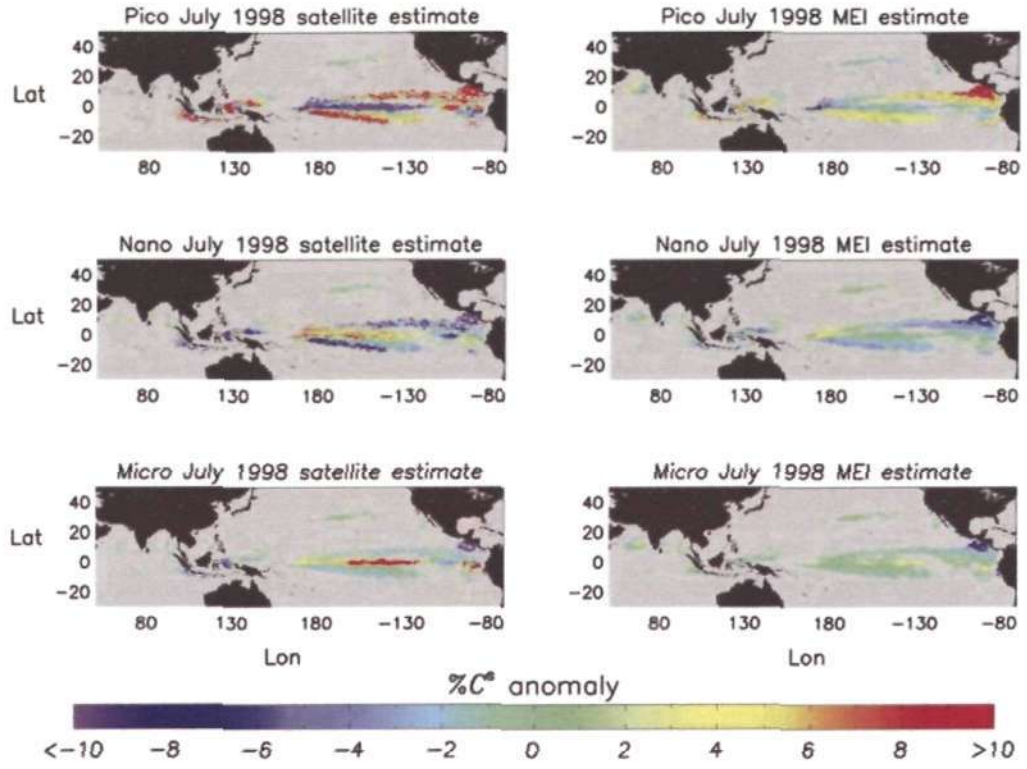

Figure 7.2: Phytoplankton size percentage chlorophyll-a anomaly maps for July 1998 from the satellite-based three-component model for the classified pixels (Figure 6.13 b) in addition to the modelled anomaly map estimates using the linear relationship between MEI and phytoplankton size percentage chlorophyll-a (Figure 6.18).

(Figure 6.19). When using such a model to hindcast it is important to be aware of its assumptions. The results in Figure 6.19 assume that the relationship between MEI and phytoplankton size class would be the same during similar ENSO events, when in fact the correlations may be different. To investigate this further one may need to compare the results to the output from multi-plankton biogeochemical models or alternatively perhaps make use of the CZCS archives (e.g. possibly during the *1982-1983 ENSO event*).

Such drastic changes in the size structure of the phytoplankton during the 1972-1973 period, as highlighted in Figure 6.19, are likely to have a huge influence on the food web. Tsukayama (1983) linked the strong ENSO event of 1972-1973 to a crash in the population of anchovy at the Peruvian coast (in addition to high exploitation), which in the 1960s reached biomass levels of 15-20 million tons, providing annual landings that exceeded 10 million tons in 1970 (Niquen and Bouchon, 2004). Together with political change in the country, the anchovy collapse in 1973 led to a temporary nationalisation of fisheries, resulting in massive layoffs and a restructuring of the fishing industry (Broad et al., 2002). This had worldwide effects on food prices (Idyll, 1973). It was not until early 1990s that the anchovy catch recuperated to near pre-1973 levels (Broad et al., 2002). Anchovy are planktonic feeders and

form the diet of large fish, guano birds, marine mammals and humans.

While it is established that larval survival is especially dependant on availability of phytoplankton, and that the reproductive success of the species will be impaired if availability of phytoplankton declines (Barber and Chavez, 1983; Platt et al., 2003), it may be that selective community-based preferences may also have a significant influence. The community size-structure shifts in phytoplankton during the 1972-1973 period highlighted in Figure 6.19, driven by the ENSO cycle, may have played a role in the population crash of anchovy at the Peruvian coast. Further investigation would need to be conducted to verify this link. The use of climate indices such as MEI or DMI may also become useful for improving the spatial availability of satellite data (note that the MEI model estimates cover a larger spatial area than the satellite estimate in Figure 6.18) and may even have potential use in the merging of satellite data from different platforms, considering such indices are available over multiple decades (for instance encompassing the CZCS and SeaWiFS period).

7.3 Future work and the impact of the work in other research fields

Future work will focus on improvements in the three-component model. Furthermore, the findings of this research have a variety of applications in the greater context of oceanography which will also form the basis of future work.

7.3.1 Improvements in the three-component model

7.3.1.1 Future improvements in the calibration of the three-component model

The applicability of the three-component model was outlined in section 7.2.2.2. A current weakness of the three-component is that it is fitted to pigment measurements and as highlighted previously, there are certain assumptions about the pigment to size-class relationship. By conducting coupled cell count, size-fractionated chlorophyll measurements, phytoplankton absorption measurements and HPLC pigment measurements, improvements in the parameterisation of the model could be made.

Through gathering measurements in case 2 waters, further investigation could be made into whether the relationship between size and chlorophyll-a concentration demonstrated for case 1 waters holds in various case 2 waters. With improvements in case 2 satellite retrievals, possibly through the further development of IOP models, this may result in the application of the model to a wider geographic region.

If a larger database became available, whereby data could be partitioned into biogeochemical provinces, and in each province the data was representative of the entire chlorophyll-a range, the performance of the three-component model may im-

prove over larger spatial scales. Furthermore, in environments that deviate from the major phytoplankton composition trends, by improving our understanding of the physical and chemical regime, additional environmental knowledge could be introduced which may improve model performance.

7.3.1.2 Extending the three-component model to more PFTs

While from the perspective of primary production, cell size, is thought to be sufficient for defining the major functional groups, a size-based approach to functionality in *phytoplankton is not fully satisfactory from a biogeochemical perspective* (Nair et al., 2008). For instance, if phytoplankton characterised by different functions fell under the same size class, a size-based approach would fail to separate the two groups (e.g. an increase in Si is likely to influence diatoms but not dinoflagellates, both of the microplankton size class). Therefore, from a biogeochemical perspective, extending the three-component model to distinguish further taxonomic phytoplankton groups would be beneficial.

Hirata et al. (2011) quantified relationships between surface chlorophyll-a and the diagnostic pigments specific to phytoplankton functional types. In addition to determining the three size classes from satellite, as with the three-component model, the approach of Hirata et al. (2011) detects diatoms, dinoflagellates, green algae, picoeukaryotes, prokaryotes and *Prochlorococcus*. Whereas such an approach appears the logical step on from size class detection, caution needs to be made when deriving six PFTs from a single variable (i.e. chlorophyll-a). Nair et al. (2008) highlight that the limited wavelength resolution of satellite data currently available, may set an upper limit on the number of functional types that can be retrieved from space. There is, however, certainly scope for further improvements as hyperspectral remote sensing from space becomes a reality.

The three-component model highlights that size-fractionated chlorophyll-a can be estimated from total chlorophyll-a using a simple exponential equation, with two parameters, the maximum chlorophyll-a concentration of the size class (C^m) and the initial slope (S), dictating the increase in the size-fractionated chlorophyll-a as a function of total chlorophyll-a. Comparing model parameters when fitting the same equation to two different size fractions ($<2\mu$m and $<20\mu$m) indicates that C^m increases with increasing size and S decreases. By using further size-fractionated measurements (e.g. $<2\mu$m, $<5\mu$m, $<10\mu$m $<20\mu$m and $<100\mu$m), it could be possible to derive quantifiable relations between phytoplankton size and these two parameters, which could present an avenue to determining the phytoplankton size distribution more fully from total chlorophyll-a.

7.3.1.3 Using the three-component model to improve satellite estimates of chlorophyll-a

Recent efforts have been made to improve remotely-sensed retrievals of the chlorophyll-a concentration by introducing phytoplankton community composition. Alvain et al. (2006) applied the PHYSAT approach to the NOMAD *in situ* dataset to derive species-dependent polynomial relationships between $L_{wn}(\lambda)$ and the chlorophyll-a concentration (similar polynomial relationships to the OC4 algorithm of O'Reilly et al. (1998)). The resulting (OC4-SD) bio-optical model starts from a classification of the dominant phytoplankton group (using PHYSAT), followed by a species-dependent estimate of chlorophyll-a using the species-dependent polynomial relationships. It was found that new algorithm (OC4-SD) led to lower chlorophyll-a concentrations in regions where the OC4 model retrievals are known to be too high, and higher concentrations in regions dominated by diatom blooms where previous studies had demonstrated a low bias in the standard OC4 algorithm.

Through discriminating diatoms from other phytoplankton using ocean colour data, Sathyendranath et al. (2004) developed a diatom-specific and non-diatom algorithm for estimating the chlorophyll-a concentration from satellite data in the North West Atlantic. Similar to Alvain et al. (2006), when diatoms were identified, the diatom-specific algorithm was used and when diatoms were not identified the non-diatom algorithm was used. The results show that the branching bio-optical algorithms often performed better than the OC4 algorithm used in standard processing of SeaWiFS data. As the three-component absorption model developed in Chapter 5 is an extension of the two-component model of Sathyendranath et al. (2001), used in the Sathyendranath et al. (2004) study, the three-component absorption model may have the potential to further improve chlorophyll-a retrievals from $R_{rs}(\lambda)$.

7.3.2 Improving our understanding of the carbon cycle

7.3.2.1 Introducing size-structure into satellite estimates of primary production

As highlighted in Chapter 4, the three-component model may be used in conjunction with procedures designed to estimate the vertical chlorophyll profile from the surface concentration (Morel and Berthon, 1989; Sathyendranath et al., 1995; Uitz et al., 2006). Furthermore, as shown in Chapter 5, specific absorption coefficients were retrieved for the three size classes by extending the Sathyendranath et al. (2001) and Devred et al. (2006) absorption models into a three-component absorption model based on phytoplankton size class. Such detailed knowledge regarding the spatial distributions of the phytoplankton size classes, and their optical properties, could be used together with other size-specific photophysiological parameters to improve

EO primary-production estimates (e.g. Silió-Calzada et al., 2008; Uitz et al., 2008, 2009, 2010; Hirata et al., 2009b).

Using the two-component model of Sathyendranath et al. (2001), Brewin et al. (2010b) developed a size-specific primary production model which was used to estimate global distributions of production by small (<20μm) and large cells (>20μm), using satellite data. It was found that smaller cells contribute highly to global production ($\sim$ 95 %) in comparison with larger cells ($\sim$ 5 %). This result was contradictory to that of Uitz et al. (2010). Interestingly, Uitz et al. (2010) estimated that smaller phytoplankton (<20μm) contribute a much smaller fraction of the global estimate ($\sim$ 68 %). Brewin et al. (2010b) found that discrepancies between the two models lie in their allocation of size-specific photophysiological parameters. The model of Uitz et al. (2010) assumes larger phytoplankton (>20μm) are more efficient in photosynthesis than smaller phytoplankton (<20μm) (consistent with Claustre, 1994; Claustre et al., 2005; Cermeno et al., 2005), alternatively, the model of Brewin et al. (2010b) assumes smaller phytoplankton (<20μm) are more efficient in photosynthesis than larger phytoplankton (>20μm) (consistent with Laws et al., 1987; Bouman et al., 2005; Kameda and Ishizaha, 2005).

The assignment of size-specific photophysiological parameters is an emerging area of research with little current consensus. Furthermore, assigning size-specific photophysiological parameters directly from globally representative data (as conducted by Brewin et al. (2010b) and Uitz et al. (2010)) may not fully capture the widescale variability in phytoplankton physiology. Future work may need to focus on seasonal and geographical differences, possibly partitioning data into biogeochemical provinces and dealing with each province independently (Sathyendranath et al., 1995; Longhurst et al., 1995).

7.3.2.2 Improving export production estimates by introducing size-structure

It is well established that the size-structure of the phytoplankton has a significant influence on the sinking rate and export of carbon (Michaels and Silver, 1988; Boyd and Newton, 1999; Laws et al., 2000). In particular, Uitz et al. (2010) found the ratio of microplankton production to total production to be a good estimate of the f-ratio (the ratio of new to total primary production) which is subsequently available for carbon export to the deep ocean.

Using a globally-representative dataset, Guidi et al. (2009) found that 68 % of the variance of the mass flux of carbon at 400 m was explained by the size structure of the phytoplankton community and integrated chlorophyll-a in the euphotic zone. Guidi et al. (2009) estimated the coefficient k, in the Martin power relationship (which describes the decrease in the vertical mass flux with depth and

generally varies between 0.2-1.0), using an empirical relationship derived from the size structure of phytoplankton biomass in the euphotic zone. Satellite retrievals of the size-structure of phytoplankton biomass in the euphotic zone, calculated using the three-component model, could be used to improve export production estimates. As suggested by Guidi et al. (2009), information such as the coefficient k, derived from satellite models of phytoplankton size class, could be used by biogeochemists and modellers to obtain a realistic description of the downward particle flux instead of using a constant k value as frequently conducted.

7.3.2.3 Size-specific CO_2 fluxes

A further step toward improving our understanding of the carbon cycle would be to investigate the role of phytoplankton size class in CO_2 flux variability. This could be conducted by comparing size-fractionated chlorophyll-a (or primary production, e.g. Brewin et al. (2010b)) derived from satellite to CO_2 flux hindcasts from biogeochemical models, in order to see how changes in phytoplankton structure have contributed to seasonal and interannual variability in air-sea CO_2 fluxes. By undertaking a multivariate evaluation, a process understanding of the functional relationships between the size structure of the phytoplankton, their environment and their influence on CO_2 fluxes may be achieved.

7.3.2.4 Metabolic-scaling

Recently, several attempts have been made to use EO data and food web models to predict consumer biomass in the global oceans. Jennings et al. (2008) used primary production estimates from processed ocean colour data as input to a food web model that predicted the abundance, distribution and role of marine animals on global scales. However, it is well established that such predicted values are dependant on the consumer size, predator-prey size relationships and the size composition of the primary producers (Borgmann, 1987). Therefore, in order to improve estimates of higher trophic levels, it may seem sensible to introduce phytoplankton size-structure, as derived from EO, into metabolic-scaling models.

Using the three-component model, Jennings et al. (2010) predicted consumer biomass and production, trophic levels and ratios between consumer production and primary production in the global oceans using simple food web model that took account of the size structure of phytoplankton communities using the three-component model. Initial results suggest further work is needed to address the link between primary production and the slopes of size spectra, and that the results may benefit from introducing size-specific primary production rates possibly derived from EO.

7.3.2.5 Multi-plankton biogeochemical models: validation and assimilation

Biogeochemical models have the potential to predict how the ocean biology will change (or not) in the face of our changing climate. However, in order to confidently use such models, observations are required for validation. Sampling limitations of ships and buoys which involve comparing measurements widely separated in space and time, limit the use of *in situ* data in validating such models. EO, however, can be used to synoptically monitor wide areas not possible by conventional *in situ* methods.

Recently much effort has been put into using ocean colour observations for both validation of, and assimilation into, biogeochemical models (Harmon and Challenor, 1997; Gregg et al., 2003; Lacroix et al., 2007; Hemmings et al., 2008; Gregg, 2008). With the development of multi-phytoplankton biogeochemical models (e.g. Taylor et al., 1993; Vanden Berg et al., 1996; Kuroda and Kishi, 2004; Blackford et al., 2004; Le Quéré et al., 2005; Kishi et al., 2007), there is increasing demand for synoptic data of the different phytoplankton communities. This thesis has shown that phytoplankton size class can be retrieved from EO with accuracy sufficient to be useful in such model comparisons. The three-component model offers an avenue to assimilate size structure into such biogeochemical models, or alternatively, verify them. Furthermore, in addition to providing information on size-structure, using the proposed three-component model, error estimates can also be provided, which are essential for validation and assimilation purposes. By doing this, such models can be improved, ultimately advancing our understanding of the ocean carbon cycle needed to improve predictions of its future influence on climate.

7.3.3 Monitoring change

7.3.3.1 Phytoplankton phenology

Remote sensing data is a useful tool in monitoring changes in phytoplankton bloom phenology (Platt et al., 2009) which can significantly influence larval fish survival (Platt et al., 2003). Information on the phenology of the different phytoplankton size classes may offer further insight into such trophic interactions. For instance, changes in phytoplankton succession associated with seasonal events such as the Spring Bloom.

7.3.3.2 Multi-decadal changes

By using a consistent, reanalyzed, ocean colour time series built from 5 years of observations of the CZCS (1979-1983) and 5 years from SeaWiFS (1998-2002) (Antoine et al., 2005), Martinez et al. (2009) linked multi-decadal changes in global

phytoplankton abundances to basin-scale oscillations of the physical ocean, specifically the Pacific Decadal Oscillation and the Atlantic Multi-decadal Oscillation. By applying the three-component model to such a dataset, further investigation could be made into links between multi-decadal basin-scale oscillations and phytoplankton size structure.

7.4 Conclusion

The aim of this thesis was to compare a variety of existing approaches that have been designed to detect phytoplankton size class from EO and develop a new modified approach that can be applied to 10-years of satellite ocean colour observations to investigate relationships between phytoplankton size structure and physical forcing on interdecadal scales. This aim was achieved by conducting an intercomparison of bio-optical techniques for detecting dominant phytoplankton size class from EO using a co-located *in situ* and satellite dataset (Chapter 3). The results of this intercomparison indicated that abundance-based models are the most robust approach for detecting dominant size class from EO. A new abundance-based model was developed based on insight into abundance-based models used in the intercomparison (Devred et al., 2006; Uitz et al., 2006), designed to calculate the fractional contributions of three phytoplankton size classes for a continuum of chlorophyll-a concentrations (Chapter 4 and 5). The model was applied to 10-years of satellite ocean colour observations and phytoplankton size structure was correlated with indices of the El Niño (La Niña) Southern Oscillation and the Indian Ocean Dipole.

The major findings of the thesis can be stated in the context of the research questions posed in Chapter 1.

How accurately can we detect phytoplankton size class from Earth Observation in the global ocean?

Based on the results from the intercomparison in Chapter 3, mean percentage accuracy combining all models, according to method 1, calculated from averaging both HPLC and cell count data, was 63.4 % (77.2 % not including the L4 data) for picoplankton, 86.6 % for combined nano-picoplankton, 61.4 % for nanoplankton and 66.8 % for microplankton. When only considering the abundance-based models of Devred et al. (2006), Uitz et al. (2006), and Hirata et al. (2008a), this percentage accuracy changes to 65.7 % (82.7 % not including the L4 data) for picoplankton, 84.3 % for combined nano-picoplankton, 65.7 % for nanoplankton and 77.9 % for microplankton.

Validation of the three-component model developed in Chapter 4 with concurrent and co-located *in situ* and satellite data, indicated the fractional contribution

of each size class to the overall biomass can be retrieved to an accuracy of within 9.2 % for microplankton, 17.1 % for nanoplankton and 16.1 % for picoplankton, in the global ocean. Based on these results it can be concluded that phytoplankton size class can be derived from EO with reasonable accuracy.

What is the most robust method for detecting phytoplankton size class from Earth Observation in the global ocean?

Results from the intercomparison in Chapter 3 indicate that spectral-response, ecological and abundance-based approaches can all perform with similar accuracy. However, abundance-based approaches were shown to provide better spatial retrieval of phytoplankton size class, supporting the theory that information on the size structure of phytoplankton is latent in the satellite derived biomass fields. The robustness of abundance-based approaches appears to be a result of their utilisation of the first order variability in the satellite ocean colour signal, whereas spectral-response-based algorithms use the second order variability which is weaker, in some respects harder to infer and more vulnerable to errors in atmospheric processing.

When applying the three-component model to absorption data (Chapter 5), the retrieved size-specific absorption coefficients were consistent with both laboratory and field studies, again supporting the assumption that there is information on the phytoplankton size structure in the chlorophyll-a concentrations. This was further supported in Chapter 6, where interannual variations using the three-component model in the Pacific and Indian Oceans were strongly correlated with physical parameters, consistent with theories on coupling between physical-chemical processes and ecosystem structure, such as that of Margalef (1978).

The proposed three-component model is an advance on previous approaches (e.g. Devred et al., 2006; Uitz et al., 2006; Hirata et al., 2008a) as the model calculates the fractional contribution of three phytoplankton size classes for a continuum of chlorophyll-a concentrations and retrieves these fractions with similar (if not better, see Figure 4.8) accuracy to the model of Uitz et al. (2006), from Earth Observation. Furthermore, unlike the statistical model of Uitz et al. (2006), the three-component model is based on ecological theory and its parameters provide biological interpretation.

Can Earth Observation estimates of phytoplankton size class be used to improve estimates of phytoplankton light absorption needed for input to satellite-based primary production models?

In Chapter 5, a new three-component absorption model was developed, extending the two-component absorption models of Sathyendranath et al. (2001) and Devred

et al. (2006). The new three-component absorption model provided a better fit to absorption and chlorophyll-a data than the two component model as indicated by retrieving lower mean errors when fitting the three models to the same dataset. The improvement over the two-component absorption models of Sathyendranath et al. (2001) and Devred et al. (2006) is a result of introducing a third component which yielded a better representation of both $a^*(\lambda)$ and $a(\lambda)$ at low chlorophyll-a concentrations.

How is phytoplankton size structure influenced by climate variability?

The three-component model developed in Chapter 4 was applied to a decade of ocean colour observations in Chapter 6. In the equatorial region of the Pacific and Indian Oceans, phytoplankton size class anomalies were highly correlated with indices of both the El Niño (La Niña) Southern Oscillation and the Indian Ocean Dipole. Furthermore, in these regions, changes in the phytoplankton size structure were highly correlated with changes in SST, SSHA and stratification, derived from both satellite and *in situ* observations. The fraction of microplankton and nanoplankton to the total chlorophyll-a biomass were negatively correlated with SST, SSHA and stratification, and the fraction of picoplankton to the total chlorophyll-a biomass positively correlated with SST, SSHA and stratification.

Under a global warming scenario, it has been projected that there will be an increase in sea surface temperature and stratification in low latitude areas of the open ocean (Doney, 2006). Under such circumstances, in the surface layer of the ocean, it may be expected to see an increase in picoplankton at the expense of nano- and microplankton in low latitude areas, which may have huge impact on the carbon cycle and on marine ecosystems.

7.4.1 Summary, recommendations and a final note

By comparing a variety of existing phytoplankton functional type satellite models using a concurrent and co-located *in situ* and satellite database of phytoplankton size measurements, it became evident that abundance-based approaches are the most robust method for detecting phytoplankton size class from EO. A new abundance-based model was developed which was then adapted to improve estimates of phytoplankton light absorption from EO and to quantify relationships between phytoplankton size structure and physical forcing on interdecadal scales.

If this research was to be repeated, future efforts need to focus on gathering more *in situ* data over larger spatial scales and clarifying uncertainty in using *in situ* proxies to infer phytoplankton size. By developing a database of concurrent and co-located *in situ* measurements of cell counts, size-fractionated chlorophyll, phytoplankton absorption measurements, HPLC pigment measurements, flow cytometry,

PSD measurements and possibly DNA measurements, the diagnostic pigment to size class procedure may be improved. A more robust intercomparison of the different approaches could then be conducted and the parameterisation of the three component model could be further improved.

The true capabilities of EO can only come to fruition when it is used in conjunction with *in situ* based measurements, for validation and calibration purposes. The synergistic benefits of using these observational techniques in conjunction allow for well-constrained, accurate biological and geophysical parameters that can then be assimilated into mathematical models to improve their parameterisation and our understanding needed to predict future change. The results of this thesis recommend that EO measurements of phytoplankton size class should be used for validation of, or assimilation into multi-plankton biogeochemical models. This will ultimately result in advancing our understanding of the ocean carbon cycle needed to improve predictions of its future influence on climate.

This thesis has for the first time quantified links between the phytoplankton community composition and physical forcing on synoptic interannual scales, using EO in conjunction with *in situ* data. Results support theories first proposed by Ramón Margalef as early as the 1960's, showing community changes of phytoplankton based on physical-chemical-ecological interactions, and cement the idea that all the components of a system (physical, biological and chemical) are intertwined and intrinsically linked (Lovelock, 1992). By facing an uncertain climate we are in fact facing uncertain changes in our marine ecosystem.

Appendices

Appendix A

Application of the three-component model to daily, 8-day and monthly satellite chlorophyll-a fields to derive monthly composites of phytoplankton size class

A.1 Introduction

Theoretically, as the three-component model is based on non-linear equations, the model needs to be applied directly to daily satellite chlorophyll-a images and then averaged to produce a monthly composite. In this appendix the three-component model is applied to 32 daily SeaWiFS chlorophyll-a images from 1st May 2005 to the 1st June 2005 to produce a 32-day (monthly) composite. In addition, the three-component model is also applied to four 8-day SeaWiFS chlorophyll-a images from the same time period and then averaged to produce a 32-day (monthly) composite. Furthermore, the three-component model is also applied to a 32-day rolling SeaWiFS composite of chlorophyll-a for the same time period. Results from the three 32-day composites are then compared to quantify differences between the three approaches.

A.2 Methodology

Thirty-two daily, global, SeaWiFS chlorophyll-a images from 1st May 2005 to the 1st June 2005 were used for analysis. In addition, four 8-day, global, SeaWiFS chlorophyll-a images were also downloaded encompassing the following time periods: 1st-8th May, 9th-16th May, 17th-24th May, and 25th May-1st June 2005. Finally a 32-day rolling, global, SeaWiFS chlorophyll-a composite, encompassing the same time period, was also used for analysis.

The three-component model (using parameters from Table 4.1) was applied to each daily image from 1st May 2005 to the 1st June 2005 to derive the chlorophyll-a concentration ($mg\,m^{-3}$) and fractional contribution (% chlorophyll-a) of the three size classes of phytoplankton (pico-, nano- and microplankton). These 32 daily images were then averaged to produce a 32-day composite for each size class, and for each product (referred to as M1 composites). Using the same model parameterisation, the three-component model was applied to the four 8-day SeaWiFS chlorophyll-a images, to derive for each size class the chlorophyll-a concentration and fractional contribution. Products from these four 8-day images were then averaged to produce a second 32-day composite for each size class (referred to as M2 composites). Finally, the three-component model was applied directly to the 32-day rolling, global, SeaWiFS chlorophyll-a image to produce a third 32-day composite for each size class, and for each product (referred to as M3 composites).

Mean Error (ME) differences were calculated between each composite (weighting each pixel's value by its area (a function of latitude)). In addition, differences were also calculated on a pixel by pixel basis by subtracting M2 from M1, M3 from M1, and M3 from M2.

A.3 Results

Figure A.1 and A.2 show the results from the three monthly images for size-specific chlorophyll-a and the percentage of each size class to the total chlorophyll-a concentration respectively. In all cases the results are shown to be very similar. Table A.1 show the global average ME between images. ME differences between images, regarding percentage contribution to total chlorophyll-a, are less than 1 % for all size classes. Regarding size-specific chlorophyll-a concentrations, differences are below $0.015\ mg\,m^{-3}$ for all size classes. These differences are well below estimated errors on the three-component model (Chapter 4) and also realistic sensitivity estimations (Appendix D).

Figure A.3 and A.4 show the differences between the monthly images for size-specific chlorophyll-a and the percentage of each size class to the total chlorophyll-a concentration respectively, on a pixel by pixel basis. In general, higher differences are observed in coastal and highly eutrophic areas for all size classes (see Figure A.3 and A.4). In such areas, the percentage of each size class to the total chlorophyll-a concentration typically varies between ± 3 % and the size-specific chlorophyll-a concentrations between $\pm 0.01\ mg\,m^{-3}$. Again these differences are well below estimated errors on the three-component model (Chapter 4) and also realistic sensitivity estimations (Appendix D).

The small differences between approaches are clearly due to the temporal sampling of satellite data. Maritorena and Siegel (2005) highlight that SeaWiFS daily

images cover typically 12-15 % of the ocean surface. When averaging over a monthly period, monthly SeaWiFS images typically cover the majority of the world ocean. Maritorena and Siegel (2005) found that by merging three ocean colour sensors, 30-35 % of the ocean surface can be covered daily, allowing almost complete coverage of the world ocean within a 4-5 day period. Larger differences in the three approaches, shown here, may be expected with satellite products that have higher temporal resolution, such as merged products (e.g. the GlobColour Project).

Table A.1: Mean Error (ME) differences between monthly processing methods.

Product	M1-M2	M1-M3	M2-M3
Pico $\%C^s$	0.45	0.53	0.62
Nano $\%C^s$	0.35	0.45	0.51
Micro $\%C^s$	0.24	0.29	0.34
Pico C_p^s ($\mathrm{mg\,m^{-3}}$)	0.0008	0.0009	0.0011
Nano C_n^s ($\mathrm{mg\,m^{-3}}$)	0.0036	0.0050	0.0055
Micro C_m^s ($\mathrm{mg\,m^{-3}}$)	0.0138	0.0097	0.0149

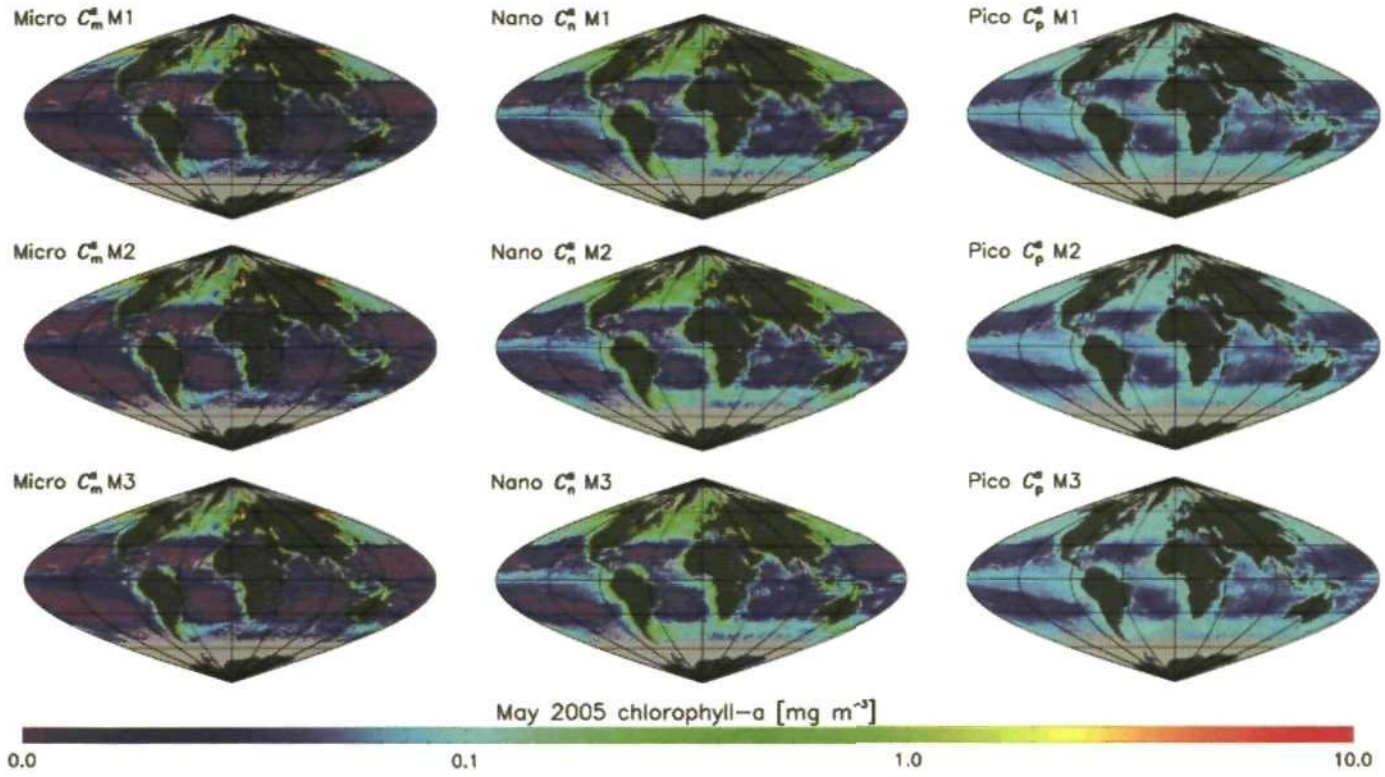

Figure A.1: The size-specific chlorophyll-a concentrations (C) of pico-, nano- and microplankton for the three monthly processing methods (M1, M2 and M3) for May 2005.

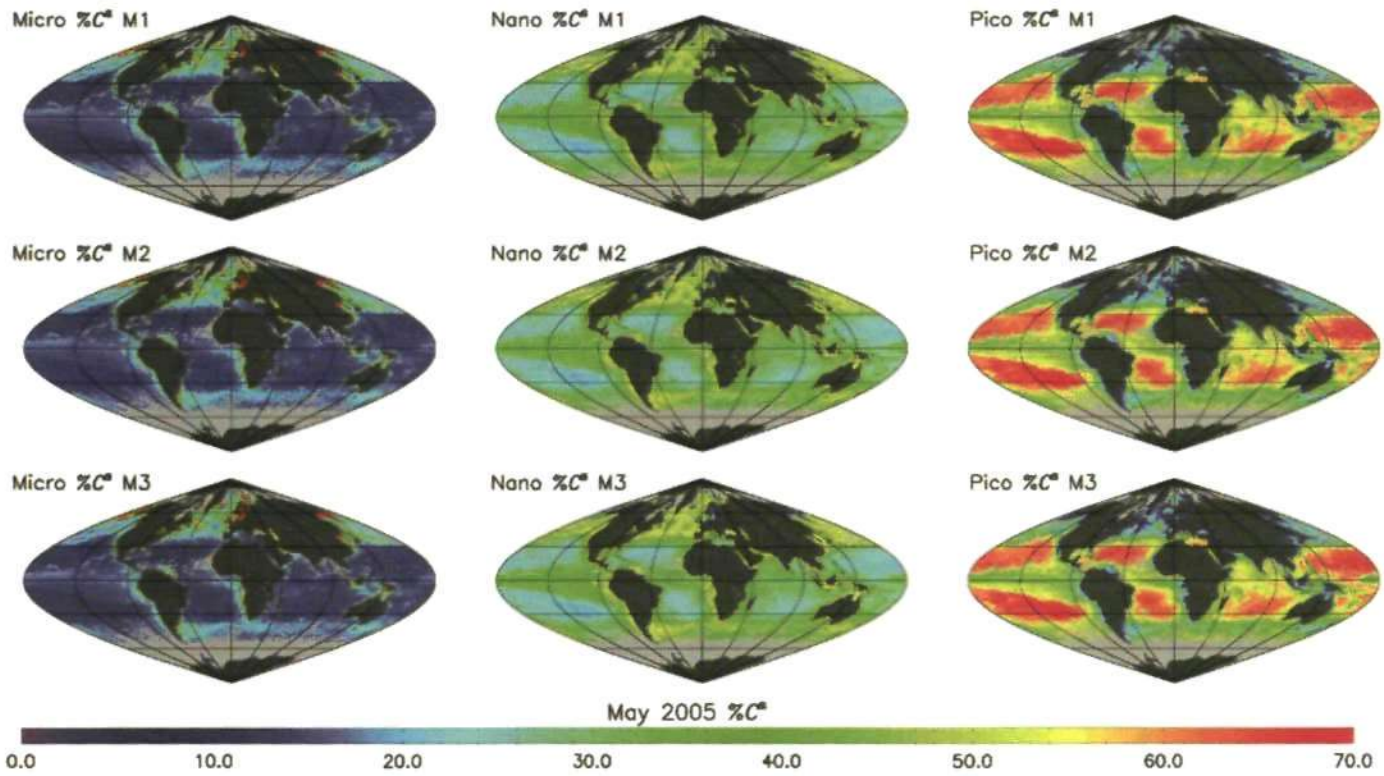

Figure A.2: The percentage contribution of the three size class to total chlorophyll-a (C), for the three monthly processing methods (M1, M2 and M3) for May 2005.

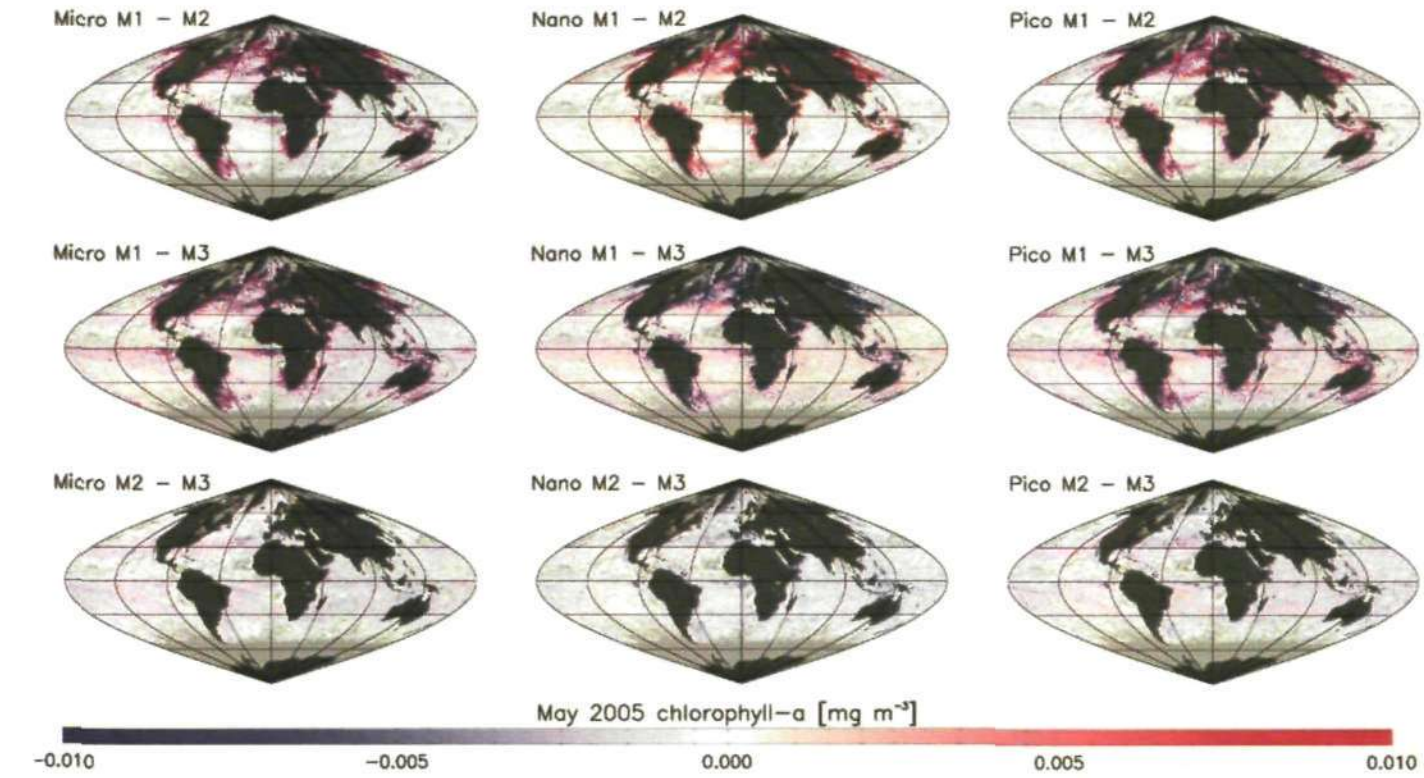

Figure A.3: Differences in the size-specific chlorophyll-a concentrations (C) of pico-, nano- and microplankton for the three monthly processing methods (M1, M2 and M3) for May 2005.

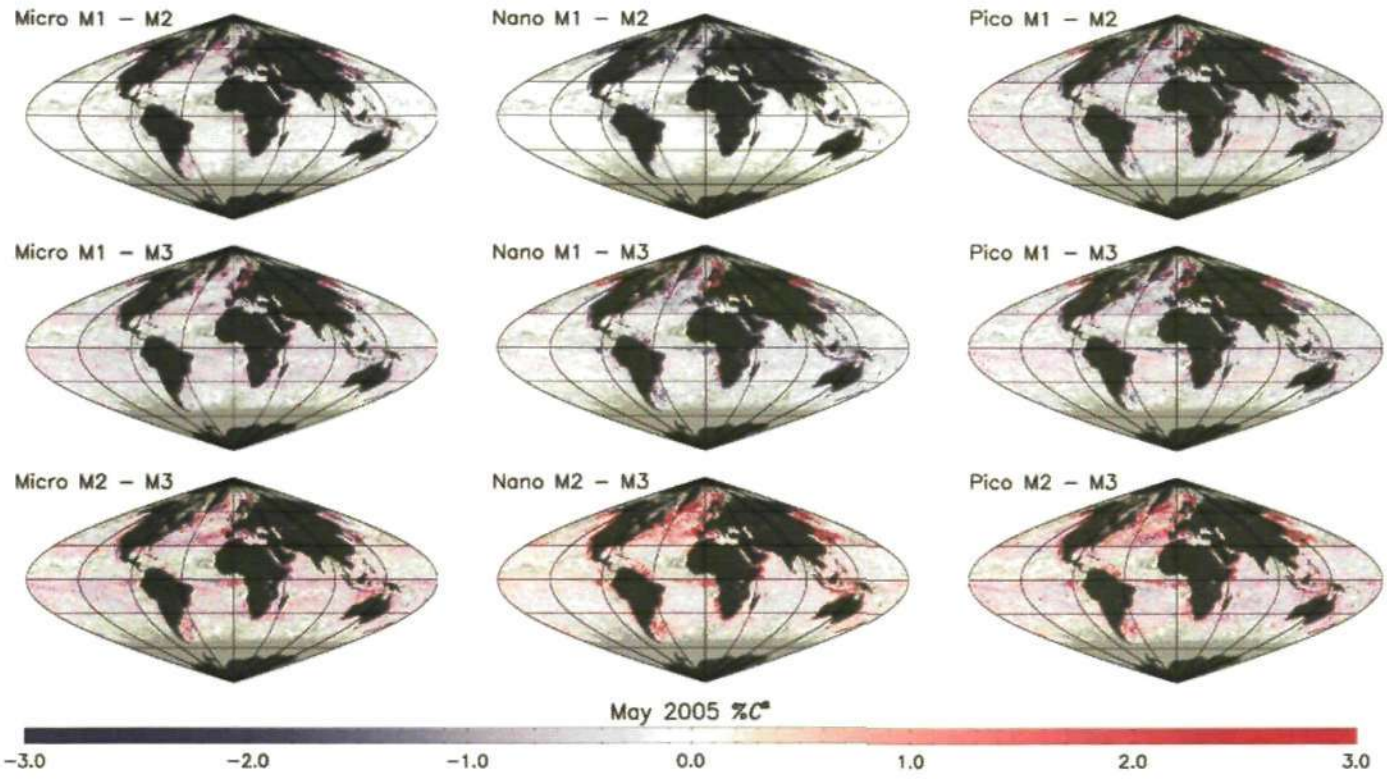

Figure A.4: Differences in the percentage contribution of the three size class to total chlorophyll-a (C), for the three monthly processing methods (M1, M2 and M3) for May 2005.

A.4 Summary

Whereas the three-component model is based on non-linear equations, results from this appendix indicate that such a model can be applied directly to either 8-day SeaWiFS chlorophyll-a composites before producing a monthly composite, or alternatively directly to monthly SeaWiFS chlorophyll-a composites. When comparing the three methods, global average ME differences between images were below 1 % and 0.015 $mg\,m^{-3}$ for the percentage total chlorophyll-a and the absolute chlorophyll-a of the three size classes, respectively. Such a result could help to reduce computational time when running the model on SeaWiFS satellite images.

Appendix B

Testing the NASA chlorophyll-a algorithm for systematic interannual variability

B.1 Introduction

The three-component model developed in Chapter 4 uses the total chlorophyll-a concentration as an input to calculate the fractional contributions of three phytoplankton size classes. When applying the model to satellite derived total chlorophyll-a data over a 10-year SeaWiFS period, it is essential to test the satellite algorithm for systematic interannual variability before applying the three-component model and using the results to analyse changes over the 10-year period. Any small systematic deviations in the input may propagate through the calculations, particularly considering the three-component model is non-linear. In this appendix, the NASA chlorophyll-a algorithm is tested for systematic interannual variability using the NASA NOMAD dataset.

B.2 Methodology

B.2.1 *In situ* data

Using the NASA NOMAD *in situ* dataset (Version 2.0w APLHA, 18/07/2008, OOXIX IOP Algorithm Workshop evaluation dataset, Werdell and Bailey, 2005; Werdell, 2009), 822 contemporary, co-located remote-sensing reflectances, at SeaWiFS visible wavelengths, and *in situ* chlorophyll-a measurements, were used to test the NASA OC4 algorithm (O'Reilly et al., 1998, 2000). The dataset incorporated measurements from 1995-2007 from various oceans insuring high variability in the dataset. It is acknowledged that some of the data in the NOMAD dataset was used to fit the OC4 algorithm. However, the purpose of this exercise is not to validate the

algorithm but to test for any systematic interannual biases and the NASA NOMAD dataset is the only freely available dataset of sufficient size to do so.

B.2.2 NASA OC4 algorithm

The remote-sensing reflectances ($R_{rs}(\lambda)$) were used to derive the near surface chlorophyll-a concentration using the OC4 algorithm (O'Reilly et al., 1998, 2000) following Equation 2.19. The *in situ* chlorophyll-a measurements were then compared with the OC4 measurements for different years to see if there is any systematic interannual variability in the OC4 estimates.

B.3 Results

The results from the test are shown in Figures B.1 and B.2. Figure B.1 shows the band ratio plotted as a function of the *in situ* chlorophyll-a concentrations with the OC4 algorithm superimposed on the data, for all the data and for each separate year. The majority of the data was sampled between 1997-2003, and for these years the model appears to fit the observations well with no systematic biases observed. Data post 2004 appears to be sparse in comparison.

Figure B.2 shows the OC4 derived chlorophyll-a concentrations plotted against the *in situ* chlorophyll-a concentrations, for all the data and for each separate year. A linear model was fitted to the data to highlight biases and the ME % are shown between the two measurements (Figure B.2). With the exception of 1995 (not a SeaWiFS year), 2004, 2005 and 2007, the OC4 algorithm appears to compare well to the *in situ* chlorophyll-a concentrations with no systematic bias, as indexed by a slope close to one, and an intercept close to zero in the linear regression. The years where the OC4 algorithm does not seem to fit the *in situ* chlorophyll-a concentrations so well, as indexed by a slope far from one and an intercept far from zero in the linear regression (1995, 2004, 2005 and 2007), there are very few measurements. Furthermore, in these years the *in situ* chlorophyll-a values appear unevenly distributed over the chlorophyll-a range (e.g. for 2005 chlorophyll-a values are nearly all over 1 $\mathrm{mg\,m^{-3}}$).

B.4 Summary

In conclusion, given the regional and seasonal variability in the NOMAD dataset, one cannot discern any systematic interannual variability in the performance of the NASA algorithm when using the NOMAD dataset. In years where there are plenty of measurements that are evenly distributed over the chlorophyll-a range, the OC4 algorithm appears to perform without any systematic bias.

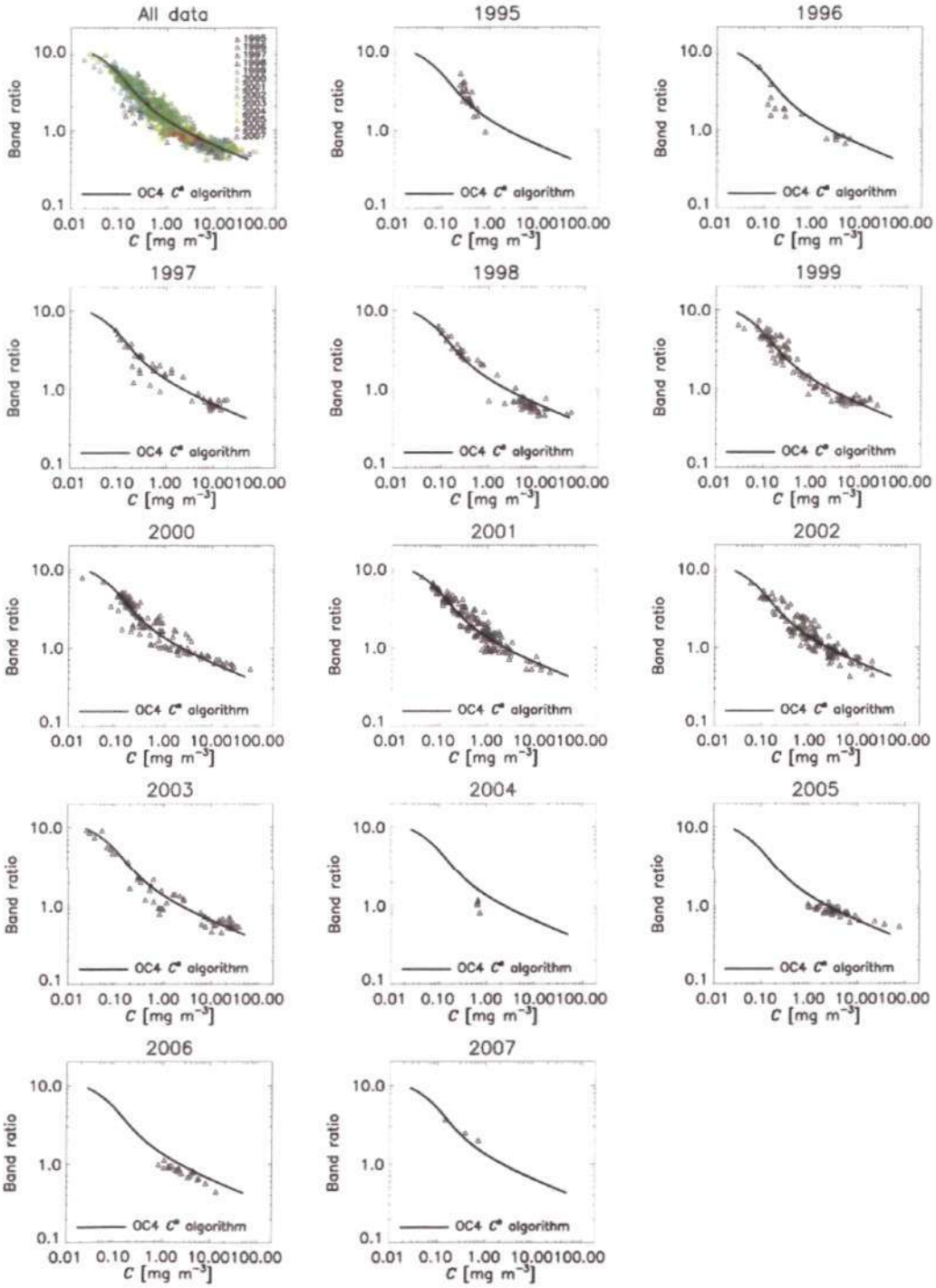

Figure B.1: The band ratio ($R_rs443 > R_rs490 > R_rs510/R_rs555$) plotted as a function of the *in situ* chlorophyll-a concentrations with the OC4 algorithm superimposed on the data, for all the data and for each separate year using the NOMAD dataset.

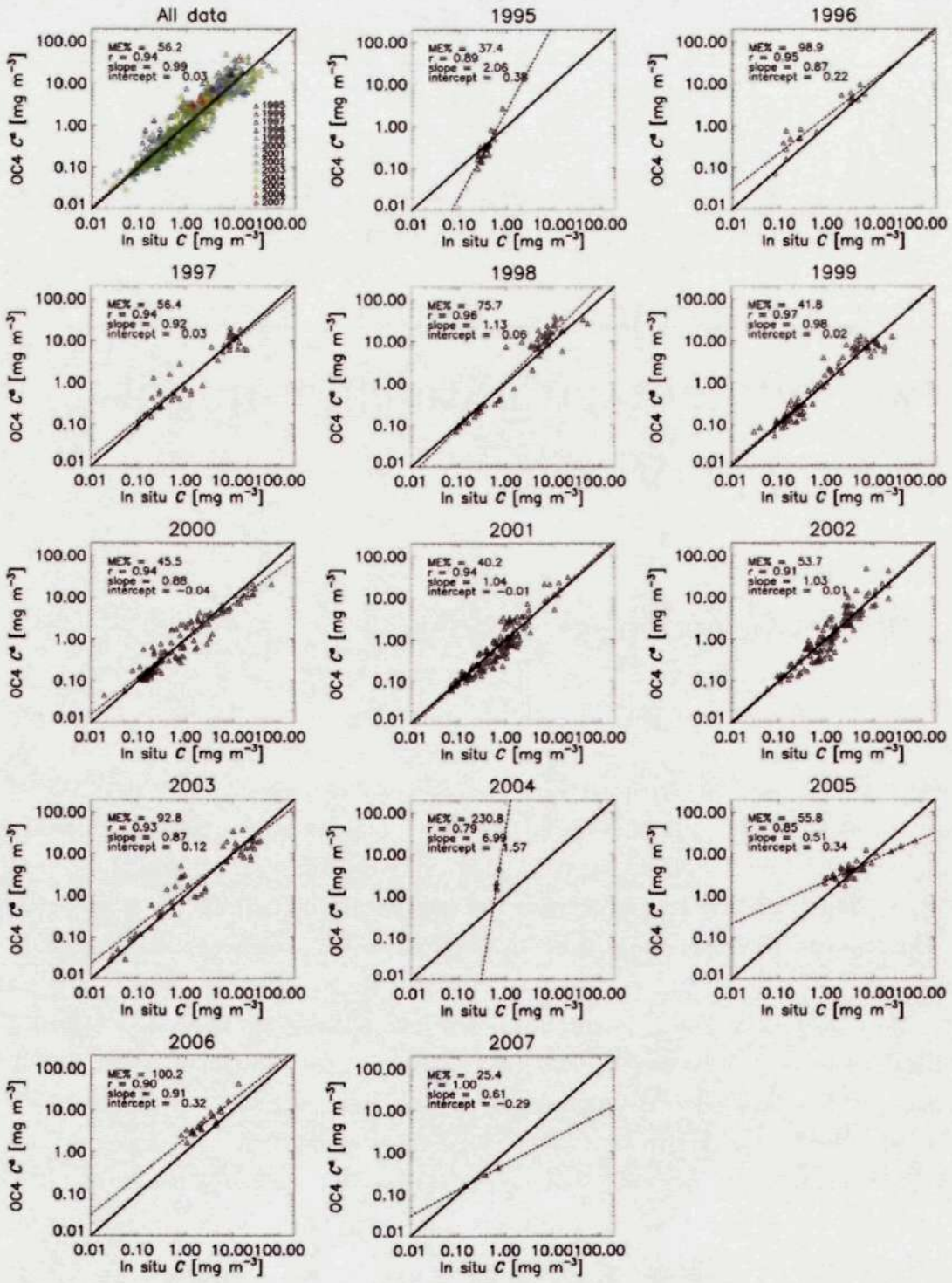

Figure B.2: The OC4 derived chlorophyll-a concentrations plotted against the *in situ* chlorophyll-a concentrations, for all the data and for each separate year using the NOMAD dataset

Appendix C

Comparing output from the three-component model when using two different satellite chlorophyll-a input algorithms

C.1 Introduction

Various algorithms have been proposed to detect the total chlorophyll-a concentration from satellite data. These include global and regional algorithms, and both empirical and semi-analytical approaches. Two common algorithms currently used for global application are the OC4 algorithm (O'Reilly et al., 1998, 2000), currently in operational use by NASA, and the semi-analytical GSM algorithm (Maritorena et al., 2002). Both these algorithms were developed using a large set of biological (chlorophyll-a concentrations) and optical (water-leaving radiance spectra) measurements.

The OC4 algorithm is based on a polynomial relationship between a band ratio (blue to green wavelengths) and the chlorophyll-a concentration, assuming the majority of optically-active components in the surface ocean covary with chlorophyll-a. The GSM algorithm treats chlorophyll-a, CDOM and SPM independently, and these properties are retrieved simultaneously from the radiance spectrum (Maritorena et al., 2002). Both approaches have been found to be good predictors of chlorophyll-a from satellite (Siegel et al., 2005).

However, a comparison of the two global chlorophyll-a climatologies have indicated large qualitative and quantitative differences. Siegel et al. (2005) found that normalised percentage differences exceed 50 % over large areas of the ocean where the OC4 chlorophyll-a values are greater than the GSM values, particularly in poleward regions. Alternatively, in subtropical gyres, the GSM chlorophyll-a retrievals were found to be greater than the OC4 chlorophyll-a retrievals by as much as 50 %.

On average over the global ocean, OC4 chlorophyll-a retrievals are 29 % higher than the GSM algorithm (Behrenfeld, 2010).

In this appendix, the three-component model is applied to input from both the OC4 algorithm and the semi-analytical GSM algorithm. Outputs from the two approaches were compared in order to quantify differences in using the two satellite chlorophyll-a inputs.

C.2 Methodology

To test the algorithms, twelve global, monthly Level 3 mapped SeaWiFS images of OC4 derived chlorophyll-a and $R_{rs}(\lambda)$ in 2003 were used for analysis. To run the GSM model IDL code was utalised (available at http://www.ioccg.org/groups/software.html) with a standard set of parameters optimised for applications to offshore oceanic waters (see Table 2 in Maritorena et al., 2002). The GSM model was run on the $R_{rs}(\lambda)$ data in order to derive chlorophyll-a according to the GSM for the 12 months of 2003. The three-component model was then run on the two separate chlorophyll-a inputs and differences between output were compared.

Hardman-Mountford et al. (2008) developed a classification system by adopting a combination of multivariate statistics and classification techniques and applying them to a time-series of satellite chlorophyll-a data. The classification scheme objectively defined six top-level biomes that each exhibited persistence. These biomes are shown in Figure C.1 (top image). Areas in white represent bathymetry <200 m and latitudes greater than 66.6°. These areas were masked from our classification as to avoid coastal (case 2) and inland waters and avoid areas that are inhibited by high sun zenith angles (Artic and Antarctic circle) in the winter months and so suffer from low sample rate of satellite observations. The Red and Black seas were also masked out of our time-series as they to suffer from non-biological optical complexity.

Oligotrophic and meso-eutrophic waters were partitioned using the Hardman-Mountford et al. (2008) system by separating meso-eutrophic waters according to *very high chlorophyll-a*, *high chlorophyll-a* and *high intermediate chlorophyll-a* and oligotrophic according to *very low chlorophyll-a*, *low chlorophyll-a* and *low intermediate chlorophyll-a* (Figure C.1, bottom image). Eutrophic waters (*very high chlorophyll-a*) were merged with mesotrophic waters as there was only a small amount of *very high chlorophyll-a* waters in Figure C.1 (top image) having removed coastal (case 2) and inland waters. When comparing models, data were partitioning into oligotrophic and meso-eutrophic areas in addition to deriving global monthly statistics (weighting each pixel's value by its area (a function of latitude)).

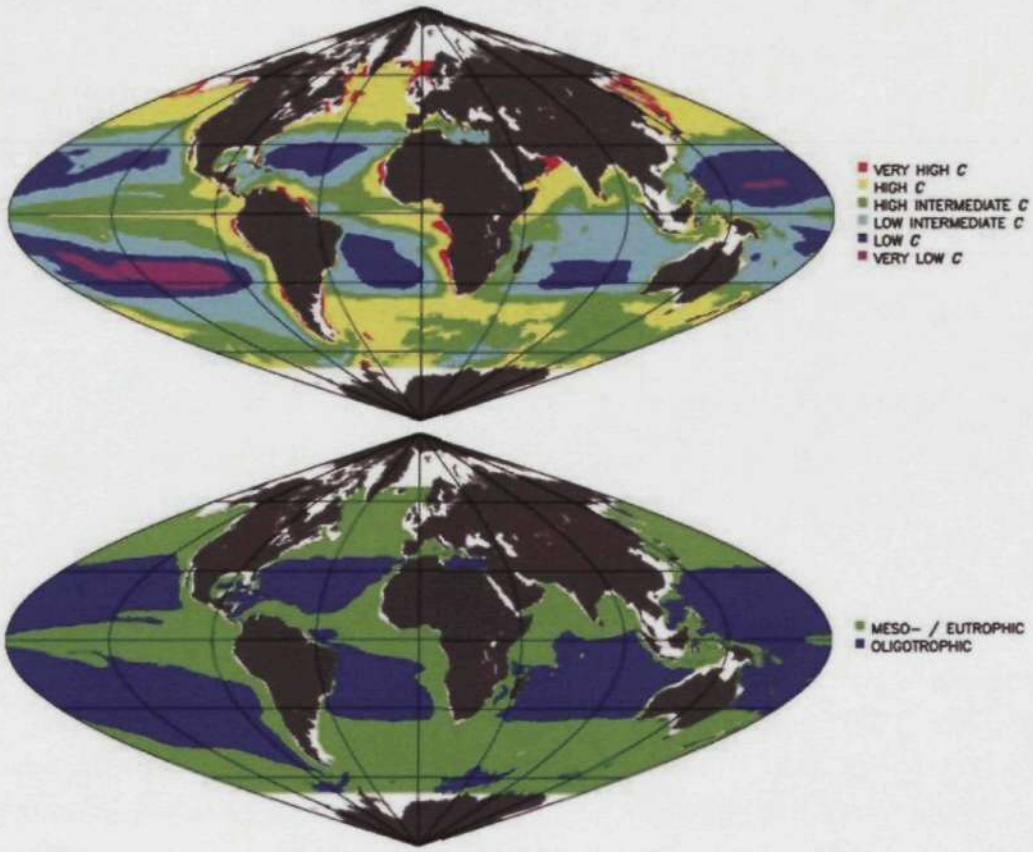

Figure C.1: Classification of oligotrophic and meso-eutrophic provinces used when comparing the GSM and OC4 inputs to the three-component model. Top image shows the classification of Hardman-Mountford et al. (2008), bottom image shows the partition of oceanic waters into oligotrophic and meso-eutrophic areas based on Hardman-Mountford et al. (2008). White areas represent bathymetry <200 m, latitudes greater than 66.6° and coastal and inland waters.

C.3 Results

Figure C.2 shows a comparison between output from the three-component model when using two different satellite chlorophyll-a algorithms for global, oligotrophic and meso-eutrophic areas over the 12 months of 2003. As highlighted by Siegel et al. (2005) and Behrenfeld (2010), the OC4 algorithm estimates higher total chlorophyll-a than the GSM globally. When applying the three-component model to the two inputs, higher micro-, nano- and picoplankton chlorophyll-a were also found when using the OC4 algorithm as input, in comparison with the GSM algorithm. This is less pronounced in the oligotrophic regions than the meso-eutrophic regions and exhibits slight seasonal variability. Note in the oligotrophic regions, from February to May the three-component model with the GSM input estimates higher levels of picoplankton chlorophyll-a when compared with the OC4 input.

On average, over the 12 months of 2003, total chlorophyll-a is 0.047 mg m^{-3}

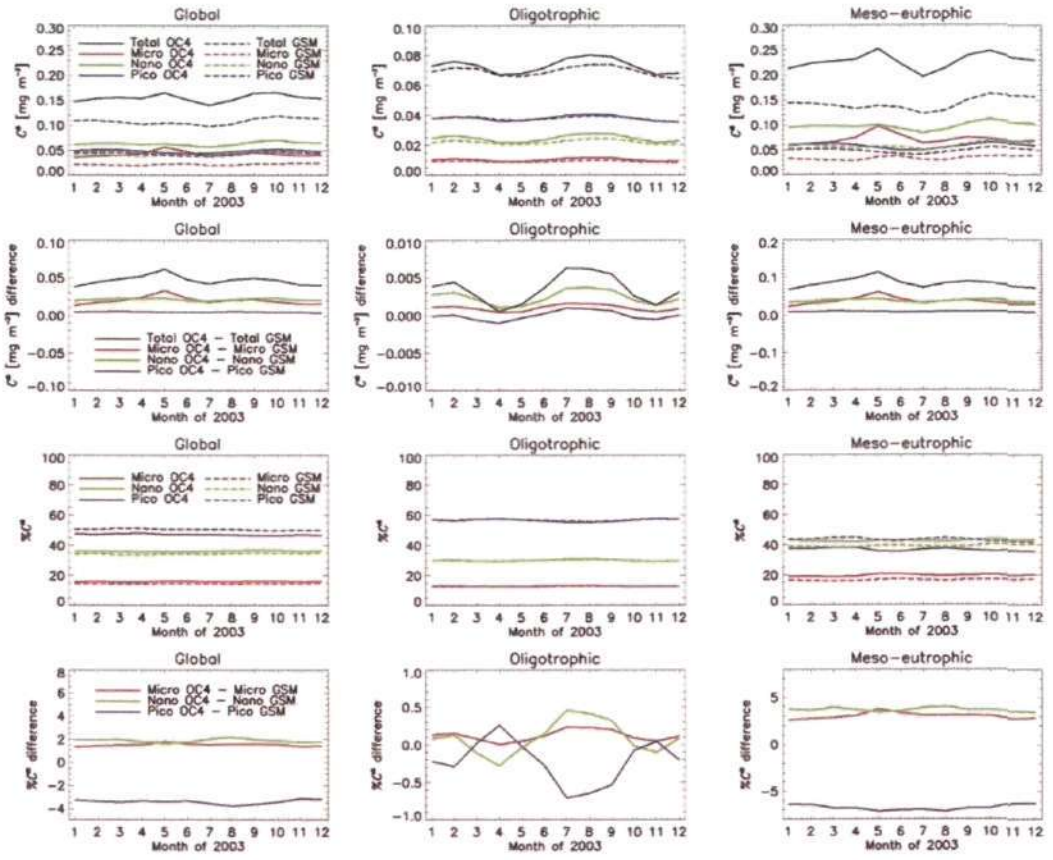

Figure C.2: A comparison between output from the three-component model when using two different satellite chlorophyll-a algorithms for global, oligotrophic and meso-eutrophic areas over the 12 months of 2003. The top row shows the total, pico-, nano- and microplankton chlorophyll-a concentration derived from the two inputs, the second row down show the difference in these concentrations when subtracting the GSM output from the OC4 output, the third row down shows the percentage of the pico-, nano- and microplankton to the total chlorophyll-a concentration derived from the two inputs and the bottom row shows the difference in the percentages when subtracting the GSM output from the OC4 output. The left column represents all case 1 global areas, the middle column the oligotrophic areas and the right column meso-eutrophic areas (see Figure C.2 for classification).

higher when using the OC4 algorithm in comparison with the GSM algorithm. When using both satellite chlorophyll-a models as input to the three-component model, picoplankton chlorophyll-a is 0.005 $\mathrm{mg\,m^{-3}}$ higher, nanoplankton chlorophyll-a is 0.022 $\mathrm{mg\,m^{-3}}$ higher and microplankton 0.020 $\mathrm{mg\,m^{-3}}$ higher when using the OC4 algorithm in comparison with the GSM algorithm.

Regarding the percentages to the total chlorophyll-a of the three size classes, when using the OC4 algorithm as input to the three-component model, higher micro- and nanoplankton percentages are found globally over the 12 months in comparison with applying the three-component model to the GSM algorithm. However, higher percentages of picoplankton are observed globally using the GSM algorithm as input in comparison with the OC4 algorithm. These differences are primarily pronounced

in the meso-eutrophic regions as opposed to the oligotrophic areas which exhibit little difference. Again these differences are seen to vary slightly seasonally. Note in the oligotrophic regions, from May to October, the three-component model with the GSM input estimates higher picoplankton and lower nanoplankton percentages when compared to the OC4 input, contradictory to March and April. Over the 12 months of 2003, on average using the OC4 algorithm as input, picoplankton chlorophyll-a percentage is -3.4 % lower, nanoplankton is 1.9 % higher and microplankton 1.5 % higher when using the OC4 algorithm in comparison with the GSM algorithm.

Table C.1 shows the Pearson correlation coefficients (r) in the seasonal time-series of 2003 from the two different satellite input chlorophyll-a algorithms (Figure C.2). With the exception of microplankton chlorophyll-a in meso-eutrophic and global waters, all r values are greater than 0.83 for micro-, nano- and picoplankton (both C^s and $\%C^s$) and on average all output products have a r value of $\sim$0.87. This implies that conclusions drawn by use of either algorithm as input, regarding phytoplankton seasonal cycles, are generally insensitive to this choice of satellite chlorophyll-a product despite slight seasonal differences noted in Figure C.2.

Table C.1: Pearson correlation coefficients from the comparison between different satellite chlorophyll-a algorithms as input to the three-component model for global, oligotrophic and meso-eutrophic areas over the 12 months of 2003.

Product	Global	Oligotrophic	Meso-eutrophic
Total C^s	0.59	0.97	0.62
Micro C^s_m	0.24	0.96	0.29
Nano C^s_n	0.91	0.98	0.90
Pico C^s_p	0.99	0.95	0.98
Micro $\%C^s$	0.83	0.99	0.88
Nano $\%C^s$	0.89	0.99	0.97
Pico $\%C^s$	0.93	0.99	0.95

Figure C.3 and C.4 show a pixel by pixel comparison between output from the three-component model when using two different satellite chlorophyll-a algorithms for January and July respectively. The results reflect those shown in Figure C.2, particularly large differences in the meso-eutrophic regions in comparison with the oligotrophic areas. However, these figures highlight additional regional variability between output when using the two different algorithms. For instance, microplankton chlorophyll-a is actually lower in mesotrophic areas (e.g. Equatorial Pacific) when using the OC4 algorithm in comparison to the GSM algorithm. In the meso-eutrophic regions shown in Figure C.2 this is masked by the very high microplankton chlorophyll-a values, when using the OC4 algorithm, in the very productive areas (e.g. Benguela upwelling, see Figure C.3 and C.4).

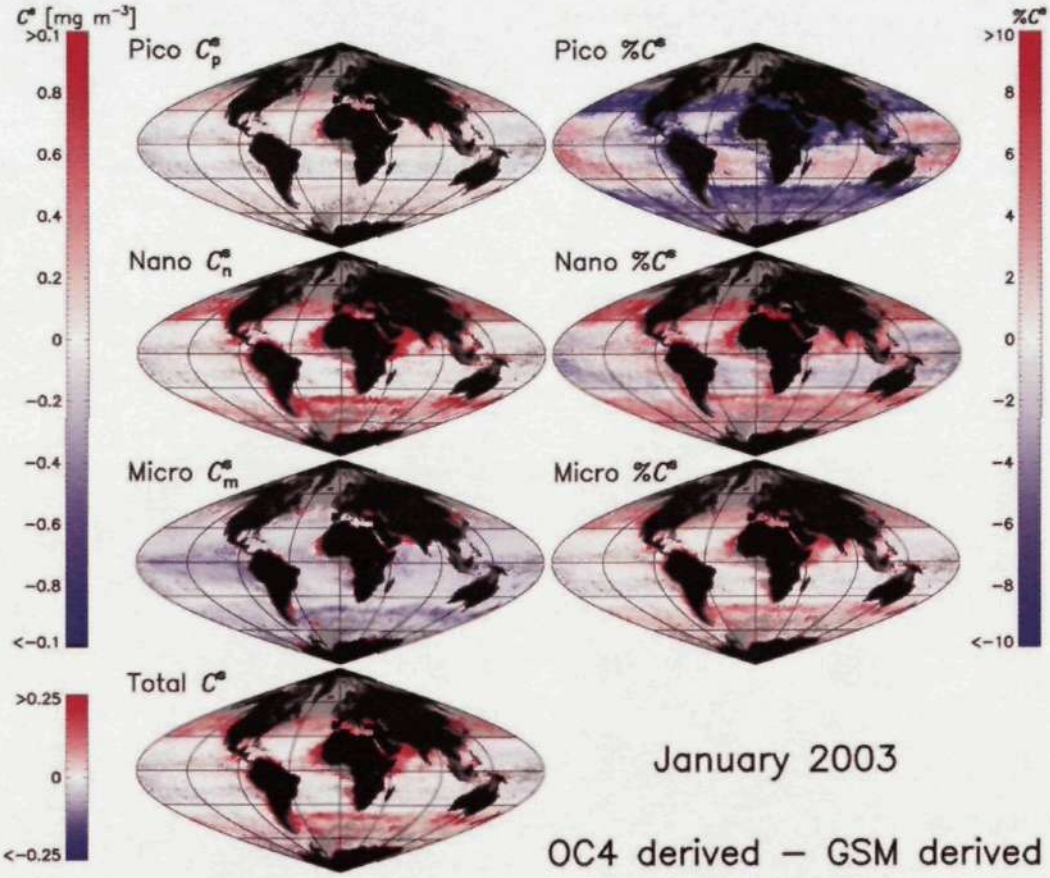

Figure C.3: A comparison between output from the three-component model when using two different satellite chlorophyll-a algorithms for January 2003. Differences were calculated by subtracting results from the three-component model when using the GSM input from the three-component model when using the OC4 input.

C.4 Summary

Over the 12 months of 2003, using the OC4 algorithm as input to the three-component model, microplankton chlorophyll-a is 0.020 mg m^{-3} higher (microplankton percentage 1.5 % higher), nanoplankton chlorophyll-a is 0.022 mg m^{-3} higher (nanoplankton percentage is 1.9 % higher) and picoplankton chlorophyll-a is 0.005 mg m^{-3} higher (picoplankton percentage is -3.4 % lower) globally, in comparison with using the with the GSM algorithm as input to the three-component model. These differences are primarily pronounced in the meso-eutrophic regions as opposed to the oligotrophic areas which exhibit smaller differences. Additional spatial differences were observed depending on seasonal and trophic level. Average r values, when analysing temporal trends over 2003 for all output products, are $\sim$0.87. This implies that conclusions drawn by use of either algorithm as input, regarding phytoplankton seasonal cycles, are generally insensitive to the choice of satellite chlorophyll-a product.

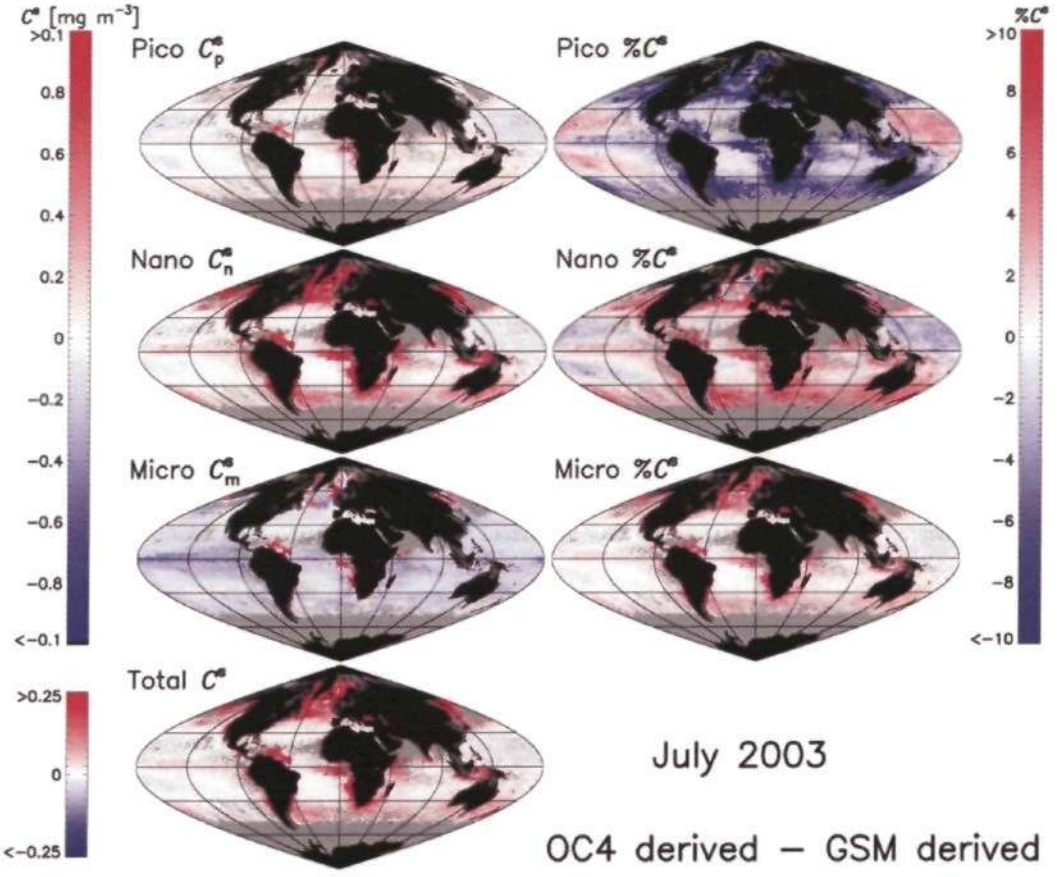

Figure C.4: A comparison between output from the three-component model when using two different satellite chlorophyll-a algorithms for July 2003. Differences were calculated by subtracting results from the three-component model when using the GSM input from the three-component model when using the OC4 input.

Appendix D

Sensitivity analysis of the three-component model for application to satellite chlorophyll-a fields

D.1 Introduction

Satellite ocean colour sensors generally penetrate the first optical depth (or penetration depth) of the water column (Morel et al., 2007c). Therefore, chlorophyll-a retrievals via ocean colour sensors are thought to be representative of the first optical depth. In Chapters 4 and 5, within the first optical depth, the parameters of the three-component model were seen to vary among datasets. When applying the three-component model to satellite chlorophyll-a retrievals it is essential to grasp how sensitive the model is to changes in its parameterisation. In this appendix, a sensitivity analysis is conducted on the three-component model in order to quantify how sensitive the model is to realistic variations in its parameterisation within the first optical depth.

D.2 Methodology

The three-component model is based essentially upon two equations (see Equations 4.4 and 4.6) that are reproduced below for convenience:

$$C_{p,n} = C^m_{p,n}[1 - \exp(-S_{p,n}C)], \tag{D.1}$$

and

$$C_p = C^m_p[1 - \exp(-S_pC)]. \tag{D.2}$$

Having derived the combined nano-picoplankton chlorophyll-a concentration ($C_{p,n}$) and the picoplankton chlorophyll-a concentration (C_p), the nano- and microplankton chlorophyll-a concentrations (C_n and C_m respectively) can be calculated according to Equations 4.5 and 4.7 that are reproduced below for convenience:

$$C_n = C_{p,n} - C_p, \tag{D.3}$$

and

$$C_m = C - C_{p,n}. \tag{D.4}$$

The percentages of each phytoplankton size class to total chlorophyll-a can then be calculated by dividing the size-specific chlorophyll-a concentrations (C_p, C_n, $C_{p,n}$ and C_m, in $\mathrm{mg\,m^{-3}}$) by the total chlorophyll-a concentration (C, in $\mathrm{mg\,m^{-3}}$) and multiplying by 100. Assuming C is known (as derived from satellite), the parameters of the three-component model are C_p^m ($\mathrm{mg\,m^{-3}}$), $C_{p,n}^m$ ($\mathrm{mg\,m^{-3}}$), S_p and $S_{p,n}$. Figure D.1 shows the retrieved model parameters for the AMT and NOMAD pigment datasets (Chapters 4 and 5), in addition to the modelled relationship between optical depth and model parameters using the AMT data (Chapter 4). Model parameters are seen to vary within the first optical depth: C_p^m from 0.09 to 1.15, $C_{p,n}^m$ from 0.77 to 1.11, S_p from 5.15 to 8.29, and $S_{p,n}$ from 0.78 to 1.16, as represented by the measured minimum and maximum lines shown in Figure D.1.

Near the origin where C is extremely low, the derivative of Equations D.1 and D.2 can be expressed according to

$$\left.\frac{dC_{p,n}}{dC}\right|_{C\to 0} = S_{p,n}C_{p,n}^m, \tag{D.5}$$

and

$$\left.\frac{dC_p}{dC}\right|_{C\to 0} = S_pC_p^m, \tag{D.6}$$

respectively. Therefore, when C is extremely low, the fractional contribution of $C_{p,n}$ to C can be expressed by $S_{p,n}C_{p,n}^m$, and the fractional contribution of C_p to C can be expressed by $S_pC_p^m$. Note that according to Equations D.3 and D.4, at extremely low C the fractional contribution of C_m, $F_m = C - S_{p,n}C_{p,n}^m$ and C_n, $F_n = S_{p,n}C_{p,n}^m - S_pC_p^m$.

Figure D.2 shows the products of $S_{p,n}C_{p,n}^m$ and $S_pC_p^m$, for the retrieved model parameters from the AMT and NOMAD pigment datasets, in addition to the modelled relationship between optical depth and model parameters using the AMT data. Using the model parameters for the different datasets, within the first optical depth, the product $S_{p,n}C_{p,n}^m$ is shown to range from 0.86 to 0.93 and $S_pC_p^m$ from to 0.67 to 0.81, as represented by the measured minimum and maximum lines (Figure D.2).

Two sensitivity procedures were set up to test the model. Test 1 was designed to test the sensitivity of the model based on measured parameter variations within

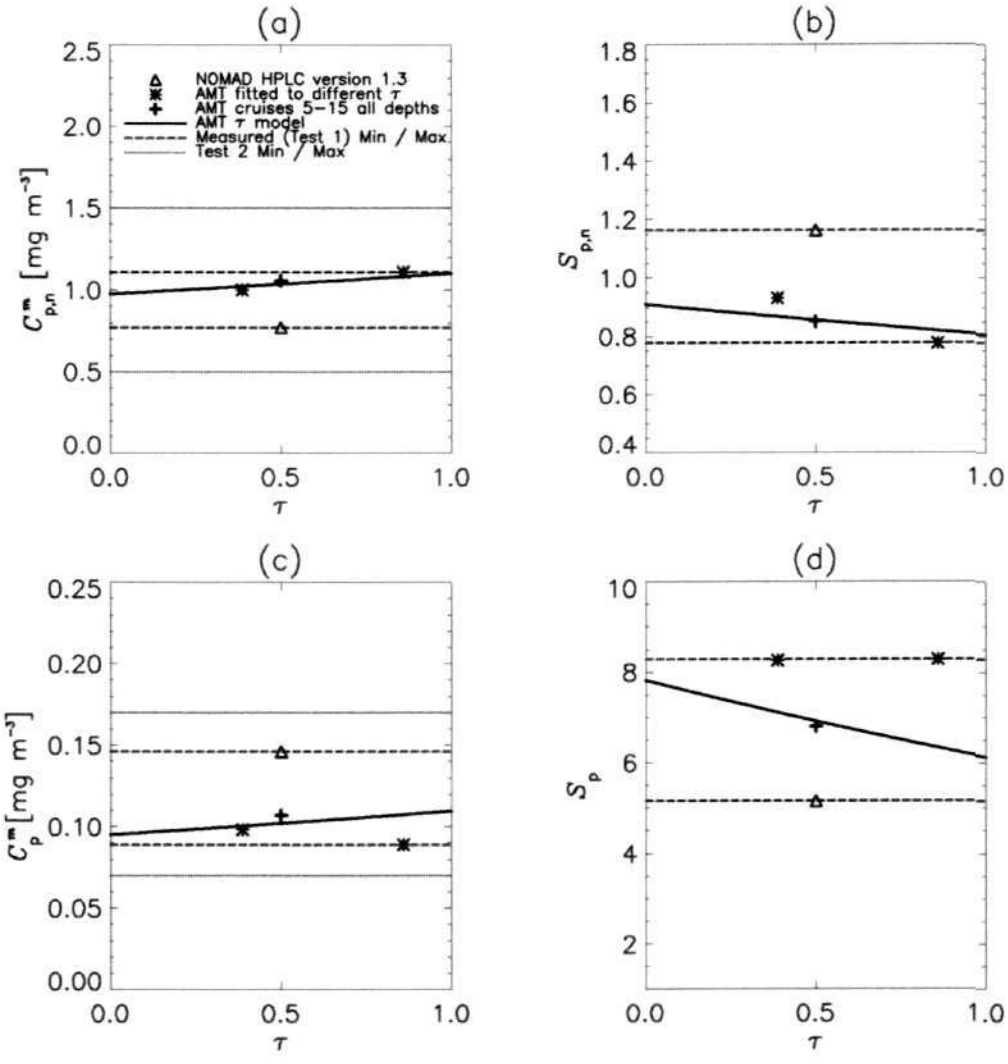

Figure D.1: Variations in the three-component model parameters in Chapters 4 and 5 with optical depth (τ). Note that the parameters derived from NOMAD and AMT cruises 5-15 are plotted at 0.5 τ. AMT τ model refers to the optical depth-dependent function described in Chapter 4.

the first optical depth, and test 2 was designed to test the sensitivity of the model beyond the measured parameter variations. Maximum and minimum values for C_p^m and $C_{p,n}^m$ were assigned for each test (Table D.1). In the first test (test 1), maximum and minimum values of C_p^m and $C_{p,n}^m$ were varied between measured values (see Figure D.1 and Table D.1). In the second test (test 2), the maximum and minimum values were varied beyond realistic parameter variations (see Figure D.1 and Table D.1).

The parameters S_p and $S_{p,n}$ were calculated based on a maximum and minimum relationships between $S_{p,n}C_{p,n}^m$ and $S_pC_p^m$. For test 1, maximum and minimum values of $S_{p,n}C_{p,n}^m$ and $S_pC_p^m$ were varied to realistic maximum and minimum values shown in Figure D.2 (see Table D.1), based on derived parameters. For test 2, the maximum and minimum values of $S_{p,n}C_{p,n}^m$ and $S_pC_p^m$ were varied beyond realistic values (0.1

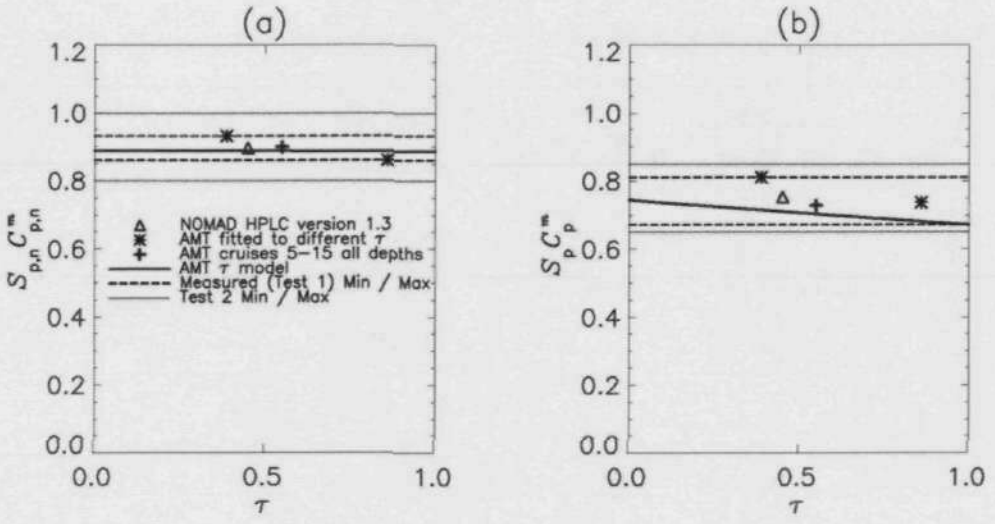

Figure D.2: Variations in (a) $S_{p,n}C^m_{p,n}$ and (b) $S_pC^m_p$ derived from the three-component model parameters in Chapters 4 and 5 with optical depth (τ). Note that the parameters derived from NOMAD and AMT cruises 5-15 are plotted at 0.45 τ and 0.55 τ respectively. AMT τ model refers to the optical depth-dependent function described in Chapter 4.

around the mean measured value of $S_{p,n}C^m_{p,n}$ and $S_pC^m_p$) shown in Figure D.2 (see Table D.1).

The model was run on 21 iterations between the minimum and maximum values of C^m_p and $C^m_{p,n}$ (Table D.1), and for each of these iterations, the parameters of S_p and $S_{p,n}$ were calculated and varied a further 21 iterations between the minimum and maximum values of $S_pC^m_p$ and $S_{p,n}C^m_{p,n}$ (Table D.1). This resulted in 441 iterations for a range of chlorophyll-a concentrations from 0.01-100 mg m^{-3}. For nanoplankton, the population is calculated according to a combination of both Equations D.1 and D.2, and hence requires all four parameters for each iteration. Therefore, for nanoplankton, the four parameters of the three-component model need to be run in every possible permutation. Therefore, each C_p run needs to be subtracted from each $C_{p,n}$ run to derive C_n. This resulted in 194,481 (441 $\times$ 441) runs for nanoplankton in comparison with 441 for the other size classes, for both test 1 and 2.

D.3 Results

The results from the sensitivity analysis are shown in Figure D.3 (a-h) with dark grey shading representing results from test 1 and light grey from test 2. Figure D.3 (i) and (j) show the percentage difference and chlorophyll-a difference from test 1 (realistic test) for the three size classes across a continuum of chlorophyll-a values (note these have been divided by two to show the + or - value around the mean). The nanoplankton are the most sensitive of the three size classes, for both the percentage and absolute chlorophyll-a concentrations (Figure D.3 (i) and (j)). This was

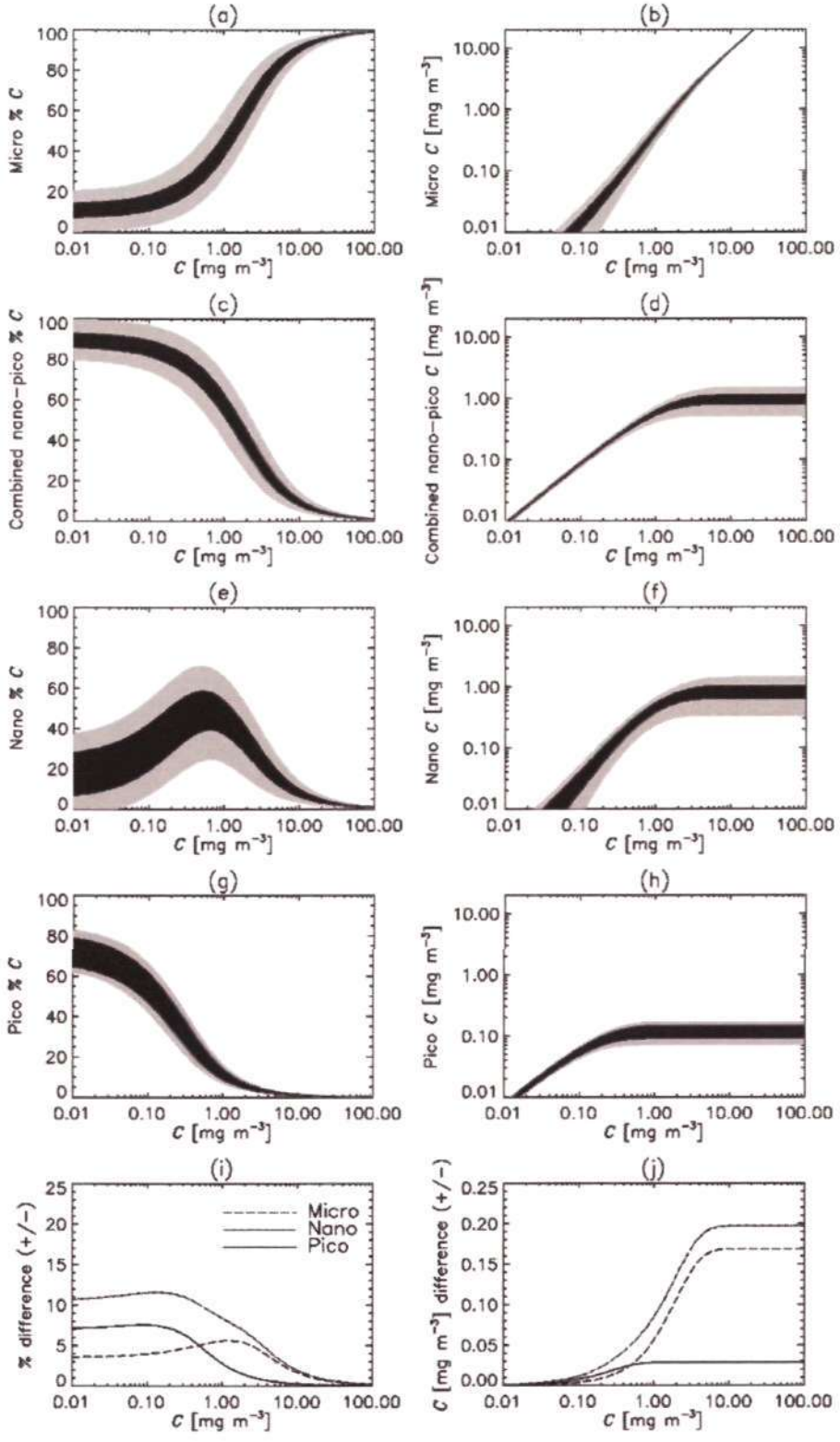

Figure D.3: Results from the sensitivity analysis. Dark grey shading represents results from test 1 and light grey from test 2 in (a) through to (k), and (i) and (j) show the percentage difference and chlorophyll-a difference from test 1 (realistic test) for the three size classes across a continuum of chlorophyll-a values.

Table D.1: Minimum and maximum parameter values for $C^m_{p,n}$ and C^m_p, in addition to minimum and maximum relationships between $S_{p,n}$ and $C^m_{p,n}$, and S_p and C^m_p, used in the sensitivity analysis for test 1 and 2.

Test	Parameter	Minimum	Maximum
1	$C^m_{p,n}$	0.711	1.108
1	C^m_p	0.089	0.146
2	$C^m_{p,n}$	0.500	1.500
2	C^m_p	0.070	0.170
1	$S_{p,n}C^m_{p,n}$	0.861	0.932
1	$S_pC^m_p$	0.671	0.811
2	$S_{p,n}C^m_{p,n}$	0.800	1.000
2	$S_pC^m_p$	0.650	0.850

expected considering that four parameters are required for nanoplankton, whereas only two are needed for the other size classes. Pico- and nanoplankton percentage differences are higher at low chlorophyll-a (<0.7 mg m−3) and microplankton percentage differences are highest between 0.7 to 3.0 mg m^{-3}. The absolute chlorophyll-a differences increase for all size classes up to a given point where they appear to saturate (i.e. at ∼1.0 mg m^{-3} for picoplankton and ∼9.0 mg m^{-3} for nano- and microplankton).

The percentage difference and chlorophyll-a difference from test 1, shown in Figure D.3 (i) and (j), were plotted on the entire mission SeaWiFS chlorophyll-a composite using a look-up table approach (Figure D.4). On average, over the global ocean (weighting each pixel's value by its area), microplankton percentage difference (+ or -) was found to be 4.3 %, nanoplankton 10.9 % and picoplankton 6.6 %. The corresponding chlorophyll-a differences from the three size classes were 0.016 mg m^{-3} for microplankton, 0.029 mg m^{-3} for nanoplankton and 0.013 mg m^{-3} for picoplankton.

D.4 Summary

The results from the sensitivity analysis indicate that nanoplankton are the most sensitive to variations in model parameters. Percentage differences from test 1 (see Figures D.3 and D.4) indicate pico- and nanoplankton are most sensitive in oligotrophic and mesotrophic areas. Absolute chlorophyll-a differences for the three size classes increase with chlorophyll-a up to a saturation point. On average, over the global ocean, microplankton percentage difference (+ or -) was found to be 4.3 % (0.016 mg m^{-3} absolute chlorophyll-a), nanoplankton 10.9 % (0.029 mg m^{-3} absolute

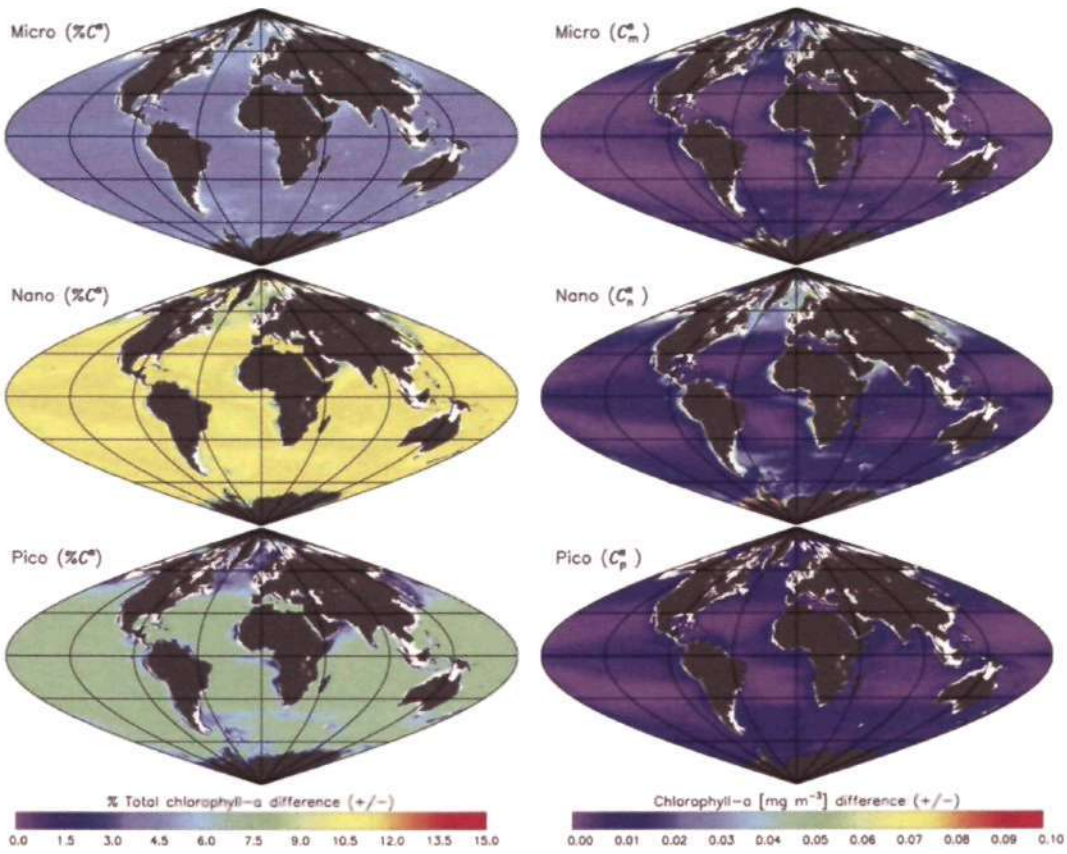

Figure D.4: Results from the sensitivity analysis applied to the entire mission SeaWiFS chlorophyll-a composite.

chlorophyll-a) and picoplankton 6.6 % (0.013 mg m^{-3} absolute chlorophyll-a).

Appendix E

Sensitivity analysis to test the correlation between MEI and phytoplankton size class percentage chlorophyll-a anomaly in the equatorial region of the Pacific and Indian Oceans

E.1 Introduction

In Chapter 6, a very strong correlation was shown between phytoplankton size class % chlorophyll-a anomaly (negative for micro- and nanoplankton, positive for picoplankton) and the MEI, in the equatorial region of the Pacific and Indian Oceans. Using the sensitivity procedure developed in Appendix E, this Appendix tests this correlation by varying the parameters of the three-component model and running a model ensemble.

E.2 Methodology

For the test case scenario, 120 monthly, Level 3 mapped, chlorophyll-a SeaWiFS images were used for analysis, encompassing the time period from October 1997 to September 2007. Each image was rescaled to $1/3°$ by $1/3°$ resolution. Then using the mask developed in Chapter 6 (Figure 6.13 b), the allocated regions of the equatorial Pacific and Indian Oceans were pooled and then averaged for each month (weighting each pixel's value by its area). Figure E.1 shows the mean monthly chlorophyll-a values for the area of interest (Figure 6.13 b, red pixels) that were used to test the correlation between MEI and phytoplankton size class % chlorophyll-a anomaly.

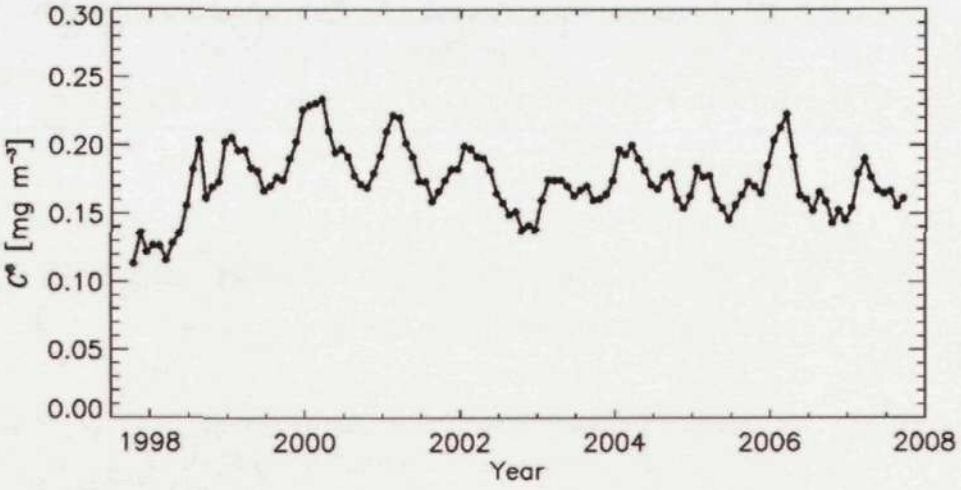

Figure E.1: The mean chlorophyll-a concentrations (C) in the equatorial region of the Pacific and Indian Oceans used to test the correlation between size class % chlorophyll-a anomaly and MEI.

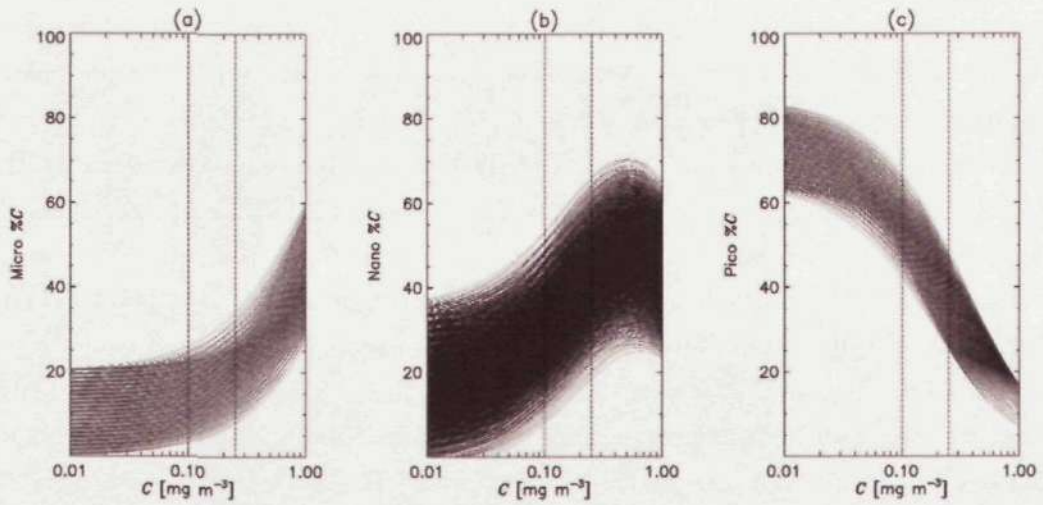

Figure E.2: Three-component model runs for the sensitivity analysis (test 2 Appendix D) for (a) microplankton, (b) nanoplankton and (c) picoplankton. For nanoplankton only the 80th of every 80 model runs are plotted, and for pico- and microplankton only the 2nd of every 2 model runs are plotted. The area between the vertical dotted lines indicate the region between the minimum and maximum chlorophyll-a values from the 10-year chlorophyll-a means show in Figure E.1.

Designed to test the sensitivity of the model beyond the measured parameter variations shown in Chapters 4 and 5, test 2 was adopted from Appendix D and used to test the correlation between MEI and phytoplankton size class % chlorophyll-a anomaly. The ensemble of model runs used for the sensitivity test are shown in Figure E.2. The model was applied to each monthly mean chlorophyll-a value over the 10-year period. Then for each model run, the anomaly was calculated by first calculating a seasonal climatology over the 10-year period, then subtracting

the corresponding monthly climatology from the same month in the time series (as conducted in Chapter 6). Each anomaly from each model run was then correlated with MEI. Overall, 441 model runs were conducted for pico- and microplankton and 194,481 for nanoplankton, and hence a total of 195,363 correlation coefficients.

E.3 Results

The results from the sensitivity analysis are shown in Figure E.3 for (a) microplankton, (b) nanoplankton and (c) picoplankton. Over the 10-year period, all microplankton anomalies (441 model runs) were significantly negatively correlated with MEI ($r < -0.85, p < 0.0001$) and all picoplankton anomalies (441 model runs) were significantly positively correlated with MEI ($r > 0.85, p < 0.0001$). Furthermore, all nanoplankton anomalies (194,481 model runs) were significantly negatively correlated with MEI ($r < -0.68, p < 0.0001$). Results from this sensitivity analysis clearly emphasis a very strong correlation between phytoplankton size class and MEI in the equatorial region of the Pacific and Indian Oceans, even when varying the parameters of the three-component model beyond the measured parameter variations shown in Chapters 4 and 5.

Whereas the results from this sensitivity test clearly support evidence of the strong correlation between phytoplankton size class and MEI in the equatorial region of the Pacific and Indian Oceans, the sensitivity test is not concrete. The use of monthly SeaWiFS chlorophyll-a composites to derive monthly phytoplankton size class products has been shown to be valid in Appendix A. However, ideally (as conducted in Chapter 6), the three-component model should be run on daily images, then produce monthly composites, climatologies and anomaly composites, before averaging over all the pixels of the region then regressing with MEI. As opposed to applying the model to each monthly mean chlorophyll-a value of the region, as conducted in this test. Particularly considering the model is non-linear. Figure E.4 shows the differences between these two approaches when running the three-component model on a single set of parameters (parameters values set from Table 4.1, method 1 refers to anomalies as calculated in Chapter 6, and method 2 refers to anomalies as calculated in the sensitivity test). Discrepancies are noticed between the two approaches. For instance, at the beginning of 1998 the method used in this sensitivity analysis (method 2, Figure E.4) predicts higher picoplankton anomalies and lower nano- and microplankton anomalies when compared with the anomalies calculated in Chapter 6 (method 1, Figure E.4). However, all anomalies are well correlated ($r > 0.87$) clearly supporting the basis for the sensitivity test and its results.

Whereas it would seem more sensible to run the sensitivity test as in method 1, on daily images between 1997-2007 ($\sim$ 3633 images), to then develop monthly

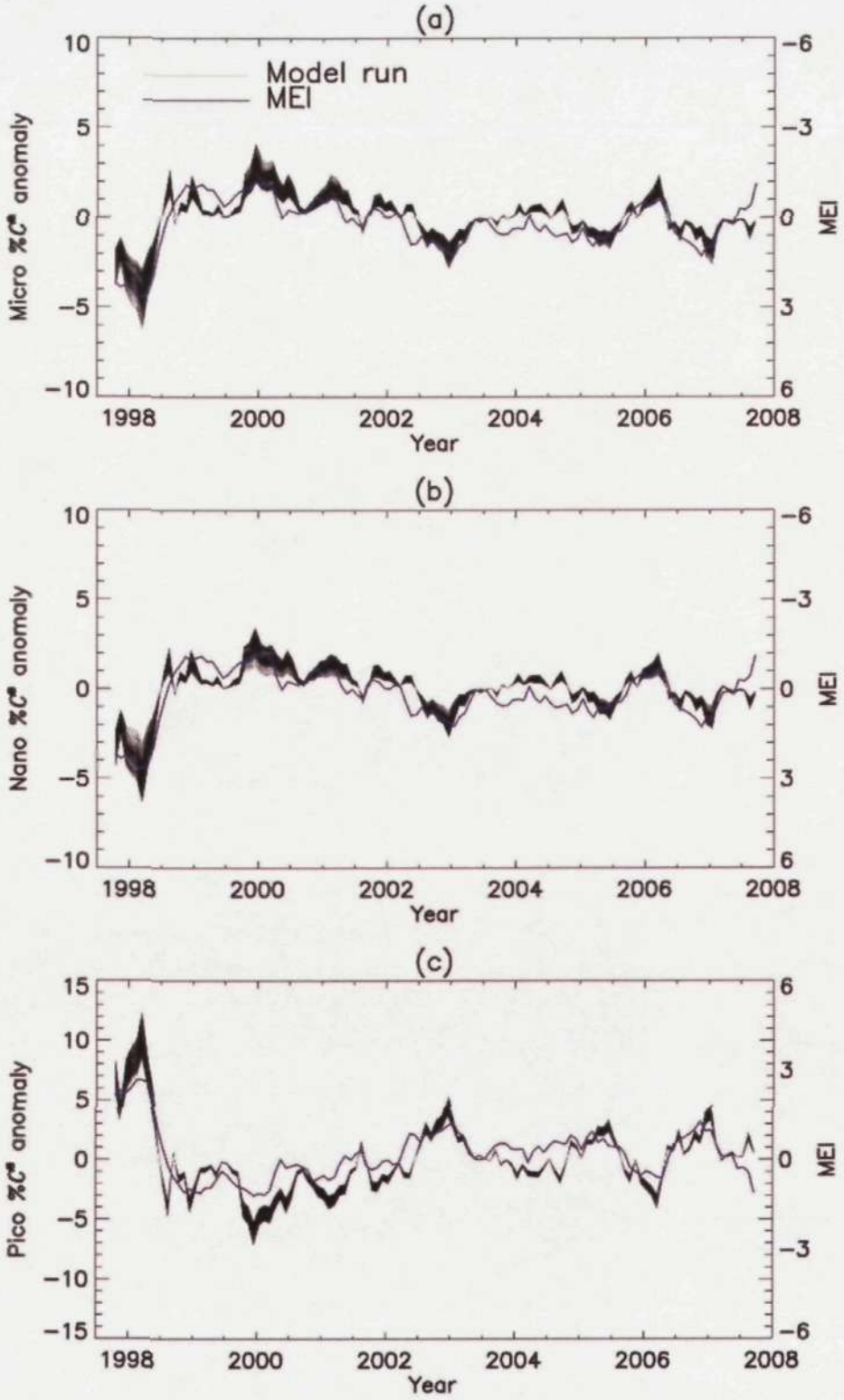

Figure E.3: Three-component model runs for the sensitivity analysis to test the correlation between MEI and phytoplankton size class % chlorophyll-a anomaly in the Equatorial region of the Pacific and Indian Oceans; (a) microplankton, (b) nanoplankton and (c) picoplankton.

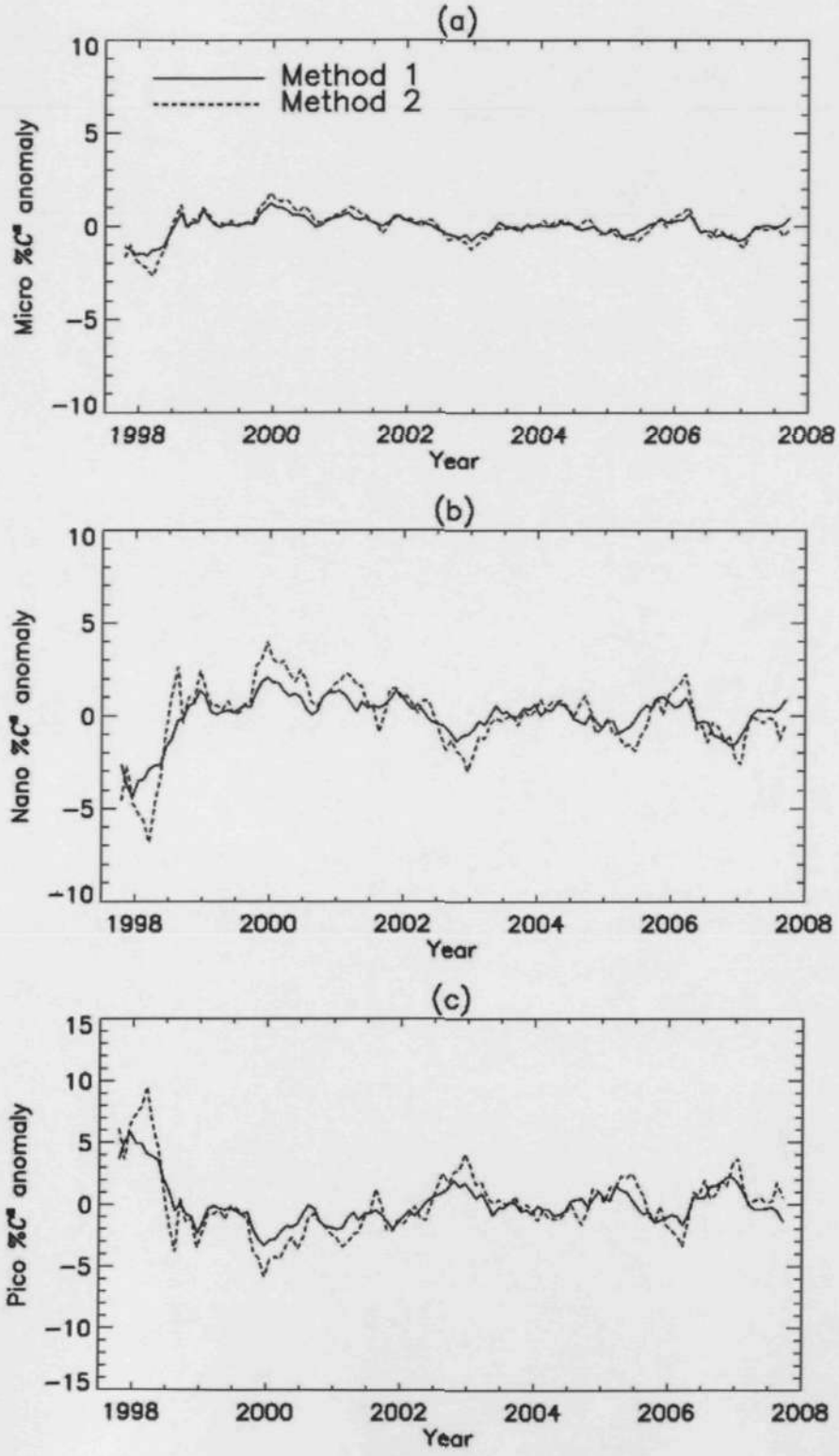

Figure E.4: Comparison between the anomalies of the three size class calculated in Chapters 6 (Method 1), and the anomalies of the three size class calculated according to the sensitivity test (Method 2), for the same set of three-component model parameters. Note the inverse Y-axis for picopkankton in (c).

composites (120 images), then climatologies (12 images) and anomalies (120 images), before averaging each anomaly in the equatorial Pacific and Indian Oceans (pixel by pixel) and then regressing with MEI, at 195,363 ensemble runs the computation time and power would be far greater than possible with a conventional desktop computer. Furthermore, the correlations between MEI and PSC from the two tests shown in Figure E.4 are -0.89, -0.89 and 0.90 for micro-, nano- and picoplankton, for method 1, and -0.85, -0.85 and 0.85 for micro-, nano- and picoplankton for method 2. The methodology for the sensitivity test (method 2) displays lower correlation coefficients than method 1. Therefore, it may be expected that the correlations between the ensemble runs and MEI would improve if the sensitivity test was run using method 1.

E.4 Summary

The results from the sensitivity analysis indicate that, even when varying the parameters of the three-component model beyond the measured parameter variations shown in Chapters 4 and 5, the very strong correlation between phytoplankton size class % chlorophyll-a anomaly (inverse for micro- and nanoplankton, positive for picoplankton) and the MEI in the equatorial region of the Pacific and Indian Oceans (Chapter 6), was still maintained, regardless of parameter variations.

Reference List

Ackleson, S G., Balch, W. M., Holligan, P M , 1994 Response of water-leaving radiance to particulate calcite and chlorophyll-a concentrations: A model for Gulf of Maine coccolithophore blooms Journal of Geophysical Research 99 (C4), 7483–7499

Agrawal, Y. C , Pottsmith, H. C , 2000. Instruments for particle size and settling velocity observations in sediment transport. Marine Geology 168, 89–114.

Aiken, J , Bale, A , 2000 An introduction to the Atlantic Meridional Transect (AMT) programme *Progress in Oceanography* 45, 251–256

Aiken, J , Fishwick, J. R , Lavender, S , Barlow, R., Moore, G. F., Sessions, H., Bernard, S , Ras, J , Hardman-Mountford, N J , 2007 Validation of MERIS reflectance and chlorophyll during the BENCAL cruise October 2002 preliminary validation of new demonstration products for phytoplankton functional types and photosynthetic parameters. International Journal of Remote Sensing 28 (3-4), 497–516.

Aiken, J., Fishwick, J R , Pemberton, K., 2004 The annual cycle of phytoplankton photosynthetic quantum efficiency, pigment composition and optical properties in the western English Channel Journal of the Marine Biological Association of the UK 84, 301–313

Aiken, J , Hardman-Mountford, N. J , Barlow, R , Fishwick, J. R , Hirata, T , Smyth, T. J , 2008 Functional links between bioenergetics and bio-optical traits of phytoplankton taxonomic groups an overarching hypothesis with applications for ocean colour remote sensing Journal of Plankton Research 30 (2), 165–181

Aiken, J., Pradhan, Y., Barlow, R , Lavender, S , Poulton, A., Holligan, P , Hardman-Mountford, N. J , 2009 Phytoplankton pigments and functional types in the Atlantic Ocean a decadal assessment, 1995-2005. AMT Special Issue. Deep-Sea Research II 56, 899–917. doi 10 1016/j dsr2 2008.09.017

Aiken, J , Rees, N , Hooker, S. B , Holligan, P., Bale, A., Robins, D , Moore, G F., Harris, R. P , Pilgrim, D , 2000. The Atlantic Meridional Transect· overview and synthesis of data Progress in Oceanography 45, 257–312

Aksnes, D. L., Egge, J. K., 1991. A theoretical model for nutrient uptake in phytoplankton. Marine Ecological Progress Series 70, 65–72.

Alvain, S., Moulin, C., Dandonneau, Y., Breon, F. M., 2005. Remote sensing of phytoplankton groups in case 1 waters from global SeaWiFS imagery. Deep-Sea Research I 1 (52), 1989–2004.

Alvain, S., Moulin, C., Dandonneau, Y., Loisel, H., 2008. Seasonal distribution and succession of dominant phytoplankton groups in the global ocean: A satellite view. Global Biogeochemical Cycles 22, GB3001, doi:10.1029/2007GB003154.

Alvain, S., Moulin, C., Dandonneau, Y., Loisel, H., Breón, F. M., 2006. A species-dependent bio-optical model of case 1 waters for global ocean color processing. Deep Sea Research I 53, 917–925.

An, S., Ye, Z., Hsieh, W. W., 2006. Changes in the leading ENSO modes associated with the late 1970s climate shift: Role of surface zonal current. Geophysical Research Letters 33, L14609, dio:10.1029/2006Gl026604.

Anderson, T. R., 2005. Plankton functional type modelling: running before we can walk? Journal of Plankton Research 27 (11), 1073–1081.

Anderson, T. R., 2006. Confronting complexity: reply to Le Quéré and Flynn. Journal of Plankton Research 28 (9), 877–878.

Annamalai, H., Xie, S. P., McCreary, J. P., Murtugudde, R., 2005. Impact of Indian Ocean sea surface temperature on developing El Niño. Journal of Climate 18, 302–319.

Antoine, D., Morel, A., Gordon, H. R., Banzon, V. F., Evans, R. H., 2005. Bridging ocean color observations of the 1980s and 2000s in search of long-term trends. Journal of Geophysical Research 110, C06009, doi:10.1029/2004JC002620.

Ashok, K., Guan, Z., Yamagata, T., 2001. Impact of the Indian Ocean dipole on the relationship between the Indian monsoon rainfall and ENSO. Geophysical Research Letters 28 (23), 4499–4502.

Babin, M., Morel, A., Claustre, H., Bricaud, A., Kolber, Z. S., Falkowski, P. G., 1996. Nitrogen- and irradiance- dependant variations of the maximum quantum yield of carbon fixation in eutrophic, mesotrophic and oligotrophic marine systems. Deep-Sea Research I 43, 1241–1272.

Bailey, S. W., Werdell, P., 2006. A multi-sensor approach for the on-orbit validation of ocean color satellite data products. Remote Sensing of Environment 102, 12–13.

Balch, W M., Kilpatrick, K. A , Trees, C C , 1996 The 1991 coccolithophore bloom in the central North Atlantic 1 optical properties and factors affecting thier distribution Limnology and Oceanography 41, 1669–1683

Barber, R T , Chavez, F P , 1983 Biological consequences of El Niño Science 222, 1203–1210

Barlow, R , Aiken, J., Holligan, P , Cummings, D G , Maritorena, S , Hooker, S B , 2002 Phytoplankton pigment and absorption characteristics along meridional transects in the Atlantic Ocean Deep-Sea Research I 47, 637–660

Batten, S D , Clark, R , Flinkman, J , Hays, G C , John, E , John, A W G , Jonas, T , Lindley, J A , Stevens, D P , Walne, A , 2003 CPR sampling. the technical background, materials and methods, consistency and comparability Progress in Oceanography 58 (2-4), 193–215.

Beaufort, L , Couapel, M , Buchet, N , Claustre, H , Goyet, C , 2008 Calcite production by coccolithophores in the south east pacific ocean Biogeosciences 5, 1101–1117, doi 10 5194/bg–5–1101–2008

Beaugrand, G , Brander, K M., Lindley, J. A , Souissi, S , Reid, P C., 2003 Plankton effect on cod recruitment in the North Sea. Nature 426, 661–664

Beaugrand, G , Reid, P C , Ibanez, F , Lindley, J A , Edwards, M , 2002 Reorganization of north atlantic marine copepod biodiversity and climate. Science 296, 1692–1694

Behera, S K , Luo, J J , Masson, S , Rao, S A , Sakuma, H , 2006 A CGCM study on the interaction between IOD and ENSO Journal of Climate 19, 1608–1705

Behrenfeld, M., Boss, E , Siegel, D. A., Shea, D M., 2005. Carbon-based ocean productivity and phytoplankton physiology from space Global Biogeochemical Cycles 19, 1–14.

Behrenfeld, M J , 2010. Abandoning Sverdrup's Critical Depth Hypothesis on phytoplankton blooms. Ecology 91 (4), 977–989

Behrenfeld, M. J , Bale, A. J , Kolber, D D , Aiken, J., Falkowski, P G , 1996 Confirmation of iron limitation of phytoplankton photosynthesis in the equatorial Pacific Ocean Nature 383, 508–511.

Behrenfeld, M J , O'Malley, R T , Siegel, D. A , McClain, C. R., Sarmiento, J. L , Feldman, G C., Milligan, A J , Falkowski, P G , Letelier, R M., Boss, E S., 2006. Climate-driven trends in contemporary ocean productivity. Nature 444, doi 10 1038/nature05317

Behrenfeld, M. J., Randerson, J. T., McClain, C. R., Feldman, G. C., Los, S. O., Tucker, C. J., Falkowski, P. G., Field, C. B., Frouin, R., Esaias, W. E., Kolber, D. D., Pollack, N. H., 2001. Biospheric primary production during an ENSO transition. Science 291(5513), 2594–2597.

Bidigare, R. R., Ondrusek, M. E., Morrow, J. H., Kiefer, D. A., 1990. In vivo absorption properties of algal pigments. Proceedings of SPIE 1302, 290–302.

Blackford, J. C., Allen, J. I., Gilbert, F. J., 2004. Ecosystem dynamics at six contrasting sites: a generic modelling study. Journal of Marine Systems 52 (1-4), 191–215.

Blanchot, J., Andre, J. M., Navarette, C., Neveux, J., Radenac, M. H., 2001. Picophytoplankton in the equatorial Pacific: vertical distributions in the warm pool and in the high nutrient low chlorophyll conditions. Deep-Sea Research I 48 (1), 297–314.

Borgmann, U., 1987. Models of the slope of, and biomass flow up, the biomass size spectrum. Canadian Journal of Fisheries and Aquatic Sciences 44, 136–140.

Bouman, H., Platt, T., Sathyendranath, S., Stuart, V., 2005. Dependence of light-saturated photosynthesis on temperature and community structure. Deep Sea Research I 52, 1284–1299.

Bouman, H. A., Ulloa, O., Scanlan, D. J., Zwirglmaier, K., Li, W. K. W., Platt, T., Stuart, V., Barlow, R., Leth, O., Clementson, L., Lutz, V., Fukasawa, M., Watanabe, S., Sathyendranath, S., 2006. Oceanographic basis of the global surface distribution of *Prochlorococcus* ecotypes. Science 312, 918–921.

Boyce, D. G., Lewis, M. R., Worm, B., 2010. Global phytoplankton decline over the past century. Nature 466, 591–596, doi:10.1038/nature09268.

Boyd, C. M., Johnson, G. W., 1995. Precision of size determination of resistive electronic particle counters. Journal of Plankton Research 17, 41–58.

Boyd, P. W., Newton, P., 1999. Does planktonic community structure determine downward particulate organic carbon flux in different oceanic provinces? Deep Sea Research I 46, 63–91.

Bracher, A., Vountas, M., Dinter, T., Burrows, J. P., Röttgers, R., Peeken, I., 2009. Quantitative observation of cyanobacteria and diatoms from space using PhytoDOAS on SCIAMACHY data. Biogeosciences 6, 751–764.

Brewin, R. J. W., Hardman-Mountford, N. J., Hirata, T., 2010a. Detecting phytoplankton community structure from ocean colour. In: Morales, J., Stuart, V.,

Platt, T., Sathyendranath, S (Eds.), Handbook of Satellite Remote Sensing Image Interpretation: Applications to Marine Living Resources Conservation and Management EU PRESPO and IOCCG, Spain

Brewin, R J W , Lavender, S J., Hardman-Mountford, N. J , 2010b Mapping size-specific phytoplankton primary production on a global scale Journal of Maps, 448–462, doi 10 4113/jom 2010.1122.

Brewin, R. J W , Lavender, S. J., Hardman-Mountford, N J , Hirata, T , 2010c A spectral response approach for detecting dominant phytoplankton size class from satellite remote sensing. Acta Oceanologica Sinica 29 (2), 14–32, doi·10.1007/s13131–010–0018–y

Bricaud, A , Babin, M , Morel, A , Claustre, H , 1995 Variability in the chlorophyll-specific absorption coefficients of natural phytoplankton Analysis and parameterization Journal of Geophysical Research 100, 13,321–13,332

Bricaud, A , Ciotti, A M , Silió-Calzada, A , Gentili, B , 2006. Retrievals of a Size Parameter for Phytoplankton and Light Absorption by Colored Detrital Matter from Ocean Color Measurements Validation and Application to SeaWiFS Images. Ocean Optics XVIII, Montréal, Québec, Oct 9-13, 2006, CD-ROM

Bricaud, A , Claustre, H., Ras, J , Oubelkheir, K , 2004 Natural variability of phytoplanktonic absorption in oceanic waters Influence of the size structure of algal populations Journal of Geophysical Research 109, C11010, doi 10 1029/2004JC002419

Bricaud, A , Mejia, C , Blondeau-Patissier, D , Claustre, H , Crepon, M , Thiria, S , 2007 Retrieval of pigment concentrations and size structure of algal populations from their absorption spectra using multilayered perceptrons. Applied Optics 46 (8), 1251–1260

Bricaud, A., Morel, A , Babin, M , Allali, K , Claustre, H., 1998 Variations of light absorption by suspended particles with the chlorophyll a concentration in oceanic (case 1) waters Analysis and implications for bio-optical models Journal of Geophysical Research 103, 31,033–31,044.

Broad, K , Pfaff, A S. P , Glantz, M H , 2002. Effective and Equitable Dissemination of Seasonal-to-Interannual Climate Forecasts Policy Implications from the Peruvian Fishery during El Niño 1997-98 Climatic Change 54 (4), 415–438, doi 10 1023/A:1016164706290

Brown, C A , Huot, Y , Werdell, P , Gentili, B., Claustre, H., 2008 The origin and global distribution of second order variability in satellite ocean color and its

potential applications to algorithm development. Remote Sensing of Environment 112, 4186 – 4203.

Brown, C. W., Podesta, G. P., 1997. Remote sensing of coccolithophore blooms in the Western South Atlantic Ocean. Remote Sensing Environment 60, 83–91.

Brown, C. W., Yoder, J. A., 1994. Coccolithophorid blooms in the global ocean. Journal of Geophysical Research 99, 7467–7482.

Brown, J., Colling, A., Park, D., Phillips, J., Rothery, D., Wright, J., 1991. Ocean Circulation. The Open University, 1991.

Burkill, P. H., 1987. Analytical flow cytometry and its application to marine microbial ecology. In: Sleigh, M. A. (Ed.), Microbes in the Sea. Ellis Horwood Ltd, Chicester, pp. 139–166.

Caddy, J. F., Fefk, R., Do-Chi, T., 1995. Productivity estimates for the Mediterranean: Evidence of accelerating ecological change. Effects of riverine inputs on coastal ecosystems and fisheries resources. FAO Tech. Rep 249, 1–17. Rome: FAO.

Campbell, L., Nolla, H. A., Vaulot, D., 1994. The importance of *Prochlorococcus* to community structure in the Central North Pacific Ocean. Limnology and Oceanography 39 (4), 954–961.

Canadell, J. G., Le Quere, C., Raupach, M. R., Field, C. B., Buitenhuis, E. T., Ciais, P., Conway, T. J., Gillett, N. P., Houghton, R. A., Marland, G., 2007. Contributions to accelerating atmospheric CO_2 growth from economic activity, carbon intensity, and efficiency of natural sinks. Proceedings of the National Academy of Sciences of the United States of America 104 (47), 18866–18870.

Cermeno, P., Estevez-Blanco, P., Maranon, E., 2005. Maximum photosynthetic efficiency of size-fractionated phytoplankton assessed by C-14 uptake and fast repetition rate fluorometry. Limnology and Oceanography 50 (5), 1438–1446.

Charlson, R. J., Lovelock, J. E., Andreae, M. O., Warren, S. G., 1987. Oceanic phytoplankton, atmospheric sulphur, cloud albedo and climate. Nature 326, 655–661.

Chavez, F. P., Buck, K. R., Bidigare, R. R., Karl, D. M., Hebel, D. V., Latasa, M., Campbell, L., Newton, J., 1995. On the chlorophyll-a retention properties of glass-fiber GF/F filters. Limnology and Oceanography 40, 428–433.

Chavez, F. P., Strutton, P. G., Friederich, G. E., Feely, R. A., Feldman, G. C., Foley, D. G., McPhaden, M. J., 1999. Biological and chemical response of the equatorial Pacific Ocean to the 1997-98 El Niño. Science 286, 2126 – 2131.

Chazottes, A , Bricaud, A., Crepon, M , Thiria, S., 2006. Statistical analysis of a database of absorption spectra of phytoplankton and pigment concentrations using self-organizing maps. Applied Optics 45 (31), 8102–8115

Chazottes, A , Crepon, M , Bricaud, A , Ras, J., Thiria, S , 2007. Statistical analysis of absorption spectra of phytoplankton and of pigment concentrations observed during three POMME cruises using a neural network clustering method. Applied Optics 46 (18), 3790–3799.

Chisholm, S W , 1992. Phytoplankton Size In Falkowski, P. G , Woodhead, A D (Eds), Primary Productivity and Biogeochemical Cycles in the Sea Springer, New York, pp 213–237.

Chisholm, S. W., Armbrust, E V , Olson, R J , 1986 The individual cell in phytoplankton ecology· cell cycles and applications of flow cytometry In Platt, T , Li, W K W (Eds), Photosynthetic Picoplankton Vol 214 Can Bull Fish Aqua Sci, pp 343–369

Chisholm, S W , Olson, R J , Zettler, E R , Waterbury, J , Goericke, R , Welschmeyer, N , 1988 A novel free-living prochlorophyte occurs at high cell concentrations in the oceanic euphotic zone Nature 334, 340–343.

Ciotti, A. M , Bricaud, A , 2006 Retrievals of a size parameter for phytoplankton and spectral light absorption by coloured detrital matter from water-leaving radiances at SeaWiFS channels in a continental shelf off Brazil. Limnology and Oceanography: Methods 4, 237–253

Ciotti, A M., Lewis, M. R , Cullen, J. J , 2002. Assessment of the relationships between dominant cell size in natural phytoplankton communities and the spectral shape of the absorption coefficient Limnology and Oceanography 47 (2), 404–417

Clarke, A , Leakey, R J G., 1996 The seasonal cycle of phytoplankton, macronutrients, and the microbial community in a nearshore Antarctic marine ecosystem Limnology and Oceanography 41, 1281–1294

Claustre, H., 1994 The trophic status of various oceanic provinces as revealed by phytoplankton pigment signitures Limnology and Oceanography 39 (5), 1206–1210

Claustre, H., Babin, M , Merien, D , Ras, J., Prieur, L , Dallot, S , Prasil, O , Dousova, H., 2005 Towards a taxon-specific parameterization of bio-optical models of primary production: A case study in the North Atlantic Journal of Geophysical Research 110, C07S12, doi:10 1029/2004JC002634

Claustre, H., Hooker, S. B., Van Heukelemc, L., Berthon, J.-F., Barlow, R., Ras, J., Sessions, H., Targad, C., Thomas, C. S., Van der Linde, D., Martya, J.-C., 2004. An intercomparison of HPLC phytoplankton pigment methods using in situ samples: application to remote sensing and database activities. Marine Chemistry 85, 41–61.

Claustre, H., Marty, J. C., 1995. Specific phytoplankton biomasses and their relation to primary production in the tropical North Atlantic. Deep Sea Research I 42 (8), 1476–1793.

Claustre, H., Morel, A., Babin, M., Cailliau, C., Marie, D., Marty, J. C., Tailliez, D., Vaulot, D., 1999. Variability in particle attenuation and chlorophyll fluorescence in the tropical Pacific: Scales, patterns, and biogeochemical implications. Journal of Geophysical Research 104 (C2), 3401–3422.

Cleveland, J. S., 1995. Regional models for phytoplankton absorption as a function of chlorophyll a concentration. Journal of Geophysical Research 100, 13,333–13,344.

Coale, K. H., Fitzwater, S. E., Gordon, R. M., Johnson, K. S., Barber, R. T., 1996. Control of community growth and export production by upwelled iron in the equatorial Pacific Ocean. Nature 379, 621–624.

Colling, A., 2001. Ocean Circulation, 2nd Edition. The Open University, Butterworth-Heinemann,, Oxford, UK.

Cullen, J. J., 1991. Hypotheses to explain high-nutrient conditions in the open sea. Limnology and Oceanography 36 (8), 1578–1599.

Cullen, J. J., Fennel, K., 2010. Modeling the dynamics of optical properties in the ocean, directly and mechanistically. In: Ocean Optics XX, SPIE proceedings, PDF No. 100928 (CDROM), Anchorage, Alaska, 27th September - 1st October 2010.

Dall'Olmo, G., Westberry, T. K., Behrenfeld, M. J., Boss, E., Slade, W. H., 2009. Significant contribution of large particles to optical backscattering in the open ocean. Biogeosciences 6, 947–967.

Dandonneau, Y., Deschamps, P. Y., Nicolas, J. M., Loisel, H., Blanchot, J., Montel, Y., Thieuleux, F., Becu, G., 2004. Seasonal and interannual variability of ocean color and composition of phytoplankton communities in the North Atlantic, equatorial Pacific and South Pacific. Deep-Sea Research II 51 (1-3), 303–318.

Davey, H. M., Winson, M. K., 2003. Using flow cytometry to quantify microbial heterogeneity. Current Issues in Molecular Biology 5, 9–15.

de Boyer Montégut, C , Madec, G , Fisher, A S , Lazar, A , Iudicone, D , 2004 Mixed layer depth over the global ocean: An examination of profile data and a profile-based climatology Journal of Geophysical Research 109, C12003, doi:10.1029/2004JC002378

DelVecchio, R , Subramaniam, A., 2004 Influence of the amazon river on the surface optical properties of the western tropical North Atlantic Ocean. Journal of Geophysical Research 109, 1–13.

Devred, E , Sathyendranath, S , Platt, T., 2007. Delineation of ecological provinces using ocean colour radiometry Marine Ecological Progress Series 346, 1–13

Devred, E , Sathyendranath, S , Platt, T , 2009 Decadal changes in ecological provinces of the Northwest Atlantic Ocean revealed by satellite observations Geophysical Research Letters 36, L19607, doi:10.1029/2009gl039896

Devred, E., Sathyendranath, S., Stuart, V , Maas, H , Ulloa, O., Platt, T , 2006. A two-component model of phytoplankton absorption in the open ocean Theory and applications Journal of Geophysical Research 111, C03011, doi 10 1029/2005JC002880.

Devred, E., Sathyendranath, S , Stuart, V., Platt, T , In revision A three component classification of phytoplankton absorption spectra Applications to ocean-colour data Remote Sensing of Environment

Diaz, H. F , Markgraf, V., 1992 El Niño: historical and paleoclimatic aspects of the southern oscillation Cambridge Univeristy Press, Cambridge, UK.

Digby, P S B., 1950. The biology of the small planktonic copepods of Plymouth Journal of the Marine Biological Association of the UK 29, 393–438

Doney, S. C , 2006 Plankton in a warmer world. Science 444, 695–696

Doney, S C , Glover, D M , Najjar, R G , 1996 A new coupled, one-dimensional biological–physical model for the upper ocean· applications to the JGOFS Bermuda Atlantic Time-series Study (BATS) site Deep Sea Research II 43, 591–624

Droppo, I. G , 2000. Filtration in Particle Size Analysis In Meyers, R A (Ed.), Encyclopedia of analytical chemistry John Wiley and Sons Ltd, Chichester, pp. 5397–5413.

DuRand, M D., Olson, R J , Chisholm, S W , 2001 Phytoplankton population dynamics at the Bermuda Atlantic Time-series station in the Sargasso Sea Deep Sea Research II 48 (8-9), 1983–2003

Duysens, L N M , 1956 The flattening of the absorption spectrum of suspensions as compared to that of solutions Biochim Biophys Acta 19, 1–12

Dythan, C., 2003. Choosing and Using Statistics: A Biologist's Guide. Second Edition. Blackwell Science Ltd, Oxford, UK.

Edwards, A. M., 2001. Adding detritus to a Nutrient-Phytoplankton-Zooplankton model: A Dynamical-Systems Approach. Journal of Plankton Research 23 (4), 389–413.

Edwards, M., Richardson, A. J., 2004. The impact of climate change on the phenology of the plankton community and trophic mismatch. Nature 430, 881–884.

Eisma, D., Kalf, J., 1996. In situ particle (floc) size measurments with the NIOZ in situ camera system. Journal of Sea Research 36, 49–53.

Eppley, R. W., Sloan, P. R., 1966. Growth rates of marine phytoplankton: Correlation with light absorption by cell chlorophyll-a. Physiologia Plantarum 19, 47–49.

Etcheto, J., Boutin, J., Dandonneau, Y., Bakker, D. C. E., Feely, R. A., Ling, R. D., Nightingale, P. D., Wanninkhof, R., 1999. Air-sea CO_2 flux variability in the equatorial Pacific Ocean near 110°W. Tellus 51B (734-747).

Fairbridge, R. W., 1966. The Encyclopedia of Oceanography. Encyclopedia of Earth Science Series. Van Nostrand Reinhold Company, New York.

Falciatore, A., d'Alcalá, M. R., Croot, P., Bowler, C., 2000. Perception of Environmental Signals by a Marine Diatom. Science 288 (5475), 2363–2366.

Falkowski, P. G., Katz, M. E., Knoll, A. H., Quigg, A., Raven, J. A., Schofield, O., Taylor, F. J. R., 2004. The evolution of modern eukaryotic phytoplankton. Science 305, 354–360.

Falkowski, P. G., Raven, J. A., 1997. Aquatic Photosynthesis. Blackwell Scientific, Oxford.

Feely, R. A., Wanninkhof, R., Takahashi, T., Tans, P., 1999. Influence of El Niño on the Equatorial Pacific contribution to atmospheric CO_2 accounts. Nature 398, 597–601.

Field, C. B., Behrenfeld, M. J., Randerson, J. T., Falkowski, P., 1998. Primary production of the biosphere: integrating terrestrial and oceanic components. Science 281, 237–240.

Finkel, Z. V., 2001. Light absorption and size scaling of light-limited metabolism in marine diatoms. Limnology and Oceanography 38, 679–687.

Fishwick, J R , Aiken, J , Barlow, R , Sessions, H , Bernard, S , Ras, J , 2006 Functional relationships and bio-optical properties derived from phytoplankton pigments, optical and photosynthetic parameters, a case study of the Benguela ecosystem. J. Mar Biol Ass U K 86, 1267–1280

Flynn, K J , 2006 Reply to Horizons Article Plankton functional type modelling running before we can walk Anderson (2005) II. Putting trophic functionality into plankton functional types. Journal of Plankton Research 28 (9), 873–875

Fowler, J , Cohen, L., Jarvis, P , 1998 Practical Statistics for Field Biology 2nd Edition WileyBlackwell

Fuller, N. J , Tarran, G A , Cummings, D. G., Woodward, E M S , Orcutt, K. M , Yallop, M , 2006. Molecular analysis of photosynthetic picoeukaryote community structure along an Arabian Sea transect Limnology and Oceanography 51, 2502–2514.

Garcia-Herrera, R., Diaz, H. F., Garcia, R. R , Prieto, M R , Barriopedro, D., Moyano, R , Hernandez, E , 2008 A chronology of el niño events from primary documentary sources in northern peru. Journal of Climate 21, 1948–1962

Garver, S. A , Siegel, D A , 1997. Inherent optical property inversion of ocean color spectra and its biogeochemical interpretation. 1 time series from the Sargasso Sea Journal of Geophysical Research 102, 18607–18625.

Garver, S A., Siegel, D A , Mitchell, B G , 1994 Variability in near-surface particulate absorption spectra What can a satellite ocean color imager see? Limnology and Oceanography 39, 1349–1367

Geider, R J., Platt, T , Raven, J A , 1986. Size dependence of growth and photosynthesis in diatoms· a synthesis. Marine Ecological Progress Series 30, 93–104

GEO, 2010. Group on Earth Observations Online http //www.earthobservations org/ (10/12/10).

Gibb, S W , Barlow, R , Cummings, D G , Rees, N W , Trees, C C , Holligan, P , Suggett, D , 2000 Surface phytoplankton pigment distributions in the Atlantic Ocean an assessment of basin scale variability between 50N and 50S Progress in Oceanography 45, 339–368

Gibson, P J , Keating, J , Power, C J , 2000. Introductory Remote Sensing Principles and concepts Routledge, London

Gin, K Y H , Lin, X , Zhang, S , 2000 Dynamics and size structure of phytoplankton in the coastal waters of Singapore Journal of Plankton Research 22 (8), 1465–1484

Gist, N., Serret, P., Woodward, E. M. S., Chamberlain, K., Robinson, C., 2009. Seasonal and spatial variability in plankton production and respiration in the Subtropical Gyres of the Atlantic Ocean. Deep Sea Research II 56 (15), 931–940.

GlobColour, 2010. The Globcolour Project. Online: http://www.globcolour.info/ (10/10/10).

Glover, H., Prezelin, B., Campbell, L., Wyman, M., Garside, C., 1988. A nitrate-dependent *Synechococcus* bloom in surface Sargasso Sea water. Nature 331, 161–163.

Goericke, R., Repeta, D. J., 1993. Chlorophylls a and b and divinylchlorophylls a and b in the open subtropical North Atlantic Ocean. Marine Ecological Progress Series 101, 307–313.

Goldman, J. C., 1993. Potential role of large oceanic diatoms in new primary production. Deep Sea Research I 40, 159–168.

Gordon, H. R., 2005. Normalized water-leaving radiance: revisiting the influence of surface roughness. Applied Optics 44 (2), 241–248.

Gordon, H. R., Brown, O. B., Jacobs, M. M., 1975. Computed Relationships Between the Inherent and Apparent Optical Properties of a Flat Homogeneous Ocean. Applied Optics 14 (2), 417–427.

Gordon, H. R., Clark, D. K., Brown, J. W., Brown, O. B., Evans, R. H., Broenkow, W. W., 1983. Phytoplankton pigment concentrations in the Middle Atlantic Blight: Comparison of ship determinations and CZCS estimates. Applied Optics 22, 20–36.

Graham, G. W., Nimmo Smith, W. A. M., 2010. The application of holography to the analysis of size and settling velocity of suspended cohesive sediments. Limnology and Oceanography Methods 8, 1–15.

Gregg, W. W., 2008. Assimilation of SeaWiFS ocean chlorophyll data into a three-dimensional global ocean model. Journal of Marine Systems 69 (3-4), 205–225.

Gregg, W. W., Casey, N. W., 2004. Global and regional evaluation of the SeaWiFS chlorophyll data set. Remote Sensing of Environment 93, 463–479.

Gregg, W. W., Casey, N. W., McClain, C. R., 2005. Recent trends in global ocean chlorophyll. Geophysical Research Letters 32, L03606, doi:10.1029/2004GL021808.

Gregg, W. W., Conkright, M. E., 2002. Decadal changes in global ocean chlorophyll. Geophysical Research Letters 29 (15), 1730.

Gregg, W W , Gmoux, P , Schopf, P S , Casey, N W., 2003 Phytoplankton and iron validation of a global three-dimensional ocean biogeochemical model Deep Sea Research II 50, 3143–3169

Groom, S , Martinez-Vicente, V , Fishwick, J , Tilstone, G , Moore, G , Smyth, T , Harbour, D , 2009 The western english channel observatory: Optical characteristics of station L4 Journal of Marine Systems 77 (3), 278–295

Guidi, L., Stemmann, L , Jackson, G A , Ibanez, F , Claustre, H , Legendre, L , Picheral, M , Gorskya, G , 2009 Effects of phytoplankton community on production, size and export of large aggregates A world-ocean analysis Limnology and Oceanography 54 (6), 1951–1963.

Guptil, S C , 1989 Inclusion of accuracy data in a feature based object-oriented data model In Goodchild, M , Gopal, S (Eds), The Accuracy of Spatial Databases Taylor & Francis, London, pp 91–97

Hansen, B , Bjørnsen, P K , Hansen, P J., 1994. The size ratio between planktonic predators and their prey Limnology and Oceanography 39, 395–403

Hardman-Mountford, N J., Hirata, T , Richardson, K A , Aiken, J , 2008 An objective methodology for the classification of ecological pattern into biomes and provinces for the pelagic ocean Remote Sensing of Environment 112, 3341–3352

Hardy, A C , 1926. The discovery expedition A new method of plankton research. Nature 118, 630–632

Hardy, A C , 1939 Ecological investigations with the continuous plankton recorder object, plan and methods Hull Bulletins of Marine Ecology 1, 1–57.

Harmon, R , Challenor, P., 1997 A Markov chain Monte Carlo method for estimation and assimilation into models *Ecological Modelling* 101 (1), 41–59

Harris, R , 2010 The L4 time-series the first 20 years Journal of Plankton Research 32 (5), 577–583.

Harvey, H W., Cooper, L. H. N., Lebour, M V , Russell, F. S , 1935 Plankton production and its control. Journal of the Marine Biological Association of the UK 20, 407–441

Hays, G C , Warner, A J., John, A. W. G , Harbour, D S , Holligan, P M., 1995. Coccolithophores and the continuous plankton recorder survey Journal of the Marine Biological Association of the UK 75, 503–506

Hemmings, J C P., Barciela, R M., Bell, M J , 2008 Ocean color data assimilation with material conservation for improving model estimates of air-sea CO_2 flux Journal of Marine Research 66 (1), 87–126.

Henson, S. A., Sarmiento, J. L., Dunne, J. P., Bopp, L., Lima, I., Doney, S. C., John, J., Beaulieu, C., 2010. Detection of anthropogenic climate change in satellite records of ocean chlorophyll and productivity. Biogeosciences 7, 621–640.

Heywood, J. L., Zubkov, M. V., Tarran, G. A., Fuchs, B. M., Holligan, P. M., 2006. Prokaryoplankton standing stocks in oligotrophic gyre and equatorial provinces of the Atlantic Ocean: evaluation of inter-annual variability. Deep Sea Research II 50, 1530–1547.

Hirata, T., Aiken, J., Hardman-Mountford, N. J., Smyth, T. J., Barlow, R. G., 2008a. An absorption model to derive phytoplankton size classes from satellite ocean colour. Remote Sensing of Environment 112 (6), 3153–3159.

Hirata, T., Brewin, R. J. W., 2009. Phytoplankton community structure from space. GLOBEC International Newsletter 15 (1), 5–6.

Hirata, T., Hardman-Mountford, N. J., Aiken, J., Fishwick, J., 2009a. Relationship between the distribution function of ocean nadir radiance and inherent optical properties for oceanic waters. Applied Optics 48 (17), 3129–3138.

Hirata, T., Hardman-Mountford, N. J., Aiken, J., Smyth, T., Barlow, R., Martines-Vicente, V., Fishwick, J., Bernard, S., 2008b. Optical approach to derive phytoplankton size classes using ocean color remote sensing. In: Ocean Optics XIX. Castelvecchio Pascoli, Italy, 6-10 Oct. 2008, SPIE proceedings, PDF No. oo080577 (CDROM).

Hirata, T., Hardman-Mountford, N. J., Barlow, R., Lamont, T., Brewin, R. J. W., Smyth, T., Aiken, J., 2009b. An inherent optical property approach to the estimation of size-specific photosynthetic rates in eastern boundary upwelling zones from satellite ocean colour: an initial assessment. Progress in Oceanography 83, 393–397, doi:10.1016/j.pocean.2009.07.019.

Hirata, T., Hardman-Mountford, N. J., Brewin, R. J. W., Aiken, J., Barlow, R., Suzuki, K., Isada, T., Howell, E., Hashioka, T., Noguchi-Aita, M., Yamanaka, Y., 2011. Synoptic relationships between surface chlorophyll-a and diagnostic pigments specific to phytoplankton functional types. Biogeosciences 8, 311–327, doi:10.5194/bg–8–311–2011.

Hirata, T., Højerslev, N., 2008. Relationship between the irradiance reflectance and inherent optical properties of seawater. Journal of Geophysical Research 113, C03030, doi:10.1029/2007JC004325.

Hoepffner, N., Sathyendranath, S., 1991. Effect of pigment composition on absorption properties of phytoplankton. Marine Ecological Progress Series 73 (1), 11–23.

Holligan, P M , Viollier, M , Harbour, D. S , Camus, P , Champagne-Philippe, M , 1983 Satellite and Ship Studies of Coccolithophore Production Along the Continental Shelf Edge Nature 304, 339–342.

Hood, R R., Bates, N. R , Capone, D J , Olson, D B , 2001. Modeling the effect of nitrogen fixation on carbon and nitrogen fluxes at BATS Deep Sea Research II 48 (8-9), 1609–1648

Hood, R R., Laws, E A , Armstrong, R A , Bates, N R , Brown, C W , Carlson, C A., Chai, F., Doney, S. C , Falkowski, P G., Feely, R. A., Friedrichs, M A M , Landry, M R , Moore, J. K., Nelson, D. M , Richardson, T. L , Salihoglu, B., Schartau, M , Toole, D A., Wiggert, J D., 2006. Pelagic functional group modeling: Progress, challenges and prospects Deep-Sea Research Part II 53 (5-7), 459–512

Hooker, S B , Esaias, W E., Feldman, G. C., Gregg, W W , McClain, C. R., 1992. SeaWiFS Technical Report Series: Volume 1. In Hooker, S B , Firestone, E. R (Eds.), An Overview of SeaWiFS and Ocean Color Vol 1 NASA Technical Memorandum, Goddard Space Flight Center, Greenbelt, Maryland 20771, p 24pp

Hooker, S B., McClain, C. R , 2000 The calibration and validation of SeaWiFS data Progress in Oceanography 45 (3-4), 427–465

Hooker, S B , Rees, N. W , Aiken, J , 2000 An objective methodology for identifying oceanic provinces Progress in Oceanography 45, 313–338

Hosie, G W , Fukuchi, M , Kawaguchi, S , 2003 Development of the Southern Ocean Continuous Plankton Recorder Survey. Progress in Oceanography 58, 263–283

House, J I , Prentice, I C , Le Quéré, C , 2002 Maximum impacts of future reforestation or deforestation on atmospheric CO_2 Global Change Biology 8, 1047–1052

Hunt, B P V , Hosie, G W , 2003 The Continuous Plankton Recorder in the Southern Ocean. a comparative analysis of zooplankton communities samples by the CPR and vertical net hauls along 140°E Journal of Plankton Research 25 (12), 1561–1579

Hurrell, J W , 1995. Decadal Trends in the North Atlantic Oscillation: Regional Temperatures and Precipitation Science 269, 676–679

Hurtt, G C., Armstrong, R A , 1996 A pelagic ecosystem calibrated with BATS data Deep Sea Research II 43, 653–683.

Idyll, C P , 1973 The Anchovy Crisis Scientific American 228 (6), 22–29.

Irigoien, X., Flynn, K. J., Harris, R. P., 2005. Phytoplankton blooms: a "loophole" in microzooplankton grazing impact? Journal of Plankton Research 27, 313–321.

Irigoien, X., Huisman, J., Harris, R. P., 2004. Global biodiversity patterns of marine phytoplankton and zooplankton. Nature 429 (6994), 863–867.

Izumo, T., Vialard, J., Lengaigne, M., de Boyer Montégut, C., Behera, S. K., Luo, J. J., Cravatte, S., Masson, S., Yamagata, T., 2010. Influence of the state of the Indian Ocean Dipole on the following year's El Niño. Nature Geoscience 3, 168–172.

Jeffrey, S. W., Hallegraeff, G. M., 1990. Phytoplankton ecology of Australian waters. In: Clayton, M. N., King, R. J. (Eds.), Biology of Marine Plants. Longman Cheshire, Melbourne, pp. 310–348.

Jeffrey, S. W., Mantoura, R. F. C., 1997. Development of pigment methods for oceanography: SCOR-supported working groups and objectives. In: Jeffrey, S. W., Mantoura, R. F. C., Wright, S. W. (Eds.), Phytoplankton Pigments in Oceanography: Guidelines to modern methods. UNESCO Publishing, Paris, pp. 38–84.

Jennings, S., Brewin, R. J. W., Hardman-Mountford, N. J., Barnes, C., 2010. Linking remote sensing data and food web models to predict consumer biomass in the global oceans, *SAFARI Remote Sensing and Fisheries International Symposium*, Kochi, India, 15th-17th February, 2010.

Jennings, S., Mélin, F., Blanchard, J. L., Forster, R. M., Dulvy, N. K., Wilson, R. W., 2008. Global-scale predictions of community and ecosystem properties from simple ecological theory. Proceedings of the Royal Society B 275 (1641), 1375–1383 doi:10.1098/rspb.2008.0192.

Jennings, S., Warr, K. J., Mackinson, S., 2002. Use of size-based production and stable isotope analyses to predict trophic transfer efficiencies and predator-prey body mass ratios in food webs. Marine Ecological Progress Series 240, 11–20.

Jerlov, N. G., 1968. Optical Oceanography. Elsevier, Amsterdam.

Jerlov, N. G., 1976. Marine Optics. Elsevier, Amsterdam.

Jordan, R. W., Chamberlain, A. H. L., 1997. Biodiversity among haptophyte algae. Biodiversity and Conservation 6 (1), 131–152.

Kameda, T., Ishizaha, J., 2005. Size-fractionated primary production estimated by a two-phytoplankton community model applicable to ocean color remote sensing. Journal of Oceanography 61, 663–672.

Karl, D M , Bidigare, R R , Letelier, R M , 2001 Long-term changes in plankton community structure and productivity in the North Pacific Subtropical Gyre The domain shift hypothesis Deep Sea Research II 48 (8-9), 1449–1470

Karl, D M , Lukas, R , 1996 The Hawaii Ocean Time-series (HOT) program Background, rationale and field implementation. Deep Sea Research II 43 (2-3), 129–156

Karp-Boss, L , Azevedo, L , Boss, E , 2007. LISST-100 measurements of phytoplankton size distribution Evaluation of the effects of cell shape Limnology and Oceanography Methods 5, 396–406

Kawamura, G S , OCTS Team, T , 1998 OCTS mission overview J. Oceanogr. 54, 383–399

Keller, M. D., 1988 Dimethyl sulfide production and marine phytoplankton The importance of species composition and cell size Biological Oceanography 6 (5-6), 375–382

Kiefer, D. A , Mitchell, B. G , 1983. A simple steady state description of phytoplankton growth based on absorption cross section and quantum efficiency Limnology and Oceanography 27, 492–499.

Kirk, J T O , 1975 A theoretical analysis of the contribution of algal cells to the attenuation of light within waters, II, Spherical cells New Phytologist 75, 21–36

Kirk, J T O , 1994 Light and photosynthesis in aquatic ecosystems Cambridge University Press, Cambridge

Kishi, M J., Kashiwai, M., Ware, D. M , Megrey, B. A., Eslinger, D L., Werner, F E., Noguchi-Aita, M , Azumaya, T., Fuji, M., Hashimoto, S , Huang, D. J , Iizumi, H , Ishida, Y , Kang, S , Kantakov, G. A , Kim, H C., Komatsu, K., Navrotsky, V V , Smith, S L , Tadokoro, K , Tsuda, A , Yamamura, O., Yamanaka, Y , Yokouchi, K , Yoshie, N , Zhang, J , Zuenko, Y I., Zvalinsky, V I , 2007 NEMURO - a lower trophic level model for the North Pacific marine ecosystem Ecological Modelling 202 (1-2), 12–25

Kitchen, J C , Zaneveld, J R V , 1992 A three-layered sphere model of the optical properties of phytoplankton. Limnology and Oceanography 37 (8), 1680–1690

Knefelkamp, B , Carstens, K , Wiltshire, K H C , 2007 Comparison of different filter types on chlorophyll-a retention and nutrient measurements Journal of Experimental Marine Biology and Ecology 345, 61–70

Kobayashi, F., Takahashi, K., 2002. Distribution of diatoms along the equatorial transect in the western and central Pacific during the 1999 La Niña conditions. Deep-Sea Research II 49 (13-14), 2801–2821.

Kostadinov, T. S., Siegel, D. A., Maritorena, S., 2009. Retrieval of the particle size distribution from satellite ocean color observations. Journal of Geophysical Research 114, C09015, 10.1029/2009jc005303.

Kostadinov, T. S., Siegel, D. A., Maritorena, S., 2010. Global variability of phytoplankton functional types from space: assessment via the particle size distribution. Biogeosciences 7, 3239–3257.

Kuroda, H., Kishi, M. J., 2004. A data assimilation technique applied to estimate parameters for the NEMURO marine ecosystem model. Ecological Modelling 172 (1), 69–85.

Lacroix, G., Ruddick, K., Park, Y., Gypens, N., Lancelot, C., 2007. Validation of the 3D biogeochemical model MIRO & CO with field nutrient and phytoplankton data and MERIS-derived surface chlorophyll a images. Journal of Marine Systems 64 (1-4), 66–88.

Landry, M. R., Constantinou, J., Latasa, M., Brown, S. L., Bidigare, R. R., Ondrusek, M. E., 2000. Biological response to iron fertilization in the eastern equatorial Pacific (ironEx II). III. dynamics of phytoplankton growth and microzooplankton grazing. Marine Ecological Progress Series 201, 57–72.

Laws, E. A., Ditullio, G. R., Redalje, D. G., 1987. High phytoplankton growth and production-rates in the North Pacific subtropical gyre. Limnology and Oceanography 32 (4), 905–918.

Laws, E. A., Falkowski, P. G., Smith Jr, W. O., Ducklow, H., McCarth, J. J., 2000. Temperature effects on export production in the open ocean. Global Biogeochemical Cycles 14, 1231–1246.

Lawson, L. M., Hofmann, E. E., Spitz, Y. H., 1996. Time series sampling and data assimilation in a simple marine ecosystem model 43 (2-3), 625–651.

Le Quéré, C., 2006. Reply to Horizons Article Plankton functional type modelling: running before we can walk Anderson (2005): I. Abrupt changes in marine ecosystems? Journal of Plankton Research 28 (9), 871–872.

Le Quéré, C., Harrison, S. P., Prentice, C. I., Buitenhuis, E. T., Aumont, O., Bopp, L., Claustre, H., Cotrim Da Cunha, L., Geider, R., Giraud, X., Klaas, C., Kohfeld, K. E., Legendre, L., Manizza, M., Platt, T., Rivkin, R., Sathyendranath, S., Uitz, J., Watson, A. J., Wolf-Gladrow, D., 2005. Ecosystem dynamics based on plankton

functional types for global ocean biogeochemistry models. Global Change Biology 11 (11), 2016–2040

Le Quéré, C., Raupach, M R., Canadell, J G , Marland, G , Bopp, L , Ciais, P , Conway, T. J , Doney, S. C , Feely, R. A , Foster, P., Friedlingstein, P , Gurney, K., Houghton, R A., House, J I., Huntingford, C., Levy, P. E , Lomas, M R , Majkut, J , Metzl, N., Ometto, J P., Peters, G. P., Prentice, I. C , Randerson, J T., Running, S W., Sarmiento, J L , Schuster, U , Sitch, S., Takahashi, T., Viovy, N., van der Werf, G R , Woodward, F. I , 2009 Trends in the sources and sinks of carbon dioxide Nature Geoscience 2 (12), 831–836.

Lee, Z P , Carder, K. L , Arnone, R A , 2002 Deriving inherent optical properties from water color a multiband quasi-analytical algorithm for optically deep waters Applied Optics 41, 5755–5772.

Lefevre, N , Moore, G , Aiken, J , Watson, A J , Cooper, D J , Ling, R , 1998 Variability of pCO_2 in the tropical Atlantic in 1995 Journal of Geophysical Research 103, 5623–5634

Letelier, R M , Bidigare, R , Hebel, D V., Ondrusek, M , Winn, C D , Karl, D. M , 1993 Temporal variability of phytoplankton community structure based on pigment analysis Limnology and Oceanography 38, 1420–1437.

Lewis, M. R , Cullen, J J , Platt, T , 1983 Phytoplankton and thermal structure in the upper ocean: Consequences of nonuniformity in chlorophyll profile. Journal of Geophysical Research 88, 2565–2570

Li, W K W , Subba-Rao, D , Harrison, W G , Smith, J C , Cullen, J. J., Irwin, B., Platt, T , 1983. Autotrophic picoplankton in the tropical ocean. Science 219, 292–295

Libicki, C., Bedford, K W , Lynch, J F , 1989 The interpretation and evaluation of a 3-Mhz acoustic backscatter device for measuring benthic boundary layer sediment dynamics Journal of the Acoustical Society of America 85 (4), 1501–1511

Litt, E J , Hardman-Mountford, N J , Blackford, J C , Mitchelson-Jacob, G , Goodman, A , Moore, G F , Cummings, D G , Butenschon, M , 2010 Biological control of pCO_2 at station L4 in the Western English Channel over 3 years. Journal of Plankton Research 32 (5), 621–629

Liu, H., Probert, I., Uitz, J , Claustre, H , Aris-Brosou, Frada, M , Not, F , Vargas, C., 2009. Extreme diversity in noncalcifying haptophytes explains a major pigment paradox in open oceans. Proceedings of the National Academy of Sciences of the United States of America 106 (31), 12803–12808.

Llewellyn, C. A., Fishwick, J. R., Blackford, J. C., 2005. Phytoplankton community assemblage in the English Channel: a comparison using chlorophyll a derived from HPLC-CHEMTAX and carbon derived from microscopy cell counts. Journal of Plankton Research 27, 103–119.

Llewellyn, C. A., Harbour, D. S., 2003. A temporal study of mycosporine-like amino acids in surface water phytoplankton from the English Channel and correlation with solar irradiation. Journal of the Marine Biological Association of the UK 83, 1–9.

Logan, B. E., 1993. Theoretical analysis of size distributions determined with screens and filters. Limnology and Oceanography 38, 372–381.

Logan, B. E., Passow, U., Alldredge, A. L., 1994. Variable retention of diatoms on screens during size separations. Limnology and Oceanography 39, 390–395.

Lohrenz, S. E., Weidemann, A. D., Tuel, M., 2003. Phytoplankton spectral absorption as influenced by community size structure and pigment composition. Journal of Plankton Research 25, 35–61.

Loisel, H., Nicolas, J. M., Sciandra, A., Stramski, D., Poteau, A., 2006. Spectral dependency of optical backscattering by marine particles from satellite remote sensing of the global ocean. Journal of Geophysical Research 111, C09024, doi:10.1029/2005JC003367.

Loisel, H., Poteau, A., 2006. Inversion of IOP based on R_{rs} and Remotely Retrieved K_d. In: Lee, Z. P. (Ed.), Remote Sensing of Inherent Optical Properties: Fundamentals, Tests of Algorithms, and Applications. Ocean-Colour Coordinating Group, No. 5, IOCCG, Dartmouth, Canada.

Loisel, H., Stramski, D., 2000. Estimation of the inherent optical properties of natural waters from irradiance attenuation coefficient and reflectance in the presence of Raman scattering. Applied Optics 41, 2705–2714.

Longhurst, A., Sathyendranath, S., Platt, T., Caverhill, C., 1995. An estimate of global primary production in the ocean from satellite radiometer data. Journal of Plankton Research 17, 1245–1271.

Longhurst, A. R., 1998. Ecological Geography of the Sea. Academic Press, San Diego.

Lovelock, J. E., 1992. A numerical model for biodiversity. Philosophical Transactions of the Royal Society of London B 338, 383–391, doi: 10.1098/rstb.1992.0156.

Luo, J J., Zhang, R., Behera, S K , Masumoto , Y , (2010) , J C , 2010 Interaction between El Niño and Extreme Indian Ocean Dipole Journal of Climate 23 (3), 726–742

Lutz, V A., Sathyendranath, S., Head, E J H , 1996. Absorption coefficient of phytoplankton Regional variations in the North Atlantic Marine Ecological Progress Series 135, 197–213

Mackey, M D , Mackey, D J., Higgins, H. W , Wright, S. W., 1996 CHEMTAX - a program for estimating class abundances from chemical markers: application to HPLC measurements of phytoplankton. Marine Ecological Progress Series 144, 265–283

Malone, T C , 1980 Algal size In Morris, I. (Ed), The Physiological Ecology of Phytoplankton Univ. of Calif., Berkeley, pp 443–463.

Manning, A , Dyer, K , 1999 A laboratory examination of floc characteristics with regard to turbulent shearing Marine Geology 160, 147–170

Marañón, E , 2009 Phytoplankton size structure In· Steele, J H , Turekian, K , Thorpe, S A (Eds), Encyclopedia of Ocean Sciences Academic Press, Oxford

Marañón, E , Holligan, P , Varela, M , Mourinõ, B , Bale, A J., 2000 Basin-scale variability of phytoplankton biomass, production and growth in the Atlantic Ocean Deep Sea Research I 47, 825–857

Mare, M., 1940 Plankton production off Plymouth and the mouth of the English Channel in 1939. Journal of the Marine Biological Association of the UK 24, 461–482

Margalef, R , 1967 Some concepts relative to the organisation of plankton. Oceanogr. Mar Biol Ann Rev 5, 257–289

Margalef, R., 1978. Life-forms of phytoplankton as survival alternatives in an unstable environment. Oceanol Acta 1, 493–509.

Maritorena, S , Siegel, D A., 2005. Consistent merging of satellite ocean color data sets using a bio-optical model Remote Sensing of Environment 94, 429–440

Maritorena, S., Siegel, D A , Peterson, A R., 2002. Optimization of a semianalytical ocean color model for global-scale applications Applied Optics 41 (15), 2705–2714.

Marra, J , Trees, C , O'Reilly, J., 2007. Phytoplankton pigment absorption: A strong predictor of primary productivity in the surface ocean. Deep-Sea Research I 54, 155–163.

Martin, J. H., 1991. Iron, Liebig's Law, and the Greenhouse. Oceanography 4 (2), 52–55.

Martin, J. H., Fitzwater, S. E., 1988. Iron deficiency limits phytoplankton growth in the north-east Pacific subarctic. Nature 331, 341–343.

Martin, S., 2004. An introduction to ocean remote sensing. Cambridge University Press, Cambridge, UK.

Martinez, E., Antoine, D., D'Ortenzio, F., Gentili, B., 2009. Climate-driven basin-scale decadal oscillations of oceanic phytoplankton. Science 326, 1253–1256, doi:10.1126/science.1177012.

McClain, C. R., 2009. A decade of satellite ocean color observations. Annual Review of Marine Science 1, 19–42.

McClain, C. R., Cleave, M. L., Feldman, G. C., Gregg, W. W., Hooker, S. B., Kuring, N., 1998. Science quality SeaWiFS data for global biosphere research. Sea Technology 39 (9), 10–16.

McClain, C. R., Esaias, W., Feldman, G., Frouin, R., Gregg, W., Hooker, S. B., 2002. The proposal for the NASA sensor intercalibration and merger for biological and interdisciplinary oceanic studies (SIMBIOS) program, 1995. Tech. rep.

McClain, C. R., Signorini, S. R., Christian, J. R., 2004. Subtropical gyre variability observed by ocean-color satellites. Deep Sea Research II 51 (1-3), 281–301.

McGillicuddy, D. J., Kosnyrev, V. K., Ryan, J. P., Yoder, J. A., 2001. Covariation of mesoscale ocean color and sea-surface temperature patterns in the Sargasso Sea. Deep Sea Research II 48 (8-9), 1823–1836.

Michaels, A. F., Knap, A. H., 1996. Overview of the U.S. JGOFS BATS and Hydrostation S program. Deep Sea Research II 43 (2-3), 157–198.

Michaels, A. F., Silver, M. W., 1988. Primary production, sinking fluxes and the microbial food web. Deep-Sea Research I 35, 473–490.

Miller, C. B., 2004. Biological Oceanography. Blackwell Publishing company, Oxford.

Millie, D. F., Schofield, O. M., Kirkpatrick, G. J., Johnsen, G., Tester, P. A., Vinyard, B. T., 1997. Detection of harmful algal blooms using photopigments and absorption signatures : A case study of the Florida red tide dinoflagellate, *Gymnodinium breve*. Limnology and Oceanography 42 (2), 1240–1251.

Milligan, T. G., Kranck, K., 1991. Electroresistance particle size analyzers. In: Syvitski, J. (Ed.), Principles, Methods, and Application of Particle Size Analysis. Cambridge University Press, Cambridge, UK.

Mitchell, B G , 1994. Ocean color from space A coastal zone color scanner retrospective special edition, Journal of Geophysical Research 97, 7429–7445

Mitchum, G T , 1996 On using satellite altimetric heights to provide a spatial context for the Hawaii Ocean Time-series measurements Deep Sea Research II 43 (2-3), 257–280.

Monger, B C , Landry, M R , Brown, S L , 1999 Feeding selection of heterotrophic marine nanoflagellates based on the surface hydrophobicity of their picoplankton prey Limnology and Oceanography 44 (8), 1917–1927.

Moore, L R , Goericke, R , Chisholm, S W., 1995. Comparative physiology of *Synechococcus* and *Prochlorococcus* Influence of light and temperature on growth, pigments, fluorescence and absorptive properties Marine Ecological Progress Series 116, 259–275

Morel, A , 1978 Available, usable, and stored radiant energy in relation to marine photosynthesis Deep-Sea Research 25 (673-688)

Morel, A , 1988 Optical modeling of the upper ocean in relation to its biogenous matter content (Case I waters). Journal of Geophysical Research 93, 749–768.

Morel, A , 1991 Light and marine photosynthesis A spectral model with geochemical and climatological implications Progress in Oceanography 26, 263–306.

Morel, A., Ahn, Y H , Partensky, F , Vaulot, D , Claustre, H , 1993 *Prochlorococcus* and *Synechococcus* A comparitive study of thier optical properties in relation to thier size and pigmentation Journal of Marine Research 51, 617–649

Morel, A , Berthon, J F , 1989 Surface pigments, algal biomass profiles, and potential production of the euphotic layer Relationships reinvestigated in view of remote-sensing applications Limnology and Oceanography 34 (8), 1545–1562

Morel, A , Bricaud, A , 1981. Theoretical results concerning light absorption in a discrete medium, and application to specific absorption of phytoplankton Deep-Sea Research 28, 1375–1393

Morel, A , Claustre, H , Antoine, D , Gentili, B , 2007a Natural variability of bio-optical properties in Case 1 waters attenuation and reflectance within the visible and near-UV spectral domains, as observed in South Pacific and Mediterranean waters Biogeosciences 4, 913–925

Morel, A , Claustre, H , Gentili, B , 2010 The most oligotrophic subtropical zones of the global ocean· similarities and differences in terms of chlorophyll and yellow substance Biogeosciences Discuss 7, 5047–5079

Morel, A., Gentili, B., 1993. Diffuse reflectance of oceanic waters. 2. Bidirectional aspects. Applied Optics 32, 6864–6872.

Morel, A., Gentili, B., 1996. Diffuse reflectance of oceanic waters. 3. Implications of Bidirectionality for the Remote-Sensing Problem. Applied Optics 35, 4850–4862.

Morel, A., Gentili, B., Claustre, H., Babin, M., Bricaud, A., Ras, J., Tiéche, F., 2007b. Optical properties of the "clearest" natural waters. Limnology and Oceanography 52, 217–229.

Morel, A., Huot, Y., Gentili, B., Werdell, P. J., Hooker, S. B., Franz, B. A., 2007c. Examining the consistency of products derived from various ocean color sensors in open ocean (case 1) waters in the perspective of a multi-sensor approach. Remote Sensing of Environment 111, 69–88.

Morel, A., Maritorena, S., 2001. Bio-optical properties of oceanic waters: A reappraisal. Journal of Geophysical Research 106 (C4), 7163–7180.

Morel, A., Prieur, L., 1977. Analysis of variations in ocean color. Limnology and Oceanography 22, 709–722.

Mouw, C. B., Yoder, J., 2010. Optical determination of phytoplankton size composition from global SeaWiFS imagery. Journal of Geophysical Research 115, C12018, doi:10.1029/2010JC006337.

Mouw, C. B., Yoder, J. A., 2005. Primary production calculations in the Mid-Atlantic Bight, including effects of phytoplankton community size structure. Limnology and Oceanography 50 (4), 1232–1243.

Muylaerta, K., Gonzalesa, R., Francka, M., Lionarda, M., Van der Zeeb, C., Cattrijssec, A., Sabbea, K., Choub, L., Vyvermana, W., 2006. Spatial variation in phytoplankton dynamics in the Belgian coastal zone of the North Sea studied by microscopy, HPLC-CHEMTAX and underway fluorescence recordings. Journal of Sea Research 55 (4), 253–265.

Nair, A., Sathyendranath, S., Platt, T., Morales, J., Stuart, V., Forget, M.-H., Devred, E., Bouman, H., 2008. Remote sensing of phytoplankton functional types. Remote Sensing of Environment 112 (8), 3366–3375.

Nathanail, C. P., Rosenbaum, M. S., 1995. The misclassification matrix: a tool for validating geotechnical data. Quarterly Journal of Engineering Geology 28, 381–384.

Nelson, D. M., Treguer, P., Brzezinski, M. A., Leynaert, A., Queguiner, B., 1995. Production and dissolution of biogenic silica in the ocean: Revised global estimates, comparison with regional data and relationships to biogenic sedimentation. Global Biogeochemical Cycles 9, 359–372.

Nimmo Smith, W A M , 2008 A submersible three-dimensional particle tracking velocimetry system for flow visualization in the coast ocean Limnology and Oceanography Methods 6, 96–104

Niquen, M., Bouchon, M., 2004 Impact of El Niñõ events on pelagic fisheries in peruvian waters Deep Sea Research II 51, 563–574

NOAA, 2010 NOAA El Niño theme page Online http://www.pmel noaa.gov/tao/elnino/nino-home html (20/12/10)

Not, F , Latasa, M , Cariou, T , Valout, D., Simon, N , 2004 A single species, *Micromonas pusilla* (Prasinophyceae), dominates eukaryote picoplankton in the Western English Channel Applied Environmental Microbiology 70, 4064–4072

Olson, R J , Shalapyonok, A A , Sosik, H M , 2003 An automated submersible flow cytometer for pico- and nanophytoplankton. FlowCytobot. Deep Sea Research I 50, 301–315

Olson, R J., Sosik, H. M , 2007 A submersible imaging-in-flow instrument to analyze nano- and microplankton Imaging FlowCytobot Limnology and Oceanography Methods 5, 195–203

Ondrusek, M. E , Bidigare, R B , Waters, K , Kar, D. M , 2001 A predictive model for estimating rates of primary production in the subtropical North Pacific Ocean. Deep Sea Research II 48 (8-9), 1837–1863

Ondrusek, M E., Bidigare, R. R , Sweet, S T , Defreitas, D. A., Brooks, J M , 1991. Distribution of phytoplankton pigments in the North Pacific Ocean in relation to physical and optical variability. Deep Sea Research I 38 (2), 243–266

O'Reilly, J E., Maritorena, S , Mitchell, B G., Siegel, D A , Carder, K L , Garver, S A , Kahru, M , McClain, C , 1998 Ocean chlorophyll algorithms for SeaWiFS Journal of Geophysical Research 103 (C11), 24,937–24,953

O'Reilly, J E , Maritorena, S., Siegel, D , O'Brien, M C , Toole, D , Mitchell, B. G , Kahru, M , Chavez, F P , Strutton, P , Cota, G , Hooker, S B , McClain, C. R , Carder, K L , Muller-Karger, F , Harding, L., Magnuson, A , Phinney, D , Moore, G. F , Aiken, J , Arrigo, K R , Letelier, R , Culver, M., 2000 Ocean color chlorophyll a algorithms for seawifs, oc2, and oc4 Version 4 In: Hooker, S B., Firestone, E. R (Eds.), SeaWiFS Postlaunch Technical Report Series. Vol. 11. SeaWiFS Postlaunch Calibration and Validation Analyses, Part 3 NASA, Goddard Space Flight Center, Greenbelt, Maryland 9-23.

Oschlies, A., Garcon, V., 1998. Eddy-induced enhancement of primary production in a model of the North Atlantic Ocean. Nature 394, 266–269.

Palmer, J. R., Totterdell, I., 2001. Production and export in a global ocean ecosystem model. Deep-Sea Research I 48, 1169–1198.

Pan, X., Mannino, A., Russ, M. E., Hooker, S. B., Harding, L., 2010. Remote sensing of phytoplankton pigment distribution in the United States northeast coast. Remote Sensing of Environment 114 (11), 2403–2416.

Parsons, T. R., Lalli, C. M., 2002. Jellyfish populations explosions: Revisiting a hypothesis of possible causes. La Mer 40, 111–121.

Partensky, F., Hess, W. R., Vaulot, D., 1999. *Prochlorococcus*, a Marine Photosynthetic Prokaryote of Global Significance. Microbiology and Molecular Biology Reviews 63 (1), 106–127.

Partensky, F., Hoepffner, N., Li, W. K. W., Ulloa, O., Vaulot, D., 1993. Photoacclimation of *Prochlorococcus sp* (prochlorophyta) strains isolated from the North Atlantic and the Mediterranean Sea. Plant Physiology 101 (1), 285–296, iSI Document Delivery No.: KG721 Times Cited: 107 Cited Reference Count: 31.

Patz, J. A., Campbell-Lendrum, D., Holloway, T., Foley, J. A., 2005. Impact of regional climate change on human health. Nature 438, 310–317.

Perry, M. J., 1994. Measurements of phytoplankton absorption other than per unit of chlorophyll a. In: Spinrad, R. W., Carder, K. L., Perry, M. J. (Eds.), Ocean Optics. Oxford University Press, New York, pp. 107–116.

Peters, R. H., 1983. The Ecological Implications of Body Size. Cambridge University Press, Cambridge.

Platt, T., Bouman, H., Devred, E., Fuentes-Yaco, C., Sathyendranath, S., 2005. Physical forcing and phytoplankton distributions. Scientia Marina 69 (1), 55–73.

Platt, T., Denman, K. L., 1976. The relationship between photosynthesis and light for natural assemblages of coastal marine phytoplankton. Journal of Phycology 12 (4), 421–430.

Platt, T., Denman, K. L., 1977. Organisation in the pelagic ecosystem. HelgoaËnder Wissenschaftliche Meeresuntersuchungen 30, 575–581.

Platt, T., Denman, K. L., 1978. The structure of pelagic marine ecosystems. Rapp. P.-v. Réun. Cons. perm. int. Explor. Mer, 60–65.

Platt, T., Fuentes-Yaco, C., Frank, K. T., 2003. Spring algal bloom and larval fish survival. Nature 423 (6938), 398–399.

Platt, T., Jassby, A. D., 1976 Relationship between photosynthesis and light for natural assemblages of coastal marine-phytoplankton Journal of Phycology 12 (4), 421–430.

Platt, T , Sathyendranath, S., 1988 Oceanic primary production Estimation by remote sensing at local and regional scales Science 241, 1613–1620

Platt, T., Sathyendranath, S , Forget, M. H , White, G N., Caverhill, C., Bouman, H., Devred, E., Son, S., 2008 Operational estimation of primary production at large geographical scales. Remote Sensing of Environment 112 (8), 3437–3448

Platt, T , Sathyendranath, S , Stuart, V , 2006 Why study biological oceanography? Aquabiology 28, 542–557

Platt, T , White, G N., Zhai, L , Sathyendranath, S , Roy, S , 2009 The phenology of phytoplankton blooms Ecosystem indicators from remote sensing Ecological Modelling 220 (21), 3057–3069

Polovina, J J , Howell, E A , Abecassis, M , 2008 Ocean's least productive waters are expanding Geophysical Research Letters 35, L03618, doi 10 1029/2007GL031745

Preisendorfer, R W , 1961 Application of radiative transfer theory to light measurments in the sea International Union of Geodesy and Geophysics Monograph (Symposium on Radiant Energy in the Sea) no. 10, 11-30

Preisendorfer, R W , 1976 Hydrologic Optics vol 1: Introduction Tech. rep., NTIS PB-259 793/8ST , National Technical Information Service , Springfield, Ill , USA,

Press, W H , Keukolsky, S A , Vettering, W T., Flannery, B P , 1992. Levenberg-Marquard Method in Numerical Recipes in C. The Art of Scientific Computation Cambridge Univ Press, New York

Prieur, L , Sathyendranath, S , 1981 An optical classification of coastal and oceanic waters based on the specific spectral absorption curves of phytoplankton pigments, dissolved organic matter and other particulate materials Limnology and Oceanography 26, 617–689

Probyn, T. A , 1985 Nitrogen uptake by size-fractionated phytoplankton populations in the southern Benguela upwelling system Marine Ecological Progress Series 22, 249–258.

Raimbault, P., Rodier, M., Taupier-Letage, I , 1988 Size fraction of phytoplankton in the Ligurian Sea and the Algerian Basin (Mediterranean Sea)· Size distribution versus total concentration. Marine Microbial Food Webs 3, 1–7

Raitsos, D. E., Lavender, S. J., Maravelias, C. D., Haralambous, J., Richardson, A. J., Reid, P. C., 2008. Identifying four phytoplankton functional types from space: An ecological approach. Limnology and Oceanography 53 (2), 605–613.

Raitsos, D. E., Lavender, S. J., Pradhan, Y., Tyrrell, T., Reid, P. C., Edwards, M., 2006. Coccolithophore bloom size variation in response to the regional environment of the subarctic North Atlantic. Limnology and Oceanography 51 (5), 2122–2130.

Raitsos, D. E., Reid, P. C., Lavender, S. J., Edwards, M., Richardson, A. J., 2005. Extending the SeaWiFS chlorophyll data set back 50 years in the Northeast Atlantic. Geophysical Research Letters 32, LO6613, doi:10.1029/ 2005 GL 022484.

Ras, J., Claustre, H., Uitz, J., 2008. Spatial variability of phytoplankton pigment distributions in the Subtropical South Pacific Ocean: a comparison between in situ and predicted data. Biogeosciences 5, 353–369.

Rast, M., Bezy, J.-L., 1999. The ESA Medium Resolution Imaging Spectrometer MERIS: A review of the intrument and its mission. International Journal of Remote Sensing 20 (9), 1681–1702.

Raven, J. A., 1998. Small is beautiful: The picophytoplankton. Functional Ecology 12, 503–513.

Richardson, A. J., Walne, A. W., John, A. W. G., Jonas, T. D., Lindley, J. A., Sims, D. W., Stevens, D., Witt, M., 2006. Using continuous plankton recorder data. Progress in Oceanography 68 (1), 27–74.

Ripley, S. J., Baker, A. C., Miller, P. I., Walne, A. W., Schroeder, D. C., 2008. Development and validation of a molecular technique for the analysis of archived formalin-preserved phytoplankton samples permits retrospective assessment of *Emiliania huxleyi* communities. Journal of Microbiological Methods 73 (2), 118–124.

Robinson, C., Poulton, A. J., Holligan, P. M., Baker, A. R., Forster, G., Gist, N., Jickells, T. D., Malin, G., Upstill-Goddardd, R., Williams, R. G., Woodward, E. M. S., Zubkov, M. V., 2006. The Atlantic Meridional Transect (AMT) Programme: A contextual view 1995-2005. Deep Sea Research II 53, 1485–1515.

Robinson, C., Serret, P., Tilstone, G., Teira, E., Zubkov, M. V., Rees, A. P., Woodward, E. M. S., 2002. Plankton respiration in the Eastern Atlantic. Deep Sea Research I 49, 787–813.

Robinson, G. A., 1970. Continuous plankton records: variation in the seasonal cycle of phytoplankton in the North Atlantic. Bulletin of Marine Ecology 6, 333–345.

Robinson, I. S., 2004. Measuring the oceans from space Praxis Publishing Ltd, Chichester, UK

Ryan, J P , Polito, P S , Strutton, P G , Chavez, F. P , 2002 Unusual large-scale phytoplankton blooms in the equatorial Pacific Progress in Oceanography 55 (3-4), 263–285.

Saba, V. S., Friedrichs, M A M , Carr, M. E , Antoine, D., Armstrong, R A , Asanuma, I., Aumont, O., Bates, N. R , Behrenfeld, M J., Bennington, V , Bopp, L , Bruggeman, J., Buitenhuis, E. T , Church, M. J , Ciotti, A. M , Doney, S C , Dowell, M , Dunne, J , Dutkiewicz, S , Gregg, W , Hoepffner, N., Hyde, K J. W., Ishizaka, J., Kameda, T , Karl, D M., Lima, I., Lomas, M W , Marra, J , McKinley, G A , Mélin, F., Moore, J. K., Morel, A., O'Reilly, J , Salihoglu, B , Scardi, M , Smyth, T J , Tang, S , Tjiputra, J , Uitz, J., Vichi, M., Waters, K., Westberry, T K , Yool, A., 2010. The challenges of modeling depth-integrated marine primary productivity over multiple decades A case study at BATS and HOT Global Biogeochemical Cycles 24, doi:10 1029/2009GB003655

Sabine, C L , Feely, R. A , Gruber, N., Key, R M , Lee, K , Bullister, J. L , Wanninkhof, R , Wong, C S , Wallace, D. W. R , Tilbrook, B , Millero, F. J , Peng, T.-H , Kozyr, A , Ono, T , Rios, A F , 2004 The oceanic sink for anthropogenic CO_2. Science 305, 367–371.

Sabins, F F , 1987 Remote Sensing Principles and Interpretation 2nd edition W H Freeman and Company, New York.

SAHFOS, 2010 Sir Alister Hardy Foundation for Ocean Science. Online http //www sahfos.ac uk/ (8/10/10)

Saji, N H , Goswami, B N , Vinayachandran, P N , Yamagata, T., 1999 A dipole mode in the tropical Indian Ocean Nature 401, 360–363

Sakshaug, E , Andresen, K , Kiefer, D A , 1989 A steady-state description of growth and light-absorption in the marine planktonic diatom *Skeletonema-Costatum* sp Limnology and Oceanography 34 (1), 198–205

Sarmiento, J L , Slater, R D , Fasham, M. J. R , Ducklow, H W , Toggweiler, J R , Evans, G T , 1993 A seasonal three-dimensional ecosystem model of nitrogen cycling in the North Atlantic euphotic zone. Global Biogeochemical Cycles 7, 417–450.

Sathyendranath, S , Lazzara, S L , Prieur, L , 1987 Variations in the spectral values of specific absorption of phytoplankton Limnology and Oceanography 32, 403–415

Sathyendranath, S., Longhurst, A. R., Caverhill, C. M., Platt, T., 1995. Regionally and seasonally differentiated primary production in the North Atlantic. Deep-Sea Research I 42 (10), 1773–1802.

Sathyendranath, S., Platt, T., 1988. The spectral irradiance field at the surface and in the interior of the ocean: A model for applications in oceanography and remote sensing. Journal of Geophysical Research 93, 9370–9280.

Sathyendranath, S., Platt, T., 1989. Remote sensing of ocean chlorophyll: consequences of non-uniform pigment profile. Applied Optics 28, 490–495.

Sathyendranath, S., Stuart, V., Cota, G., Maas, H., Platt, T., 2001. Remote sensing of phytoplankton pigments: a comparison of empirical and theoretical approaches. International Journal of Remote Sensing 22, 249–273.

Sathyendranath, S., Watts, L., Devred, E., Platt, T., Caverhill, C., Maass, H., 2004. Discrimination of diatoms from other phytoplankton using ocean-colour data. Marine Ecological Progress Series 272, 59–68.

Scharf, F. S., Juanes, F., Rountree, R. A., 2000. Predator size - prey size relationships of marine fish predators: interspecific variation and effects of ontogeny and body size on trophic-niche breadth. Marine Ecology Progress Series 208, 229–248.

Schlesinger, D. A., Molot, L. A., Shuter, B. J., 1981. Specific growth rates of freshwater algae in relation to cell size and light intensity. Canadian Journal of Fisheries and Aquatic Sciences 38, 1052–1058.

Schwarz, J. N., Kowalczuk, P., Kaczmarek, S., Cota, G. F., Mitchell, B. G., Kahru, M., Chavez, F. P., Cunningham, A., McKee, D., Gege, P., Kishino, T., Phinney, D. A., Raine, R., 2002. Two models for absorptions by coloured dissolved organic matter (CDOM). Oceanologia 44, 209–241.

SCOR, 1987. The joint global ocean flux study: background, goals, organization, and next steps. Tech. rep., Dalhousie University, Halifax, Nova Scotia, Canada.

SeaBASS, 2010. The SeaWiFS Bio-optical Archive and Storage System. Online http://seabass.gsfc.nasa.gov/seabass/index.htm (10/10/10).

Secchi, P. A., 1866. Esperimento per determinare la transparanza del mare. In: Cialdi, A. (Ed.), Sul Moto Ondoso del Mare. Rome, pp. 258–288.

Serret, P., Fernández, E., Robinson, C., Woodward, E. M. S., Pérez, V., 2006. Local production does not control the balance between plankton photosynthesis and respiration in the open Atlantic Ocean. Deep Sea Research II 53 (14-16), 1611–1628.

Serret, P., Robinson, C , Fernández, E , Teira, E , Tilstone, G , 2001 Latitudinal variation of the balance between plankton photosynthesis and respiration in the E Atlantic Ocean Limnology and Oceanography 46, 1642–1652

Serret, P , Robinson, C , Fernández, E , Teira, E , Tilstone, G , Pérez, V , 2009 Predicting plankton net community production in the atlantic ocean Deep Sea Research II 56 (15), 941–953

Sheldon, R W , 1972 Size separation of marine seston by membrane and glass-fiber filters Limnology and Oceanography 17, 494–498

Sheldon, R W , Parsons, T R , 1967 A practical manual on the use of the Coulter Counter in marine science Tech. rep.

Sheldon, R W , Prakash, A , Sutcliffe, W H , 1972 The size distribution of particles in the ocean Limnology and Oceanography 17, 327–340

Sieburth, J. M , Smetacek, V , Lenz, J , 1978. Pelagic ecosystem structure· Heterotrophic compartments of the plankton and their relationship to plankton size fractions Limnology and Oceanography 23, 1256–1263

Siegel, D A., Maritorena, S , Nelson, N B , Behrenfeld, M J , McClain, C R , 2005 Colored dissolved organic matter and its influence on the satellite-based characterization of the ocean biosphere Geophysical Research Letters 32, L20605, doi 10 1029/2005GL024310

Siegel, D A , Westberry, T K , O'Brien, M C , Nelson, N. B , Michaels, A F., Morrison, J R , Scott, A , Caporelli, E A , Sorensena, J C , Maritorena, S , Garvere, S A , Brody, E A , Ubante, J , Hammerc, M A , 2001 Bio-optical modeling of primary production on regional scales· the Bermuda BioOptics project Deep Sea Research II 48 (8-9), 1865–1896.

Sieracki, C K , Sieracki, M. E , Yentsch, C S , 1998 An imaging-in-flow system for automated analysis of marine microplankton. Marine Ecological Progress Series 168, 285–296

Signorini, S , McClain, C R , Dandonneau, Y , 1999 Mixing and phytoplankton bloom in the wake of the marquesas island. Geophysical Research Letters 26, 3121–3124

Silió-Calzada, A., Bricaud, A., Uitz, J., Gentili, B , 2008 Estimation of new primary production in the Benguela upwelling area, using ENVISAT satellite data and a model dependent on the phytoplankton community size structure Journal of Geophysical Research 113, C11023, doi.10.1029/2007JC004588.

Six, K. D., Maier-Reimer, E., 1996. Effects of plankton dynamics on seasonal carbon fluxes in an ocean general circulation model. Global Biogeochemical Cycles 10, 559–583.

Slade, W. H., Boss, E., 2006. Calibrated near-forward volume scattering function obtained from the LISST particle size. Optics Express 14, 3602–3615.

Smyth, T. J., Moore, G. F., Hirata, T., Aiken, J., 2006. Semianalytical model for the derivation of ocean color inherent optical properties: description, implementation, and performance assessment. Applied Optics 45 (31), 1–16.

Smyth, T. J., Tilstone, G. H., Groom, S. B., 2005. Integration of radiative transfer into satellite models of ocean primary production. Journal of Geophysical Research 110, doi:10.1029/2004GB002784.

Son, S., Platt, T., Fuentes-Yaco, C., Bouman, H., Devred, E., Wu, Y. S., Sathyendranath, S., 2007. Possible biogeochemical response to the passage of hurricane fabian observed by satellites. Journal of Plankton Research 29 (8), 687–697.

Southward, A. J., Langmead, O., Hardman-Mountford, N. J., Aiken, J., Boalch, G. T., Dando, P. R., Genner, M. J., Joint, I., Kendall, M. A., Halliday, N. C., Harris, R. P., Leaper, R., Mieszkowska, N., Pingree, R. D., Richardson, A. J., Sims, D. W., Smith, T., Walne, A. W., Hawkins, S. J., 2005. Long-term oceanographic and ecological research in the western English Channel. Advances In Marine Biology 47, 1–105.

Steinberg, D. K., Carlson, C. A., Bates, N. R., Johnson, R. J., Michaels, A. F., Knap, A. H., 2001. Overview of the US JGOFS Bermuda Atlantic Time-series Study (BATS): a decade-scale look at ocean biology and biogeochemistry. Deep Sea Research II 48 (8-9), 1405–1447.

Stramski, D., Boss, E., Boguckic, D., Voss, K. J., 2004. The role of seawater constituents in light backscattering in the ocean. Progress In Oceanography 61 (1), 27–56.

Stramski, D., Kiefer, D. A., 1991. Light scattering by microorganisms in the open ocean. Progress in Oceanography 28, 343–383.

Strutton, P. G., Chavez, F. P., 2000. Primary productivity in the equatorial Pacific during the 1997-1998 el niño. Journal of Geophysical Research 105 (C11), 26089–26101.

Stuart, V., Sathyendranath, S., Head, E. J. H., Platt, T., Irwin, B., Maass, H., 2000. Bio-optical characteristics of diatom and prymnesiophyte populations in the Labrador Sea. Marine Ecological Progress Series 201, 91–106.

Stuart, V., Sathyendranath, S , Platt, T , Maass, H , Irwin, B D , 1998. Pigments and species composition of natural phytoplankton populations· Effects on the absorption spectra. Journal Plankton Research 20, 187–217.

Subramaniam, A., Brown, C W., Hood, R. R , Carpenter, E. J., Capone, D G , 2002. Detecting *Trichodesmium* blooms in SeaWiFS imagery. Deep Sea Research II II 49, 107–121

Subramaniam, A., Carpenter, E J , Karentz, D , Falkowski, P. G , 1999 Bio-optical properties of the marine diazotrophic cyanobacteria Trichodesmium spp i Absorption and photosynthetic action spectra Limnology and Oceanography 44 (3), 608–617

Subramaniam, A , Yager, P L., Carpenter, E J , Mahaffey, C , Bjorkman, K , Cooley, S., Kustka, A B , Montoya, J P., Sanudo-Wilhelmy, S. A , Shipe, R , Capone, D G , 2008 Amazon River enhances diazotrophy and carbon sequestration in the tropical North Atlantic Ocean Proceedings of the National Academy of Sciences of the United States of America 105 (30), 10460–10465

Sun, D , Lau, K M , Kafatos, M., 2008 Contrasting the 2007 and 2005 hurricane seasons: Evidence of possible impacts of Saharan dry air and dust on tropical cyclone activity in the Atlantic basin Geophysical Research Letters 35, L15405, doi·10.1029/2008GL034529

Sunda, W G , Huntsman, S A , 1997 Interrelated influence of iron, light and cell size on marine phytoplankton growth Nature 390, 389–392

Sze, P , 1993 A biology of the Algae, 2nd edition Wm C Brown Publishers, Iowa

Takahashi, T., Sutherland, S C., Sweeney, C., Poisson, A , Metzl, N., Tilbrook, B , Bates, N , Wanninkhof, R , Feely, R. A , Sabine, C., Olafsson, J , Nojiri, Y., 2002 Global sea-air CO_2 flux based on climatological surface ocean pCO_2 and seasonal biological and temperature effects Deep-Sea Research II 49, 1601–1622

Tarran, G A., Heywood, J L., Zubkov, M V., 2006 Latitudinal changes in the standing stocks of nano- and picoeukaryotic phytoplankton in the Atlantic Ocean Deep-Sea Research II 53, 1516–1529

Taylor, A H , Harbour, D S , Harris, R P., Burkill, P H , Edwards, E S., 1993 Seasonal succession in the pelagic ecosystem in the North Atlantic and the utilization of nitrogen. Journal of Plankton Research 15, 875–891

Thingstad, T. F , Sakshaug, E., 1990 Control of phytoplankton growth in nutrient recycling ecosystems. theory and terminology Marine Ecological Progress Series 63, 261–272

Thomas, W. H., 1979. Anomalous nutrient-chlorophyll interrelationships in the offshore eastern tropical Pacific Ocean. Journal of Marine Research 37, 327–335.

Thorne, P. D., Agrawal, Y. C., Cacchione, D. A., 2007. A Comparison of Near-Bed Acoustic Backscatter and Laser Diffraction Measurements of Suspended Sediments. IEEE Journal of Oceanic Engineering 32 (1), 225–235.

Throndsen, J., 1978. Preservation and storage. In: Sournia, A. (Ed.), Phytoplankton manual. UNESCO, Paris, pp. 69–74.

Tilstone, G., Smyth, T., Poulton, A., Hutson, R., 2009. Measured and remotely sensed estimates of primary production in the Atlantic Ocean from 1998 to 2005. Deep-Sea Research II 56 (15), 918–930.

Toggweiler, J. R., Carson, S., 1995. What are upwelling systems contributing to the ocean's carbon and nutrient budgets? In: Summerhayes, C. P., Emeis, K. C., Angel, M. V., Smith, R. L., Zeitzschel, B. (Eds.), Upwelling in the ocean. Modern processes and ancient records. John Wiley and Sons, Chichester, UK.

Trees, C. C., Clark, D. K., Bidigare, R. R., Ondrusek, M. E., Mueller, J. L., 2000. Accessory pigments versus chlorophyll a concentrations within the euphotic zone: A ubiquitous relationship. Limnology and Oceanography 45 (5), 1130–1143.

Trenberth, K., 2005. Uncertainty in hurricanes and global warming. Science 308, 1753 –1754.

Trenberth, K. E., Hurrell, J. W., 1994. Decadal atmosphere-ocean variations in the Pacific. Climate Dynamics 9, 303–319.

Tsukayama, I., 1983. Recursos pelágicos y sus pesquerias en Perú. Rev. Com. Perm. Pacifico Sur 13, 25–63.

Twardowski, M. S., Claustre, H., Freeman, S. A., Stramski, D., Huot, Y., 2007. Optical backscattering properties of the "clearest" natural waters. Biogeosciences 4, 1041–1058.

Uitz, J., Claustre, H., Brian Griffiths, F., Ras, J., Garcia, N., Sandroni, V., 2009. A phytoplankton class-specific primary production model applied to the Kerguelen Islands region (Southern Ocean). Deep-Sea Research II 56, 541–560.

Uitz, J., Claustre, H., Gentili, B., Stramski, D., 2010. Phytoplankton class-specific primary production in the world's oceans: Seasonal and interannual variability from satellite observations. Global Biogeochemical Cycles 24, doi:10.1029/2009GB003680.

Uitz, J., Claustre, H , Morel, A , Hooker, S B., 2006 Vertical distribution of phytoplankton communities in open ocean: An assessment based on surface chlorophyll. Journal of Geophysical Research 111, CO8005, doi 10 1029/2005JC003207.

Uitz, J , Huot, Y , Bruyant, F , Babin, M , Claustre, H , 2008 Relating phytoplankton photophysiological properties to community structure on large scales. Limnology and Oceanography 52 (2), 614–630

Van de Hulst, H C , 1957 Light scattering by Small Particles Wiley, New York

van Dijk, M A , Gregori, G , Hoogveld, H L , Rijkeboer, M , Denis, M , Malkassian, A , Gons, H J , 2010 Optimizing the setup of a flow cytometric cell sorter for efficient quantitative sorting of long filamentous cyanobacteria Cytometry 77, 911–924.

Vanden Berg, A J., Ridderinkhof, H , Riegman, R , Ruardija, P , Lenhart, H , 1996 Influence of variability in water transport on phytoplankton biomass and composition in the southern North Sea: a modelling approach (FYFY) Continental Shelf Research 16, 907–931

Vaulot, D., Courties, C., Partensky, F , 1989 A simple method to preserve oceanic phytoplankton for flow cytometric analyses Cytometry 10, 629–635.

Vidussi, F , Claustre, H , Manca, B B , Luchetta, A., Marty, J C , 2001 Phytoplankton pigment distribution in relation to upper thermocline circulation in the eastern Mediterranean Sea during winter Journal of Geophysical Research 106 (C9), 19,939–19,956

Vinayachandran, P. N., Kurian, J , Neema, C P , 2007 Indian Ocean response to anomalous conditions in 2006 Geophysical Research Letters 34, L15602, doi.10 1029/2007GL030194.

Walsh, J J., 1976 Herbivory as a factor in patterns of nutrient utilization in sea. Limnology and Oceanography 21 (1), 1–13

Wara, M W , Ravelo, A C., Delaney, M. L., 2005. Permanent El Nino-like conditions during the Pliocene warm period. Science 309 (5735), 758–761

Warner, A. J , Hayes, G C , 1994 Sampling by the Continuous Plankton Recorder survey Progress in Oceanography 34, 237–256

Webster, P J , Holland, G. J , Curry, J A , Chang, H R , 2005 Changes in tropical cyclone number, duration, and intensity in a warming environment. Science 309, 1844 –1846 10.1126/science 1116448.

Webster, P. J , Moore, A , Loschnigg, J , Leban, M , 1999 Coupled ocean dynamics in the Indian Ocean during the 1997-1998 Nature 401, 356–360.

Werdell, J., 2009. Global bio-optical algorithms for ocean color satellite applications. Eos Trans. AGU 90 (1), doi:10.1029/2009EO010005.

Werdell, P., Bailey, S. W., 2002. The SeaWiFS Bio-optical Archive and Storage System (SeaBASS): Current architecture and implementation. Tech. rep., NASA Goddard Space Flight Center, Greenbelt, Maryland, 45 pp.

Werdell, P., Bailey, S. W., Fargion, G. S., Pietras, C., Knobelspiesse, K. D., Feldman, G. C., McClain, C. R., 2003. Unique data repository facilitates ocean color satellite validation. EOS Trans. AGU 84 (38), 337.

Werdell, P. J., Bailey, S. W., 2005. An improved in situ bio-optical data set for ocean colour algorithm development and satellite data production validation. Remote Sensing Environment 98, 122–140.

Westberry, T. K., Behrenfeld, M. J., Siegel, D., Boss, E., 2008. Carbon-based primary productivity modeling with vertically resolved photoacclimation. Global Biogeochem Cycles 22 (2), GB2024, doi:10.1029/2007GB003078.

Westberry, T. K., Dall'Olmo, G., Boss, E., Behrenfeld, M. J., Moutin, T., 2010. Coherence of particulate beam attenuation and backscattering coefficients in diverse open ocean environments. Optics Express 18 (15), 15419–15425.

Widdicombe, C. E., Eloire, D., Harbour, D. S., Harris, R. P., Somerfield, P. J., 2010. Long-term phytoplankton community dynamics in the Western English Channel. Journal of Plankton Research 32, 643–655.

Wolter, K., 1987. The Southern Oscillation in surface circulation and climate over the tropical Atlantic, Eastern Pacific, and Indian Oceans as captured by cluster analysis. J. Clim. Appl. Meteorol 26 (540-558).

Wolter, K., Timlin, M. S., 1993. Monitoring ENSO in COADS with a seasonally adjusted principal component index.

Wolter, K., Timlin, S. M., 1998. Measuring the strength of ENSO events - how does 1997/98 rank? Weather 53, 315–324.

Wright, S. W., Thomas, D. P., Marchant, H. J., Higgins, H. W., Mackey, M. D., Mackey, D. J., 1996. Analysis of phytoplankton of the Australian sector of the Southern Ocean: comparisons of microscopy and size frequency data with interpretations of pigment HPLC data using the CHEMTAX matrix factorisation program. Marine Ecological Progress Series 144, 285–298.

Wright, S. W., van den Enden, R. L., 2000. Phytoplankton community structure and stocks in the East Antarctic marginal ice zone (BROKE survey, January-March

1996) determined by CHEMTAX analysis of HPLC pigment signatures. Deep Sea Research II 47 (12-13), 2363–2400

Yentsch, C S., Phinney, D A., 1989. A bridge between ocean optics and microbial ecology Limnology and Oceanography 34, 1694–1704.

Yoder, J., Kennelly, M A , Doney, S C , Lima, I D , 2010 Are trends in SeaWiFS chlorophyll time-series unusual relative to historic variability Acta Oceanologica Sinica 29 (2), 1–4

Zaneveld, J R. V , 1995 A theoretical derivation of the dependence of the remotely sensed reflectance on the inherent optical properties. Journal of Geophysical Research 100 (C7), 13135–13142.

Zhang, X., Lewis, M R , Johnson, B , 1998 The influence of bubbles on scattering of light in the ocean Applied Optics 37, 6525–6536

Zubkov, M V., Sleigh, M A., Burkill, P H., Leakey, R J G , 2000 Picoplankton community structure on the Atlantic Meridional Transect: a comparison between seasons Progress in Oceanography 45, 369–386.

Zubkov, M V , Sleigh, M A , Tarran, G A , Burkill, P H , Leaky, R J G , 1998 Picoplankton community structure on an Atlantic transect from 50°N to 50°S Deep Sea Research I 45, 1339–1355

Zwirglmaier, K , Heywood, J L , Chamberlain, K., Woodward, E M S., Zubkov, M V , Scanlan, D. J , 2007 Basin-scale distribution pattern of picocyanobacterial lineages in the Atlantic Ocean. Environmental Microbiology 9, 1278–1290.

Zwirglmaier, K , Jardillier, L , Ostrowski, M , Mazard, S., Garczarek, L , Not, F , 2008 Global phylogeography of marine *Synechococcus* and *Prochlorococcus* reveals a distinct partitioning of lineages amongst oceanic biomes Environmental Microbiology 10, 147–161.